26810

National Library of Canada | Bibliothèque nationale du Canada

CANADIAN THESES ON MICROFICHE | THÈSES CANADIENNES SUR MICROFICHE

NAME OF AUTHOR/*NOM DE L'AUTEUR* PANDE, B B. Lal

TITLE OF THESIS/*TITRE DE LA THÈSE* ~~An Experimen~~ A Theoretical and Experimental Study of Heated discharges into Quiescent Ambients

UNIVERSITY/*UNIVERSITÉ* University of Alberta,

DEGREE FOR WHICH THESIS WAS PRESENTED/*GRADE POUR LEQUEL CETTE THÈSE FUT PRÉSENTÉE* Ph. D.

YEAR THIS DEGREE CONFERRED/*ANNÉE D'OBTENTION DE CE GRADE* 1975

NAME OF SUPERVISOR/*NOM DU DIRECTEUR DE THÈSE* DR. N. Rajaratnam

Permission is hereby granted to the NATIONAL LIBRARY OF CANADA to microfilm this thesis and to lend or sell copies of the film.

The author reserves other publication rights, and neither the thesis nor extensive extracts from it may be printed or otherwise reproduced without the author's written permission.

L'autorisation est, par la présente, accordée à la BIBLIOTHÈQUE NATIONALE DU CANADA de microfilmer cette thèse et de prêter ou de vendre des exemplaires du film.

L'auteur se réserve les autres droits de publication; ni la thèse ni de longs extraits de celle-ci ne doivent être imprimés ou autrement reproduits sans l'autorisation écrite de l'auteur.

DATED/*DATÉ* 12/9/75 SIGNED/*SIGNÉ* B Lal Pande

PERMANENT ADDRESS/*RÉSIDENCE FIXE* Assistant Professor, M.M.M. Engg College, Gorakhpur, (U.P.) India

NL-91 (3-74)

THE UNIVERSITY OF ALBERTA

A THEORETICAL AND EXPERIMENTAL STUDY OF HEATED SURFACE DISCHARGES INTO QUIESCENT AMBIENTS

by

PANDE B.B. LAL

A THESIS

SUBMITTED TO THE FACULTY OF GRADUATE STUDIES AND RESEARCH

IN PARTIAL FULFILMENT OF THE REQUIREMENTS FOR THE DEGREE

OF DOCTOR OF PHILOSOPHY

DEPARTMENT OF CIVIL ENGINEERING

EDMONTON, ALBERTA

FALL 1975

THE UNIVERSITY OF ALBERTA

FACULTY OF GRADUATE STUDIES AND RESEARCH

The undersigned certify that they have read, and recommend to the Faculty of Graduate Studies and Research, for acceptance, a thesis entitled A THEORETICAL AND EXPERIMENTAL STUDY OF HEATED SURFACE DISCHARGES INTO QUIESCENT AMBIENTS submitted by PANDE B.B. LAL in partial fulfilment of the requirements for the degree of Doctor of Philosophy.

.....
N. Rajaratnam,
Supervisor

.....
A.W. Peterson

.....
D.J. Wilson

.....
R. Gerard

.....
E. Silberman,
External Examiner

DATE 2 Sept., 1975

ABSTRACT

This study presents a theoretical and experimental investigation of the near field regime of heated water discharge from a thermal power plant into lakes or cooling ponds.

The theoretical study begins with an order of magnitude study of the Reynold's equation of motion, this leads to the recognition of three regimes of flow characterised by small, moderate and large (source) Richardson number, Ri. For each of these three cases, the equations of motion and the heat transport equation are integrated and then subjected to a similarity analysis. The results of this analysis indicate the manner of variation of the significant scale factors of this phenomenon as a function of longitudinal distance from the inlet section, where the heated water enters the lake. An equation for the temperature distribution for the large Richardson number flows is also derived.

Experimental investigation of the near field has been carried out for two aspect ratios for both moderate and large Richardson numbers. For temperature measurements a rake of thermistors with an automatic data acquisition system has been used. Velocity has been measured by the hydrogen bubble technique. The Richardson number at which the flow changes from moderate to large Richardson has been found. For the two ranges of Richardson numbers, the velocity and temperature profiles in both lateral and vertical directions are found to be similar. The value of the coefficients for the variation of velocity, temperature,

width and depth scales, are found experimentally for all Richardson numbers. The experimental findings confirm, in general, the theoretical predictions.

Equation of the isotherms and the areas contained within them are then derived for the entire range of Richardson numbers based on the present experimental results, as also those of Jen, Wiegel and Mobarek.

ACKNOWLEDGEMENTS

I wish to express my sincere gratitude to my supervisor, Dr. N. Rajaratnam, for his suggestions, constructive criticism, guidance and encouragement throughout the course of this study.

I am indebted to Dr. R. Gerard for his many useful suggestions and review of the manuscript. Thanks are also due to Professor A.W. Peterson for his invaluable advice during the experimental work.

Messers S. Lovell assisted in erecting and maintaining most of the experimental setup, R. Gitzel designed and kept the electronic equipment in working order and [redacted] McGowan assisted in erecting the flume and hot water system. Their valuable assistance is greatly appreciated.

My special thanks are due to many others, whose names are not mentioned here, who directly and indirectly contributed towards the completion of this thesis.

The present study was supported by the National Research Council of Canada through a grant to Dr. N. Rajaratnam (No. A-3365). I have been supported by a scholarship award given by the Commonwealth Scholarship and Fellowship Committee of the Government of Canada. The help of these authorities is gratefully acknowledged.

Finally, I am immeasurably indebted to my wife, Sudha, for her forbearance and sympathetic understanding throughout the busy years of my graduate studies.

TABLE OF CONTENTS

Page

CHAPTER 3 THEORETICAL ANALYSIS

LIST OF TABLES

LIST OF FIGURES

LIST OF SELECTED SYMBOLS

A	=	area covered under isotherm either A_y or A_z
A_y	=	area covered under isotherm in lateral directions
A_z	=	area covered under isotherm in vertical directions
A_o	=	area of inlet
A_1	=	area contained within 1°C excess isotherm
A_r	=	area normal to jet centerline
a	=	exponent of velocity scale, also suffix to denote ambient
B	=	suffix to denote effect of buoyancy
b	=	length scale in y direction (half width of jet)
C, C_1 to C_5	=	constants
c	=	exponent in depth scale
D_f	=	friction drag
D	=	critical mixing depth as given by Equation 2.9.7
d	=	exponent in excess temperature scale
F	=	integrals (see Appendix A)
F_w	=	wind shear force per unit depth
$\overline{F}$	=	a parameter to represent momentum perpendicular to ambient currents
F_i	=	body force in i direction
f_i	=	function for different values of i (see Appendix A)
$\overline{f}$	=	fraction of control volume that is ambient fluid
$\overline{g}$	=	function for shear stress (see Appendix A)
g	=	acceleration due to gravity
h	=	length scale in z direction
$H(s)$	=	heat flux
J	=	integral (see Appendix A)

k_e = surface heat transfer coefficient

$\bar{k}$ = thermal conductivity

k = parameter invariant with x_*

L = length scale

$\bar{L}$ = parameter to represent momentum of jet in direction of ambient current

m = suffix to denote maximum or axial value

m_1 = exponent of Ri to correlate the data

m_2 = constant in Equation 2.13.1

$M(s)$ = momentum flux

n = exponent for b_*, also to represent normal direction in curvilinear coordinate system

n_1 = constant in Equation 2.13.1

o = suffix to denote conditions at the inlet

P = drag force due to ambient current

p = pressure

p_s = static pressure

p_o = pressure at surface caused by ambient current, wind, etc.

p_d = dynamic pressure

Q = discharge in cfs of thermal effluents

$Q(s)$ = volume flux

R = ratio of inlet velocity to cross flow velocity

R_1 = radius of curvature of jet trajectory

Ri = Richardson number equal to $[g(\Delta\rho_o/\rho_a)h_o] / U_o^2$

S = axial direction in curvilinear coordinate system

s = suffix to denote (water) surface values

s_f = scale factor

T	=	temperature, as a suffix to denote length scale for temperature
T_a	=	ambient temperature
T_e	=	equilibrium temperature
T_o	=	temperature of the effluent
T'	=	turbulent fluctuation in temperature
ΔT	=	temperature excess
t	=	suffix to denote turbulence property
U_o	=	source velocity or velocity of the effluent at the inlet structure
U	=	velocity in the direction of streak line
U_x	=	velocity scale
u	=	turbulent mean velocity in the x direction, as a suffix to represent length scale for velocity
u'	=	turbulent fluctuating velocity in the x direction
v	=	turbulent mean velocity in the y direction
v_e	=	entrainment velocity in lateral direction
v'	=	turbulent fluctuating velocity in the y direction
w	=	turbulent mean velocity in the z direction
w_1	=	wind velocity
w_e	=	entrainment velocity in the z direction
W	=	mean width of the isotherm
w'	=	turbulent fluctuating velocity in the z direction
x	=	longitudinal distance from the outlet (or suitable virtual origin)
x_p	=	length of potential core
y	=	lateral distance in the y direction
z	=	distance measured in the z direction

δ = small quantity, compared to unity

ε = turbulent kinematic viscosity

η = non-dimensional y distance

ξ = non-dimensional z distance

ρ = mass density of the fluid

ρ_a = ambient density

ρ_{air} = density of overlying layer

$\Delta\rho$ = density difference

$\Delta\rho_o$ = density difference between the ambient fluid and the thermal discharge at the inlet

τ = turbulent shear stress

τ_w = shear stress created by wind force

$*$ = suffix to denote dimensionless quantity

$\overline{\quad}$ = time average (when used over fluctuating quantities)

$\bar{\alpha}$ = ratio of lateral velocity to longitudinal centerline velocity

$\alpha, \alpha_1, \alpha_2$ = coefficients of entrainment

α_h = horizontal entrainment coefficient

α_v = vertical entrainment coefficient

a = $\Delta\rho/\Delta T$

β = angle between ambient cross current and centerline of jet

λ_H = ratio of half temperature width to half velocity width

λ_v = ratio of half temperature depth to half velocity depth

C_D = coefficient of drag

c_f = coefficient of friction

α_3 = correction factor for velocity

β_1 = correction factor for momentum

i,j = suffix in tensorial equation to denote the component of a quantity in a particular direction

μ	=	dynamic viscosity
$\bar{\phi}$	=	viscous generation of heat
δ_a	=	thickness of air boundary layer
ν_a	=	kinematic viscosity of air
θ	=	angle between ambient current and wind

CHAPTER 1

INTRODUCTION

1.1 General

The addition of concentrated heat load to a water body, as may be caused by the addition of condenser cooling water of a powerhouse, can bring about an ecological change. The important parameters which govern such a change are the changes in temperature and temperature gradient, and not the total heat addition. Many species of the aquatic life are quite sensitive to temperature change and although they may be physiologically tolerant to it, their behaviour alters. Biochemical processes are speeded up in slightly warmer water and species may appear to thrive and grow better. However, it is the lower forms of life, the parasites and bacilli, that adapt and respond more readily to the temperature changes than the higher and organised species. Thus the ecosystem is disrupted.

Besides the above changes, excessive temperature causes sublethal effects on certain fishes and higher evaporation leading to increased levels of salinity. It causes vertical stratification which in turn cuts down oxygen circulation to lower layers leading to the death of organisms there in. The stratification also controls the flow regimes and dispersal processes within water. The above ill effects are usually lumped together under the title of thermal pollution. In a cold country like Canada there is apt to be wishful thinking that it would be environmentally beneficial to warm up the rivers and lakes which are so cold. In fact, the addition of substantial amounts of heat into cold

water is relatively much more of an environmental shock than it would be in warmer waters where the temperature contrast would not be so high.

Industries, particularly fossil and nuclear fueled power plants, discharge large amounts of waste heat into the water ways. This leads to thermal pollution. The problem has been further aggravated by the increasing size of central electricity generating plants and the transition from fossil to nuclear fuels; the latter having lower thermal efficiency. Apart from the power plants, some relatively minor sources of waste heat additions are industry, municipal and irrigation return waters. However, a breakup of total waste heat at Thames estuary (Parker and Krenkel, 1969) indicates that 75% of waste heat comes from power station discharges. Hence the discharge of cooling water from power stations needs to be given special attention.

1.1.1 Growth in Energy Requirements

Canada stands second among all countries of the world in per capita use of electrical energy. The total requirements for electric energy have been growing steadily at a compound rate of 7.1 percent per annum during the past thirty-five years. Energy demand projection in Canada, up to the year 2000, is shown in Figure 1.1 (An Energy Policy of Canada, Phase 1, 1973), and the corresponding forecast rate for the U.S.A., up to the year 2020, is shown in Figure 1.2 (Parker and Krenkel, 1969). The total consumption of 2,02,300 millions of kwh in 1970 in Canada corresponds to an average use of 9500 kwh per capita. This estimated three and one-half fold increase in per capita use from 1970 to 2000 compares with the historical four fold increase experienced from 1935 to 1970 and reflects the trend towards an electrical society.

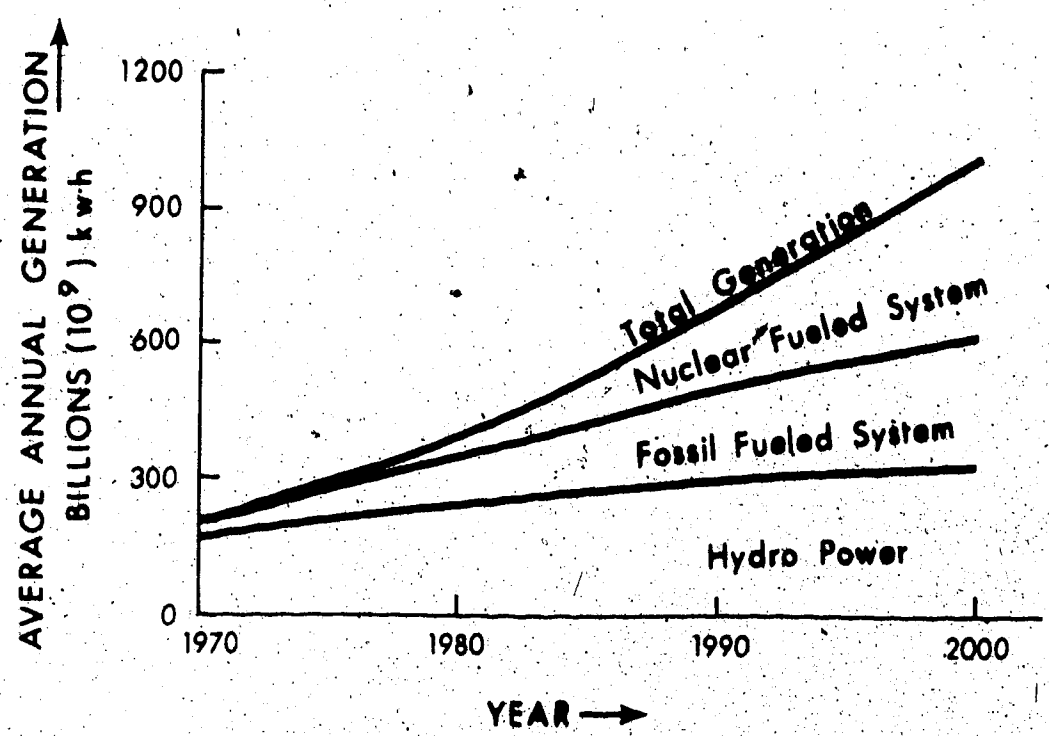

FIGURE 1.1 ELECTRIC ENERGY DEMAND PROJECTION IN CANADA UP TO THE YEAR 2000

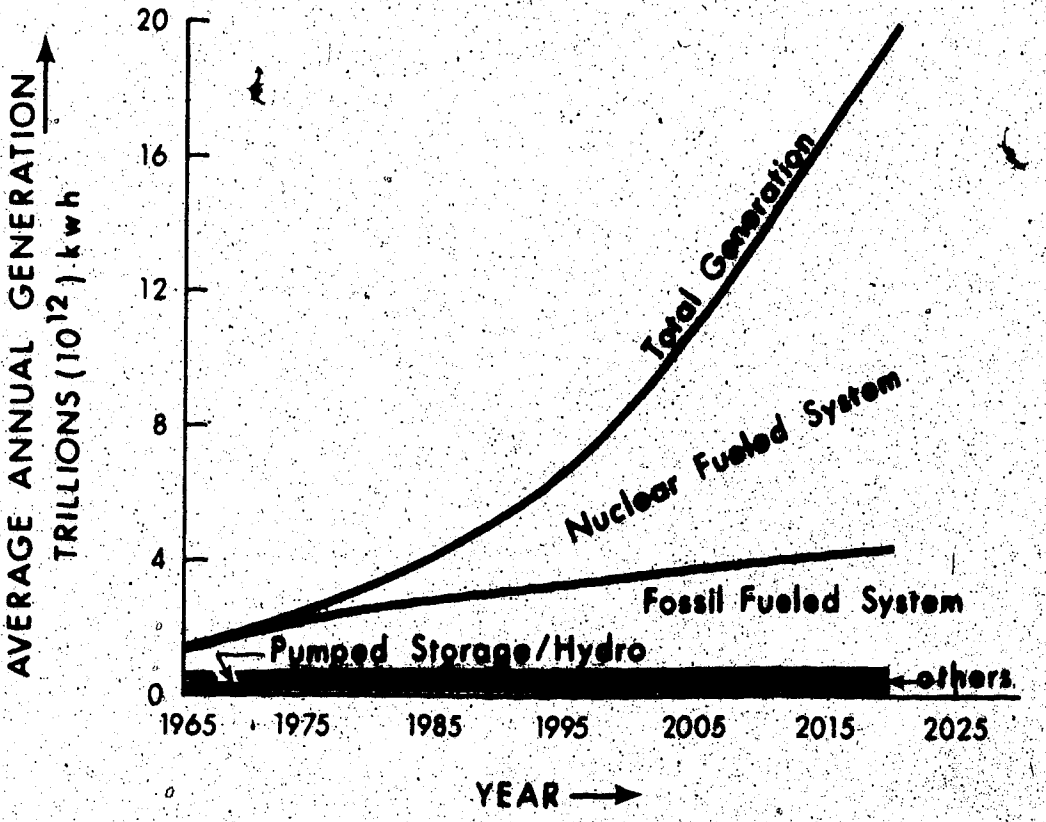

FIGURE 1.2 ELECTRIC ENERGY DEMAND PROJECTION IN U.S.A. UP TO THE YEAR 2020

The projections shown in Figure 1.3 indicate that a decreasing proportion of electricity will be derived from hydroelectric generation and an increasing proportion from nuclear plants. The undeveloped hydro resources in Canada are either more remote or economically less attractive due to the high transmission cost. Energy generation from tides such as the Bay of Fundy still seems to be far from being economically feasible. Thermal generating plants are becoming increasingly competitive as efficiencies are improved and costs reduced with large scale higher temperature units. In addition, there is a movement away from rapidly depleting fuel (oil and natural gas) to coal and nuclear fuel. The significant promise of the CANDU system which requires no enrichment facilities and the large reserves of nuclear fuel in Canada all combine to ensure that this system will make a very important contribution to Canada's electrical energy needs for many decades to come.

1.2 Cooling Water Requirements and Efficiencies

The present day fossil fueled plants operate at a thermal efficiency of 35 to 40% which leads to a waste heat of 1.5 to 1.8 times the electric energy produced. Nuclear plants operate at 30 to 35% efficiency leading to a waste heat production of 1.8 to 2.3 times the electric energy produced. Efficiencies of nuclear powered stream plants will probably catch up to conventional steam plants in another decade. Nevertheless, safety requirements and the limitation of material may not permit any substantial increase in efficiency over the 40% of the present steam cycle.

Parker and Krenkel (1969) report that with the present and

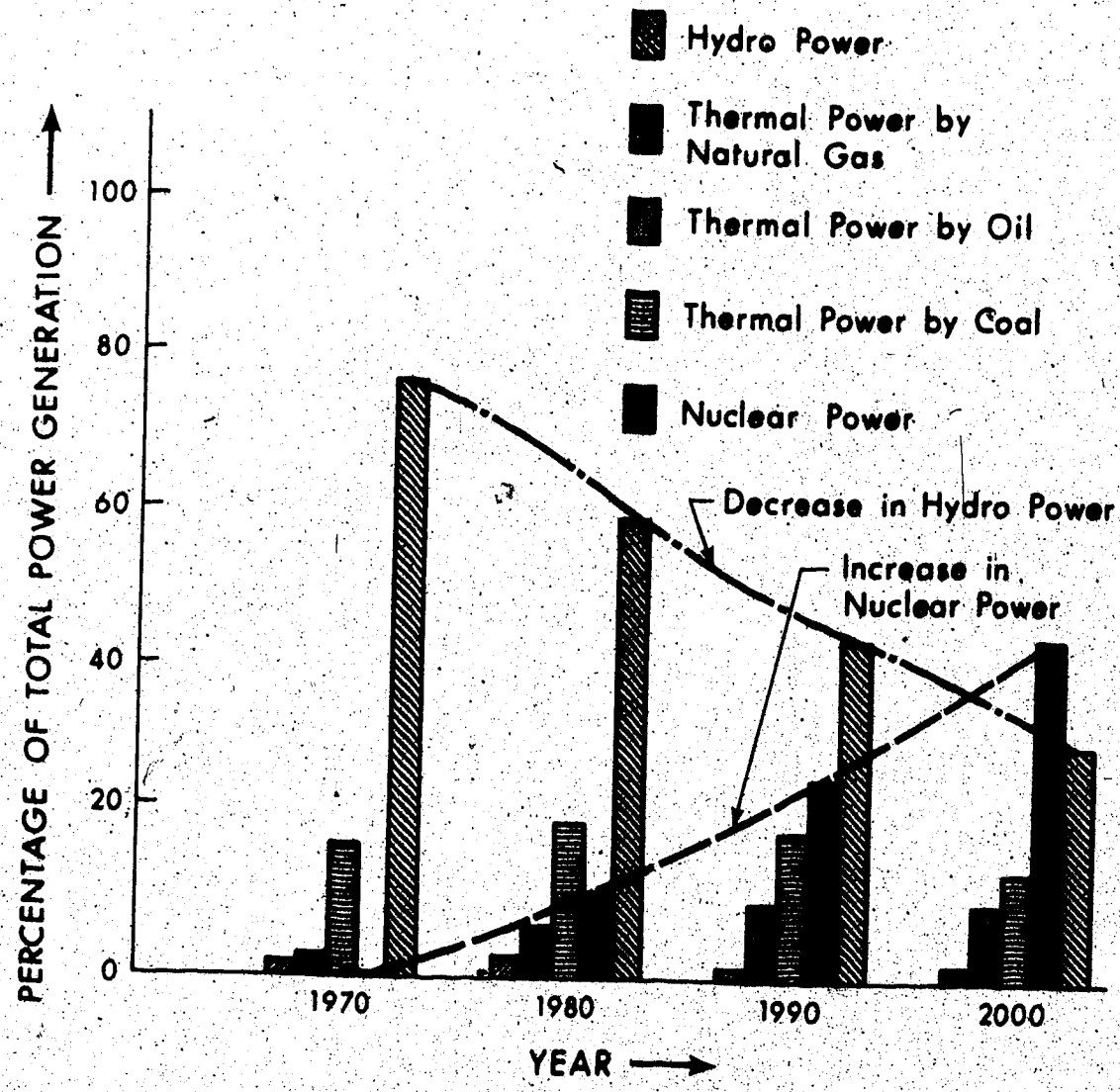

FIGURE 1.3 PROJECTED COMPARATIVE ENERGY PRODUCTION BY VARIOUS SOURCES IN CANADA

foreseeable technology there is not much hope of decreasing, to any substantial degree, the total amount of heat rejected to stream from these central steam generation plants. Based on the above figures on efficiencies, the report on energy policy of Canada, phase 1, mentions the order of magnitude of known heat discharges into Canadian waters from various sources for the year 1970 as well as the projected figures for the year 2000, if the present energy and industrial trends continue. Table 1.1 summarises these data.

Table 1.1 Heat discharge into Canadian waters from power generation and industrial processes

	Great Lakes		Other Fresh Water		Total Water		Total	
Year	1970	2000	1970	2000	1970	2000	1970	2000
Heat rejection BTU/hr x 10^{10}	3.165	60	1.65	38.6	1.21	38.1	6.025	136.7
Water loss by evaporation to dispose of added heat US gal/day x 10^{6}	69	1308	36	846	28	838	133	2292

It is clear from the above that if the current trends were to continue to the year 2000, the heat discharged into Canadian waters and consequent increased evaporation will have an important impact on the environment. The study of the temperature distribution should, therefore, be of an immediate concern.

1.3 Alternative Cooling Methods

The addition of heat discharge as discussed in the previous

section is usually accomplished by what is termed as "once through cooling". Here, water is piped directly to the source after cooling the condensers. This is the cheapest available mode of heat disposal. In order that the water bodies be safeguarded from thermal pollution caused by the continued growth rate in the electrical energy production, the alternative methods of heat disposal into the atmosphere are:

i) Cooling ponds: Cooling of the discharge water occurs through evaporative cooling, direct transfer of heat to the air, and radiation.

ii) Spray ponds: This is a cooling pond fixed with spray modules. The heated effluent is sprayed on to the surface of the pond from a height of a few meters thus increasing the evaporative cooling.

iii) Wet cooling towers: In this device, the heated effluent is sprayed on to a wooden lattice network ("fill") inside a large tower which is open at the bottom. Evaporative cooling is promoted by movement of air over the water which now has a large surface area. The air may be moved either by natural convective cooling or by large fans at the bottom of the tower. The cooled water collects in the basin at the bottom of the tower.

iv) Dry cooling towers: The dry tower cooling system operates much like the cooling system of an automobile. The heated effluent is circulated through a giant radiator through which air is blown by large fans, and thus the water is cooled by heat transfer through the walls of the radiator to the air.

However, a very high capital cost associated with dry cooling towers and a high capital cost along with fog and icing problems associa-

ted with evaporative cooling still make the "once through cooling" method preferable where feasible.

1.4 Alternative Methods of Effluent Discharge in "Once Through Cooling"

In the once through cooling, there are two distinct modes of outfall discharges; these must be considered in order to evaluate the impact of heated discharge upon a natural body of water:

i) Surface discharge of hot water from an effluent channel.

ii) Sub-surface discharge from submerged outfalls:
   a) Single jet, no diffuser.
   b) Multiple jet line diffuser.

Thermal effluents can also be discharged as a shallow submerged jet. The shallow submerged jet comes up quickly to the water surface due to the coanda effect. This type has features common to both of the above categories. The two modes of flow are quite different and the choice depends upon objectives to be attained. Umrath (1971) favours the scheme of heated discharge as a surface jet. He concludes that if the cooling water is discharged at the bottom of the receiving water, essentially all its heat is absorbed by the cooler water body due to wide dispersal of heat as it slowly reaches the surface thus affecting the natural water body and aquatic life to a maximum. On the other hand, if the plant cooling water is discharged at the surface level of the water body, relatively little of its heat is transferred down to the cooler water body. Hence, the aquatic life is affected to a minimum and more heat is released to the atmosphere by evaporation.

The scheme of discharging heated water as a surface jet has therefore been selected for the present study. The discharge of heated water on the surface of a lake has to pass through three distinct regions (Bauer, et al. 1973) given as:

i) Near field region or jet regime where momentum characteristics of heated discharge must be considered.

ii) The intermediate region where surface transfer and diffusion are the most significant mechanisms for heat redistribution.

iii) The far region where surface transfer aspects are dominant.

The near field region or jet regime is of significant interest as the so-called mixing zone is usually treated synonymous with the jet regime as discussed in the next section.

1.5 Description of the Problem

Ill effects of thermal water discharges causing ecological imbalances have aroused unprecedented public awareness. Strict laws have been framed in various parts of the USA that define thermal water quality criteria limiting the temperature rise in thermal plumes to a prescribed distance from the point of discharge. This is commonly referred to as mixing zone limitation.

From a regulatory point of view, the jet regime is of particular interest. It is often within this region that outfall must be designed so that its effluent meet the prescribed temperature criteria. Thus the jet regime is synonymous with mixing zone. Some states in the

USA have adopted a very restrictive mixing zone criteria while others have none at all. Thus each of the plant outfall designs must be based upon size of the plant, nature of the receiving body of water, thermal criteria and several other factors.

On the various lakes in Canada, such as Lake Wabamun and the Great Lakes, the predominant outfall design happens to be shoreline, open, rectangular discharge canals. The present investigation considers the problem of surface jets as discharged from these open rectangular discharge canals. The investigation is confined only to the jet regime. No cross flow or wind effects have been considered. Surface heat loss to the atmosphere is generally considered negligible and has been neglected. The justifications and objectives of the present study are described at the end of Chapter 2 in Section 2.18.

CHAPTER 2

REVIEW OF EXISTING WORK

2.1 General

As a heated effluent enters an ambient environment from a plant outfall, it acquires a jet-like character (Figure 2.1) possessing both velocity and temperature disparity with respect to the receiving body. As it enters the ambient water it creates a tangential separation surface. The instability of the tangential separation surface causes eddies which move in a disorderly fashion both along and across the stream bringing about an exchange of matter between the ambient water and the jet. This turbulence travels both inwards to the jet centerline and outwards towards the ambient fluid. A transverse transfer of momentum and heat therefore takes place as the turbulent eddies move both along and across the stream. As a result, a region of finite width and thickness with a continuous distribution of velocity and temperature is formed. The thickening and widening of the jet eats up the nonviscous core after some distance from the outfall. The velocity and temperature excess on the centerline thereafter starts to decay. This region is known as the zone of fully established flow. The region before the turbulence reaches the center of the jet is known as potential core (nonviscous core, or zone of flow establishment). Due to a large expansion of the heated jet, the zone of flow establishment appears to be very short (approximately equal to $4.2\, b_o$ as found by Paddock, 1973) and is of no practical importance in heated water discharges. The zone of established flow appears to be of considerable practical importance.

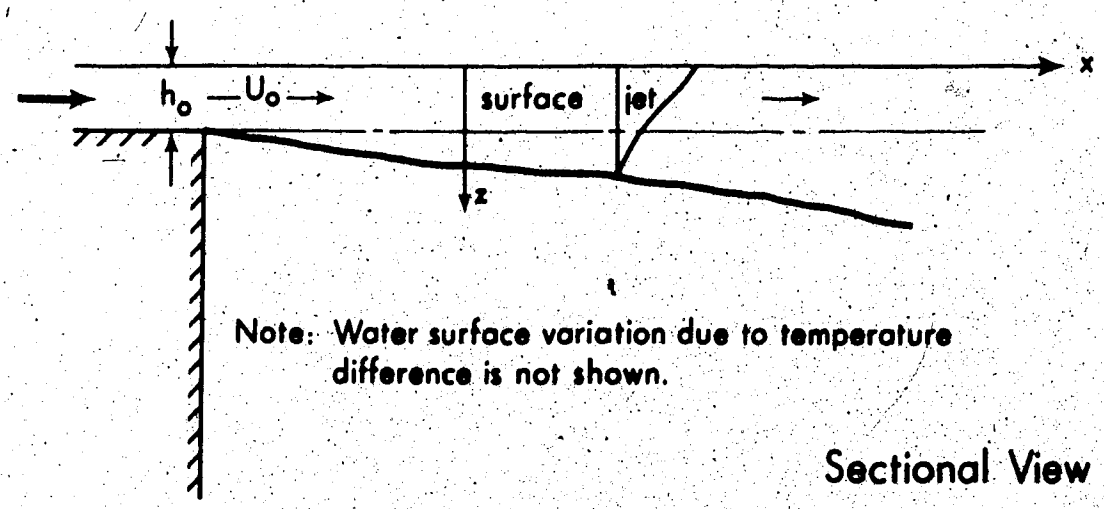

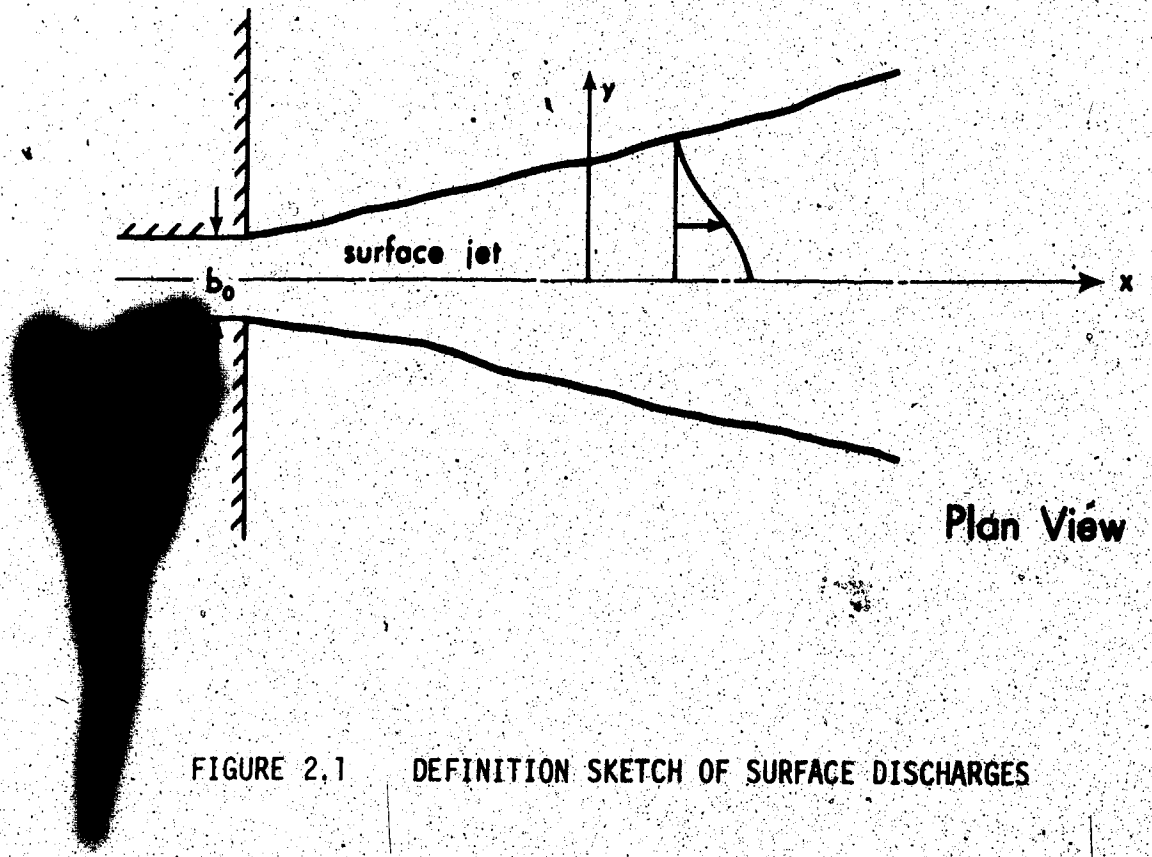

FIGURE 2.1 DEFINITION SKETCH OF SURFACE DISCHARGES

The velocity and temperature excess undergo considerable decay in this region and various "limiting temperature excess" criteria have to be satisfied in this region.

Within the jet regime the turbulence of the jet dominates the ambient turbulence. At some distance from outfall, however, kinetic energy of the discharge would be sufficiently dissipated. The ambient turbulence now dominates the jet turbulence and dictates the effluent mixing; the effluent loses its jet like character. This region is classified as the far field region.

2.1.1 Classification of Surface Jets

As described in Chapter 1, heated surface jets can be classified into two broad categories:

Class I. Three dimensional momentum jet discharged either by canals or by pipe flows.

Class II. Jets discharged at the bottom of lakes by single or multiport diffusers, rising up to the free surface, and then spreading radially as a surface layer.

These can be further subdivided into:

i) Discharge flowing into a deep quiescent water with no cross flow and no wind shear.

ii) Discharge flowing over a sloping bottom (such as on a lake beach).

iii) Discharge flowing into shallow waters.

iv) Discharge flowing into a significant cross flow (such as those occurring in a river).

v) Discharge flowing into a small cross flow (such as in a lake).

vi) Discharge flowing under influence of wind shear.

2.2 Development of Governing Equations

It would be well to commence by listing certain assumptions made by various investigators. Some of these are as follows. Fluids are incompressible and fully turbulent. Longitudinal diffusion is small compared to lateral diffusion. The largest variation of fluid density throughout the flow field is small compared with reference density so that the density variation need be considered only insofar as it gives rise to buoyant forces but neglected in inertial terms; and that the density variation is small enough so that the conservation of mass flux can be approximated by conservation of volume flux. (This assumption of small density variation is commonly called the Boussinesq assumption.)

The basic equations of mass, momentum and heat conservation are, respectively:

$$\frac{\partial u_i}{\partial x_i} = 0 \qquad (2.2.1)$$

where u_i is the mean velocity in the x_i direction (written without bar on it).

$$\rho u_j \frac{\partial u_i}{\partial x_j} = - \frac{\partial p}{\partial x_i} + \frac{\partial}{\partial x_j} (\mu \frac{\partial u_i}{\partial x_j}) + \frac{\partial}{\partial x_j} (- \rho \overline{u_i' u_j'}) + F_i \qquad (2.2.2)$$

where μ is the dynamic viscosity, F_i is the body force, u_i' and u_j' are fluctuating velocity components, ρ is the mass density of the

fluid and $\overline{\rho u_i' u_j'}$ are Reynold's stresses.

$$\frac{\partial}{\partial x_i}(u_i T) = \frac{\partial}{\partial x_i}\left(\bar{k}\frac{\partial T}{\partial x_i}\right) + \frac{\partial}{\partial x_i}\left(\overline{u_i' T'}\right) + \bar{\phi} \qquad (2.2.3)$$

where $\bar{k}$ is the thermal conductivity, $\bar{\phi}$ is the viscous generation of heat, T is the temperature and T' is fluctuation in T. As shown in Figure 2.1, $i,j = 1,2,3$ represents x,y and z directions, respectively. The subscripts indicate which components of a quantity are considered and repetition of a subscript in a term indicates a summation to be carried over possible components.

The pressure at any point is p and it is equal to the sum of the static pressure p_s and the dynamic pressure p_d. Consider first the static pressure term:

$$\frac{\partial p_s}{\partial z} = \rho g \qquad (2.2.4a)$$

Integrating Equation 2.2.4a from the water surface (where $z = \Delta z$) downwards:

$$p_s \Big|_{\Delta z}^{z} = p_s - p_o = \int_{\Delta z}^{z} \rho g dz \qquad (2.2.4b)$$

or:
$$p_s = p_o + \int_{\Delta z}^{z} \rho g dz \qquad (2.2.4c)$$

where p_o is the atmospheric pressure or pressure created due to jet bending, etc. Since Δz is generally small, as a first approximation we rewrite Equation 2.2.4c as:

$$p_s = \int_o^z \rho g dz + p_o \qquad (2.2.4d)$$

with $\rho = \rho_a - \Delta\rho$, where ρ_a is the ambient fluid density. Then Equation 2.2.4d becomes:

$$p_s = g\rho_a z - g\int_o^z \Delta\rho dz + p_o$$

$$= g\rho_a z + ga\int_o^z \Delta T dz + p_o \qquad (2.2.5a)$$

where $\partial\rho/\partial T = -a$, a being the thermal expansion coefficient. With the value of p_s given by Equation 2.2.5a, the value of:

$$p = (g\rho_a z + ag\int_o^z \Delta T dz) + p_d + p_o \qquad (2.2.5b)$$

on the further assumption that molecular heat diffusion $\bar{k}$, viscous heat generation $\bar{\phi}$, and dynamic viscosity μ are negligible since in practical turbulent jets and plume problems these are much smaller than the corresponding turbulence stress terms. Using Equation 2.2.5b, Equation 2.2.2 reduces to Equation 2.2.6, as:

$$\rho u_j \frac{\partial u_i}{\partial x_j} = g\frac{\partial}{\partial x_i}\int_o^z (-a\Delta T)\, dz - g_i'\Delta\rho + \frac{\partial}{\partial x_j}(-\overline{\rho u_i' u_j'}) - \frac{\partial}{\partial x_i}(p_d + p_o) \qquad (2.2.6)$$

where $g_i' = 0$ when $i = 1,2$ and $g_i' = g$ when $i = 3$. Consequently:

$$\left[g \frac{\partial}{\partial x_i} \int_o^z (-a\Delta T)\, dz - g_i' \Delta\rho \right] = 0 \quad \text{when} \quad i = 3 \qquad (2.2.7a)$$

and:

$$= - ag \frac{\partial}{\partial x_i} \int_o^z \Delta T dz \quad \text{when} \quad i = 1 \text{ and } 2 \qquad (2.2.7b)$$

Heat transportation Equation 2.2.3 can be reduced to Equation 2.2.8 where $\Delta T = T - T_a$. T and T_a are, respectively, the temperature at any point in the surface jet and in the ambient fluid, and $\Delta T'$ is the temperature fluctuation at any point in the surface jet. Thus:

$$\frac{\partial}{\partial x_i} (u_i \Delta T) = - \frac{\partial}{\partial x_i} (\overline{u_i' \Delta T'}) \qquad (2.2.8)$$

The term:

$$- ag \frac{\partial}{\partial x_i} \int_o^z \Delta T dz$$

in the x direction tends to accelerate the jet while in the y direction it increases lateral convection.

2.2.1 Integral Methods

The most common approach used so far in the model development is the integral analysis. A set of integral equations for conservation of volume, momentum and heat energy can be obtained by integrating Equations 2.2.1, 2.2.6 and 2.2.8 first in the vertical direction and

then in lateral directions. The most frequently used integral approach was introduced by Morton, et al. (1956). Although their work and that of Fan (1967) does not consider surface discharges, yet they need a brief discussion here as most of the models on heated surface jets are based on the pioneering work of these authors. In addition to the Boussinesq assumption, velocity profiles are assumed to be similar in consecutive transverse sections of the jet. Morton, et al. added to this the assumption of similar profiles for buoyancy and temperature. Work on non-buoyant jets indicated that a Gaussian profile was appropriate. However, Morton (1961) states that the assumption of similar profiles suppresses all details of the transverse structure of the jet. Therefore any profile shape can be used without loss of additional physical information.

Morton, et al. (1956) developed three differential equations based on the conservation of volume, momentum and heat energy of a control volume although, as mentioned earlier, these equations can also be derived by integrating Equations 2.2.1, 2.2.6 and 2.2.8.

Some kind of assumption for entrainment velocity has to be made in order to solve the above derived differential equations. Morton, et al. (1956) assumed this entrainment velocity (v_e) to be proportional to the magnitude of difference between some characteristic velocity (u_m) in the jet and the velocity of ambient (u_a) unaffected by the jet. Thus:

$$v_e = \alpha (u_m - u_a \cos \beta) \qquad (2.2.9a)$$

where β is the angle of flow between centerline velocity u_m and ambient

velocity u_a.

A more general expression for entrainment velocity under cross flow is given by Platten and Keffer (1968) and Hoult (1969) as:

$$v_e = \alpha_1(u_m - u_a \cos\beta) + \alpha_2 u_a(\cos\beta - \cos\beta_o) \qquad (2.2.9b)$$

where β_o is the angle between direction of cross flow velocity and centerline of outlet. The additional term in Equation 2.2.9b as compared to Equation 2.2.9a is included to account for the entraining effects of internal rotation imparted to the jet by cross flowing current.

Using Equation 2.2.9a and considering $u_a = 0$, Morton, et al. (1956) solved the differential equations and determined the value of centerline velocity u_m, centerline excess temperature ΔT_m, and half width of jet in terms of longitudinal distance x. Fan (1967) used Morton's work to study buoyant jets under cross flow. The important aspect of Fah's analysis is that he approximated the effect of pressure gradient across the jet parallel to ambient current by a drag coefficient. He determined the entrainment coefficient from jet centerline dilution ratios and noted that the cross-sectional concentration profiles were horseshoe shaped (Figure 2.2) with maximum concentration at two sides of the plane of symmetry.

2.3 Reduction of Governing Equations for Two Dimensional Models

2.3.1 Equation of Motion for Two Dimensional Model in Cartesian Coordinates

Hoopes, et al. (1968), Motz and Benedict (1970) considered a two dimensional surface discharge under cross flow. Their methods are based on formulation of three differential equations by control volume approach and assumption of an external equation in the form of entrainment velocity as was done by Morton, et al. (1956). Carter (1969) does the same thing, but instead of making an assumption for entrainment velocity, relates dilution with decay of centerline excess temperature. Each of these authors claim their method to be different from the other. In the following, an attempt is made to derive all these models from Equations 2.2.1 to 2.2.8.

Ignoring the coupling between hydrodynamic forces with those of buoyancy, as was done in the models under discussion, and neglecting the dynamic pressure and applying boundary layer approximations, Equations 2.2.1, 2.2.6 and 2.2.8 reduce to:

$$\frac{\partial u}{\partial x} + \frac{\partial u}{\partial y} = 0 \qquad (2.3.1)$$

$$\rho \left(u \frac{\partial u}{\partial x} + v \frac{\partial u}{\partial y}\right) = - \frac{\partial p_o}{\partial x} + \frac{\partial}{\partial y} \left(-\overline{\rho u' v'}\right) \qquad (2.3.2)$$

$$\frac{\partial}{\partial x} (u\Delta T) + \frac{\partial}{\partial y} (v\Delta T) = \frac{\partial}{\partial y} \left(-\overline{v'\Delta T'}\right) \qquad (2.3.3)$$

These equations are not applicable when the jet trajectory is curved under the effect of cross current and wind shear. Schlichting (1960) has given an expression for complete Navier-Stokes equation on a curved wall. An examination of those equations reveal that Equations 2.3.1 to 2.3.3 can still apply approximately if the following two conditions are

satisfied:

i) Thickness of jet is small compared to the radius of curvature of the jet trajectory.

ii) No large variation in trajectory curvature may occur.

As far as jet discharges on lakes are concerned, the ambient cross velocities are small and the second assumption is likely to be satisfied. A buoyant heated jet grows very fast and therefore its width is much larger than the width of a nonbuoyant jet. But if the jet curvature is large, the width of the jet could still be considered much smaller than its radius of curvature. The assumptions (i and ii) may therefore be considered to be an approximation to the flow situation.

2.3.2 Equations of Motion in Terms of S and n Coordinates

A new coordinate system, shown in Figure 2.3, is now chosen with centerline trajectory represented as S axis and direction perpendicular to it represented as n axis. Equations 2.3.1 to 2.3.3 will be applicable to this system with the direction of x represented as S and direction y represented as n.

The new set of equations for a two dimensional flow in terms of surface velocities u_s and v_s and surface excess temperature ΔT_s are represented as:

$$\frac{\partial u_s}{\partial S} + \frac{\partial v_s}{\partial n} = 0 \qquad (2.3.4)$$

$$\rho \left(u_s \frac{\partial u_s}{\partial S} + v_s \frac{\partial u_s}{\partial n}\right) = - \frac{\partial p_o}{\partial S} + \frac{\partial}{\partial n} \left(-\rho \overline{u_s' v_s'}\right) \qquad (2.3.5)$$

$$\frac{\partial}{\partial S}(u_s \Delta T_s) + \frac{\partial}{\partial n}(v_s \Delta T_s) = \frac{\partial}{\partial n}(-\overline{v_s' \Delta T_s'}) \qquad (2.3.6)$$

The pressure gradient term in Equation 2.3.5 represents the effect of wind shear or ambient cross flow.

A similarity function for velocity and temperature excess can now be assumed:

$$\frac{(u_s - u_a \cos\beta)}{u_m - u_a \cos\beta} \triangleq \frac{u_s}{u_m} = f_1\left(\frac{\hat{n}}{b_u}\right) = f_1(\eta) \qquad (2.3.7)$$

$$\frac{(T_s - T_a)}{T_m - T_a} = \frac{\Delta T_s}{\Delta T_m} = f_1\left(\frac{n}{\lambda_H b_u}\right) = f_3(\eta) \qquad (2.3.8)$$

u_m and ΔT_m are, respectively, the centerline velocity and temperature at the surface. T_a is the ambient temperature. The authors under discussion have totally ignored the effect of cross flow on similarity and have considered the effect of cross flow on pressure gradient alone.

Heat diffuses more than velocity and half width of velocity (b_u) is smaller than half width of temperature b_T ($= \lambda_H b_u$). Thus λ_H was usually taken as 1.16 in plumes. Paddock, et al. (1973) later found this value as 2 for heated surface discharges.

There is a marked difference between windward and leeward sides of the jet. Thus the assumption of similarity when the jet is bending under a cross flow is only a rough approximation as are the simplifications suggested in Equation 2.3.7 and Equation 2.3.8. However, if cross flow velocities are low as discussed earlier these approximations may

not be far from the truth.

2.3.3 Development of Governing Equations

Equation 2.3.5 can now be resolved in x and y directions as given below:

Momentum equation in the x direction

$$\frac{\partial}{\partial S}(u_s \sin\beta)\, u_s + \frac{\partial}{\partial n}(u_s \sin\beta)\, v_s =$$

$$-\frac{1}{\rho}\frac{\partial p_o}{\partial S}\sin\beta + \frac{\partial}{\partial n}(-\overline{\rho u_s' v_s'}\sin\beta) \qquad (2.3.9a)$$

Momentum equation in the y direction

$$\frac{\partial}{\partial S}(u_s \cos\beta)\, u_s + \frac{\partial}{\partial n}(u_s \cos\beta)\, v_s =$$

$$-\frac{1}{\rho}\frac{\partial p_o}{\partial S}\cos\beta + \frac{\partial}{\partial n}(-\overline{\rho u_s' v_s'}\cos\beta) \qquad (2.3.9b)$$

When the similarity relations are substituted, Equation 2.3.4, 2.3.6 and 2.3.9 can be integrated in lateral (n) direction under the following boundary conditions:

$$n = 0, \quad u_s \cos\beta = u_m \cos\beta$$
$$u_s \sin\beta = u_m \sin\beta$$
$$v_s = 0$$
$$n = \infty, \quad u_s \cos\beta = u_a$$
$$u_s \sin\beta = 0$$
$$v_s = -v_e$$

The integration yields:

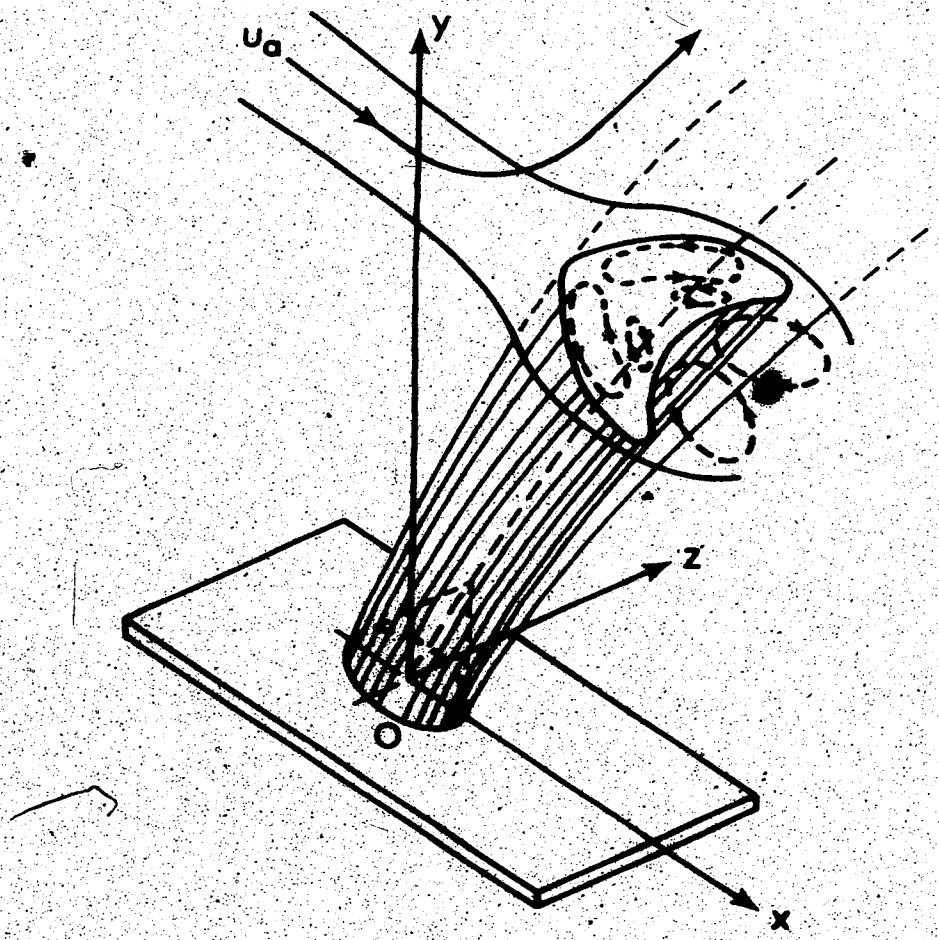

FIGURE 2.2 JET IN A LATERAL DEFLECTING FLOW

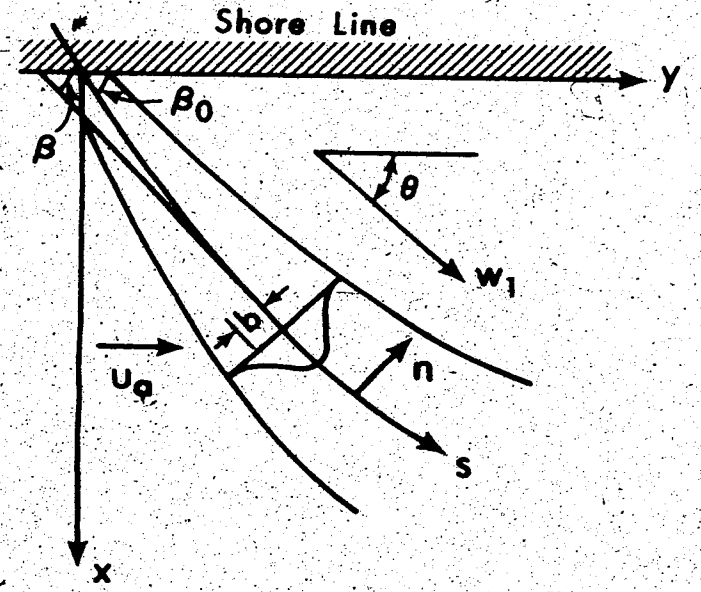

FIGURE 2.3 GENERAL COORDINATE SYSTEM FOR DEFLECTED JET (ALSO FOR HOOPES' MODEL)

$$\frac{d}{dS}(u_m b) = \frac{v_e}{I_1'} \tag{2.3.10}$$

$$\frac{d}{dS}(u_m \Delta T_m b)\, I_3' = 0 \tag{2.3.11}$$

$$\frac{d}{dS}(u_m^2 b)\, I_2' \sin\beta = -\frac{\sin\beta}{\rho}\int_o^\infty \frac{\partial p_o b}{\partial S}\, d\eta \tag{2.3.12a}$$

and:
$$\frac{d}{dS}(u_m^2 b)\, I_2' \cos\beta - u_a v_e = -\frac{\cos\beta}{\rho}\int_o^\infty \frac{\partial p_o b}{\partial S}\, d\eta \tag{2.3.12b}$$

where:
$$I_1' = \int_o^\infty f_1 d\eta \tag{2.3.13a}$$

$$I_2' = \int_o^\infty f_1^2 d\eta \tag{2.3.13b}$$

$$I_3' = \int_o^\infty f_1 f_3 d\eta \tag{2.3.13c}$$

Equation 2.3.12 states that the rate of change of momentum in the x and y directions equals the component of drag force in these directions. The term $u_a v_e$ in Equation 2.3.12b represents the lateral entrainment of momentum flux and has been obtained by integrating the second term in Equation 2.3.9b.

2.3.4 Effect of Wind Shear

Wind stress, depending upon its direction, has the effect of either increasing or decreasing the momentum flux without affecting the mass flux through any control volume. Hoopes, et al. (1968) used the following formula for wind shear:

$$\tau_w = \rho_{air} C_D W_1^2 \qquad (2.3.14)$$

where [redacted] wind stress, ρ_{air} = density of overlying air, C_D = drag coef[redacted] = wind speed. Stefan (June, 1970) defines the [redacted] of [redacted]ssius equation for skin friction coefficient o[redacted] a [redacted]. Thus:

$$C_D = 0.0225 \left(\frac{\nu_a}{W_1 \delta_a}\right)^{1/4} \qquad (2.3.15a)$$

w[redacted] $_a$ is the kinematic viscosity of air in sq.ft./sec, and δ_a is th[redacted]ickness of the air boundary layer in feet above the water surface. Use[redacted] Equation 2.3.15a is likely to be true only for smooth water which is p[redacted]ible only if W_1 is quite small. Usually, the value of W_1 is quit[redacted]rge and the water surface is wavy. Hence, Equation 2.3.15a is not likely to be true.

[redacted]u (1969) defines C_D by the following equation:

$$\frac{1}{\sqrt{C_D}} = 2.5 \ln \left(\frac{91 - gh}{C_D W_{1h}^2}\right) \qquad (2.3.15b)$$

where W_{1h} is the wind velocity measured at an elevation h above water surface.

Equation 2.3.14 actually represents the wind shear past a solid body and its use for plumes in lakes yields only a first approximation to the actual value of τ_w. In fact, modelling of wind shear is rather complex. The ambient current structure is generally non-uniform with depth. The top layers of ambient water typically travel at a higher

velocity and are strongly influenced by wind and its variations. It can be argued that wind induced stresses act not only on the plume but also on ambient lake waters (Policastro, 1972) and provide no incremental momentum flux to the plume. It appears as if the wind shear affects plume dispersion by the introduction of wind induced currents and waves.

2.4 Hoopes' Model

The details of Hoopes' model can now be considered. The coordinate system chosen by Hoopes, et al. (1968) is shown in Figure 2.3. In Equation 2.13.12a, the term:

$$-\sin\beta \int_o^\infty \frac{\partial p_o b}{\partial S}\, d\eta = \left(\frac{\tau_w b}{h_o}\right) \sin\theta$$

where h_o is the depth of the jet assumed constant. In Equation 2.3.12b the term:

$$-\cos\beta \int_o^\infty \frac{\partial p_o b}{\partial S}\, d\eta = \left(\frac{\tau_w b}{h_o}\right) \cos\theta$$

Hoopes also chose an approximation to Equation 2.2.9a and assumed $v_e = \alpha u_m$. Substituting these values in Equation 2.3.12, one gets:

$$\rho h_o dS \frac{d}{dS}(u_m^2 b)\, I_2' \sin\beta = \tau_w (bdS) \sin\theta \qquad (2.4.1a)$$

$$\rho h_o dS \left[\frac{d}{dS}(u_m^2 b)\, I_2' \cos\beta - \alpha u_a u_m\right] = \tau_w (bdS) \cos\theta \qquad (2.4.1b)$$

Since the mass flux and the buoyancy flux remains unaffected Equation 2.3.10 and Equation 2.3.11 remain unaltered. Hoopes, et al. further

assumed a linear spread for the jet width b and solved the set of Equations 2.3.10, 2.3.11 and 2.4.1 by numerical integration.

2.4.1 Remarks on Hoopes' Model

A weak point of the model involves the author's analysis of entrainment. A more exact definition is given by Equation 2.2.9a or 2.2.9b. The assumption of similar profiles for velocity and temperature makes the model capable of handling only very small cross flows. The authors consider the value of $\lambda_H = 1$ in the form of similarity function which is inconsistent with actual observations. They assume a linear spread of the jet and this may not be true if the level of the ambient turbulence is low and buoyancy effects are predominant. In view of the discussion suggesting that the wind shear provides no incremental momentum flux to the plume, their consideration of the effect of wind shear stress may be in error.

Carter's model is next in the order of development. But before considering Carter's model, the drag force formulation as done by various authors are discussed in detail to clarify the limitations involved in the model formulation.

2.5 Drag Force Due to Cross Currents

Hoopes, et al. considered only the entrainment of momentum flux due to cross current. An ambient current can influence the jet in ways other than through direct momentum exchange (Silberman, 1972). A net pressure force occurs across the jet and is caused by separation and eddying of the ambient fluid on the far side and by distortion of jet

boundaries. The ambient flow is being retarded by the jet at the near side of the jet, creating an increased pressure, while rarefaction occurs at the rear side. This force is usually represented by a drag coefficient much as though the jet were a solid body. Although, because of the inflow of the ambient into the jet, this force should be somewhat less than it would be at the wall of a solid body of the same form as a curved jet. Stefan (1972) considers a friction drag also acting on the jet but if the form drag has been created due to the separation and eddying and the momentum of the entrained ambient fluid properly accounted for, there is no frictional drag occurring on the jet. Fan (1967) originally accounted for this form drag force as:

$$P = \frac{1}{2} \rho_a C_D u_a^2 A_r \sin^2 \beta \qquad (2.5.1a)$$

where A_r is the area normal to the jet centerline. Motz and Benedict define this force as:

$$P = \frac{1}{2} \rho_a C_D u_a^2 A_r \sin \beta \qquad (2.5.1b)$$

and Carter defines this force as:

$$P = \frac{1}{2} \rho_a C_D A_r u_a^2 \qquad (2.5.1c)$$

The basic difference between these formulations is the inclusion of sin β term. Motz and Benedict argue that if sin β is not included then P cos β would go on deflecting the jet even after the jet has aligned itself parallel to ambient currents. Whereas, if sin β were included,

the term P becomes zero as $\beta \triangleq 0$, Motz and Benedict intuitively think this to be more realistic. In Carter's formulation the jet goes on bending till it reaches the near shore. Rouse, as reported by Carter, has carried out some experiments on air jets under cross flow and has experimentally found that it is indeed possible for the jet axis to bend inwards or towards the shore. Fan uses the term $u_a^2 \sin^2\beta$ as the square of the ambient velocity component normal to the projected area. Based on the arguments that pressure drag depends more on the form of body and on separation at the rear of the body than on the conditions at the front of the body, Motz and Benedict reject Fan's definition as an unnecessary refinement.

Which of these formulations is near truth is not clear. However, Policastro, et al. (1972) argues that none of these formulations will yield pressure distributions according to experimental plots of Rouse. Hence the drag formulation by any of these authors should be considered as no more than mere artifacts in an attempt to account for the pressure distribution over the jet due to flow separation.

2.6 Carter's Model

Carter (1969) assumes a "top hat" distribution for velocity and temperature yielding a value of $I_1' = I_2' = I_3' = 1$. If we replace the wind shear force used in Equations 2.3.1 and 2.3.2 acting on surface area bdS by the drag force P acting on area $h_o dS$, we get Carter's equation. Since the drag force P acts normal to the jet centerline, $\theta = \beta$ in Equation 2.3.1 and 2.3.2. The coordinate axis chosen by Carter is shown in Figure 2.4. The choice of axis by Zeller and Carter

are different. The coordinate system chosen by Carter is shown in Figure 2.4. The component of drag force in y direction in the present case is opposite to the component of wind shear in x direction in Zeller's model. Equation 2.4.1a and Equation 2.4.1b can be written as:

$$d(\rho u_m^2 h_o b) \sin\beta = -\frac{1}{2}\rho_a C_D u_a^2 h_o dS \cos\beta \qquad (2.6.1a)$$

and:
$$d(\rho u_m^2 b h_o) \cos\beta - u_a v_e dS \rho_a h_o = \frac{1}{2}\rho_a C_D u_a^2 h_o dS \sin\beta \qquad (2.6.1b)$$

Carter defines $\bar{f}$ as the fraction of control volume that is ambient fluid. He also defines the component of jet centerline velocity in x and y directions as u and v respectively. Thus in Carter's model:

$$v_e dS h_o = d(\bar{f} u_m b h_o) \qquad (2.6.2a)$$

$$u_m \cos\beta = u \qquad (2.6.2b)$$

$$u_m \sin\beta = v \qquad (2.6.2c)$$

$$dS \cos\beta = dx \qquad (2.6.2d)$$

$$dS \sin\beta = dy \qquad (2.6.2e)$$

So the two Equations 2.6.1a and 2.6.1b now read:

$$d(\rho u_m b v) = -\frac{1}{2}\rho_a C_D u_a^2 \, dx \qquad (2.6.3a)$$

and:

$$d(\rho u_m b u) - d(\bar{f} u_m b u_a \rho_a) = \frac{1}{2} \rho_a C_D u_a^2 dy \qquad (2.6.3b)$$

Carter then integrates Equation 2.6.3a and Equation 2.6.3b from the orifice $S = 0$ to an arbitrary centerline position S with boundary conditions $x = 0$, $y = 0$, $u_m = U_o$, $u = u_1$, $v = v_1$, $\bar{f} = 0$ and $b = b_o$. Assume $\rho = \rho_a$, also:

$$\frac{u}{u_m} = \cos \phi_1 ; \frac{u_1}{U_o} = \cos \phi_o ; \frac{v_1}{U_o} = \sin \phi_o ; \frac{v}{u_m} = \sin \phi_1 \qquad (2.6.4)$$

The integration of these equations with the above boundary conditions and division of the integrated form of Equation 2.6.3b with Equation 2.6.3a yields:

$$\tan \phi_1 = \frac{dy}{dx} = \frac{(\sin \phi_o - \frac{C_D}{2R^2 b_o} x)(1 - \bar{f} \frac{u_a}{u})}{\cos \phi_o + \frac{C_D}{2R^2 b_o} y} \qquad (2.6.5)$$

where $R = U_o / u_a$. Carter derives the equation for jet trajectory for both the zone of flow establishment and zone of fully established flow.

For the zone of flow establishment, Carter assumes no dilution, i.e., $\bar{f} = 0$, which does not appear a correct assumption. Equation 2.6.5 can then be integrated to yield the trajectory of the jet as a circular arc given by:

$$(y + \frac{2R^2 b_o \cos \phi_o}{C_D})^2 + (x - \frac{2R^2 b_o \sin \phi_o}{C_D})^2 = (\frac{2R^2 b_o}{C_D})^2 \qquad (2.6.6)$$

For a zone of fully established flow, Carter assumes $u = u_a$

for all points. This also does not seem to be a logical assumption and there is no hard evidence to support this assumption other than the author's own observation that the flow rapidly turned parallel to the ambient current. Thus:

$$(1 - \bar{f}\frac{u_a}{u}) = (1 - \bar{f}) \qquad (2.6.7)$$

For $(1 - \bar{f})$ = constant, Equation 2.6.5 can again be integrated to yield the trajectory of the jet as an ellipse with the same center as that of the circular trajectory but with the semi-major and minor axes as:

$$\frac{2R^2 b_o}{C_D(1 - \bar{f})^{1/2}} (1 - \bar{f} \sin^2 \phi_o)^{1/2} \qquad (2.6.8a)$$

and:

$$\frac{2R^2 b_o}{C_D} (1 - \bar{f} \sin^2 \phi_o)^{1/2} \qquad (2.6.8b)$$

Carter then relates the value of $\bar{f}$ with temperature. He defines dilution as a fraction of unit volume that was initially part of the jet discharge, the remainder was part of ambient stream. Thus:

$$\Delta T_m = (1 - \bar{f}) \Delta T_o + f\Delta T_a \qquad (2.6.9)$$

where ΔT_o = initial excess temperature of the jet and ΔT_a = excess temperature of ambient, which is treated as zero. So:

$$(1 - \bar{f}) = \frac{\Delta T_m}{\Delta T_o} \qquad (2.6.10)$$

Laboratory experiments carried out by Carter showed that:

$$\left(\frac{\Delta T_m}{\Delta T_o}\right) = \left(\frac{S}{b_o}\right)^{-1/4} \qquad (2.6.11)$$

and: Length of flow establishment = $2.5\, b_o$ (2.6.12)

The value of ϕ_o and C_D are the only unknown parameters in Equations 2.6.6 and 2.6.8. The author determines these from Rouse's experimentation on slot jets. The methodology of determining ϕ_o is approximate and the analysis yields:

$$\cos \phi_o = \frac{1}{R} \sqrt{C_D/2} \qquad (2.6.13)$$

The value of C_D has been determined as a function of R from Rouse's experimental data on boundary pressure distribution. An independent estimate of C_D was also made for the length of zone of flow establishment. Since the trajectory in the region of flow establishment is a circle, the arc length can be found as the product of radius with included angle:

$$2.5\, b_o = \left(\frac{2R^2 b_o}{C_D}\right) \left[(\phi_o - \phi_e) \frac{2\pi}{360}\right] \qquad (2.6.14a)$$

or: $$(\phi_o - \phi_e) = \frac{225}{\pi} \frac{C_D}{R^2} \qquad (2.6.14b)$$

As already assumed, the x component of velocity in the established flow region equals u_a. Thus:

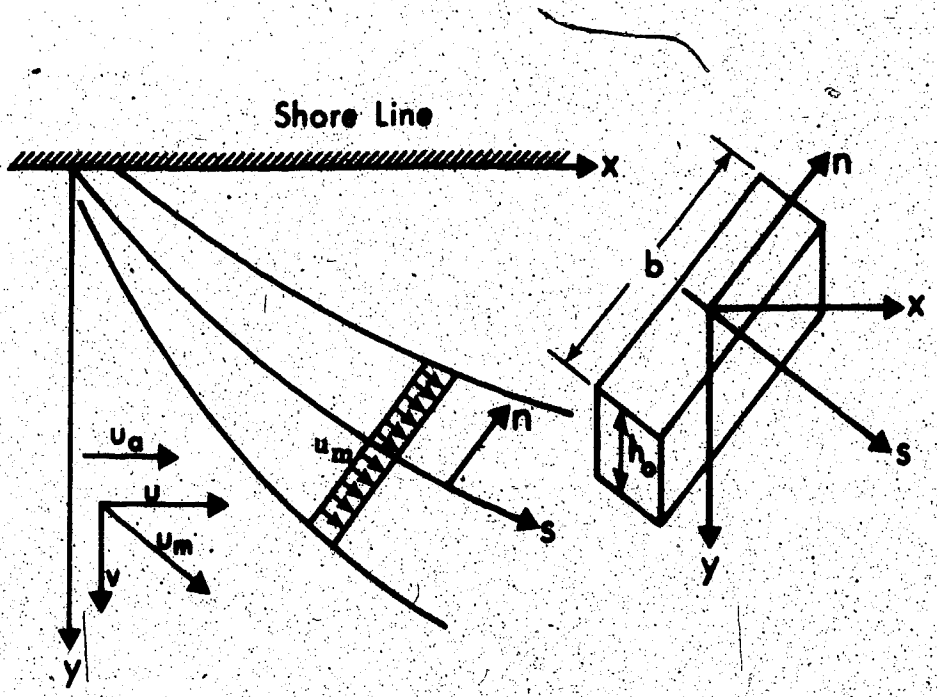

FIGURE 2.4 COORDINATE SYSTEM AND FORCES USED IN CARTER'S MODEL

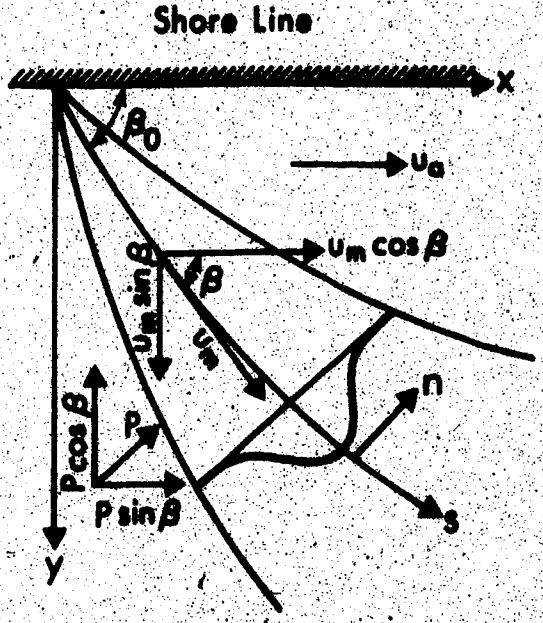

FIGURE 2.5 COORDINATE SYSTEM FOR MOTZ AND BENEDICT'S MODEL

$$\cos \phi_e = \frac{u_a}{U_o} = \frac{1}{R} \qquad (2.6.15)$$

Using Equations 2.6.13 and 2.6.15, the values of ϕ_o and C_D can be determined.

The theoretical model considered by Carter differs from that of Zeller in several respects. The decrease in temperature along the jet axis was related to dilution, but the entrainment mechanism causing the dilution was not specifically considered. The equation of volume continuity was not used. The length of flow establishment was assumed constant with respect to velocity ratio but this assumption was not supported with experimental proofs. Recently, Stefan (1975) worked out the length of flow establishment as a function of R. The increase in width of the jet cannot be predicted by the solution presented by Carter. The assumption that the x component of jet velocity equals ambient velocity in established flow region is also a doubtful approximation. However, inspite of these limitations, Carter's methodology is quite impressive.

2.7 Motz and Benedict's Model

Motz and Benedict (1970) developed a model built basically on the then existing models. They also considered a two dimensional surface jet deflected downstream by ambient velocity and incorporated a better form of entrainment velocity as given by Equation 2.2.9a. This is an improvement over Hoopes and Carter. But the authors assume the similarity function given by the approximate form of Equation 2.3.7. Although any profile for lateral distribution could have been assumed,

Motz and Benedict chose an exponential form. Further, they assumed the value of λ_H equal to 1. These are rather gross approximations which the authors resorted to in order to get a solution of governing equations. Thus:

$$f_1\left(\frac{n}{b}\right) = f_3\left(\frac{n}{b}\right) = \exp\left(-\eta^2/2\sigma^2\right) = \exp\left(-\eta^2\right) \qquad (2.7.1a)$$

and: $$b = \sigma\sqrt{2} \qquad (2.7.1b)$$

The value of various integrals becomes:

$$I_1' = \frac{\sqrt{\pi}}{2} \quad \text{and} \quad I_2' = I_3' = \frac{\sqrt{\pi}}{2\sqrt{2}} \qquad (2.7.2)$$

Using Equation 2.7.1a, 2.3.10 gives the equation for volume flux as:

$$\frac{d}{dS}\left(u_m b\right) = \frac{2\alpha}{\sqrt{\pi}}\left(u_m - u_a \cos\beta\right) \qquad (2.7.3)$$

The integration of pressure gradient over the cross-section should equal P (Equation 2.5.1b) as shown in Figure 2.5.

$$\sin\beta \int_0^\infty \frac{\partial p_o}{\partial S}\, b\, d\eta = \frac{P\cos\beta}{2h_o d_s} \qquad (2.7.4a)$$

Also: $$\cos\beta \int_0^\infty \frac{\partial p_o}{\partial S}\, b\, d\eta = \frac{P\sin\beta}{2h_o d_s} \qquad (2.7.4b)$$

Substituting Equations 2.7.4a, 2.7.4b and 2.5.1b in Equation 2.3.12, one gets:

$$\frac{d}{dS}\left(u_m^2 b \sin\beta\right) = -\frac{C_D u_a^2}{\sqrt{2\pi}} \sin\beta\cos\beta \qquad (2.7.5a)$$

$$\frac{d}{dS}\left(\overline{u_m^2} b \cos\beta\right) = \frac{2\sqrt{2}}{\sqrt{\pi}} \alpha \left(u_m - u_a \cos\beta\right) u_a + \frac{C_D u_a^2}{\sqrt{2\pi}} \sin^2\beta \qquad (2.7.5b)$$

Equation 2.3.11 remains unchanged and thus:

$$\frac{d}{dS}\left(u_m \Delta T_m b\right) = 0 \qquad (2.3.11)$$

In addition to the above, we can relate:

$$\frac{dx}{dS} = \cos\beta \qquad (2.7.6a)$$

$$\frac{dy}{dS} = \sin\beta \qquad (2.7.6b)$$

There are now six unknowns, u_m, ΔT_m, b, β, x and y. Assuming α and C_D as already known, the six unknowns can be found from Equations 2.7.3, 2.7.5a, 2.7.5b, 2.3.11, 2.7.6a and 2.7.6b.

In order to solve these equations numerically, the authors define:

$$\bar{L} = \frac{u_m^2 b}{U_o^2 b_o} \cos\beta_1 \quad ; \quad X = \frac{2\alpha}{\sqrt{\pi}\, b_o} x \quad ;$$

$$\bar{F} = \frac{u_m^2 b}{U_o^2 b_o} \sin\beta_1 \quad ; \quad Y = \frac{2\alpha}{\sqrt{\pi}\, b_o} y$$

$$V = \frac{u_m b}{U_o b_o} \quad ; \quad S = \frac{2\alpha}{\sqrt{\pi}\, b_o} s \qquad (2.7.7)$$

$$R = u_a / U_o$$

Thus Equation 2.7.3 becomes:

$$\frac{dV}{dS} = \frac{(\bar{L}^2 + \bar{F}^2)^{1/2}}{V} - \frac{\bar{L}}{R(\bar{L}^2 + \bar{F}^2)^{1/2}} \qquad (2.7.8)$$

Equations 2.7.5a and 2.7.5b become:

$$\frac{dL}{dS} = \frac{\sqrt{2}}{R}\left[\frac{(\bar{L}^2 + \bar{F}^2)^{1/2}}{V} - \frac{\bar{L}}{R(\bar{L}^2 + \bar{F}^2)^{1/2}} + \frac{C_D}{4\alpha R}\frac{\bar{F}^2}{\bar{L}^2 + \bar{F}^2}\right] \qquad (2.7.9)$$

and:
$$\frac{dF}{dS} = -\sqrt{2}\,\frac{C_D}{4\alpha}\frac{\overline{FL}}{(\bar{F}^2 + \bar{L}^2)R^2} \qquad (2.7.10)$$

The geometric equations now are:

$$\frac{dX}{dS} = \frac{\bar{L}}{(\bar{L}^2 + \bar{F}^2)^{1/2}} \qquad (2.7.11)$$

and:
$$\frac{dY}{dS} = \frac{\bar{F}}{(\bar{L}^2 + \bar{F}^2)^{1/2}} \qquad (2.7.12)$$

These are five first order differential equations which are solved by a fourth order Runge Kutta method.

Motz and Benedict have carried out laboratory experiments to determine the relation between α, C_D, zone of flow establishment and velocity ratio R and the initial angle β_o. They also relate the width of the jet at the end of the zone of flow establishment to the outlet width b_o' by equating the heat flux at the outlet to that at the end of the flow establishment where u_m and ΔT_m still equal U_o and ΔT_o. Thus, from Equation 2.3.11:

$$U_o \Delta T_o b_o I_3' = U_o b_o' \Delta T_o \qquad (2.7.13)$$

and:
$$b_o = \frac{b_o'}{I_3'} = 1.60\, b_o' \qquad (2.7.14)$$

The length of established flow has been obtained by plotting the value of temperature versus distance on log-log graph paper and finding the maximum distance up to which temperature equals the outlet temperature. The value of α and C_D has also been determined graphically. The value C_D obtained from laboratory and field data is approximately 0.5 and is reasonable. However, the value of α differs by as much as ten times between different locations. This casts a great doubt on the validity of the model.

Motz and Benedict later modified their model to include surface heat loss. Their results show that surface cooling plays no significant effect until the lower excess temperature contours (1 ~ 2°F) are reached. The model was also modified to include the

effects of non-uniform ambient currents. For most field cases of practical interest they conclude that there is little difference between predictions obtained by choosing some suitable average of ambient current over the reach influenced by the jet as compared to the inclusion of a more refined profile.

2.7.1 Field Test of Motz's Model

Paddock, et al. (1973) have tested Motz and Benedict's model with the field data obtained at Point Beach Nuclear Power Plant and Palisades Nuclear Power Plant on Lake Michigan, U.S.A. They summarize the inadequacies of the model as below:

i) Buoyant forces as well as vertical entrainment are ignored in the model development. For densimetric Froude numbers less than about 2, buoyant spreading is quite important; for densimetric Froude numbers exceeding about 5, a substantial amount of vertical entrainment may be expected. Consequently, the types of discharge for which the model may be used is limited. The entrainment coefficient determined from data fitting must actually account for spreading due to buoyancy as well as from jet entrainment.

ii) Data presented by Motz and Benedict show considerable variation in the value of entrainment coefficient from one situation to another. Particularly for lake data, the value of α is shown to be extremely small (~ 0.04) compared to riverine situations where it is about an order of magnitude higher. A particularly interesting contrast is observed when one compares the Motz-Benedict laboratory data for 90° discharge to the Romberg-Ayers lake data. Although most of the initial conditions are similar, the entrainment coefficients are different by a factor of 10. But limited field results indicated that the entrainment coefficient α remained

essentially constant at a particular location with changing values of R ; this behaviour being consistent with their laboratory findings showing α to be relatively independent of R.

iii) The model is actually restricted to small ambient currents. The simulation assumes that the jet velocity approaches zero at large distances normal to the jet centerline. The assumption of Gaussian profiles for temperature and velocity and the assumption of equal rates of entrainment on offshore and lee sides of the jet are not valid for ambient currents that are not very small.

iv) The model does not simulate unequal rates of spread for momentum and heat. These have been observed to be significant in the Point Beach and Palisades data.

v) The model does not treat turbulence intensity in the cross flow due to the assumption that such turbulence and its effects on mixing are negligible. Although some account of this effect may be made in the choice of entrainment coefficients, any such treatment would only be qualitative.

2.8 Koh's Analysis for Two Dimensional Surface Jets

Koh (1971) wrote a very interesting paper concerning an infinitely wide (slot) jet with no lateral spreading. The author's model was the first to consider any coupling between hydrodynamic and buoyancy forces. The author provides a clear definition of four regimes possible with such a mode of discharge:

i) Zone of flow establishment.

ii) Supercritical flow (jet zone).

iii) Internal hydraulic jump.

iv) Subcritical flow (no entrainment across horizontal interface).

Field and laboratory data presented so far suggest that hydraulic jumps are much less likely to occur than would be expected from the author's analysis. The author's method assumes a slot jet which prohibits lateral dispersion and reduces the number of degrees of freedom by one. This loss of freedom for the jet accounts for the increased predictions of jump by his method. In a practical field situation, surface jets are not discharged by an infinite rectangular slot and hence we shall not discuss Koh's method in any greater detail.

2.9 Two Dimensional Model Accounting for Vertical Spreading Correction

Prichard's model (1971)[1] is basically a two dimensional empirical one but accounts for vertical spreading correction, background temperature correction, etc., thus making it suitable to be applied to the field. The model is based upon observations at Waukegan Power Station at Lake Michigan. Pritchard uses an integral technique in which plume velocity and excess temperature are assumed to have a "top hat" distribution both laterally and vertically. Buoyancy forces in the equation of motion are not considered. The effluent is assumed to discharge in a quiescent ambient water.

Prichard's theoretical development is carried out in four consecutive stages:

i) A two dimensional plane jet is considered without any coupling of hydrodynamic and buoyant forces which yields well known results of nonbuoyant jets. These can be written as:

---

[1] Review material extracted from Policastro, et al. (1972).

a) $b = x/6$ (assumed) (2.9.1)

b) Length of flow establishment $x_e = 6\, b_o$ (2.9.2)
(assumed)

c) $u_m = U_o \sqrt{x_e/x}$ (derived from momentum principle) (2.9.3)

d) $\Delta T_m = \Delta T_o \sqrt{x_e/x}$ (2.9.4)

The variation of velocity and temperature is assumed to hold for $0.2\ \Delta T_o \leq \Delta T_m \leq \Delta T_o$. Beyond this point, the dilution of excess heat in the plume is assumed to be primarily the result of mixing processes. The jet decays as a three dimensional jet. Hence:

$$\frac{\Delta T_m}{\Delta T_o} = 30\, b_o/x \qquad (2.9.5)$$

The constant 30 was calculated matching Equations 2.9.4 and 2.9.5 at $\Delta T_m = 0.2\ \Delta T_o$.

ii) Vertical spreading correction. The author defines a "critical depth of mixing". If the initial depth of the jet is less than critical depth D, plume entrains vertically till the depth becomes critical, thereafter the depth remains constant. If the initial depth is greater than the critical depth, the depth of the plume remains constant throughout the near field. Vertical rate of growth found by this author is 0.002 ft/ft. He uses the method of reflection to calculate the distance between source and the critical mixing depth. This distance is given by:

$$x_1 = \frac{12\, h_o}{(1 - \sqrt{1 - h_o/D})^2} \qquad (2.9.6)$$

Then; $$h = h_o + \left(\frac{D - h_o}{x_1}\right)x \quad \text{for } x < x_1 \qquad (2.9.7)$$

$$= D \quad \text{for } x > x_1 \qquad (2.9.8)$$

The value of ΔT_m calculated from Equation 2.9.4 is corrected as:

$$\Delta T_m = \frac{h_o}{h} \Delta T_m \qquad (2.9.9)$$

iii) Background temperature correction. This correction is done to account for the possible recirculation of dilution water in the model development. The background temperature is estimated by calculating the excess temperature that would exist if the heated effluent were completely mixed into the available rate of supply of diluting water to the inshore area where the heated effluent is being discharged. Then the corrected excess temperature is given by:

$$\Delta T_m' = \Delta T_m + (1 - \frac{\Delta T_m}{\Delta T_o}) \Delta T_b \qquad (2.9.10)$$

where $\Delta T_m'$ = corrected excess temperature and ΔT_b = background temperature above ambient. The area within an isotherm is calculated empirically. The author assumes the maximum width of the area having an excess temperature equal to or greater than ΔT as:

$$\bar{b} = x/4 \qquad (2.9.11)$$

To account for a bell-shaped distribution instead of the assumed top hat distribution, the author writes:

$$A_{\Delta T} = 0.86\, \bar{b}\, x = 0.215\, x^2 \qquad (2.9.12)$$

iv) Surface cooling correction. Surface heat loss is related to the decrease in source strength. This is then included in the analysis as a correction to the areas derived in Step iii. This surface heat loss correction yields the final two dimensional temperature field and the isotherm areas.

The model is simple and considers plume dispersion to be governed solely by momentum-jet entrainment, turbulent diffusion and surface

heat loss. Buoyancy induced convective motions have not been explicitly considered. No ambient current is assumed to exist in the theoretical development; yet, the author expects that the predicted centerline-temperature decay and areas within isotherms would still be accurate in the presence of currents less than 10% of the initial discharge velocity. The model is not expected to perform well when buoyancy is significant (Ri > 0.25) or when the dilution capacity of the receiving water is significantly restricted by lateral or bottom boundaries.

2.10 Three Dimensional Models

The models discussed so far are two dimensional in character. In these models either lateral or vertical spreading is restricted. In a field problem, the jet is usually three dimensional where both the lateral and vertical processes are important and thus a two dimensional description of the jet does not describe its features properly. The models to be discussed under this heading are those of Hayashi (1967), Engelund and Pedersen (1973), Stefan and Vidayaraman (1972), Prych (1972) and Stolzenbach and Harleman (1971).

Hayashi's model is of historical interest only. Engelund and Pedersen use a control volume approach and solve the differential equations so obtained for small Richardson numbers only. Stefan and Vidayaraman's model is again based on control volume approach but there are many assumptions involved so that it looks like an empirical model. This model considered the effects of wind shear and cross flow. Prych's model is also based on control volume approach and takes into account the effect of cross flow. Stolzenbach and Harleman's model is based on

much sounder theoretical reasonings and appears the most sophisticated amongst all three dimensional models for the surface discharge. The details of these models are discussed in separate sections.

2.10.1 Similarity Assumptions for Three Dimensional Models

For three dimensional discharges, the usual similarity assumptions are:

$$\frac{u - u_a \cos\beta}{u_s - u_a \cos\beta} = f_1(z/h) = f_1(\xi) \qquad (2.10.1a)$$

$$\frac{u_s - u_a \cos\beta}{u_m - u_a \cos\beta} = f_1(y/b) = f_1(\eta) \qquad (2.10.1b)$$

or:

$$\frac{u - u_a \cos\beta}{u_m - u_a \cos\beta} = f_1(\xi) \cdot f_1(\eta) \qquad (2.10.1c)$$

In the abscence of a cross flow:

$$u/u_s = f_1(\xi) \qquad (2.10.1d)$$

$$u_s/u_m = f_1(\eta) \qquad (2.10.1e)$$

and:

$$u/u_m = f_1(\xi) f_1(\eta) \qquad (2.10.1f)$$

$$v/v_s = f_2(\xi) \qquad (2.10.2)$$

$$\Delta T/\Delta T_s = f_1(\xi/\lambda_v) = f_3(\xi) \qquad (2.10.3a)$$

$$\Delta T_s/\Delta T_m = f_1(\eta/\lambda_H) = f_3(\eta) \qquad (2.10.3b)$$

and: $$\Delta T/\Delta T_m = f_3(\xi)\, f_3(\eta) \qquad (2.10.3c)$$

In Equations 2.10.1 and 2.10.3 the length scales for velocity and temperature have been considered to be proportional to each other with the value of λ_v and λ_H being greater than 1.

2.10.2 Entrainment Velocity for Three Dimensional Jets

The horizontal entrainment velocity is considered to be the same as for two dimensional jets as given by Equation 2.2.9a or 2.2.9b. Ellison and Turner's experimentation (1959) is heavily relied upon to find the value of vertical entrainment. Stolzenbach and Harleman (1971) derive a formula based on Phillip's theory (1966) and Ellison's experimentation. This formula is given as:

$$w_{em} = \alpha u_m \exp\left(-5.0 \frac{\alpha g h_m T_m}{\rho_a u_m^2}\right) \qquad (2.10.4a)$$

where h_m is the thickness of the jet on the centerline. Stefan and Vidayaraman (1972) give this value as:

$$w_{em} = \alpha u_m \left\{1 - 1.33 \log\left[\frac{\left(\frac{\Delta\rho_m}{\rho_a} g\lambda_v h\right)^{1/2}}{(u_m - u_a \cos\beta)}\right]\right\} \qquad (2.10.4b)$$

where β is the angle between u_m and u_a

2.11 Hayashi's Model

Hayashi's model (1967) for three dimensional heated surface discharges is merely of historical interest. He first considers the general Equations 2.2.1, 2.2.2 and 2.2.8 and then assumes:

$$\frac{\partial}{\partial x_j}\left(\rho \overline{u_i' u_j'}\right) = A_j \frac{\partial^2 u_i}{\partial x_j^2} \qquad (2.11.1)$$

where A_j has been defined as turbulent diffusion coefficient with A_1 and A_2 being equal but different from A_3. The author then assumes:

i) The quadratic terms with respect to u_i in the governing equations are negligible.

ii) The vertical component of u_i is very small.

iii) No shearing force acts either on water surface or on the sea bottom.

In essence, therefore, the author assumes a surface discharge having so large a buoyant stability that vertical entrainment is zero and that all inertial terms in the governing equations are negligible. The governing equations are then integrated over the jet depth using a similarity function chosen the same as for u and v to describe vertical temperature and velocity distribution. This yields the following equations:

Continuity Equation

$$\frac{\partial}{\partial x}\left(u_s I_1 h\right) + \frac{\partial}{\partial y}\left(v_s I_1 h\right) = 0 \qquad (2.11.2)$$

Momentum equation in the x direction

$$A_1 \left(\frac{\partial^2}{\partial x^2} + \frac{\partial^2}{\partial y^2}\right)(u_s I_1 h) - \frac{\partial p}{\partial x} = 0 \qquad (2.11.3)$$

Momentum equation in the y direction

$$A_1 \left(\frac{\partial^2}{\partial x^2} + \frac{\partial^2}{\partial y^2}\right)(v_s I_1 h) - \frac{\partial p}{\partial y} = 0 \qquad (2.11.4)$$

where: $$I_1 = \int_0^\infty f_1(\xi)d\xi \qquad (2.11.5)$$

The author then defines:

$$u_s I_1 h = \frac{\partial \psi}{\partial y} \qquad (2.11.6)$$

$$v_s I_1 h = -\frac{\partial \psi}{\partial x} \qquad (2.11.7)$$

Solving Equation 2.11.3 and Equation 2.11.4 with the help of Equations 2.11.6 and 2.11.7, we get:

$$\left(\frac{\partial^4}{\partial x^4} + \frac{2\partial^4}{\partial x^4 \partial y^4} + \frac{\partial^4}{\partial y^4}\right)\psi = 0 \qquad (2.11.8)$$

with boundary conditions:

$$x = 0 \text{ and } -b_o/2 < y < b_o/2 \; ; \; u_s I_1 h = Q/b_o$$
$$\text{and } -b_o/2 > y > b_o/2 \; ; \; u_s I_1 h = 0 \qquad (2.11.9)$$

where Q is the rate of discharge of warm water. The solution of Equation 2.11.8 is:

$$\psi = \frac{1}{\pi}\frac{Q}{b_o}\left[(y+\frac{b_o}{2})\tan^{-1}\frac{y+\frac{b_o}{2}}{x} - (y-\frac{b_o}{2})\tan^{-1}\frac{y-\frac{b_o}{2}}{x}\right] \qquad (2.11.10)$$

The values of $u_s I_1 h$ and $v_s I_1 h$ can be approximated for $x >> b_o/2$:

$$u_s I_1 h = \frac{2Q}{\pi}\frac{1(y/x)^2}{[1+(y/x)^2]^2}\frac{1}{x} \qquad (2.11.11)$$

$$v_s I_1 h = \frac{2Q}{\pi}\frac{y/x}{[1+(y/x)^2]^2}\frac{1}{x} \qquad (2.11.12)$$

The author's solution here seems to be in error. Neglecting the term $\partial/\partial y\ (\overline{v'\Delta T'})$ and considering surface heat loss, Equation 2.2.8 can be integrated to yield:

$$\frac{\partial}{\partial x}(u_s \Delta T_s h)\, I_8 + \frac{\partial}{\partial y}(v_s \Delta T_s I_8 h) = -\frac{k_e}{\rho C_p}(\Delta T_s) \qquad (2.11.13)$$

Substituting for v_s and u_s, we get:

$$\frac{I_8}{I_1}\frac{2Q}{\pi}\frac{1}{(1+\frac{y^2}{x^2})^2}\frac{1}{x}\left(\frac{\partial \Delta T_s}{\partial x} + \frac{y}{x}\frac{\partial \Delta T_s}{\partial y}\right) = -\frac{k_e}{\rho C_p}\Delta T_s \qquad (2.11.14)$$

The solution of the above equation is:

$$\frac{\Delta T_s}{\Delta T_o} = \exp\left\{-\frac{k_e}{\rho C_p}\frac{I_1}{I_8}\frac{\pi}{4Q/b_o}\left[1+(\frac{y}{x})^2\right]^2(\frac{x}{b_o})\right\} \qquad (2.11.15)$$

in which ΔT_o is the excess temperature at the outlet, and:

$$I_8 = \int_0^\infty f_1(\xi) f_3(\xi) d\xi \qquad (2.11.16)$$

Experiments done by Hayashi do not agree with his theory and show a large amount of scatter. Since the author neglected inertial terms in the equations of motion, his theory is valid only for $Ri = \infty$ and thus will not apply to actual heated discharges.

2.12 Engelund's Model

The governing equations of Engelund and Pedersen's model was derived by using a control volume of unit base area and height h. The equations of volume continuity, momentum and heat conservation are written as:

$$\frac{\partial}{\partial x_i}(\alpha_3 u_i h) = \alpha(\alpha_3 u_m) \qquad (2.12.1)$$

$$\frac{\partial}{\partial x_j}(\beta_1 u_i u_j h) = -\frac{1}{\rho}\frac{\partial p_s}{\partial x_i} \qquad (2.12.2)$$

$$\frac{\partial}{\partial x_i}\left(u_i h \frac{\Delta T_s}{\Delta T_a}\right) = 0 \qquad (2.12.3)$$

where α_3 and β_1 are correction factors for velocity and momentum ($i = 1,2$). Engelund assumes these corrections to be equal for both longitudinal and lateral velocity which does not appear to be correct. The distribution of pressure p_s along any vertical is assumed to be hydrostatic. However, because the density varies vertically, this does not imply a linear, but a parabolic variation of the pressure as indicated

in Figure 2.6(b).

If h denotes the local thickness of the jet and z is the corresponding difference in level between the interface and surface of ambient water, the following hydrostatic relation is obtained:

$$(\rho_a - \frac{1}{2}\Delta\rho)h = \rho_a z \tag{2.12.4}$$

or simply:

$$h - z = \frac{1}{2}\frac{\Delta\rho}{\rho_a} h \tag{2.12.5}$$

which is the super elevation of the jet surface over the ambient water level. Thus the total difference in pressure per unit width over the vertical is:

$$\frac{1}{6} g \frac{\Delta\rho h^2}{\rho_a} \frac{(\rho_a + \rho)}{2} \tag{2.12.6}$$

corresponding to the shaded area in Figure 2.6(b). Equations 2.12.1 to 2.12.3 are then expanded as:

$$\frac{\partial}{\partial x}(uh) + \frac{\partial}{\partial y}(vh) = u_m \tag{2.12.7}$$

$$\frac{\partial}{\partial x}(u^2 h) + \frac{\partial}{\partial y}(uvh) = 0 \tag{2.12.8a}$$

$$\frac{\partial}{\partial x}(uvh) + \frac{\partial}{\partial y}(v^2 h) = -\frac{1}{6} g \frac{\partial}{\partial y}\left(\frac{\Delta T_s h^2}{T_a}\right) \tag{2.12.8b}$$

$$\frac{\partial}{\partial x}(u T_s h) + \frac{\partial}{\partial y}(v T_s h) = 0 \tag{2.12.9}$$

The pressure term in Equation 2.12.8 is approximated by considering $\rho_a + \rho = 2\rho$. Engelund, et al. neglected the pressure gradient term in the x equation of motion by explaining that for small Richardson number longitudinal momentum is dominating as compared with pressure. The model was thus recommended to be applicable only for Ri below 0.11.

The authors then non-dimensionalized these equations, assumed a similarity for velocity and temperature profile and carried out a similarity analysis to determine the variation of scale parameters for velocity, temperature, width and thickness of the jet. This is used as an input into the governing equations to reduce them to a set of ordinary differential equations which are then solved to yield a closed form solution for similarity profiles as:

$$\frac{u_s}{u_m} = \exp\left(-\frac{7}{9}\eta^2\right) \quad \text{and} \quad \frac{\Delta T_s}{\Delta T_m} = \exp\left(-\frac{14}{9}\eta^2\right)$$

This is contrary to the general belief that the width of temperature profile is greater than that of the velocity profile, and indicates that there is something erroneous in the model development.

The governing equations developed by the author become a special case of the equations developed in the present thesis from basic principles. This special case is that the vertical distribution for velocity and temperature profile must be treated as "top hat" instead of Gaussian. For small Ri this is not likely to be a true assumption. Engelund also does not consider Reynolds stresses in the momentum equation and heat diffusion terms in the heat conservation equation.

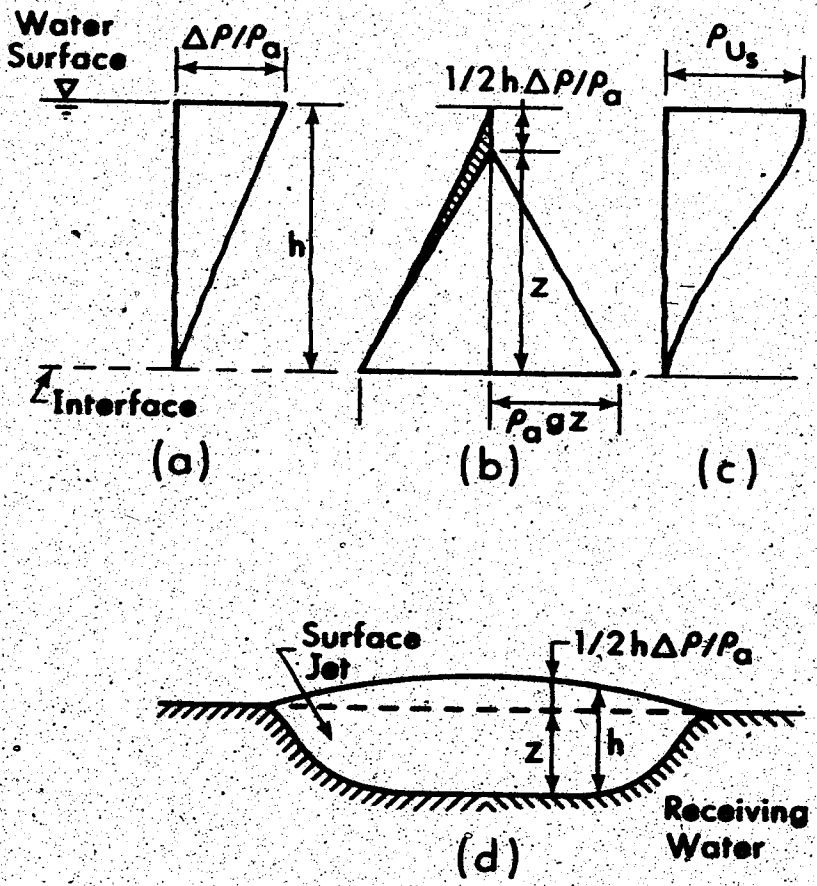

FIGURE 2.6 ENGELUND'S MODEL
(a) Distribution of Density Profile
(b) Pressure Distribution in Jet (left) and ambient (right)
(c) Distribution of Longitudinal Velocity
(d) Cross-Section of Surface Jet

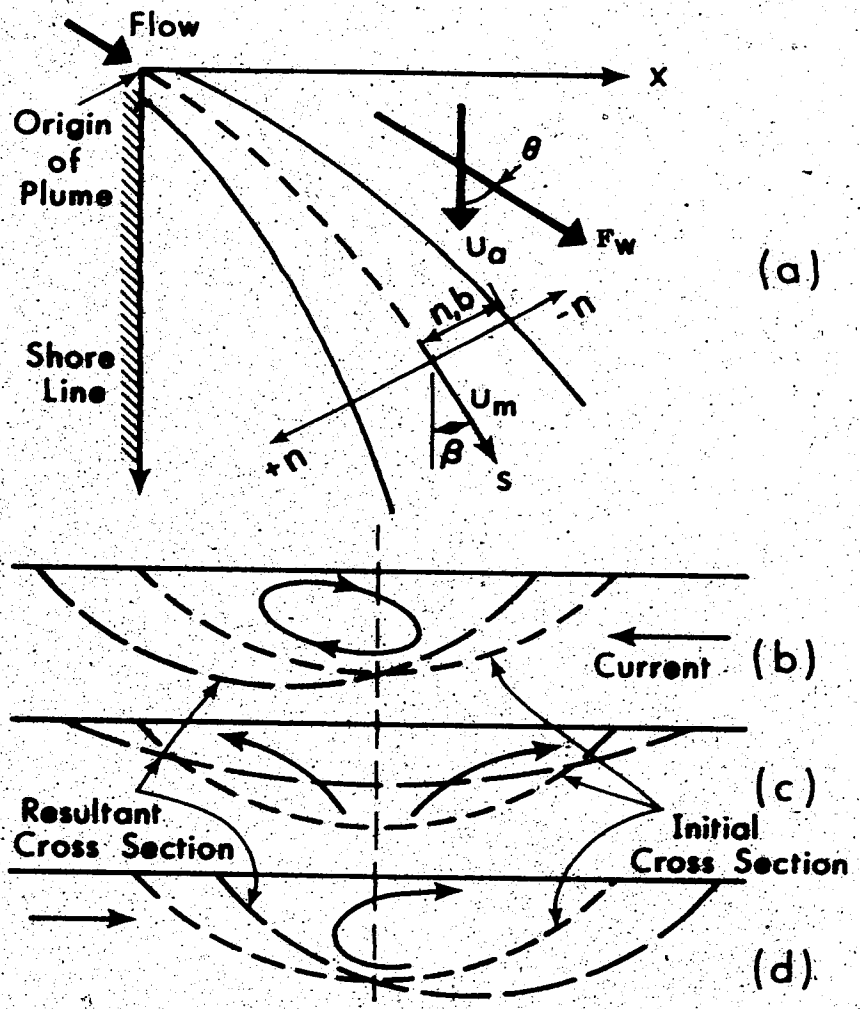

FIGURE 2.7 STEFAN AND VIDAYARAMAN'S MODEL
(a) Coordinate System
(b) Deformation of Cross-Section by Current
(c) Deformation of Cross-Section by Buoyancy
(d) Deformation of Cross-Section by Wind

For small Richardson numbers this does not seem appropriate.

2.13 Stefan and Vidayaraman's Model

Stefan and Vidayaraman (1972) developed a model for three dimensional surface jets under wind and cross flow in terms of experimentally supported empirical relationships. Similarity of velocity and temperature profiles are assumed as per Equations 2.10.1 and 2.10.3; their forms are assumed to be Gaussian. The value of λ_H and λ_v are both assumed equal to 1.05. The assumption of similarity profile and such a low value for λ_H indicate that the model results should be applicable for small values of Richardson numbers.

The values of volume, heat and momentum flux are defined as:

$$\text{volume flux} = Q(s) = \int_{-n_1/b}^{+n_1/b} \int_{o}^{m_2 h} u\,dz\,dr \qquad (2.13.1a)$$

$$\text{heat flux} = H(s) = \int_{-n_1/b}^{+n_1/b} \int_{o}^{m_2 h} \rho C_D u T\,dz\,dr \qquad (2.13.1b)$$

$$\text{momentum flux} = M(s) = \int_{-n_1/b}^{+n_1/b} \int_{o}^{m_2 h} u^2\,dz\,dr \qquad (2.13.1c)$$

The values of b and h in the present formulation are defined as standard deviations. For Gaussian distribution a value of $n_1 = m_2 = 3$ was assumed by the authors as adequate.

Mortan's entrainment principle with variable values of entrainment coefficients is utilized for further development. They define:

$$\frac{dQ(S)}{dS} = \alpha \frac{u_m (h+b)\pi}{\sqrt{2}} \qquad (2.13.2)$$

where: $$\alpha = (\alpha_h h + \alpha_v b)/(h + b) \qquad (2.13.3)$$

and α_h is the horizontal entrainment coefficient with an average value of 0.059 as in the plane jet.

Vertical entrainment coefficient decreases with an increase in Richardson number. Thus the authors assume:

$$\frac{\alpha_v}{\alpha_h} = 1.0 - 1.33 \log (6.32 \sqrt{Ri_L}) \qquad (2.13.4)$$

where: $$Ri_L = \frac{(\Delta\rho_m/\rho_a)\, g\lambda_v h}{u_m} \qquad (2.13.5)$$

Equation 2.13.4 fits experimental data of Ellison and Turner and is applicable for $0.79 < Ri < 0.025$

The rate of plume spread horizontally and vertically is broken into two parts, those represented by the suffix t are due to turbulence and those represented by B are due to buoyancy. Thus:

$$(db/dS) = (db/dS)_B + (db/dS)_t \qquad (2.13.6a)$$

$$(dh/dS) = (dh/dS)_B + (dh/dS)_t \qquad (2.13.6b)$$

Thus, according to the authors, turbulence and buoyancy act as separate

phenomena and their effects can be superimposed over each other. This does not appear to be logical as the buoyancy force suppresses turbulence due to stratification.

The horizontal spread due to turbulence is assumed equal to that of the nonbuoyant jet. Thus:

$$(db/dS)_t = \bar{C}_1 \frac{u_m}{u_m + u_a \cos \beta} \qquad (2.13.7)$$

where $\bar{C}_1 = 0.081$., This value of $\bar{C}_1$ is lower than the average value of 0.097 taken for nonbuoyant jets. Vertical and horizontal spreading ratios are proportional to the square root of vertical and horizontal entrainment coefficients. Or:

$$(dh/dS)_t = (\alpha_v/\alpha_h)^{1/2}(db/dS)_t \qquad (2.13.8)$$

The rate of lateral spread due to buoyancy is expressed on the basis of Abbott (1961) as:

$$(db/dt)_B = \bar{C}_2 \left(gh\lambda_v \frac{\Delta\rho_m}{\rho_a}\right)^{1/2} \qquad (2.13.9)$$

where the value of $\bar{C}_2$ equals 0.4 as recommended. Abbott developed Equation 2.13.9 for oil slicks. The development of this equation did not follow any theoretical reasoning; dimensional compatibility was the sole argument behind Abbott's proposed hypothesis. Moreover, the spread of an oil slick can only be compared to the spread of a plume when $Ri > 0.80$. Also:

$$(db/dS)_B \triangleq (db/dt) \frac{1}{u_{s \text{ at } b}}$$

but: $$u_{s \text{ at } b} = u_m \exp(-1/2)$$

so: $$(db/dS)_B = \frac{\bar{C}_2}{\exp(-0.5)} \sqrt{Ri_L} \qquad (2.13.10)$$

By continuity the depth of plume should decrease as the width increases, thus:

$$(dh/dS)_B = -\frac{h}{b} (db/dS)_B \qquad (2.13.11)$$

The wind shear stress is given by:

$$F_w = 2n_1 b \tau_w \qquad (2.13.12)$$

where τ_w is given by Equation 2.3.14. The rate of change of heat flux is written as:

$$-\frac{dH(S)}{dS} = k_e \int_{-n_1 b}^{n_1 b} (T_s - \bar{T}_e)\, dr \qquad (2.13.13)$$

where k_e is the surface heat loss coefficient. The form drag P exerted due to cross current is defined as:

$$P = \frac{1}{2} C_D \rho (u_a \sin\beta)^2 h \qquad (2.13.14)$$

The value of C_D is assumed to be as high as 1.0. In addition, a

friction drag force parallel to the main trajectory is also defined as:

$$D_f = C_f \rho (u_m - u_a \cos \beta)^2 (b + h) \frac{\pi}{\sqrt{2}} \qquad (2.13.15)$$

The consideration of a friction drag when a form drag due to separation has been considered does not appear to be realistic.

In summary, the momentum equations in terms of all external forces are:

$$\frac{dM(S)}{dS} = D_f + F_w \cos (\theta - \beta) + \frac{dQ(S)}{dS} \rho u_a \cos \beta \qquad (2.13.16)$$

$$\frac{dM(S)}{dn} = P - F_w \sin (\theta - \beta) + \frac{dQ(S)}{dS} \rho u_a \sin \beta - \frac{M(S)}{R_1} = 0 \qquad (2.13.17)$$

where θ, β are as given in Figure 2.7 and $d\beta = dS/R_1$. Equations 2.13.16 and 2.13.17 are solved numerically to yield the various jet trajectories of radius of curvature R_1. An examination of these equations reveals that an important force created due to density differential between jet fluid and ambient has been ignored thus limiting the model's applicability for small Richardson numbers only whereas the use of Abbott's equation suggests its applicability for large Richardson numbers. The formulation of the model is thus open to questions.

2.14 Prych's Model

The Prych model (1972) is based on three dimensional integral analysis of a turbulent heated surface jet into a large body of water

with cross flow. The similarity assumption for velocity and temperature is described by Equations 2.10.1 and 2.10.3 with $\lambda_v = \lambda_H = 1.0$. This is a weak point in formulation of the model as $\lambda_H \simeq 2.0$. Prych computes horizontal and vertical entrainment in a manner similar to Stolzenbach and Harleman.

Prych considers four force terms in x and y momentum equations:

i) Ambient momentum flux in the direction of the ambient current.

ii) Pressure due to density differential between the fluid in the jet region and the ambient fluid.

iii) A form drag due to the pressure difference between off-shore and lee side of the jet.

iv) Interfacial shear stress between jet fluid and underlying ambient fluid. Prych approximates this force by modifying an expression for the shear stress at the base of a turbulent boundary layer on a smooth flat solid surface.

The basic conservation equations are integrated over the jet cross-section using the above assumptions. The resulting system of ordinary differential equations are solved for jet trajectory, jet width and depth, centerline temperature, and velocity.

Paddock compared Prych's model with the field data and found that the Prych model gives reasonable areas for isotherm but too rapid a decay in centerline temperature and velocity and too great a lateral spread. Due to the assumption of similarity for temperature and velocity profiles as well as equal entrainment on off-shore and lee side of the jet, the model can be considered to be valid only for small

or zero ambient currents.

2.15 Stolzenbach and Harleman's Model

The development of this model starts from the basic Equations 2.2.1, 2.2.6 and 2.2.8. If no cross flow is acting on the system, there will be no horizontal pressure gradient on the jet and thus in Equation 2.2.6:

$$\frac{\partial p_o}{\partial x} \simeq \frac{\partial p_o}{\partial y} \simeq 0$$

The authors then carry out an order of magnitude analysis to retain only the dominant terms in the governing equations. The scale of the fluctuating components $\overline{u'^2}$, $\overline{v'^2}$ and $\overline{w'^2}$ are of the same order of magnitude which is an order lower than the time averaged mean velocity square u^2. Gradients of dynamic pressure in all directions are considered to be negligible. Density variation being small, the authors assume:

$$\frac{1}{\rho_a - \Delta\rho} \simeq \frac{1}{\rho_a}$$

The order of magnitude analysis with these assumptions and boundary layer type of approximations yields the following set of governing equations:

$$\frac{\partial u}{\partial x} + \frac{\partial v}{\partial y} + \frac{\partial w}{\partial z} = 0 \qquad (2.15.1)$$

$$\frac{\partial u^2}{\partial x} + \frac{\partial uv}{\partial y} + \frac{\partial uw}{\partial z} = -\frac{ag}{\rho}\int_z^{-\infty} \frac{\partial T}{\partial x}\, dz - \frac{\partial \overline{u'v'}}{\partial y} - \frac{\partial \overline{u'w'}}{\partial z} \qquad (2.15.2)$$

$$\frac{\partial uv}{\partial x} + \frac{\partial v^2}{\partial y} + \frac{\partial vw}{\partial z} = -\frac{ag}{\rho}\int_z^{-\infty} \frac{\partial T}{\partial y}\, dz \qquad (2.15.3)$$

$$\frac{\partial uT}{\partial x} + \frac{\partial vT}{\partial y} + \frac{\partial wT}{\partial z} = -\frac{\partial \overline{v'T'}}{\partial y} - \frac{\partial \overline{w'T'}}{\partial z} \qquad (2.15.4)$$

The first terms on the right in Equation 2.15.2 and in Equation 2.15.3 represent the effect of buoyancy in the flow equations and the coupling between hydrodynamic and buoyant forces.

The governing Equations 2.15.2 to 2.15.4 cannot be solved without further manipulation since the turbulence transfer terms are not determined. The technique used to develop the solution is to assume the similarity function for velocity and temperature within the jet, and boundary conditions at the outer edges, leaving as unknown only certain values such as centerline velocity and temperature. The governing equations may then be integrated over a cross-section perpendicular to the discharge centerline. This procedure eliminates the unknown turbulence terms and yields a set of first order differential equations which may be solved for the variables describing the discharge behaviour. The assumed structure is shown in Figure 2.8.

The form of similarity functions assumed by the authors were suggested by Abramovich (1963) and are:

$$f_1(\xi) = f_1(\eta) = (1 - \eta^{3/2})^2 \qquad (2.15.5)$$

and: $$f_3(\xi) = f_3(\eta) = (1 - \eta^{3/2}) \qquad (2.15.6)$$

The authors do not appear to be correct in formulating Equation 2.15.3 which expresses a balance between the lateral density gradient and lateral convective motions. In fact, the order of magnitude analysis carried out by the authors yields:

$$\frac{\partial uv}{\partial x} + \frac{\partial v^2}{\partial y} + \frac{\partial vw}{\partial z} =$$

$$\frac{ag}{\rho_a} \int_z^{-\infty} \frac{\partial \Delta T}{\partial y}\, dz - \frac{1}{\rho} \frac{\partial p_d}{\partial y} - \frac{\partial \overline{v'^2}}{\partial y} - \frac{\partial \overline{v'w'}}{\partial z} \qquad (2.15.7)$$

For a nonbuoyant jet the corresponding equation is written as:

$$0 = -\frac{1}{\rho_a} \frac{\partial p_d}{\partial y} - \frac{\partial \overline{v'^2}}{\partial y} - \frac{\partial \overline{v'w'}}{\partial z} \qquad (2.15.8)$$

Equation 2.15.3 is thus written as the difference between Equations 2.15.7 and 2.15.8. But this does not appear to be a correct procedure as is explained below.

The right hand side of Equation 2.15.8 has the same order of magnitude as convective terms in Equation 2.15.2, and the left hand side of Equation 2.15.8 was an order of magnitude lower and as such were dropped. When buoyancy becomes important all terms in Equation 2.15.7 become of the same order of magnitude and thus Equation 2.15.8 becomes invalid. In a later publication by the authors (user's manual report No. 156), Equation 2.15.3 is explained on the basis that for buoyant jets the balance between dynamic preasure and Reynold's

stresses is of the second order and so is neglected. The authors' argument here seems to have no apriori basis unless it is assumed that increase in buoyancy leads to a reduction in turbulence fluctuations. The turbulence terms thus attain a small order of magnitude. But then the turbulence terms in x equation of motion also become of a smaller order of magnitude as compared to convective terms. This is to be discussed in detail in Chapter 3, where the governing equations have been classified under separate ranges of Richardson numbers.

The lateral spreading velocity is assumed by these authors to be:

$$V = \left(\frac{db}{dx} - \alpha\right) u \sqrt{\eta_*} \quad \text{for} \quad S < |y| < S + b \qquad (2.15.9a)$$

where; $\frac{db}{dx}$ = growth rate of buoyant jet

$$\eta_* = \frac{|y| - s}{b} \qquad (2.15.9b)$$

The assumption of lateral spreading velocity is based more on intuition than on physical data but it does not work as Paddock, et al. (1973) found the predicted lateral spread for field data greatly exceeding the observed spread.

With the help of Equations 2.10.1, 2.10.3, 2.15.5, 2.15.6 and 2.15.9 the governing equations are integrated over four assumed rectangular shaped regions of the jet cross-sections as shown in Figure 2.8. These regions are an unsheared core region (No. 1), a vertically sheared region (No. 2), a horizontally sheared region (No. 3), and a region

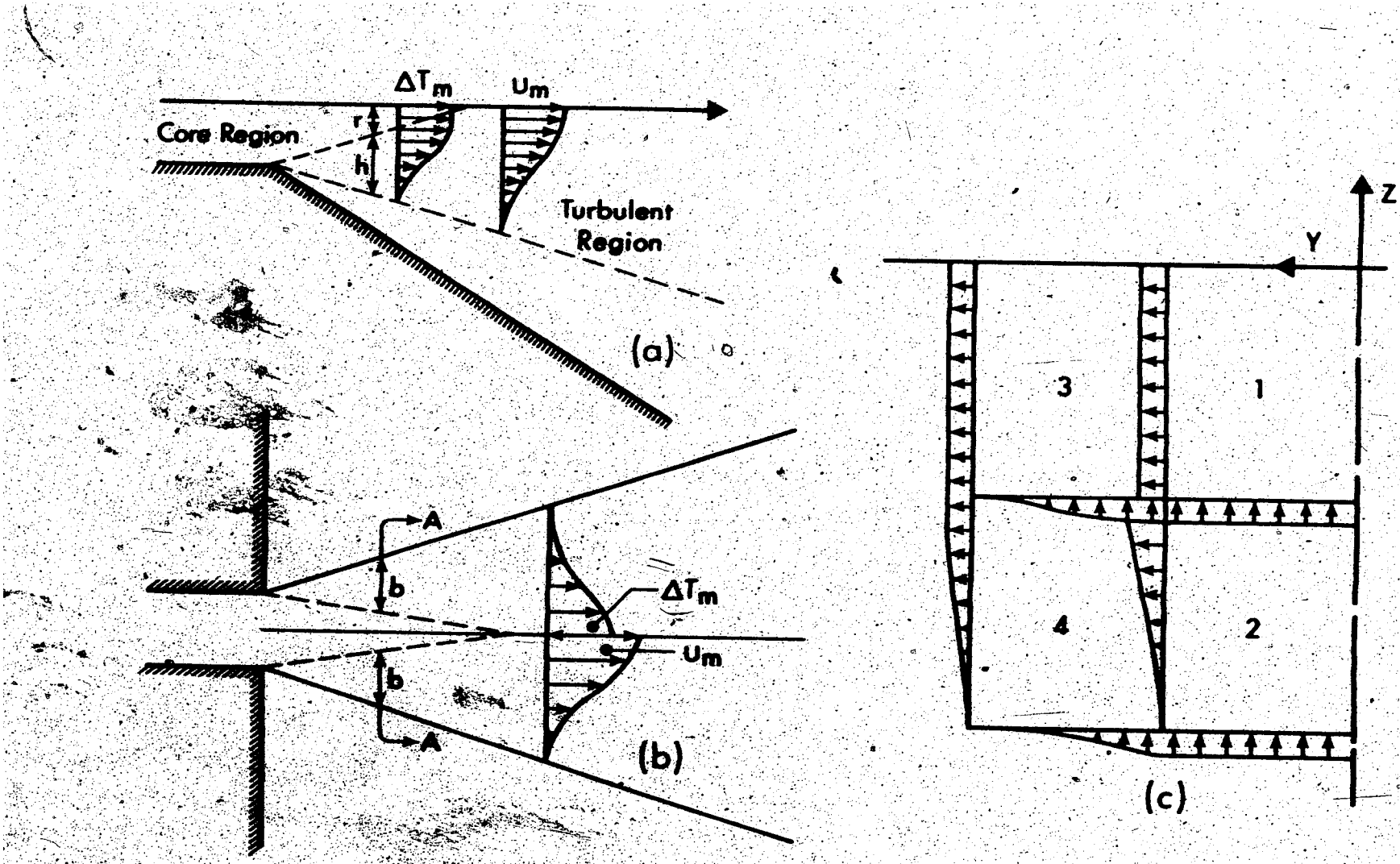

FIGURE 2.8 DIAGRAM FOR STOLZENBACH AND HARLEMAN'S MODEL
(a) Sectional View
(b) Plan View
(c) Four Zones along the Cross-Section on Section AA

sheared in both directions (No. 4). The core regions eventually disappear due to the advancing turbulent region and a single region, No. 4, exists. In reality, a jet is more trough shaped than rectangular, and each of the above shearing characteristics may be found intermixed in all four regions represented. The integration of continuity and the x momentum equations is carried over all of the four regions yielding eight equations. The y momentum equation is integrated over the entire half cross-section to yield the ninth equation. In this manner, the coupled flow and heat conservation equations reduce to a system of ordinary differential equations which are then solved numerically. The solution of model equations yields three dimensional temperature and velocity predictions as well as physical characteristics of the jet.

The division of the jet cross-section into four rectangular regions is a hypothesis that does not seem quite appropriate. The interregional velocities at the boundaries of each region have to be specified. Their forms are unknown and must be guessed. The models also permit no turbulence momentum transfer between regions of jet or between jet and ambient water. This is tantamount to dropping the Reynolds stress terms in the equation of motion or equivalently dropping turbulence diffusion mechanism.

2.15.1 Stolzenbach and Harleman's Model of Buoyant Jets in Cross Flow

For a small cross flow, the radius of curvature changes very slowly and the governing Equations 2.15.1, 2.15.2 and 2.15.4 remain the same. The y momentum Equation 2.15.3 gets modified and a term,

$u^2(\partial\beta/\partial x)$, is added to its right hand side. The value of similarity has now been chosen by the help of Equation 2.10.1 but with an approximation:

$$\frac{u - u_a \cos\beta}{u_m - u_a \cos\beta} \simeq \frac{u - u_a \cos\beta}{u_m} = f_1(\xi) f_1(\eta) \qquad (2.15.10)$$

The form of similarity functions is assumed to remain the same. There are some minor changes in the boundary conditions. But the procedure followed in integration and formulation of differential equations is exactly the same as that of buoyant jets with no cross flow.

Stolzenbach and Harleman do not use the drag force in their momentum equation. They include the appropriate buoyant force term in the x and z direction but neglect interfacial shear stress if one exists. Besides the above comments mostly associated with analytical modelling, there are practical difficulties in actually obtaining a numerical solution to the set of ordinary differential equations. Due to the complexity of the set, derivatives must be found by solving a linear set of algebraic equations before applying the Runge-Kutta scheme (Paddock, et al. 1973). For many cases the matrix which must be reduced is nearly singular and much precision is lost in solving for the derivatives.

2.16 Phenomenological Model

Elliot and Harkness (1972) presented a phenomenological model for the prediction of size, shape and orientation of thermal plumes produced by surface discharges. The model is based on statistical analy-

sis of an extensive set of measurements made near Lake View outfall on Lake Ontario, with source Richardson numbers varying from 0.25 to 0.027. The authors set out three objectives in the construction of the model.

2.16.1 Determination of a Relation Between Temperature and Area

Least squares analysis was used to determine a functional relationship between temperature, T , and area, A , (sq.ft.) of an isotherm of the form.

$$\frac{\Delta T}{\Delta T_o} = C_1 \left(\frac{A}{Q\Delta T_o}\right)^{C_2} \qquad (2.16.1)$$

where Q is the cooling water discharge (ft^3/s). The term $Q\Delta T_o$ is proportional to the total heat outflow and is included to make these expressions valid for arbitrary values. However, the area enclosed by an isotherm should also depend upon the initial momentum, aspect ratio and source Richardson number. Thus the choice of $Q\Delta T_o$ alone to correlate the data does not seem to be adequate. The available data have been classified under three groups; winter, spring and fall, and summer. The values of C_1 and C_2 for these three conditions are given in Table 2.1. Asbury and Frigo (1971) present a similar phenomenological relationship and the values of C_1 and C_2 from their data are also given in Table 2.1. The variation in the values of C_1 and C_2 found in the two sets of data are quite large to permit any generalization. However, a trend is apparent that the value of C_2 decreases as the value of the temperature or Richardson number increases.

Table 2.1 Values of C_1 and C_2

Season	Temp. Range	C_1	C_2
Winter	< 38°F	0.307	0.712
Spring and Fall	38°F - 62°F	0.354	0.478
Summer	> 62°F	0.336	0.364
Asbury and Frigo		0.456	0.297

2.16.2 Determination of Mean Width of an Isotherm

Elliot and Harkness report that the measured isotherm exhibit a perplexing irregularity in shape that would seem to defy any systematization attempts. Measurements taken under nominally identical conditions produce radically different shapes. The plumes do, however, occupy a certain region of lake surface near the outfall and they are elongated in the direction of the flow away from the outfall. It was therefore postulated that a shape factor and not the shape was contained in the data. The authors thus defined a mean width as:

$$W = A/\bar{x}_2 = C_3 \left[\frac{A}{(1 + 1/\sqrt{Ri})^{1/2}}\right]^{C_4} \qquad (2.16.2)$$

where $\bar{x}_2$ is the length of the isotherm along the axis and $C_3 = 0.717$ and $C_4 = 0.552$.

A lemniscate has been chosen to represent the isotherm with its polar coordinates as:

$$r = \bar{x}_2 \cos\left(\frac{A}{4W^2}\theta\right) \qquad (2.16.3)$$

The length $\bar{x}_2$ here is the axis length of the lemniscate. Thus if ΔT and Ri are known, the lemniscate representing the isotherm is completely specified.

2.16.3 Determination of an Expression for Plume Centerline

Elliot and Harkness chose an analytical rather than a statistical method to determine the trajectory of the jet as the locus of the trajectory depends upon many factors such as the shape of the outlet structure, the outfall velocity, the source Richardson number, the wind speed and direction, the lake current, and the lake bottom topography. However, the authors do not clarify as to why the effect of these parameters should not be considered on the area and mean width of the plume. Although various effects are mentioned, these are not considered any where in formulating centerline trajectory.

The authors use essentially the method of Platten and Keffer (1968) to derive the jet trajectory. To simplify the problems they use a similarity assumption $f_1(\eta) = \bar{e}^{\eta^2/2}$, thus limiting the analysis only to very small cross flow velocities. The derivation of the trajectory path (Figure 2.7) is formularised as follows:

i) Momentum of the jet perpendicular to ambient current is preserved, so that:

$$d/dS\ (bu^2 \sin\beta) = 0 \qquad (2.16.4)$$

The component of drag force due to lake current, wind shear buoyant force, etc., on the right side has been ignored.

ii) Momentum of the jet in the direction the ambient current is increased by the momentum of the entrained fluid. Thus:

$$\frac{d}{dS}\left(b_u^2 \cos\beta\right) = \frac{2u_a v_e}{\bar{I}_2} \qquad (2.16.5)$$

where:

$$\bar{I}_2 = \int_{-1}^{+1} e^{-2(n/b)^2} d(n/b) = \sqrt{\pi/2}$$

In this equation also, various forces as mentioned previously have been neglected.

iii) Increase in the mass flux of the jet is due to the entrainment of the free stream fluid:

$$\frac{d}{dS}\left(b_u\right) = \frac{2v_e}{\bar{I}_1} \qquad (2.16.6)$$

where:

$$\bar{I}_1 = \int_{-1}^{+1} e^{-(n/b)^2} d(n/b) = \sqrt{\pi}$$

Solving the Equations 2.16.4, 2.16.5 and 2.16.6, we get:

$$\frac{d\beta}{dS} = \frac{2v_e u_a}{I_2 b_o u_o^2 \sin\beta_o} \sin^2\beta \qquad (2.16.7)$$

where v_e is given by Equation 2.2.9b, i.e.:

$$v_e = \alpha_1(u_m - u_a \sin\beta) + \alpha_2 u_a(\sin\beta - \sin\beta_o) \qquad (2.2.9b)$$

Equations 2.2.9b and 2.16.7 have to be numerically solved to get the trajectory of the jet. Elliot and Harkness find a value of

α_1 and α_2 by fitting the field data to the trajectory. The values of α_1 and α_2 so obtained are, respectively, 0.14 and 0.60. The corresponding values recommended for nonbuoyant jets by Platten and Keffer are 0.06 and 0.30. This indicates that entrainment velocity for buoyant jets is roughly two times greater than those of nonbuoyant jets.

2.16.4 Other Phenomenological Models

There are other phenomenological models developed similar to those of Elliot and Harkness. Results of the model of Ashbury and Frigo (1971) have already been discussed in Section 2.16.1. Palmer (1972) also used data from the Lake View site but proposed an equation of the form:

$$\ln \left(\frac{Q}{A}\right) = C_1 + C_2 \ln (\Delta T) \qquad (2.16.8)$$

However, the scatter of the data about his prediction equations were very large.

Kenny (1973) proposed a model in which the area contained within 1°C excess temperature isotherm, A_1, was related to the source strength S of the power plant. The source strength is the amount of heat discharged into the lake per unit time expressed as BTU/sec. Data from a number of surveys at various generating stations were correlated and the following equation was obtained:

$$A_1 = 111.13\ S^{0.8117}$$

The equations listed above, all fitted the data because they were derived

from regression analysis which enabled the exponents and constants to be varied until a fit was obtained.

However, it appears that these equations cannot be applicable when extrapolating to a different range of variables. Furthermore, the equations are not dimensionally correct and the proportionality constants and empirical exponents include the effects of parameters not considered in the analysis.

2.17 Review of Laboratory Experiments Done on Surface Jets

Jen, Wiegel and Mobarek (1966) carried out an extensive set of experiments with the heated jet discharged from a pipe with densimetric Froude number varying from 18 to 180. Only temperature measurements were carried out using a rake of copper-constantan thermocouples. A similarity of temperature profile in the lateral direction was established. Temperatures at different locations along the centerline were measured for different values of densimetric Froude numbers. Unfortunately, there is no set available which describes temperature measurements along the whole length of centerline for one particular value of densimetric Froude number. However, the authors plotted their data to show that centerline temperature decay shows no trend of variation with change in densimetric Froude number and the best fit line lies close to those of Albertson, et al. (1950) with an equation of:

$$\frac{\Delta T_m}{\Delta T_o} = 7.0 \frac{D_o}{x}$$

The distribution of the temperature concentration at the surface on an average can be expressed as:

$$\frac{\Delta T_s}{\Delta T_m} = \exp\ (-\ 0.9747\ \eta^2) \qquad (2.17.1)$$

although considerable variation must be expected from the mean values predicted by the use of the formula, particularly for $x/D_o > 100$.

The mixing has been found to be less in depth by a factor of about 2. The slope of the bottom of the mixing jet beneath the axis of the jet is between 1/8 and 1/5.5. The value of half width, b , was found to be given by:

$$b = 0.57 \cdot x \cdot Ri^{1/8} \qquad (2.17.2)$$

Wood, et al, (1967) reported measurements of total width of the jet and found an expression:

$$\bar{b} = 1.25 \cdot x \cdot Ri^{1/8} - 4.0$$

for: $1/36000 < Ri < 1/100$ (2.17.3)

Tamai, et al. (1969) extended Jen, et al.'s work for a range of Ri from 0.0078 to 0.147. They found considerable temperature fluctuations along the centerline of the jet. The fluctuations generally varied between 10% to 30% of mean temperature. Their experiments were carried out in a narrow flume with considerable side wall effects. The authors could not draw any conclusive results from their experiments.

Hayashi and Shuto (1967) carried out experiments for Richardson numbers 0.54, 0.41, 0.27, 0.147 and 0, and plotted temperature variations along centerline. They show the temperature profiles to be similar along the vertical section for two sets. The depth chosen for non-dimensionalizing the vertical depths for these sets is the value of h where the temperature is 5% of the maximum temperature in the same vertical section; usually this value chosen is the jet half depth where temperature becomes 50% of the surface temperature. There is also a very large scatter in the data. This prevents any quantitative deductions to be drawn from Hayashi's data.

A series of papers were written by Stefan. Most of these papers (June 1970, July 1970 and January 1972) pertain to two dimensional surface discharges[1]. The author also carried out an experimental investigation for a three dimensional discharge into a wide and deep impoundment. Centerline temperature decay was measured for Ri = 0.104 and 0.059 which, according to the author, follow an exponential decay of e^{-cx^2}. Isotherms along few vertical cross sections have been drawn for a very high value of Richardson number such as 2.6. The velocity measurement was done by a tethered sphere[2]. These also have been presented for a few vertical sections for Ri = 2.6. The data presented by the author are again so meager as to prevent any quantitative deductions to be made.

---

[1] Flow was carried out in a 0.6" wide flume inhibiting lateral spread.

[2] An instrument which statically balances the drag and buoyancy forces of a 1/16" diameter to 1/8" diameter plastic sphere against the tension in a 0.002" rayon tethering line.

Stolzenhach and Harleman have done some temperature measurements primarily to verify their theory. The authors assume similarity profiles for temperature but did not establish it experimentally. In most of the experiments only centerline temperature, half width and depth were presented. Table 2.2 summarises the experimental investigation done by various workers. This short experimental review shows that experimental data for Richardson number higher than 0.10 are lacking. None of the research workers have made any detailed measurements for velocity distribution and similarity for velocity profiles.

2.17.1 Review of Field Work Done on Surface Jets

Most of the experiments done in the field and data collected therefrom pertain to the far field region, and as such are not relevant to the present study. Some of it which appear to be close to our study are described below.

Paddock, et al. (1973) made simultaneous temperature and velocity measurements in the near field region of the surface thermal discharges at Point Beach Unit 1, and Palisades Nuclear Power Plants on Lake Michigan. Data collected include measurements of temperature and velocity at 0.5m to 3.0m depth along with measurements of ambient lake and meteorological conditions. Bottom depth was also measured at various locations.

The significant results derived from the jet characteristics determined after smoothening the data were given by the following expressions:

TABLE 2.2 SUMMARY OF PREVIOUS LABORATORY WORK

Investigators	Reynolds Number	Receiving Basin	Range of Richardson Numbers Covered	Measurement of		Measurement of Similarity				Lateral and Entrainment Velocity	Remarks
						Temperature		Velocity			
				Temperature	Velocity	Lateral	Vertical	Lateral	Vertical		
Jen & Wiegel	8300-21000	26'×15'×1.5' Jet dia 0.0164' to 0.0361 ft	3.08×10^{-3} to 3.08×10^{-5}	Yes	No	Yes	No	No	No	No	Thermo couples scanned each cross-section, then moved.
Tamai	7100-21300	25'×3.5'×2.0'	0.173 to 7.83×10^{-3}	Yes	No	No	No	No	No	No	Fixed thermistors scanned.
Hayashi	3000-5600	36'×17'×1.5'	0.51 to 3.8×10^{-3}	Yes	No	No	Yes	No	No	No	Fixed thermocouples scanned. Data have too much scatter.
Stefan	1590-9500	40'×0.5'×1.25' and 40'×17'×1.6'	2.6 to 7.18×10^{-2}	Yes	Yes	No	No	No	No	No	1 thermistor temp. probe to measure anywhere. Tethered sphere for velocity.
Motz and Benedict	43[illegible]-5400	60'×2.0'×1.0'	1.18 to 3.8×10^{-2}	Yes	No	No	No	No	No	No	Single Cole Parmer #8432-1 Probe, 11 probes spread laterally across. Limited data gathered to work out some coeff for his model.
Stolzenbach and Harleman	9000-15000	46'×28'×15'	1 to 1.88×10^{-6}	Yes	No	No	No	No	No	No	67 fixed thermistor probes connected to a digitec scanning and printing system.
Present Experiment	7500-8000	50'×15'×1.5'	0.15 to 1.14	Yes	Yes	Yes	Yes	Yes	Yes	Yes	14 thermistor probes scanned laterally and vertically. Velocity by hydrogen bubble technique.

$$\frac{u_s}{u_m} = \left(\frac{1}{2}\right)^{(y/b_u)^2} \qquad (2.17.4)$$

$$\frac{\Delta T_s}{\Delta T_m} = \left(\frac{1}{2}\right)^{(y/b_T)^2} \qquad (2.17.5)$$

$$\frac{\Delta T_{b_s}}{\Delta T_m} \triangleq \frac{u_s}{u_m} \approx \sqrt{\frac{4.2\ b_o}{x}} \qquad (2.17.6)$$

Field experiments conducted by Elliot and Harkness (1972), Palmer (1972), and Kenny (1973) were mainly concerned with temperature surveys of thermal plumes. It is not clear whether their data pertain to the far field, but Elliot and Harkness's treatment of the jet trajectory, discussed in Section 2.16.3, indicates that the field data should belong to jet regime. The data obtained by all of these investigators were correlated in terms of the area enclosed by an isotherm to the total heat outflow from the outlet and the temperature excess causing the isotherm. These equations have been presented in Section 2.16.4.

Barr (1958-1968) made several studies on lock exchange flow and thermal wedge formations. For flow situations where densimetric Froude number and Reynolds number are both important, he suggests a new non-dimensional term known as densimetric Froude-Reynolds number ($F_D R_e$) and defined as:

$$F_D R_e = [(\Delta\rho_o/\rho_a)^{1/2} g^{1/2} h_o^{3/2}] / \nu \qquad (2.17.7)$$

This number is recommended to be greater than 1000 in order to simulate

turbulent flows.

Barr's other significant contribution is the preparation of a congruency diagram for the travel of an overflow front such as the spread of heated water from a power plant outfall, or an underflow front from a lock exchange. This diagram represents the relationship:

$$\frac{T_i \ (L/h_o)}{\sqrt{\frac{h_o}{(\Delta\rho/\rho)g}}} = \phi \ (F_D R, \ L/h_o) \qquad (2.17.8)$$

where $T_i \ (L/h_o)$ = elapsed time after lifting the barrier for front travel, and L/h_o = relative travel.

2.18 Objective of Present Study

The objective of the present study can be divided into two parts. The first part deals with the objectives of theoretical investigation and the second part with the objectives of experimental investigation.

2.18.1 Objective of Theoretical Investigation

A review of the existing literature shows that a major part of the literature is devoted to two dimensional surface jet discharges. The work on three dimensional surface discharge is rather scanty. The structure of three dimensional flow shows strong dependence on Richardson number. For low Richardson number, the buoyant surface jet behaves as an ordinary jet with temperature in the water acting like a tracer. For very high Richardson number, the vertical entrainment

stops and the jet becomes two dimensional. For the intermediate range, to be classified as moderate Richardson number, the flow has yet another character. The existing work on three dimensional jets does not study the flow problem in any systematic manner. A study, starting from Reynold's equation of motion for momentum and heat is thus needed which can yield a set of governing equations for the three ranges of Richardson number. This needs a different approach (other than that of Morton) for looking at lateral entrainment velocity linking its evaluation with changed governing conditions for the three ranges of Richardson number. A similarity analysis of these equations of motion, combined with experimental verification of similarity, can yield parameters needed for an almost complete solution of the problem.

Some of the phenomenological models have proposed functional relationships between temperature, ΔT , and area, A , of an isotherm. This seems to be quite a practical approach for field problems. None of the existing analytical models attempt to do it. The equation of isotherms is therefore proposed to be worked out along with areas contained in each isotherm for the three ranges of Richardson number as a part of this investigation.

2.18.2 Objectives of Experimental Investigation

A discussion of unresolved near field issues has been given by Policastro (1972). Based on this and the previous summary the areas which need investigation and verification are:

1) To establish similarity of velocity distribution in lateral and vertical directions. This has been assumed in the models

but never proved experimentally, especially for higher ranges of Richardson number.

ii) To determine the form of similarity profiles; as to whether it is Gaussian.

iii) To determine the variation of centerline velocity decay for higher ranges of Richardson number.

iv) To determine the value of lateral entrainment coefficient and to find out as to whether it depends upon buoyant or nonbuoyant factors.

v) To determine the similarity of temperature profiles and their form for "excess temperature distribution" both in the lateral and vertical directions. Some evidence exists for the similarity of temperature profiles for the lower ranges of Richardson number, but no information is available for higher ranges of Richardson number.

vi) To determine the centerline temperature decay for higher ranges of Richardson number.

Vii) To ascertain whether velocity and temperature distribution profiles are equal in the lateral and vertical directions. Most of the models have assumed that velocity and temperature profiles are equal. However, experiments on two dimensional air jets indicates that a half-width of the jet for heat is considerably greater than half-width of the jet for velocity. This value for buoyant surface jets should be determined.

CHAPTER 3

THEORETICAL ANALYSIS

3.1 Development of Governing Equations

3.1.1 Reynolds Equation

For turbulent heated surface discharges in which the primary flow is steady, the tensor Equations 2.2.6 and 2.2.1 can be reduced to the following equations in cartesian coordinates:

$$u\frac{\partial u}{\partial x} + v\frac{\partial u}{\partial y} + w\frac{\partial u}{\partial y} =$$

$$-\frac{ag}{\rho}\frac{\partial}{\partial x}\int_0^z \Delta T dz - \left(\frac{\partial \overline{u'^2}}{\partial x} + \frac{\partial \overline{u'v'}}{\partial y} + \frac{\partial \overline{u'w'}}{\partial z}\right) - \frac{1}{\rho}\frac{\partial p_d}{\partial x} \qquad (3.1.1)$$

$$u\frac{\partial v}{\partial x} + v\frac{\partial v}{\partial y} + w\frac{\partial v}{\partial z} =$$

$$-\frac{ag}{\rho}\frac{\partial}{\partial y}\int_0^z \Delta T dz - \left(\frac{\partial \overline{u'v'}}{\partial x} + \frac{\partial \overline{v'^2}}{\partial y} + \frac{\partial \overline{v'w'}}{\partial z}\right) - \frac{1}{\rho}\frac{\partial p_d}{\partial y} \qquad (3.1.2)$$

$$u\frac{\partial w}{\partial x} + v\frac{\partial w}{\partial y} + w\frac{\partial w}{\partial z} =$$

$$-\left(\frac{\partial \overline{u'w'}}{\partial x} + \frac{\partial \overline{u'w'}}{\partial y} + \frac{\partial \overline{w'^2}}{\partial z}\right) - \frac{1}{\rho}\frac{\partial p_d}{\partial z} \qquad (3.1.3)$$

and:
$$\frac{\partial u}{\partial x} + \frac{\partial v}{\partial y} + \frac{\partial w}{\partial z} = 0 \qquad (3.1.4)$$

The heat transport Equation 2.2.8 is simply written as:

$$\frac{\partial(u\Delta T)}{\partial x} + \frac{\partial(v\Delta T)}{\partial y} + \frac{\partial(w\Delta T)}{\partial z} =$$

$$- \left(\frac{\partial \overline{u'\Delta T'}}{\partial x} + \frac{\partial \overline{v'\Delta T'}}{\partial y} + \frac{\partial(\overline{w'\Delta T'})}{\partial z} \right) \qquad (3.1.5)$$

3.1.2 Continuity Equations

In this and the next few sections, simplified forms of the continuity equation, the three Reynolds equations and the heat transport equation using the order of magnitude analysis are developed. In this process, relevant boundary layer approximations have been made.

In a surface jet, in general, $v \sim w$ and, $u >> v$ and $u >> w$. Further, it is reasonable to assume that:

$$\frac{\partial v}{\partial y} \sim \frac{\partial w}{\partial z} \qquad (3.1.6)$$

Then, from the continuity equation, it follows that:

$$\frac{\partial u}{\partial x} \sim \frac{\partial v}{\partial y} \quad \text{and} \quad \frac{\partial u}{\partial x} \sim \frac{\partial w}{\partial z} \qquad (3.1.7)$$

One can now introduce three characteristic velocities U_x, U_y and U_z and three characteristic lengths L_x, L_y and L_z for the x, y and z directions respectively. Since the flow in a surface jet (generally) occupies a slender region in the y and z directions, $L_y/L_x << 1$ and $L_z/L_x << 1$. We select a quantity δ such that:

$$\frac{L_y}{L_x} \sim \delta \quad \text{and} \quad \frac{L_z}{L_x} \sim \delta \qquad (3.1.8)$$

From the continuity equation:

$$\frac{U_x}{L_x} \sim \frac{U_y}{L_y} \sim \frac{U_z}{L_z} \tag{3.1.9}$$

Hence one could write:

$$\frac{U_y}{U_x} \sim \frac{L_y}{L_x} \sim \delta \tag{3.1.10}$$

$$\frac{U_z}{U_x} \sim \frac{L_z}{L_x} \sim \delta \tag{3.1.11}$$

3.1.3 Simplification of Reynold's Equations

Considering firstly the Reynolds equation in the x direction, one has:

$$u\frac{\partial u}{\partial x} + v\frac{\partial u}{\partial y} + w\frac{\partial u}{\partial z} =$$

$$\downarrow \qquad \downarrow \qquad \downarrow$$

$$\left(\frac{U_x^2}{L_x}\right);\left(\frac{U_x^2}{L_x}\right);\left(\frac{U_x^2}{L_x}\right)$$

$$-\frac{ag}{\rho}\frac{\partial}{\partial x}\int_o^z \Delta T dz - \frac{1}{\rho}\frac{\partial p_d}{\partial x} - \frac{\partial \overline{u'^2}}{\partial x} - \frac{\partial \overline{u'w'}}{\partial y} - \frac{\partial \overline{u'w'}}{\partial z} \tag{3.1.12}$$

$$\downarrow \qquad \downarrow \qquad \downarrow \qquad \downarrow \qquad \downarrow$$

$$\left(\frac{ag}{\rho}\frac{\Delta T_x}{L_x}z\right) \; ; \; \left(\frac{1}{\rho}\frac{\Delta p_d}{L_x}\right);\left(\frac{U_t^2}{L_x}\right);\left(\frac{U_t^2}{L_y}\right);\left(\frac{U_t^2}{L_z}\right)$$

with the magnitude of each term in terms of the scales written directly under it, where U_t is the scale for turbulent velocity fluctuations.

Further, ΔT_x and Δp_d are, respectively, the scales for the temperature change and dynamic pressure. Multiplying right through by (L_x/U_x^2), the magnitude of the terms in Equation 3.1.12 become, in their respective order:

$$1 \; ; \; 1 \; ; \; 1 \; ; \; \frac{g\frac{\Delta\rho}{\rho}z}{U_x^2} \; ; \; \frac{\Delta p_d}{\rho U_x^2} \; ; \; \frac{U_t^2}{U_x^2} \; ; \; \frac{U_t^2}{U_x^2}\frac{L_x}{L_y} \; ; \; \frac{U_t^2}{U_x^2}\frac{1}{\delta}$$

Considering flows in which the buoyancy forces are negligible and inertial terms are balanced by the turbulence terms in the x direction equation of motion:

$$\left(\frac{U_t}{U_x}\right)^2 \sim \delta \quad \text{or} \quad \frac{U_t}{U_x} \sim \sqrt{\delta} \quad \text{and} \quad \frac{g(\frac{\Delta\rho}{\rho})z}{U_x^2} \sim \delta \quad \text{or} \quad \delta^2 \qquad (3.1.13)$$

Considering the equation of motion in the y direction, one could write (following the procedure used for the x direction equation):

$$u\frac{\partial v}{\partial x} + v\frac{\partial v}{\partial y} + w\frac{\partial v}{\partial z} =$$

$$\downarrow \qquad \searrow \qquad \searrow$$

$$\left(\frac{U_x^2}{L_x}\frac{L_y}{L_x}\right); \left(\frac{U_x^2}{L_x}\frac{L_y}{L_x}\right); \left(\frac{U_x^2}{L_x}\frac{L_y}{L_x}\right)$$

$$\downarrow \qquad \downarrow \qquad \downarrow$$

$$\frac{L_y}{L_x} \; ; \; \frac{L_y}{L_x} \; ; \; \frac{L_y}{L_x}$$

$$-\frac{ag}{\rho}\frac{\partial}{\partial y}\int_0^z \Delta T dz - \frac{1}{\rho}\frac{\partial p_d}{\partial y} - \frac{\partial \overline{u'v'}}{\partial x} - \frac{\partial \overline{v'^2}}{\partial y} - \frac{\partial (\overline{v'w'})}{\partial z} \qquad (3.1.14)$$

$$\downarrow \quad \downarrow \quad \downarrow \quad \downarrow \quad \downarrow$$

$$\left(\frac{g\left(\frac{\Delta\rho}{\rho}\right)z}{L_y}\right);\left(\frac{\Delta p_d}{\rho L_y}\right);\left(\frac{U_t^2}{L_x}\right);\left(\frac{U_t^2}{L_y}\right);\left(\frac{U_t^2}{L_z}\right)$$

$$\downarrow \quad \downarrow \quad \downarrow \quad \downarrow \quad \downarrow$$

$$\frac{g\left(\frac{\Delta\rho}{\rho}\right)z}{U_x^2}\frac{L_x}{L_y};\ \frac{\Delta p_d}{\rho U_x^2}\frac{L_x}{L_y};\ \frac{U_t^2}{U_x^2};\ \frac{U_t^2}{U_x^2}\frac{L_x}{L_y};\ \frac{U_t^2}{U_x^2}\frac{L_x}{L_z}$$

Assuming $\dfrac{g\frac{\Delta\rho}{\rho}z}{U_x^2} \sim \delta^2$ at the most, then:

$$\frac{\Delta p_d}{\rho U_x^2} \sim \delta \qquad (3.1.15)$$

Following a similar procedure, one could write, for the equation of motion in the z direction:

$$u\frac{\partial w}{\partial x} + v\frac{\partial w}{\partial y} + w\frac{\partial w}{\partial z} = -\frac{1}{\rho}\frac{\partial p_d}{\partial z} - \frac{\partial \overline{u'w'}}{\partial x} - \frac{\partial \overline{v'w'}}{\partial y} - \frac{\partial \overline{w'^2}}{\partial z} \qquad (3.1.16)$$

$$\downarrow \quad \downarrow \quad \downarrow \quad \downarrow \quad \downarrow \quad \downarrow \quad \downarrow$$

$$\left(\frac{U_x^2}{L_x}\frac{L_z}{L_x}\right);\left(\frac{U_x^2}{L_x}\frac{L_z}{L_x}\right);\left(\frac{U_x^2}{L_x}\frac{L_z}{L_x}\right);\left(\frac{\Delta p_d}{\rho L_z}\right);\left(\frac{U_t^2}{L_x}\right);\left(\frac{U_t^2}{L_y}\right);\left(\frac{U_t^2}{L_z}\right)$$

$$\downarrow \quad \downarrow \quad \downarrow \quad \downarrow \quad \downarrow \quad \downarrow \quad \downarrow$$

$$\frac{L_z}{L_x};\ \frac{L_z}{L_x};\ \frac{L_z}{L_x};\ \frac{\Delta p_d}{\rho U_x^2}\frac{L_x}{L_z};\ \frac{U_t^2}{U_x^2};\ \frac{U_t^2}{U_x^2}\frac{L_x}{L_y};\ \frac{U_t^2}{U_x^2}\frac{L_x}{L_z}$$

from which it could again be deduced that, at most:

$$\frac{\Delta p_d}{\rho U_x^2} \sim \delta \qquad (3.1.17)$$

It could be recognised that $(g \frac{\Delta\rho}{\rho} z / U_x^2)$ is some form of Richardson number (Ri) and let us call the case considered above as that of Small Richardson Number.

Consider now the other extreme case where inertial forces and buoyant forces are equally important in the x direction equation and turbulence terms are negligible (because of the suppression of the production of turbulence by density stratification) in comparison. From the x direction equation, one could write:

$$\frac{g \frac{\Delta\rho}{\rho} z}{U_x^2} \sim 1 \qquad (3.1.18)$$

and: $$(\frac{U_t}{U_x})^2 \frac{1}{\delta} \sim \delta \quad \text{or} \quad \delta^2$$

or: $$(\frac{U_t}{U_x}) \sim \delta \quad \text{or} \quad \delta\sqrt{\delta} \qquad (3.1.19)$$

Assuming arbitrarily $(U_t/U_x) \sim \delta$. From the y direction equation of motion, if:

$$\frac{g (\frac{\Delta\rho}{\rho}) z}{U_x^2} \sim 1$$

then it must be that unless $L_y/L_x \sim 1$, there will be no term in the y equation to balance the buoyancy term. Thus under this condition the lateral extent of the jet becomes of the same order of magnitude as

the longitudinal extent. From Equation 3.1.16, it follows that at the most:

$$\frac{\Delta p_d}{\rho U_x^2} \sim \delta^2 \qquad (3.1.20)$$

One could call the case discussed above as that of Large Richardson Number.

For the intermediate case, which could be referred to as that of Moderate Richardson Number:

$$\frac{g\,(\frac{\Delta\rho}{\rho})\,z}{U_x^2} \sim \delta$$

For this case, it is not unreasonable to set down the turbulence terms as $U_t/U_x \sim \delta^{3/4}$. With these stipulations, considering Equation 3.1.14 for inertial, buoyancy and (largest) turbulence terms to be of the same order:

$$\frac{L_y}{L_x} \sim \sqrt{\delta} \qquad (3.1.21)$$

which indicates that the lateral expansion becomes smaller than that for Large Richardson Number, and Equation 3.1.16 indicates that, at the most:

$$\frac{\Delta p_d}{\rho U_x^2} \sim \delta\sqrt{\delta} \qquad (3.1.22)$$

In Equation 3.1.12, the inertial terms dominate over both the buoyancy and the turbulence terms.

With these simplifications, the reduced form of the Reynolds

equations for the three ranges of Richardson number are given below:

For $[g(\Delta\rho/\rho)z]/U_x^2 \sim 1$ (Large Richardson Number)

$$u\frac{\partial u}{\partial x} + v\frac{\partial u}{\partial y} + w\frac{\partial u}{\partial z} = -\frac{\alpha g}{\rho}\frac{\partial}{\partial x}\int_o^z \Delta T dz \qquad (3.1.23)$$

$$u\frac{\partial v}{\partial x} + v\frac{\partial v}{\partial y} + w\frac{\partial v}{\partial z} = -\frac{\alpha g}{\rho}\frac{\partial}{\partial y}\int_o^z \Delta T dz \qquad (3.1.24)$$

For $[g(\Delta\rho/\rho)z]/U_x^2 \sim \delta$ (Moderate Richardson Number)

$$u\frac{\partial u}{\partial x} + v\frac{\partial u}{\partial y} + w\frac{\partial u}{\partial z} = -\frac{\partial \overline{u'w'}}{\partial z} \qquad (3.1.25)$$

$$u\frac{\partial v}{\partial x} + v\frac{\partial v}{\partial y} + w\frac{\partial v}{\partial z} = +\frac{\alpha g}{\rho}\frac{\partial}{\partial y}\int_o^z \Delta T dz - \frac{\partial \overline{v'w'}}{\partial z} \qquad (3.1.26)$$

$$0 = \frac{1}{\rho}\frac{\partial p_d}{\partial z} - \frac{\partial \overline{w'^2}}{\partial z} \qquad (3.1.27)$$

For $[g(\Delta\rho/\rho)z]/U_x^2 \sim \delta^2$ (Small Richardson Number)

$$u\frac{\partial u}{\partial x} + v\frac{\partial u}{\partial y} + w\frac{\partial u}{\partial z} = -\frac{\partial \overline{u'v'}}{\partial y} - \frac{\partial \overline{u'w'}}{\partial z} \qquad (3.1.28)$$

$$0 = -\frac{\partial \overline{v'^2}}{\partial y} - \frac{\partial \overline{v'w'}}{\partial z} - \frac{1}{\rho}\frac{\partial p_d}{\partial y} \qquad (3.1.29)$$

$$0 = -\frac{1}{\rho}\frac{\partial p_d}{\partial z} - \frac{\partial \overline{v'w'}}{\partial y} - \frac{\partial \overline{w'^2}}{\partial z} \qquad (3.1.30)$$

3.1.4 Equation of Heat Transport

Assuming a scale for $\Delta T'$ as ΔT_t and letting ΔT_x be the

scale for ΔT, the equation of heat transport along with the order of magnitude of the different terms is written below:

$$\frac{\partial(u\Delta T)}{\partial x} + \frac{\partial(v\Delta T)}{\partial y} + \frac{\partial(w\Delta T)}{\partial z} = - \frac{\partial(\overline{u'\Delta T'})}{\partial x} - \frac{\partial(\overline{v'\Delta T'})}{\partial y} - \frac{\partial(\overline{w'\Delta T'})}{\partial z} \qquad (3.1.5)$$

$$\frac{U_x \Delta T_x}{L_x} ; \frac{U_y \Delta T_x}{L_y} ; \frac{U_z \Delta T_x}{L_z} \quad ; \quad \frac{U_t \Delta T_t}{L_x} ; \frac{U_t \Delta T_t}{L_y} ; \frac{U_t \Delta T_t}{L_z}$$

$$1 \; ; \; 1 \; ; \; 1 \; ; \left(\frac{U_t}{U_x}\right)\left(\frac{\Delta T_t}{\Delta T_x}\right) ; \left(\frac{U_t}{U_x}\right)\left(\frac{\Delta T_t}{\Delta T_x}\right)\left(\frac{L_x}{L_y}\right) ; \left(\frac{U_t}{U_x}\right)\left(\frac{\Delta T_t}{\Delta T_x}\right)\left(\frac{L_x}{L_z}\right)$$

For the largest turbulent heat flux term to be comparable to the mean flow convection terms, and for small Ri:

$$\frac{U_t}{U_x}\frac{\Delta T_t}{\Delta T_x}\frac{L_x}{L_z} \sim 1 \quad \text{or} \quad \sqrt{\delta}\,\frac{\Delta T_t}{\Delta T_x}\frac{1}{\delta} \sim 1$$

or:
$$\frac{\Delta T_t}{\Delta T_x} \sim \sqrt{\delta} \qquad (3.1.31)$$

and similarly for large Ri:

$$\frac{\Delta T_t}{\Delta T_x} \sim 1 \qquad (3.1.32)$$

Using the simplifications developed in the previous section, the heat transport equation reduces to the following forms for the different ranges of the Richardson number.

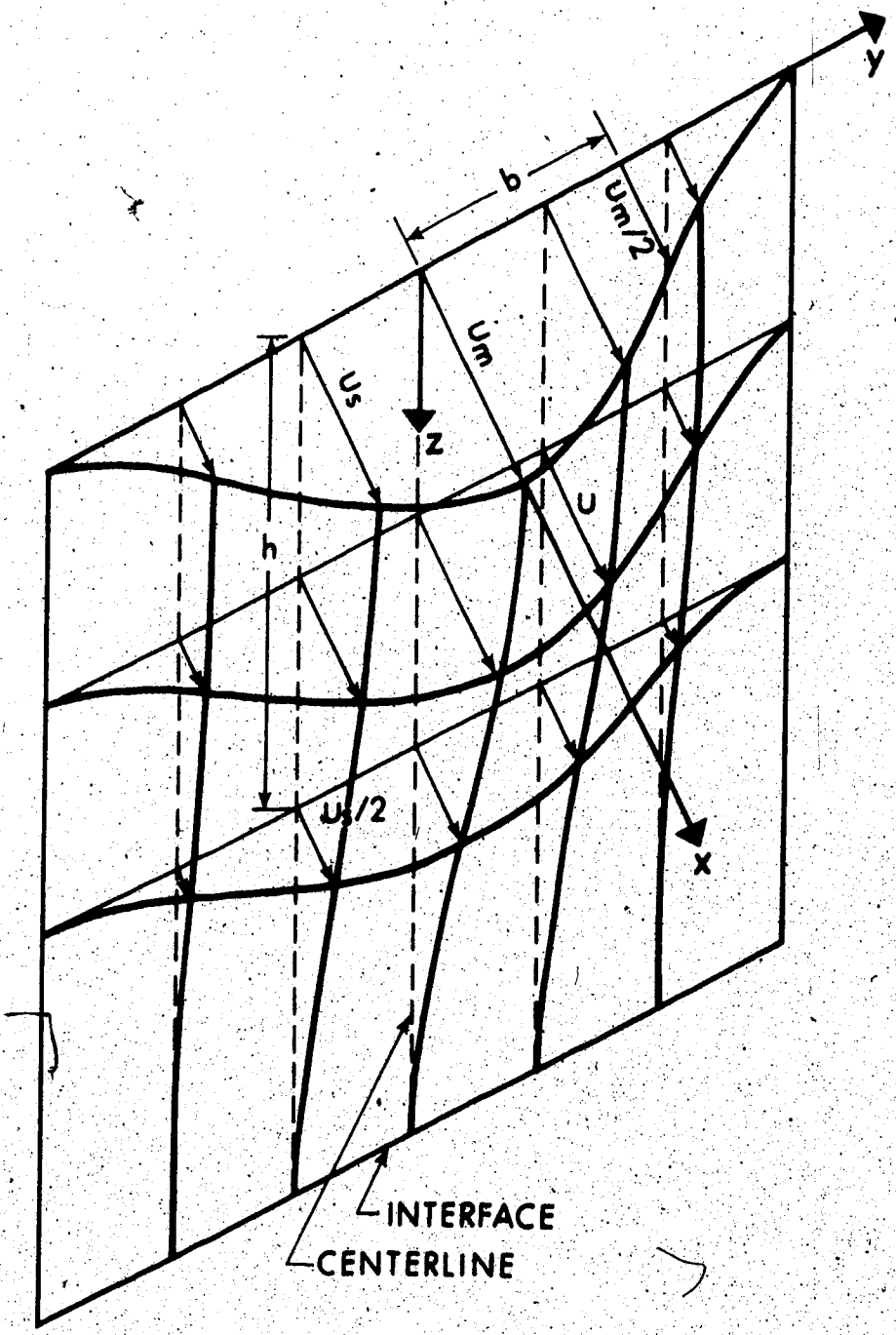

FIGURE 3.1 IDEAL MODEL OF A VELOCITY DISTRIBUTION IN A SURFACE JET FOR VELOCITY U

Large and Moderate Ri

$$\frac{\partial(u\Delta T)}{\partial x} + \frac{\partial(v\Delta T)}{\partial y} + \frac{\partial(w\Delta T)}{\partial z} = -\frac{\partial\overline{w'\Delta T'}}{\partial z} \qquad (3.1.33)$$

Small Ri

$$\frac{\partial(u\Delta T)}{\partial x} + \frac{\partial(v\Delta T)}{\partial y} + \frac{\partial(w\Delta T)}{\partial z} = -\frac{\partial\overline{v'\Delta T'}}{\partial y} - \frac{\partial\overline{w'\Delta T'}}{\partial z} \qquad (3.1.34)$$

3.1.5 Similarity of Velocity and Temperature Profiles

Before proceeding with an integral treatment of the equations derived in the previous section, similarity of velocity and excess temperature profiles is to be assumed. The similarity assumptions for three dimensional models have been described in Section 2.10.1. Rajaratnam and Pani (1970) used a similar scheme in their study of three dimensional turbulent wall jets. The similarity assumptions are again presented here in detail for convenience. With reference to Figure 3.1 to 3.3, for any non-central x-z plane:

$$\frac{u}{u_s} = f_1\left(\frac{z}{h}\right) = f_1(\xi) \qquad (3.1.35)$$

where u_s is the surface velocity $[u_s = u(x,y,z=0)]$ which is a function of x and y, and h is the length scale in the z direction taken conveniently as the value of z when $u = 1/2\ u_s$. Further, considering the y axis lying on the (level) water surface:

$$\frac{u_s}{u_m} = f_1\left(\frac{y}{b}\right) = f_1(\eta) \qquad (3.1.36)$$

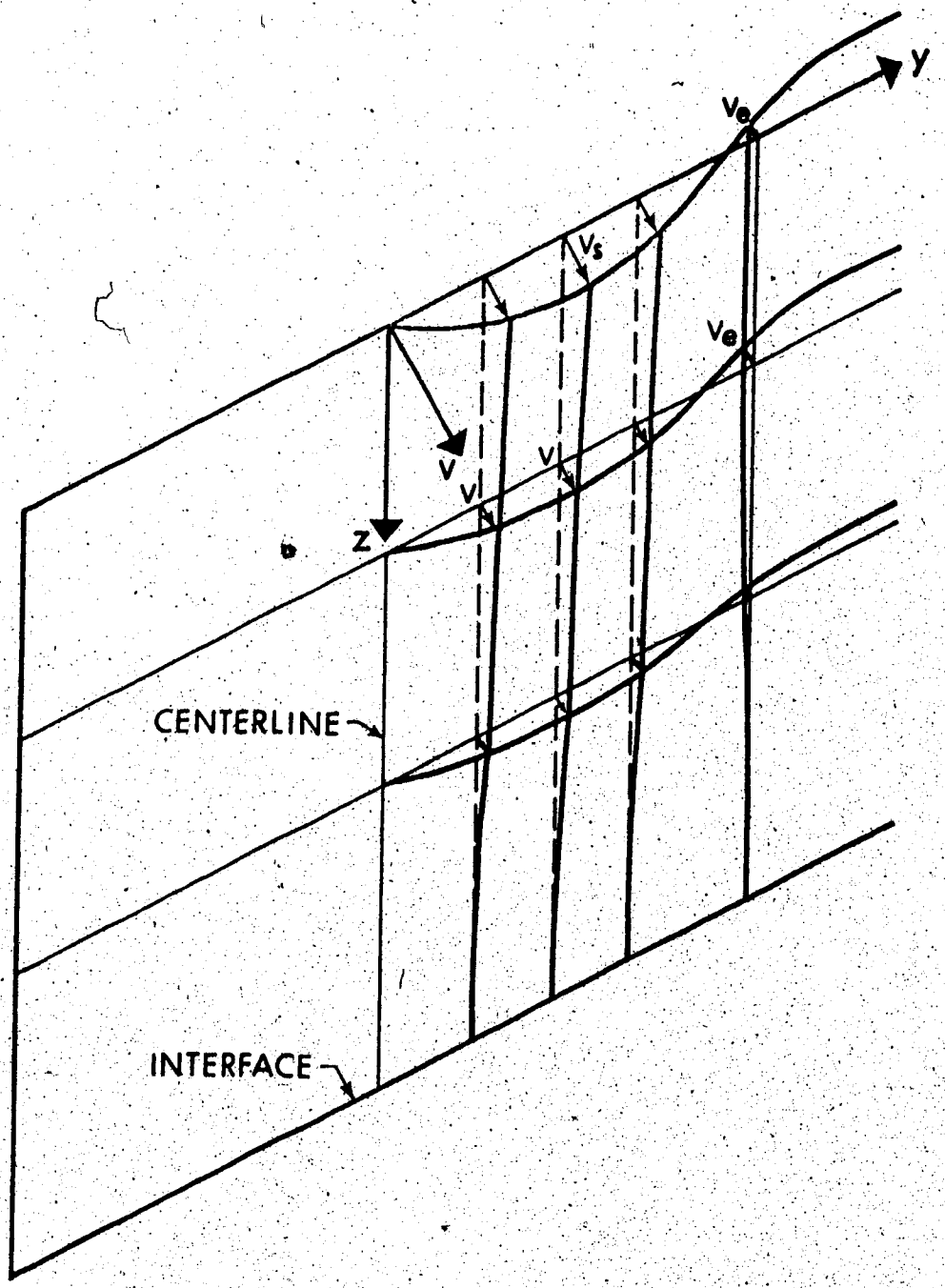

FIGURE 3.2 IDEAL MODEL FOR A VELOCITY DISTRIBUTION IN A SURFACE JET FOR VELOCITY v

where $u_m = u_s(x,y=0)$ and b is a length scale taken as the value of y where $u_s = 1/2\ u_m$. Combining Equations 3.1.35 and 3.1.36:

$$\frac{u}{u_m} = f_1(\xi)\ f_2(\eta) \qquad (3.1.37)$$

Regarding the velocity component in the y direction, it is assumed that (see Figure 3.2):

$$\frac{v}{v_s} = f_2(\xi) \qquad (3.1.38)$$

For the temperature profiles:

$$\frac{\Delta T}{\Delta T_s} = f_3(\xi) \qquad (3.1.39)$$

and:

$$\frac{\Delta T_s}{\Delta T_m} = f_3(\eta) \qquad (3.1.40)$$

and hence:

$$\frac{\Delta T}{\Delta T_m} = f_3(\xi)\ f_3(\eta) \qquad (3.1.41)$$

where $\Delta T_s = \Delta T(x,y,0)$; $\Delta T_m = \Delta T(x,0,0) = \Delta T_s(x,0)$. Experimental observations during the present investigations have indicated that Equations 3.1.35, 3.1.36, 3.1.39, and 3.1.40 are reasonable approximations. The details are discussed in Chapter 5.

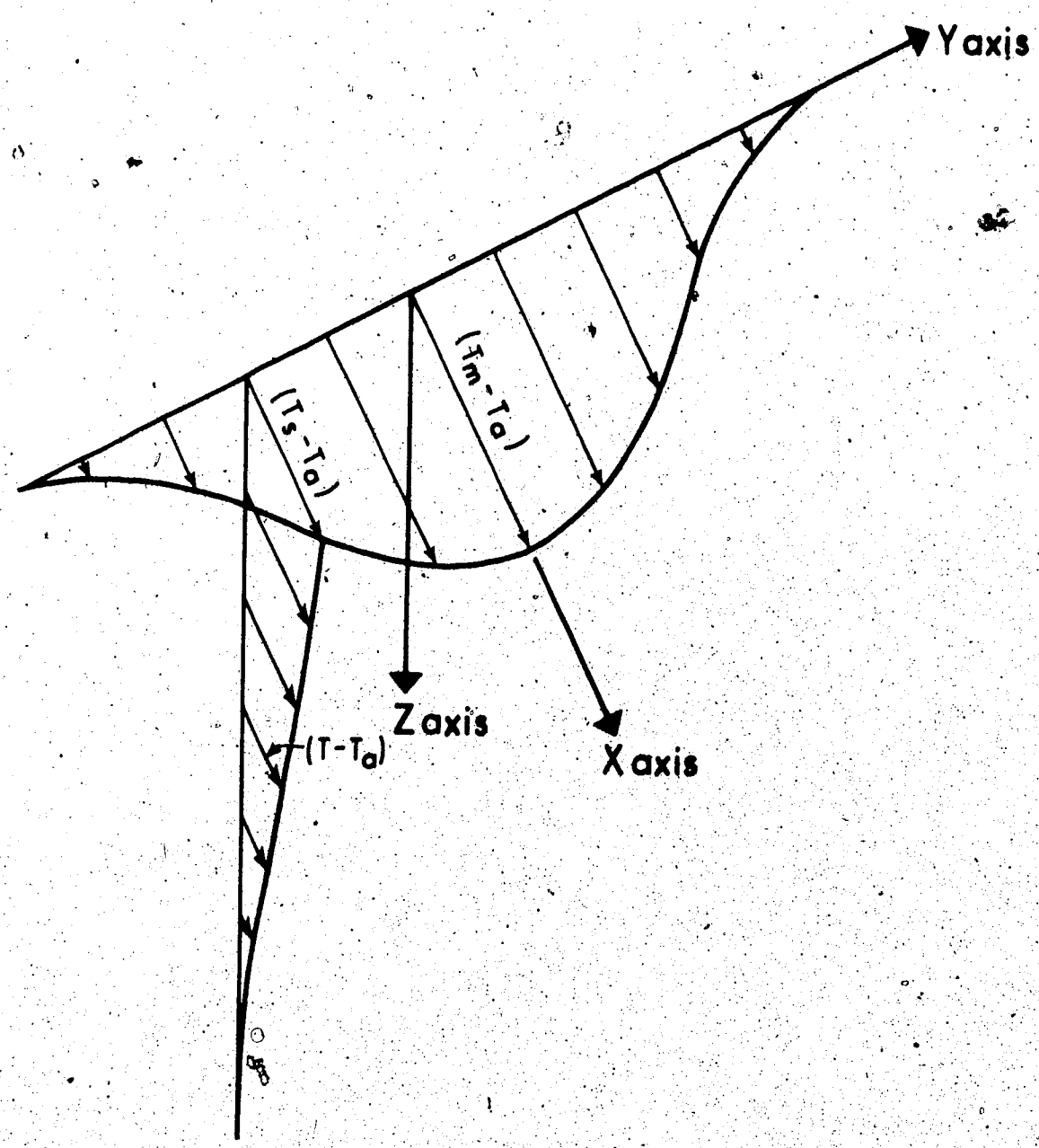

FIGURE 3.3 IDEAL MODEL OF TEMPERATURE DISTRIBUTION IN A SURFACE JET FOR EXCESS TEMPERATURE $T_m - T_a$

3.2 Integration of Equations of Motion in the z Direction

3.2.1 Integration of Continuity Equation

Integrating the equation of continuity in the z direction from $z = 0$ to $z = \infty$, we get:

$$\int_0^\infty \frac{\partial u}{\partial x}\, dz + \int_0^\infty \frac{\partial v}{\partial y}\, dz + \int_0^\infty \frac{\partial w}{\partial z}\, dz = 0 \qquad (3.2.1)$$

Substituting for u and v from Equations 3.1.35 and 3.1.38 and integrating:

$$\frac{\partial}{\partial x}(u_s h) \int_0^\infty f_1(\xi)d\xi + \frac{\partial}{\partial y}(v_s h) \int_0^\infty f_2(\xi)d\xi = - w_e \qquad (3.2.2)$$

where w_e is the entrainment velocity in the z direction. Letting:

$$I_1 = \int_0^\infty f_1(\xi)d\xi \quad \text{and} \quad I_2 = \int_0^\infty f_2(\xi)d\xi$$

Equation 3.2.2 reduces to:

$$\frac{\partial}{\partial x}(u_s h) + \frac{I_2}{I_1}\frac{\partial}{\partial y}(v_s h) = - \frac{w_e}{I_1} \qquad (3.2.3)$$

It should be noted that I_1 and I_2 are constants.

3.2.2 Integration of Equations of Motion for Small Ri

Consider first flows with small Richardson numbers. The equation of motion, Equation 3.1.28, could be written as:

$$\frac{\partial u^2}{\partial x} + \frac{\partial uv}{\partial y} + \frac{\partial uw}{\partial z} = - \frac{\partial(\overline{u'v'})}{\partial y} - \frac{\partial \overline{u'w'}}{\partial z} \qquad (3.2.4)$$

Integrating Equation 3.2.4 with respect to z, we get:

$$\int_0^\infty \frac{\partial u^2}{\partial x} dz + \int_0^\infty \frac{\partial uv}{\partial y} dz + \int_0^\infty \frac{\partial uw}{\partial z} dz =$$

$$- \int_0^\infty \frac{\partial \overline{u'v'}}{\partial y} dz - \int_0^\infty \frac{\partial \overline{u'w'}}{\partial z} dz \qquad (3.2.5)$$

Equation 3.2.5 could be reduced to the form:

$$\frac{\partial}{\partial x}(u_s^2 h) \int_0^\infty f_1^2(\xi)d\xi + \frac{\partial}{\partial y}(u_s v_s h) \int_0^\infty f_1(\xi) f_2(\xi) d\xi$$

$$+ uw \Big|_0^\infty = -\frac{\partial}{\partial y} \int_0^\infty \overline{u'v'}\, h d\xi - \overline{u'w'} \Big|_0^\infty \qquad (3.2.6)$$

Using the boundary conditions $\overline{u'w'} = 0$ at $z = 0$ and $\overline{u'w'} = 0$ at $z = \infty$, Equation 3.2.6 reduces to:

$$\frac{\partial}{\partial x}(u_s^2 h) + \frac{I_4}{I_3} \frac{\partial}{\partial y}(u_s v_s h) = \frac{1}{I_3} \frac{\partial}{\partial y} \int_0^\infty (-\overline{u'v'})\, h d\xi \qquad (3.2.7)$$

where: $I_3 = \int_0^\infty f_1^2(\xi)d\xi$ and $I_4 = \int_0^\infty f_1(\xi) f_2(\xi) d\xi$

Integrating the equation of motion in the y direction:

$$0 = - \int_0^\infty \frac{\partial \overline{v'^2}}{\partial y} dz - \int_0^\infty \frac{\partial \overline{v'w'}}{\partial z} dz - \frac{1}{\rho} \int_0^\infty \frac{\partial p_d}{\partial y} dz \qquad (3.2.8)$$

which reduces to:

$$0 = -\frac{\partial}{\partial y}\int_0^\infty \overline{v'^2}\, h d\xi - \frac{1}{\rho}\int_0^\infty \frac{\partial p_d}{\partial y} h d\xi \qquad (3.2.9)$$

Integrating the z direction equation (Equation 3.1.30) in a similar way from z to ∞ results in:

$$\frac{p_d}{\rho} = \int_z^\infty \frac{\partial(\overline{v'w'})}{\partial y} dz - \overline{w'^2} \qquad (3.2.10)$$

Differentiating Equation 3.2.10 with respect to x:

$$\frac{1}{\rho}\frac{\partial p_d}{\partial x} = \frac{\partial}{\partial x}\int_z^\infty \frac{\partial(\overline{v'w'})}{\partial y} dz - \frac{\partial \overline{w'^2}}{\partial x} \qquad (3.2.11)$$

From this equation, one could see that the pressure gradient term in the x direction momentum equation is of the order of δ, compared to the dominant order of unity and hence its neglect is justified. Differentiating Equation 3.2.10 with respect to y:

$$\frac{1}{\rho}\frac{\partial p_d}{\partial y} = \frac{\partial}{\partial y}\int_z^\infty \frac{\partial(\overline{v'w'})}{\partial y} dz - \frac{\partial \overline{w'^2}}{\partial y} \qquad (3.2.12)$$

With Equation 3.2.12, Equation 3.2.9 becomes:

$$0 = \int_0^\infty \left[\frac{\partial(\overline{w'^2} - \overline{v'^2})}{\partial y} - \frac{\partial}{\partial y}\int_z^\infty \frac{\partial(\overline{v'w'})}{\partial y}\right] h d\xi \qquad (3.2.13)$$

Since generally $\overline{v'^2} \sim \overline{w'^2}$, Equation 3.2.13 is reduced to:

$$\int_0^\infty \left[\int_\xi^\infty \frac{\partial^2}{\partial y^2} (\overline{v'w'})\, h^2 d\xi \right] d\xi = 0 \qquad (3.2.14)$$

3.2.3 Integration of Equations of Motion for Moderate Ri

The equation of motion in the x direction being the same as that for small Ri, except for the absence of the first term on the right hand side, the integrated form will be the same as Equation 3.2.7 with the right hand side equal to zero. Considering the y direction, integration of Equation 3.1.26 gives:

$$\int_0^\infty \frac{\partial uv}{\partial x} dz + \int_0^\infty \frac{\partial v^2}{\partial y} dz + \int_0^\infty \frac{\partial vw}{\partial z} dz =$$

$$- \int_0^\infty \left(\frac{\alpha g}{\rho} \frac{\partial}{\partial y} \int_0^z \Delta T dz \right) dz - \int_0^\infty \frac{\partial \overline{v'w'}}{\partial z} dz \qquad (3.2.15)$$

The above equation could be reduced to:

$$\frac{\partial}{\partial x} \int_0^\infty (uv) dz + \frac{\partial}{\partial y} \int_0^\infty v^2 dz + vw \Big|_0^\infty =$$

$$- \int_0^\infty \left(\frac{\alpha g}{\rho} \frac{\partial}{\partial y} \int_0^z \Delta T dz \right) dz \qquad (3.2.16)$$

Equation 3.2.16 could be further reduced to:

$$\frac{\partial}{\partial x}(u_s v_s h)\int_o^\infty f_1(\xi)f_2(\xi)d\xi + \frac{\partial}{\partial y}(v_s{}^2 h)\int_o^\infty f_2{}^2(\xi)d\xi =$$

$$-\frac{ag}{\rho_a}\frac{\partial}{\partial y}\int_o^\infty\left[\int_o^\xi(\Delta T d\xi)h^2\right]d\xi \qquad (3.2.17)$$

wherein the following approximation has been made:

$$\frac{1}{\rho} = \frac{1}{\rho_a - \Delta\rho} \simeq \frac{1}{\rho_a} \qquad (3.2.18)$$

The above equation can be rewritten as:

$$\frac{\partial}{\partial x}(u_s v_s h) + \frac{I_6}{I_4}\frac{\partial}{\partial y}(v_s{}^2 h) = -\frac{ag}{\rho_a}\frac{\partial}{\partial y}(\Delta T_s h^2)\frac{I_5}{I_4} \qquad (3.2.19)$$

wherein:

$$I_5 = \int_o^\infty\left[\int_o^\xi f_3'(\xi)d\xi\right]d\xi \quad \text{and} \quad I_6 = \int_o^\infty f_2(\xi)d\xi$$

3.2.4 Integration of Equations of Motion for Large Ri

Considering the x direction equation, using the continuity equation and Equation 3.2.18, one could rewrite Equation 3.1.23 as:

$$\frac{\partial u^2}{\partial x} + \frac{\partial uv}{\partial y} + \frac{\partial uw}{\partial z} = -\frac{ag}{\rho_a}\frac{\partial}{\partial x}\int_o^z \Delta T dz \qquad (3.2.20)$$

Integrating Equation 3.2.20 with respect to z:

$$\int_0^\infty \frac{\partial u^2}{\partial x}\,dy + \int_0^\infty \frac{\partial uv}{\partial y}\,dz + \int_0^\infty \frac{\partial uw}{\partial z}\,dz =$$

$$-\frac{ag}{\rho_a}\int_0^\infty \left(\frac{\partial}{\partial x}\int_0^z \Delta T dz\right) dz \qquad (3.2.21)$$

which could be further reduced to:

$$\frac{\partial}{\partial x}(u_s^2 h) + \frac{I_4}{I_3}\frac{\partial}{\partial y}(u_s v_s h) = -\frac{ag}{\rho_a}\frac{\partial}{\partial x}(\Delta T_s h^2)\frac{I_5}{I_3} \qquad (3.2.22)$$

Similarly the equation of motion (Equation 3.1.24) in the y direction could be reduced to:

$$\frac{\partial}{\partial x}(u_s v_s h) + \frac{I_6}{I_4}\frac{\partial}{\partial y}(v_s^2 h) = -\frac{ag}{\rho_a}\frac{\partial}{\partial y}(\Delta T_s h^2)\frac{I_5}{I_4} \qquad (3.2.23)$$

3.2.5 Integration of the Heat Transport Equation

Integrating Equation 3.1.34 with respect to z from 0 to ∞, one gets:

$$\int_0^\infty \frac{\partial(u\Delta T)}{\partial x}\,dz + \int_0^\infty \frac{\partial(v\Delta T)}{\partial y}\,dz + \int_0^\infty \frac{\partial(w\Delta T)}{\partial z}\,dz =$$

$$-\int_0^\infty \frac{\partial \overline{v'\Delta T'}}{\partial y}\,dz - \int_0^\infty \frac{\partial \overline{w'\Delta T'}}{\partial z}\,dz \qquad (3.2.24)$$

which reduces to:

$$\frac{\partial}{\partial x}(u_s \Delta T_s h) + \frac{I_7}{I_8}\frac{\partial}{\partial y}(v_s \Delta T_s h) = - \frac{1}{I_8}\int_0^\infty \frac{\partial(\overline{v'\Delta T'})}{\partial y} h d\xi - \overline{w'\Delta T'}\Big|_0^\infty \qquad (3.2.25)$$

One could write:

$$\overline{w'\Delta T'}\Big|_0^\infty = - K_e (T_s - T_e) \qquad (3.2.26)$$

where K_e is the surface heat transfer coefficient and T_e is the equilibrium temperature (Edinger and Geyer, 1965). With Equation 3.2.26, Equation 3.2.25 for small Ri becomes:

$$\frac{\partial}{\partial x}(u_s \Delta T_s h) + \frac{I_7}{I_8}\frac{\partial}{\partial y}(v_s \Delta T_s h) + \frac{K_e}{I_8}(T_s - T_e) = - \frac{1}{I_8}\int_0^\infty \frac{\partial(\overline{v'\Delta T'})}{\partial y} h d\xi \qquad (3.2.27)$$

In Equations 3.2.25 and 3.2.27, the integrals I_7 and I_8 are defined as:

$$I_7 = \int_0^\infty f_2(\xi) f_3(\xi) d\xi \quad \text{and} \quad I_8 = \int_0^\infty f_1(\xi) f_3(\xi) d\xi$$

For large and moderate Richardson numbers, integrating Equation 3.1.33 in a similar manner results in:

$$\frac{\partial}{\partial x}(u_s \Delta T_s h) + \frac{I_7}{I_8}\frac{\partial}{\partial y}(v_s \Delta T_s h) + \frac{K_e}{I_8}(T_s - T_e) = 0 \qquad (3.2.28)$$

3.2.6 Dimensionless Forms of Integral Equations

The integral equations derived in the previous sections can now be expressed in non-dimensional forms. The velocities are made dimensionless using the velocity at the efflux section U_o. Similarly, L is used as the length scale for lengths in the x and y directions and, h_o, the depth of the hot water discharge at the efflux section is used as the scale for distances in the z direction. For temperatures, ΔT_o, the excess temperature at the efflux section, is used as the scale.

The dimensionless quantities are written below:

$$u_{s_*} = \frac{u_s}{U_o} \; ; \; u_{m_*} = \frac{u_m}{U_o} \; ; \; v_{s_*} = \frac{v_s}{U_o} \; ; \; x_* = \frac{x}{L}$$

$$y_* = \frac{y}{L} \; ; \; h_* = \frac{h}{h_o} \; ; \; \Delta T_{s_*} = \frac{\Delta T_s}{\Delta T_o} \; ; \; \Delta T_{m_*} = \frac{\Delta T_m}{\Delta T_o} \qquad (3.2.29)$$

In terms of these dimensionless quantities, the equations of motion as well as the heat transport equation for small, moderate, and large Richardson numbers are written below for further use.

Continuity equation for all cases

$$\frac{\partial}{\partial x_*}(u_{s_*} h_*) + \frac{I_2}{I_1}\frac{\partial}{\partial y_*}(v_{s_*} h_*) = -\frac{w_e L}{U_o h_o}\frac{1}{I_1} \qquad (3.2.30)$$

Momentum equations in the x and y directions for Small Richardson Number

$$\frac{\partial}{\partial x_*}(u_{s_*}^2 h_*) + \frac{I_4}{I_3}\frac{\partial}{\partial y_*}(u_{s_*} v_{s_*} h_*) =$$

$$\frac{1}{I_3}\int_0^{\infty}\frac{\partial}{\partial y_*}\left(-\frac{\overline{u'v'}}{U_o^2}h_*\right)d\xi \qquad (3.2.31S)$$

$$0 = \frac{U_o^2 h_o^2}{L^2}\int_0^{\infty}\left[\int_{\xi}^{\infty}\frac{\partial^2}{\partial y_*^2}\left(\frac{\overline{u'w'}}{U_o^2}\right)h_*^2 d\xi\right]d\xi \qquad (3.2.32S)$$

Momentum equations in the x and y directions for Moderate Richardson Number

$$\frac{\partial}{\partial x_*}\left(u_{s_*}^2 h_*\right) + \frac{I_4}{I_3}\frac{\partial}{\partial y_*}\left(u_{s_*}v_{s_*}h_*\right) = 0 \qquad (3.2.31M)$$

$$\frac{\partial}{\partial x_*}\left(u_{s_*}v_{s_*}h_*\right) + \frac{I_6}{I_4}\frac{\partial}{\partial y_*}\left(v_{s_*}^2 h_*\right) = -\frac{ag}{\rho_a}\frac{h_o\Delta T_o}{U_o^2}\frac{\partial}{\partial y_*}\left(\Delta T_{s_*}h_*^2\right)\frac{I_5}{I_4} \qquad (3.2.32M)$$

Momentum equations in the x and y directions for Large Richardson Number

$$\frac{\partial}{\partial x_*}\left(u_{s_*}^2 h_*\right) + \frac{I_4}{I_3}\frac{\partial}{\partial y_*}\left(u_{s_*}v_{s_*}h_*\right) = -\frac{ag}{\rho_a}\frac{h_o\Delta T_o}{U_o^2}\frac{\partial}{\partial x_*}\left(\Delta T_{s_*}h_*^2\right)\frac{I_5}{I_3} \qquad (3.2.31L)$$

$$\frac{\partial}{\partial x_*}\left(u_{s_*}v_{s_*}h_*\right) + \frac{I_6}{I_4}\frac{\partial}{\partial y_*}\left(v_{s_*}^2 h_*\right) = -\frac{ag}{\rho_a}\frac{h_o\Delta T_o}{U_o^2}\frac{\partial}{\partial y_*}\left(\Delta T_{s_*}h_*^2\right)\frac{I_5}{I_4} \qquad (3.2.32L)$$

Heat transport equation for
Small Richardson Number

$$\frac{\partial}{\partial x_*}\left(u_{s_*}\Delta T_{s_*} h_*\right) + \frac{I_7}{I_8}\frac{\partial}{\partial y_*}\left(v_{s_*}\Delta T_{s_*} h_*\right) + \frac{1}{I_8}\frac{K_e L}{U_o h_o}\left[\Delta T_{s_*} - \frac{(T_e - T_a)}{\Delta T_o}\right] = -\frac{1}{I_8}\int_o^\infty \frac{\partial}{\partial y_*}\frac{\overline{v'\Delta T'}}{U_o \Delta T_o} h_* d\xi \qquad (3.2.33S)$$

Heat transport equation for
Moderate and Large Richardson Numbers

$$\frac{\partial}{\partial x_*}\left(u_{s_*}\Delta T_{s_*} h_*\right) + \frac{I_7}{I_8}\frac{\partial}{\partial y_*}\left(v_{s_*}\Delta T_{s_*} h_*\right) + \frac{1}{I_8}\frac{K_e L}{U_o h_o}\left[\Delta T_{s_*} - \frac{(T_e - T_a)}{\Delta T_o}\right] = 0 \qquad (3.2.33ML)$$

Equations 3.2.30 to 3.2.33ML derived above are more general than those derived by Engelund and Pederson (1973). These equations have indicated that the solution to this problem depends upon the source Richardson number written as:

$$Ri = -\frac{\alpha g \Delta T_o h_o}{\rho_a U_o^2} = \frac{g\Delta\rho_o h_o}{\rho_a U_o^2} \qquad (3.2.34)$$

3.3 Surface Discharges with Small Ri

3.3.1 Summary of the Equations for Small Ri

For convenience in further development, the equation of continuity, the simplified equations of motion, and the heat transport equation which were developed in the preceding section for heated sur-

face discharges with small Richardson number are presented below:

Continuity Equation

$$\frac{\partial}{\partial x_*}(u_{s_*} h_*) + \frac{I_2}{I_1}\frac{\partial}{\partial y_*}(v_{s_*} h_*) = -\frac{w_e L}{U_o h_o}\frac{1}{I_1} \qquad (3.3.1)$$

Equations of Motion

$$\frac{\partial}{\partial x_*}(u_{s_*}^2 h_*) + \frac{I_4}{I_3}\frac{\partial}{\partial y_*}(u_{s_*} v_{s_*} h_*) =$$

$$\frac{1}{I_3}\int_o^\infty \frac{\partial}{\partial y_*}\left(-\frac{\overline{u'v'}}{U_o^2} h_*\right) d\xi \qquad (3.3.2)$$

$$\frac{U_o^2 h_o^2}{L^2}\int_o^\infty \left[\int_\xi^\infty \frac{\partial^2}{\partial y_*^2}\left(\frac{\overline{u'w'}}{U_o^2}\right) h_*^2 \, d\xi\right] d\xi = 0 \qquad (3.3.3)$$

Equation of Heat Transport

$$\frac{\partial}{\partial x_*}(u_{s_*} \Delta T_{s_*} h_*) + \frac{I_7}{I_8}\frac{\partial}{\partial y_*}(v_{s_*} \Delta T_{s_*} h_*)$$

$$+ \frac{1}{I_8}\frac{K_e L}{U_o h_o}\left[\Delta T_{s_*} - \frac{(T_e - T_a)}{\Delta T_o}\right]$$

$$= -\frac{1}{I_8}\int_o^\infty \frac{\partial}{\partial y_*}\frac{\overline{v'\Delta T'}}{U_o \Delta T_o} h_* d\xi \qquad (3.3.4)$$

3.3.2 Integral Momentum Equation in the x Direction

Integrating Equation 3.3.2 with respect to y_* from $y_* = 0$ to $y_* = \infty$ (that is, large values of y_*). One obtains:

$$\int_0^\infty \frac{\partial}{\partial x_*} (u_{s_*}^2 h_*)\, dy_* + \frac{I_4}{I_3} \int_0^\infty \frac{\partial}{\partial y_*} (u_{s_*} v_{s_*} h_*)\, dy_* =$$

$$\frac{1}{I_3} \int_0^\infty \left[\int_0^\infty \frac{\partial}{\partial y_*} \left(- \frac{\overline{u'v'}}{U_o^2} h_*\right) d\xi \right] dy_* \qquad (3.3.5)$$

In the term on the right hand side of Equation 3.3.5, $-\overline{u'v'} = \tau_{xy}/\rho_a$ where τ_{xy} is the turbulent shear stress and $-\overline{u'v'}/U_o^2 = \tau_{xy}/\rho_a U_o^2$. Integration of Equation 3.3.5 with reversing the order of integration in the last term gives:

$$\int_0^\infty \frac{\partial}{\partial x_*} (u_{s_*}^2 h_*)\, dy_* + \frac{I_4}{I_3} \left| u_{s_*} v_{s_*} h_* \right|_0^\infty =$$

$$\frac{1}{I_3} \int \left| \frac{\tau_{xy}}{\rho_a U_o^2} h_* \right|_0^\infty d\xi \qquad (3.3.6)$$

The boundary conditions could be written as at $y_* = 0$, $v_{s_*} = 0$, $\tau_{xy} = 0$ and $u_{s_*} = u_{m_*}$. For $y_* \to \infty$ (that is, large values of y_*), $v_{s_*} = v_{e_*}$ (which is the dimensionless entrainment velocity), $u_{s_*} = 0$ and $\tau_{xy} = 0$. With these boundary conditions, and using the Liebnitz theorem for interchanging the order of integration, Equation 3.3.6 reduces to:

$$\frac{d}{dx_*} \int_0^\infty u_{s_*}^2 h_* dy_* = 0 \qquad (3.3.7)$$

Equation 3.3.7 says that the momentum flux in the x direction is preserved.

3.3.3 Integral Energy Equation

Multiplying Equation 3.3.2 by u_{s_*} and integrating with respect to y_* from $y_* = 0$ to $y_* = \infty$, one gets:

$$\underbrace{\int_0^\infty u_{s_*} \frac{\partial}{\partial x_*} (u_{s_*}^2 h_*)\, dy_*}_{A} + \frac{I_4}{I_3} \underbrace{\int_0^\infty u_{s_*} \frac{\partial}{\partial y_*} (u_{s_*} v_{s_*} h_*)\, dy_*}_{B}$$

$$= \frac{1}{I_3} \underbrace{\int_0^\infty u_{s_*} \left[\int_0^\infty \frac{\partial}{\partial y_*} \left(\frac{\tau_{xy}}{\rho_a U_o^2} h_* \right) d\xi \right] dy_*}_{C} \qquad (3.3.8)$$

$$\text{Term A} = \int_0^\infty \left[u_{s_*}^2 \frac{\partial}{\partial x_*} (u_{s_*} h_*) + u_{s_*}^2 h_* \frac{\partial u_{s_*}}{\partial x_*} \right] dy_*$$

$$\text{Term B} = I_4 \left\{ \int_0^\infty \left[u_{s_*}^2 \frac{\partial}{\partial y_*} (v_{s_*} h_*)\, dy_* + u_{s_*} v_{s_*} h_* \frac{\partial u_{s_*}}{\partial y_*} dy_* \right] \right\}$$

$$= \frac{I_1}{I_2} \int_0^\infty u_{s_*}^2 \left[\frac{w_e L}{I_1 U_o h_o} + \frac{\partial}{\partial x_*} (u_{s_*} h_*) \right] dy_*$$

$$+ \int_0^\infty \frac{v_{s_*} h_*}{2} \frac{\partial}{\partial y_*} u_{s_*}^2 dy_* \Bigg\}$$

$$= \frac{I_4}{I_3} \left\{ \left(-\frac{I_1}{I_2}\right) \int_0^\infty u_{s_*}^2 \left[\frac{w_e L}{I_1 U_o h_o} + \frac{\partial}{\partial x_*} (u_{s_*} h_*) \right] dy_* \right.$$

$$\left. + \underbrace{\left| \frac{v_{s_*} h_* u_{s_*}^2}{2} \right|_0^\infty}_{\text{zero}} - \frac{1}{2} \int_0^\infty u_{s_*}^2 \frac{\partial}{\partial y_*} v_{s_*} h_* dy_* \right\}$$

$$= \frac{1}{2}\frac{I_4}{I_3}\left\{(-\frac{I_1}{I_2})\int_o^\infty u_{s_*}^2\left[\frac{w_e L}{I_1 U_o h_o} + \frac{\partial}{\partial x_*}(u_{s_*} h_*)\right] dy_*\right\}$$

$$= -\frac{1}{2}\frac{I_4 I_1}{I_3 I_2}\left\{\int_o^\infty u_{s_*}^2\left[\frac{w_e L}{I_1 U_o h_o} + \frac{\partial}{\partial x_*}(u_{s_*} h_*)\right] dy_*\right\}$$

Since u_{s_*} is independent of ξ, Term C could be written as:

$$\text{Term C} = \frac{1}{I_3}\int_o^\infty\int_o^\infty\left(u_{s_*}\frac{\partial}{\partial y_*}\frac{\tau_{xy} h_*}{\rho_a U_o^2}\right) d\xi dy_*$$

and one could reduce Term C to the final form:

$$\text{Term C} = -\frac{1}{I_3}\int_o^\infty\left[\int_o^\infty\left(\frac{\tau_{xy}^*}{\rho_a U_o^2} h_* \frac{\partial u_{s_*}}{\partial y_*}\right) d\xi\right] dy_*$$

Combining the expressions developed for the terms A, B and C, Equation 3.3.8 reduces to the form:

$$\int_o^\infty\left[u_{s_*}^2\frac{\partial}{\partial x_*}(u_{s_*} h_*) + u_{s_*}^2 h_* \frac{\partial u_{s_*}}{\partial x_*}\right] dy_*$$

$$-\frac{1}{2}\frac{I_4 I_1}{I_3 I_2}\left\{\int_o^\infty u_{s_*}^2\left[\frac{w_e L}{I_1 U_o h_o} + \frac{\partial}{\partial x_*}(u_{s_*} h_*)\right] dy_*\right\} =$$

$$-\frac{1}{I_3}\int_o^\infty\left[\int_o^\infty\left(\frac{\tau_{xy}}{\rho_a U_o^2} h_* \frac{\partial u_{s_*}}{\partial y_*}\right) d\xi\right] dy_* \qquad (3.3.9)$$

Equation 3.3.9 could be referred to as the integral energy equation.

3.3.4 An Expression for the Entrainment Velocity w_{em}

Equation 3.3.9 is rewritten to provide an expression for the

entrainment velocity w_e in the z direction as:

$$\int_0^\infty \frac{w_e L}{I_1 U_o h_o} u_{s_*}^2 \, dy_* = \frac{2I_2 I_3}{I_1 I_4} \left[\frac{1}{I_3} \int_0^\infty \left(\int_0^\infty \frac{\tau_{xy}}{\rho_a U_o^2} h_* \frac{\partial u_{s_*}}{\partial y_*} d\xi \right) dy_* \right.$$

$$\left. + \int_0^\infty u_{s_*}^2 h_* \frac{\partial u_{s_*}}{\partial x_*} dy_* + \left(1 - \frac{I_4 I_1}{2 I_3 I_2} \right) \int_0^\infty u_{s_*}^2 \frac{\partial}{\partial x_*} (u_{s_*} h_*) dy_* \right] \quad (3.3.10)$$

To reduce Equation 3.3.10 to a tractable form, let:

$$w_e = w_{em} f\left(\frac{y}{b}\right) = w_{em} f(\eta) \quad (3.3.11)$$

where w_{em} is the vertical component of velocity in the central plane.

$$\frac{\tau_{xy}}{\rho_a U_m^2} = \bar{g}(\eta, \xi) \quad (3.3.12)$$

$$u_{m_*} = k_1 x_*^a \quad (3.3.13)$$

$$b_* = k_2 x_*^n \quad (3.3.14)$$

$$h_* = \frac{h}{h_o} = \frac{h}{h_m} \frac{h_m}{h_o} = f_4(\eta) k_4 x_*^c \quad (3.3.15)$$

where h_m is the central value of h, that is, $h_m = h(y=0)$ and k_1, k_2 and k_4 are independent of x_*.

Using Equations 3.3.11 to 3.3.15 and some of the equations introduced before, and after a considerable amount of algebraic manipulations, Equation 3.3.10 could be reduced to the form:

$$\frac{w_{em}L}{U_o h_o} = \frac{2I_3 I_2}{I_1 I_4 I_9}\left[I_{10}\, x_*^{a+c-n} + x_*^{a+c-1}\,(I_{11} - I_{12} - I_{13} - I_{14} - I_{15})\right] \qquad (3.3.16)$$

or:
$$\frac{w_{em}L}{U_o h_o} = I_{16}\, x_*^{a+c-n} + I_{17}\, x_*^{a+c-1} \qquad (3.3.17)$$

where the integrals I_1 to I_{17} are either constants or simply invariant with x_* and I_9 to I_{17} are defined below:

$$I_9 = \int_o^\infty f f_1^{\,2} d\eta$$

$$I_{10} = \frac{1}{I_3}\int_o^\infty \left[\int_o^\infty \frac{\bar{g}}{} \frac{k_1}{k_2} f_1' f_4 k_4 d\xi\right] d\eta$$

$$I_{11} = \int_o^\infty f_1^{\,3} f_4 k_4 k_1 a d\eta$$

$$I_{12} = \int_o^\infty f_1^{\,2} f_4 f_1' k_4 k_1 n\eta d\eta$$

$$I_{13} = \left(\frac{I_4 I_1}{2I_3 I_2} - 1\right)\int_o^\infty f_1^{\,3} f_4 k_4 c k_1 d\eta$$

$$I_{14} = \left(\frac{I_4 I_1}{2I_3 I_2} - 1\right)\int_o^\infty f_1^{\,3} k_4 f_4 k_1 a d\eta$$

$$I_{15} = \left(\frac{I_4 I_1}{2I_3 I_2} - 1\right)\left[\int_o^\infty f_1^{\,2} k_1 n\,(f_1' f_4 + f_4' f_1)\, k_4 \eta d\eta\right]$$

$$I_{16} = \frac{2I_3 I_2 I_{10}}{I_4 I_9 I_1}$$

$$I_{17} = (I_{11} - I_{12} - I_{13} + I_{14} - I_{15})/(I_4 I_9 I_1 / 2 I_3 I_2$$

3.3.5 An Expression for the Transverse Velocity v_{s_*}

Substituting Equation 3.3.17 for w_{em} into Equation 3.3.1 and simplifying:

$$v_{s_*} = -\frac{k_2}{k_4 f_4}\left\{x_*^{a}\,\frac{I_{16}}{I_2}\int_0^{\infty} f\,d\eta + x_*^{a+n-1} k_4\left[\frac{I_{17}}{I_2}\int_0^{\eta} f\,d\eta + F_1(\eta)\right]\right\} \qquad (3.3.18)$$

where:

$$F_1(\eta) = \left[\int_0^{\eta} f_1 f_4 c k_1\,d\eta + \int_0^{\eta} f_1 f_4 k_1 a\,d\eta - \int_0^{\infty} k_1 n(f_1' f_4 + f_4' f_1)\eta\,d\eta\right]$$

Equation 3.3.18 could be rewritten as:

$$v_{s_*} = F_2(\eta) x_*^{a} + F_3(\eta) x_*^{a+n-1} \qquad (3.3.19)$$

where:

$$F_2(\eta) = -\frac{k_2}{f_4}\,\frac{I_{16}}{I_2}\int_0^{\eta} f(\eta)\,d\eta$$

$$F_3(\eta) = -\frac{k_2}{f_4}\left[\frac{I_{17}}{I_2}\int_0^{\eta} f(\eta)\,d\eta - F_1(\eta)\right]$$

Dividing Equation 3.3.19 by u_{m_*}, one obtains:

$$\frac{v_s}{u_m} = \frac{F_2(\eta)}{k_1} + \frac{F_3(\eta)}{k_1} x_*^{n-1} \qquad (3.3.20)$$

For v_s/u_m to be the same at all x stations, $n = 1$. That is, the jet should expand linearly in the x-y plane. In other words, v_s/u_m will be similar only when the jet expands linearly.

3.3.6 Similarity of the Equations of Motion

The expressions developed in the preceding sections may now be substituted into the equation of motion in the x direction, that is, Equation 3.3.2. Performing this substitution and after some rearrangement, one gets:

$$x_*^{n-1}\left[(2a + c - 1)\, k_1^2 f_1'^2 f_4 - k_1^2 n\eta\, (f_1'^2 f_4)' + \frac{I_4}{I_3}\frac{k_1}{k_2}(f_1 f_4 F_3)'\right] = \frac{1}{I_3}\frac{k_1^2}{k_2}\int_0^\infty (\bar{g} f_4)'\, d\xi - \frac{I_4}{I_3}\frac{k_1}{k_2}(f_1 f_4 F_2)' \qquad (3.3.21)$$

For similarity:

$$x_*^{n-1} \propto x_*^0 \quad \text{or} \quad n = 1$$

Considering the integral momentum equation in the x direction (Equation 3.3.7), it could be rewritten as:

$$\frac{\partial}{\partial x_*}\left(u_{m_*}^{2} h_* b_*\right) \int_0^\infty f_1^{2} f_4 d\eta = 0 \qquad (3.3.22)$$

From Equation 3.3.22:

$$u_{m_*}^{2} h_* b_* \propto x_*^{o} \qquad (3.3.23)$$

or: $$2a + c + n = 0 \qquad (3.3.24)$$

or: $$2a = -(c + 1) \qquad (3.3.25)$$

3.3.7 Similarity of Heat Transport Equations

Assuming:

$$-\overline{v'\Delta T'} = \varepsilon \frac{\partial \Delta T}{\partial y} \qquad (3.3.26)$$

where ε is constant at any x station, that is, independent of η and ξ and on the basis of Prandtl's new theory of turbulence is taken as:

$$\varepsilon = k u_m \sqrt{bh} \qquad (3.3.27)$$

where k is a constant, Equation 3.3.27 reduces to the form:

$$\varepsilon = k k_1 \sqrt{k_2 k_4}\, U_o \sqrt{L h_o}\, x_*^{a + n/2 + c/2} \qquad (3.3.28)$$

Let: $$\Delta T_{m_*} = k_3 x_*^{d} \qquad (3.3.29)$$

where k_3 is another parameter independent of x_* and d is an unknown exponent. In this report, the surface heat transfer term in Equation 3.3.4 has been neglected.

With these assumptions and substituting for the various terms in Equation 3.3.4, the expressions developed in the preceding sections and after some simplifications, one could write:

$$F_4(\eta)x_*^{a+2n-1} + \frac{I_7}{I_8} k_1 k_3 F_5(\eta) x_*^{a+n} = x_*^{a + n/2 + c/2} F_6(\eta,\xi) \qquad (3.3.30)$$

where:

$$F_4(\eta) = k_4 k_1 k_3 \ (a+c+d)(f_1 f_3 f_4) - k_1 k_3 k_4 \ (f_1 f_3 f_4)'$$

$$F_5(\eta) = \frac{I_7}{I_8} k_1 k_3 k_4 \ (F_3 f_3 f_4)'$$

$$F_6(\eta,\xi) = \frac{1}{I_8} k_4 k k_1 \sqrt{k_2 k_4} \ \sqrt{L_o h_o} \ \Delta T_o \int_o^\infty [f_3(\eta) f_3(\xi) f_4(\eta)]'' d\xi$$

From Equation 3.3.30, for similarity, one could write:

$$a + 2n - 1 = a + n = a + \frac{n}{2} + \frac{c}{2} \qquad (3.3.31)$$

from which $n = 1$ and $n = c$. Hence $c = 1$. Using Equation 3.3.25, $a = -1$.

An integral equation for the buoyancy (or heat) flux is obtained by integrating the heat transport equation with respect to y_*

from $y_* = 0$ to $y_* = \infty$. Integrating Equation 3.3.4 after neglecting the surface heat transfer term, one obtains:

$$\int_0^\infty \frac{\partial}{\partial x_*} (u_{s_*} \Delta T_{s_*} h_*)\, dy_* + \frac{I_7}{I_8} \int_0^\infty \frac{\partial}{\partial y_*} (v_{s_*} \Delta T_{s_*} h_*)\, dy_*$$

$$= -\frac{1}{I_8} \int_0^\infty \left(\int_0^\infty \frac{\partial}{\partial y_*} \frac{\overline{v'\Delta T'}}{U_o \Delta T_o} h_* d\xi \right) dy_* \qquad (3.3.32)$$

Interchanging the order of integration, the last term in Equation 3.3.32 could be reduced to zero. After integration, the second term on the left hand side also disappears, leaving the final form of Equation 3.3.32 as:

$$\int_0^\infty \frac{\partial}{\partial x_*} (u_{s_*} \Delta T_{s_*} h_*)\, dy_* = 0$$

or:
$$\frac{d}{dx_*} \int_0^\infty (u_{s_*} \Delta T_{s_*} h_*)\, dy_* = 0 \qquad (3.3.33)$$

Equation 3.3.33 states that the heat flux in the surface jet is constant in the x direction. This equation could again be rewritten as:

$$\frac{d}{dx_*} (u_{m_*} \Delta T_{m_*} b_* x_*^c) \int_0^\infty k_1 k_2 k_3 k_4 f_1 f_3 f_4 d\eta = 0 \qquad (3.3.34)$$

or:
$$x_*^{2+d+n+c} \propto x_*^o \qquad (3.3.35)$$

or:
$$a + d + n + c = 0 \qquad (3.3.36)$$

With $a = -1$, $c = 1$ and $n = 1$, using Equation 3.3.36, $d = -1$.

With all the exponents evaluated, the full set of equations is written as:

$$u_{m_*} \propto \frac{1}{x_*} \quad ; \quad \Delta T_{m_*} \propto \frac{1}{x_*}$$
$$b_* \propto x_* \quad ; \quad h_{m_*} \propto x_* \qquad (3.3.37)$$

or:

$$u_m \propto \frac{1}{x} \quad ; \quad \Delta T_m \propto \frac{1}{x}$$
$$b \propto x \quad ; \quad h_m \propto x \qquad (3.3.38)$$

It should be noted that the exponents for the various scales given in Equations 3.3.37 and 3.3.38 are precisely the same as those for the non-buoyant three dimensional surface jet.

3.4 Surface Discharges with Large Ri

3.4.1 Summary of the Equations for Large Ri

For convenience in further development, relevant equations for surface discharges with large Richardson number are rewritten as:

Continuity Equation

$$\frac{\partial}{\partial x_*}(u_{s_*} h_*) + \frac{I_2}{I_1}\frac{\partial}{\partial y_*}(v_{s_*} h_*) = -\frac{w_e L}{U_o h_o}\frac{1}{I_1} \qquad (3.4.1)$$

Equations of Motion

$$\frac{\partial}{\partial x_*}(u_{s_*}^2 h_*) + \frac{I_4}{I_3}\frac{\partial}{\partial y_*}(u_{s_*} v_{s_*} h_*) =$$

$$-\frac{ag}{\rho_a}\frac{h_o \Delta T_o}{U_o^2}\frac{\partial}{\partial x_*}(\Delta T_{s_*} h_*^2)\frac{I_5}{I_3} \qquad (3.4.2)$$

$$\frac{\partial}{\partial x_*}(u_{s_*} v_{s_*} h_*) + \frac{I_6}{I_4}\frac{\partial}{\partial y_*}(v_{s_*}^2 h_*) =$$

$$-\frac{ag}{\rho_a}\frac{h_o \Delta T_o}{U_o^2}\frac{\partial}{\partial y_*}(\Delta T_{s_*} h_*^2)\frac{I_5}{I_4} \qquad (3.4.3)$$

Equation of Heat Transport

$$\frac{\partial}{\partial x_*}(u_{s_*} \Delta T_{s_*} h_*) + \frac{I_7}{I_8}\frac{\partial}{\partial y_*}(v_{s_*} \Delta T_{s_*} h_*)$$

$$-\frac{1}{I_8}\frac{K_e L}{U_o h_o}\left(\Delta T_{s_*} - \frac{T_e - T_a}{\Delta T_o}\right) = 0 \qquad (3.4.4)$$

3.4.2 Integral Momentum Equation in the x Direction

Equation 3.4.2 is integrated with respect to y_* from $y_* = 0$ to $y_* = \infty$. One obtains:

$$\int_0^\infty \frac{\partial}{\partial x_*}(u_{s_*}^2 h_*)\, dy_* + \frac{I_4}{I_3}\int_0^\infty \frac{\partial}{\partial y_*}(u_{s_*} v_{s_*} h_*)\, dy_* =$$

$$Ri\,\frac{I_5}{I_3}\int_0^\infty \frac{\partial}{\partial x_*}(\Delta T_{s_*} h_*^2)\, dy_* \qquad (3.4.5)$$

Integrating:

$$\frac{d}{dx_*}\int_0^\infty u_{s_*}^2 h_* dy_* + \frac{I_4}{I_3}\left| u_{s_*} v_{s_*} h_* \right|_0^\infty =$$

$$\frac{I_5}{I_3} Ri \frac{d}{dx_*}\int_0^\infty \Delta T_{s_*} h_*^2 dy_* \qquad (3.4.6)$$

which reduces to:

$$\frac{d}{dx}\int_0^\infty u_{s_*}^2 h_* dy_* = \frac{I_5}{I_3} Ri \frac{d}{dx}\int_0^\infty \Delta T_{s_*} h_*^2 dy_* \qquad (3.4.7)$$

Equation 3.4.7 is further reduced to:

$$\frac{d}{dx}\left[x_*^{(2a+c+n)} k_1^2 k_2 k_4 I_{18}\right] =$$

$$\frac{I_5}{I_3} Ri \frac{d}{dx_*}\left[x_*^{(2c+d+n)} k_2 k_3 k_4^2 I_{19}\right]$$

or: $$k_1^2 k_2 k_4 I_{18} \frac{d}{dx} x_*^{2a+c+n} = k_2 k_3 k_4^2 \frac{I_5}{I_3} I_{19} Ri \frac{d}{dx_*} x_*^{2c+d+n} \qquad (3.4.8)$$

where: $$I_{18} = \int_0^\infty f_1^2(\eta) f_4(\eta) d\eta \quad \text{and} \quad I_{19} = \int_0^\infty f_3(\eta) f_4^2(\eta) d\eta$$

From Equation 3.4.8, one could write:

$$2a + c + n - 1 = 2c + d + n - 1 \qquad (3.4.9)$$

or: $$2a = c + d \qquad (3.4.10)$$

3.4.3 Integral Heat Transport Equation

Neglecting the surface heat transfer term and integrating the remaining terms of Equation 3.4.4 with respect to y_* from $y_* = 0$ to $y_* = \infty$, one gets:

$$\int_0^\infty \frac{\partial}{\partial x_*} (u_{s_*} \Delta T_{s_*} h_*) \, dy_* + \frac{I_7}{I_8} \int_0^\infty \frac{\partial}{\partial y_*} (v_{s_*} \Delta T_{s_*} h_*) \, dy_* = 0 \qquad (3.4.11)$$

which could be reduced to:

$$k_1 k_2 k_3 k_4 I_{20} \frac{d}{dx_*} x_*^{a+c+d+n} = 0$$

where: $$I_{20} = \int_0^\infty f_1(\eta) f_3(\eta) f_4(\eta) d\eta$$

or: $$\frac{d}{dx_*} x_*^{a+c+d+n} = 0 \qquad (3.4.12)$$

resulting in the following equation for the unknown exponents:

$$a + c + d + n = 0 \qquad (3.4.13)$$

Using Equation 3.4.10, one could reduce Equation 3.4.13 to:

$$3a + n = 0 \qquad (3.4.14)$$

or $a = - n/3$.

3.4.4 An Expression for w_{em} and v_s

In an attempt to solve for the unknown exponents, one could

obtain an integral of the y momentum equation. But for obtaining this integral in an usable form, an expression for v_{s_*} is needed. This is developed in this section using the integral energy equation and integral continuity equations.

Multiplying Equation 3.4.2 by u_{s_*} and integrating with respect to y_* from $y_* = 0$ to $y_* = \infty$:

$$\int_0^\infty u_{s_*} \frac{\partial}{\partial x_*} (u_{s_*}^2 h_*)\, dy_* + \frac{I_4}{I_3} \int_0^\infty u_{s_*} \frac{\partial}{\partial y_*} (u_{s_*} v_{s_*} h_*)\, dy_*$$

$$= \frac{I_5}{I_3} Ri \int_0^\infty [illegible]_* \frac{\partial}{\partial x_*} (\Delta T_{s_*} h_*^2)\, dy_* \qquad (3.4.15)$$

Integrating by using Equation 3.4.1 and simplifying, Equation 3.4.15 is reduced to:

$$-\int_0^\infty \frac{w_e}{U_o} u_{s_*}^2 \frac{L}{h_o}\, dy_* = \frac{2I_2 I_3}{I_1 I_4} \left\{ \frac{I_5}{I_3} Ri \right.$$

$$\left[\int_0^\infty \frac{\partial}{\partial x_*} (u_{s_*} \Delta T_{s_*} h_*^2)\, dy_* - \int_0^\infty \Delta T_{s_*} h_* \frac{\partial}{\partial x_*} u_{s_*}\, dy_* \right]$$

$$+ \left(\frac{I_4 I_1}{2I_2 I_3} - 1\right) \int_0^\infty u_{s_*}^2 \frac{\partial}{\partial x_*} (u_{s_*} h_*)\, dy_*$$

$$\left. - \int_0^\infty u_{s_*}^2 h_* \frac{\partial}{\partial x_*} u_{s_*}\, dy_* \right\} \qquad (3.4.16)$$

One could further reduce Equation 3.4.16 to the form:

$$-\frac{w_{em}}{U_o} \frac{L}{h_o} = x_*^{a+c-1} \left(I_{17} + \frac{I_{23}}{I_9 k_1 k_2}\right) \qquad (3.4.17)$$

where:

$$I_{23} = \frac{I_5}{I_3} \text{ Ri } k_1 k_2 k_3 \left[(a+d+n+2c)\, I_{21} - I_{22} - n\right]$$

$$I_{21} = \int_0^{\eta} f_3(\eta) f_4(\eta) d\eta$$

$$I_{22} = \int_0^{\eta} f_3(\eta) f_4^{\,2}(\eta) f_1(\eta) d\eta$$

Using Eq. 3.4.17, the integral continuity equation could be reduced to the f

$$= x_*^{a+n-1} F_7 \qquad (3.4.18)$$

where:

$$F_7(\eta) = \left[\left(I_{17} + \frac{I_{14}}{I_9 k_1 k_2}\right) \frac{1}{I_2} \frac{k_2}{k_4} \frac{1}{f_4(\eta)} \int_0^{\eta} f d\eta - \frac{k_1 k_2 I_1}{I_2} \frac{1}{f_4(\eta)} \int_0^{\eta} f_1(\eta) f_4(\eta) d\eta\right]$$

3.4.5 Integral Momentum Equation in the y Direction

Integrating the momentum equation in the y direction from $y_* = 0$ to $y_* = \infty$:

$$\int_0^{\infty} \frac{\partial}{\partial x_*} (u_{s_*} v_{s_*} h_*)\, dy_* + \frac{I_6}{I_4} \int_0^{\infty} \frac{\partial}{\partial y_*} (v_{s_*}^{\,2} h_*)\, dy_* = \frac{I_5}{I_4} \text{Ri} \int_0^{\infty} \frac{\partial}{\partial y_*} (\Delta T_{s_*} h_*^{\,2})\, dy_* \qquad (3.4.19)$$

Integrating and simplifying with the substitution of Equation 3.4.18:

$$\frac{d}{dx_*}\int_0^\infty u_{s_*} v_{s_*} h_* dy_* + \frac{I_6}{I_4}\left| v_{s_*}^2 h_* \right|_0^\infty =$$

$$\frac{I_5}{I_4}\ Ri\left| \Delta T_{s_*} h_*^2 \right|_0^\infty$$

or:
$$k_1 k_2 k_4 \int_0^\infty f_1(\eta) f_4(\eta) F_7 d\eta \frac{d}{dx}\left(x_*^{2a+c+2n-1}\right) +$$

$$\frac{I_6}{I_4}\ (F_7)_\infty^2\ f_4(\infty) k_4 x_*^{2a+c+2n-2} = -\frac{I_5}{I_4}\ Ri\ k_3 k_4^2 x_*^{2c+d} \qquad (3.4.20)$$

From Equation 3.4.20, one gets:

$$2a + c + 2n - 2 = 2c + d \qquad (3.4.21)$$

or:
$$2a + 2n - 2 = c + d \qquad (3.4.22)$$

Using Equation 3.4.10:

$$2(n - 1) = 0 \qquad (3.4.23)$$

which gives the result $n = 1$. With Equation 3.4.14, $a = -1/3$. Equation 3.4.10 indicates $c + d = -2/3$.

It does not appear to be possible to obtain the value of the exponent c, but experiments for large values of Ri indicate that $c \simeq 0$. Taking c as zero, $d = -2/3$. Hence, for surface discharges

with large Richardson number, one has:

$$u_{m_*} \propto \frac{1}{x_*^{1/3}} \quad ; \quad \Delta T_{m_*} \propto \frac{1}{x_*^{-(2/3 + c)}}$$
$$b_* \propto x_* \quad ; \quad h_* \propto x_*^{c} \qquad (3.4.24)$$

From Equation 3.4.24 one finds that the decay of centerline temperature depends upon c which is the exponent of x assigned for the variation of depth h, whereas the decay of centerline velocity does not depend upon c. However, the decay of centerline velocity and temperature should be closely linked. Thus if the decay of u_m does not depend upon c the value of ΔT_m also should not depend upon c. The only way this is possible is that the value of $c = 0$. Thus assuming $c = 0$, Equation 3.4.24 reduces to:

$$u_{m_*} \propto \frac{1}{x_*^{1/3}} \quad ; \quad \Delta T_{m_*} \propto \frac{1}{x_*^{2/3}}$$
$$b_* \propto x_* \qquad h_* = \text{constant} \qquad (3.4.25)$$

or:

$$u_m \propto \frac{1}{x^{1/3}} \quad ; \quad \Delta T_m \propto \frac{1}{x^{2/3}}$$
$$b \propto x \qquad h_m = \text{constant} \qquad (3.4.26)$$

3.4.6 Solution of Equations of Motion for Velocity and Temperature Distributions

For surface discharges with large Richardson number ($Rf \gtrsim 1$)

the growth in the z direction appears to be negligible. It may be assumed that the thickness of the jet in the z direction is constant and equals h_o. Further, if as an approximation, one assumes that the distribution of the velocity and temperature in the z direction is uniform, then the distribution of the velocity and temperature could be predicted in the y direction as shown in this section.

The relevant equations of motion are written as below:

Continuity Equation

$$\frac{\partial u_{s_*}}{\partial x_*} + \frac{\partial v_{s_*}}{\partial y_*} = 0 \qquad (3.4.27)$$

Equations of Motion in the x and y directions (after integration in the z direction)

$$u_{s_*} \frac{\partial u_{s_*}}{\partial x_*} + v_{s_*} \frac{\partial u_{s_*}}{\partial y_*} = \frac{1}{2} Ri \frac{\partial \Delta T_{s_*}}{\partial x_*} \qquad (3.4.28)$$

$$u_{s_*} \frac{\partial v_{s_*}}{\partial x_*} + v_{s_*} \frac{\partial v_{s_*}}{\partial y_*} = \frac{1}{2} Ri \frac{\partial \Delta T_{s_*}}{\partial y_*} \qquad (3.4.29)$$

Equation of Heat Transport

$$\frac{\partial}{\partial x_*} u_{s_*} \Delta T_{s_*} + \frac{\partial}{\partial y} v_{s_*} \Delta T_{s_*} = 0 \qquad (3.4.30)$$

A dimensionless stream function, ψ_*, is now defined by:

$$u_{s_*} = \frac{\partial \psi_*}{\partial y_*} \qquad (3.4.31a)$$

and $$v_{s_*} = -\frac{\partial \psi_*}{\partial x_*} \qquad (3.4.31b)$$

Integrating Equation 3.4.31a:

$$\psi_* = \int_0^{y_*} u_{s_*} dy_* = u_{m_*} b_* \int_0^{\eta} f_1(\eta) d\eta$$

or: $$\psi_* = u_{m_*} b_* J_1(\eta) \qquad (3.4.32)$$

where: $$J_1(\eta) = \int_0^{\eta} f_1(\eta) d\eta$$

It is to be noted that $J_1'(\eta) = f_1(\eta)$, where the prime on J_1 denotes differentiation with respect to η. Using Equation 3.4.31b, it can be shown that:

$$v_{s_*} = k_1 k_2 \left[\eta J_1'(\eta) - \frac{2}{3} J_1(\eta)\right] x_*^{-1/3} \qquad (3.4.33)$$

Next, the following expressions are developed for substitution into Equations 3.4.28 and 3.4.29:

$$u_{s_*} \frac{\partial u_{s_*}}{\partial x_*} = -k_1^2 x_*^{-5/3} \left[\frac{1}{3} J_1'(\eta)^2 + \eta J_1'(\eta) J_1''(\eta)\right]$$

$$v_{s_*} \frac{\partial u_{s_*}}{\partial y_*} = k_1^2 x_*^{-5/3} \left[\eta J_1'(\eta) J_1''(\eta) - \frac{2}{3} J_1(\eta) J_1''(\eta)\right]$$

$$\frac{\partial}{\partial x_*} \Delta T_{s_*} = -k_3 x_*^{-5/3} \left[\frac{2}{3} f_3(\eta) + \eta f_3'(\eta)\right]$$

$$u_{s_*} \frac{\partial v_{s_*}}{\partial x_*} = k_1^2 k_2 f_1(\eta) x_*^{-5/3} \left[\frac{2}{9} J_1(\eta) - \frac{2}{3} \eta J_1'(\eta) - \eta^2 J_1''(\eta)\right] \qquad (3.4.34)$$

$$v_{s_*} \frac{\partial v_{s_*}}{\partial y_*} = k_1^2 k_2 x_*^{-5/3} \left[\eta J_1'(\eta) - \frac{2}{3} J_1(\eta)\right] \cdot \left[\frac{1}{3} J_1'(\eta) + \eta J_1''(\eta)\right]$$

$$\frac{\partial}{\partial y_*} \Delta T_{s_*} = \frac{k_3}{k_2} x_*^{-5/3} f_3'(\eta)$$

Substituting the relevant expressions into Equations 3.4.28 and 3.4.29, one obtains:

$$\frac{k_1^2}{3} [J_1'^2(\eta) + 2J_1(\eta)J_1''(\eta)] = \frac{1}{2} Ri \; k_3 \left[\frac{2}{3} f_3(\eta) + \eta f_3'(\eta)\right] \qquad 3.4.35)$$

and: $$-\frac{1}{3} k_1^2 k_2 [\eta J_1'^2(\eta) + 2\eta J_1(\eta) J_1''(\eta)] = \frac{Ri}{2} \frac{k_3}{k_2} f_3'(\eta) \qquad (3.4.36)$$

Dividing Equation 3.4.35 by Equation 3.4.26 and simplifying:

$$k_2^2 \eta \left[\frac{2}{3} f_3(\eta) + \eta f_3'(\eta)\right] + f_3'(\eta) = 0 \qquad (3.4.37)$$

or: $$\frac{f_3'(\eta)}{f_3(\eta)} = \frac{-\frac{2}{3} k_2^2 \eta}{1 + k_2^2 \eta^2} \qquad (3.4.38)$$

Integrating and simplifying, one obtains:

$$f_3(\eta) = \frac{C_1}{(1 + k_2^2 \eta^2)^{1/3}} \tag{3.4.39}$$

where C_1 is a constant of integration, which can be seen to be unity because of the boundary condition $f_3(o) = 1$. Hence, the temperature distribution is written as:

$$\frac{\Delta T_{s_*}}{\Delta T_{m_*}} = f_3(\eta) = \frac{1}{(1 + k_2^2 \eta^2)^{1/3}} \tag{3.4.40}$$

To solve for the velocity distribution function $f_1(\eta)$, the procedure used previously is applied so that Equation 3.4.30 could be reduced to the form:

$$-\frac{2}{3} x_*^{-2} k_1 k_3 [f_3(\eta) J_1'(\eta) + J_1(\eta) f_3'(\eta)] = 0 \tag{3.4.41}$$

or: $$f_3(\eta) J_1'(\eta) + J_1(\eta) f_3'(\eta) = 0$$

or: $$\frac{d}{d\eta} [f_3(\eta) J_1(\eta)] = 0 \tag{3.4.42}$$

Integrating:

$$f_3(\eta) J_1(\eta) = C_2 \tag{3.4.43}$$

where C_2 is a constant of integration. Using Equation 3.4.40 for $f_3(\eta)$, one could show that:

$$f_1(\eta) = \frac{2}{3} C_2 k_2^2 \frac{\eta}{(1 + k_2^2 \eta^2)^{2/3}} \qquad (3.4.44)$$

In this particular form, it is not possible to satisfy the important boundary condition of $f_1(o) = 1.0$. Hence, Equation 3.4.44 is left in this incomplete form.

3.5 Surface Discharges with Moderate Ri

3.5.1 Summary of the Equations for Moderate Ri

For the convenience of further development, equations governing the behaviour of surface discharges with moderate Richardson number are reproduced below:

Continuity Equation

$$\frac{\partial}{\partial x_*} (u_{s_*} h_*) + \frac{I_2}{I_1} \frac{\partial}{\partial y_*} (v_{s_*} h_*) = - \frac{w_e L}{U_o h_o} \frac{1}{I_1} \qquad (3.5.1)$$

Equations of Motion

$$\frac{\partial}{\partial x_*} (u_{s_*}^2 h_*) + \frac{I_4}{I_3} \frac{\partial}{\partial y_*} (u_{s_*} v_{s_*} h_*) = 0 \qquad (3.5.2)$$

$$\frac{\partial}{\partial x_*} (u_{s_*} v_{s_*} h_*) + \frac{I_6}{I_4} \frac{\partial}{\partial y_*} (v_{s_*}^2 h_*) =$$

$$- \frac{\alpha g}{\rho_a} \frac{h_o \Delta T_o}{U_o^2} \frac{\partial}{\partial y_*} (\Delta T_{s_*} h_*^2) \frac{I_5}{I_4} \qquad (3.5.3)$$

Equation of Heat Transport

$$\frac{\partial}{\partial x_*}\left(u_{s_*}\Delta T_{s_*} h_*\right) + \frac{I_7}{I_8}\frac{\partial}{\partial y_*}\left(v_{s_*}\Delta T_{s_*} h_*\right) = 0 \qquad (3.5.4)$$

wherein the surface heat transfer term has been dropped.

3.5.2 Integral Momentum Equation in the x Direction

Using our earlier results of articles 3.3 and 3.4, one could write the equation of motion in the x direction integrated with respect to y_* from $y_* = 0$ to $y_* = \infty$ for the moderate Richardson number as:

$$\frac{d}{dx_*}\int_0^\infty u_{s_*}^2 h_* dy_* = 0 \qquad (3.5.5)$$

or:
$$\frac{d}{dx_*}\left\{x_*^{(2a+c+n)}\left[k_1^2 k_2 k_4 \int_0^\infty f_1'^2(\eta) f_4(\eta) d\eta\right]\right\} = 0 \qquad (3.5.6)$$

From Equation 3.5.6, one could write:

$$2a + c + n = 0 \qquad (3.5.7)$$

3.5.3 Integral Momentum Equation in the y Direction

Using the earlier results in articles 3.3 and 3.4, one could write the following expressions:

$$\frac{w_e L}{U_o h_o} = I_{17}\, x_*^{a+c-1} \tag{3.5.8}$$

$$v_{s_*} = F_3(\eta)\, x_*^{a+n-1} \tag{3.5.9}$$

where: $$F_3(\eta) = -\frac{k_2}{f_4}\left[\frac{I_{17}}{I_2}\int_o^\eta f d\eta + F_1(\eta)\right]$$

The integral y direction equation becomes:

$$\frac{d}{dx}\int_o^\infty u_{s_*} v_{s_*} h_* dy_* + \frac{I_6}{I_4}\left| v_{s_*}^2 h_* \right|_o^\infty =$$

$$\frac{I_5}{I_4} Ri \left| \Delta T_{s_*} h_*^2 \right|_o^\infty \tag{3.5.10}$$

Equation 3.5.10 is further reduced to:

$$\left[k_1 k_2 k_4 \int_o^\infty f_1(\eta) f_4(\eta) F_3(\eta) d\eta\right] \frac{d}{dx}\left(x_*^{2a+c+2n-1}\right) +$$

$$\left[\frac{I_6}{I_4} F_3^2(\infty) f_4(\infty) k_4\right] x_*^{2a+c+2n-2} =$$

$$\left[-\frac{I_5}{I_4} Ri\, k_3 k_4^2\right] x_*^{2c+d} \tag{3.5.11}$$

From Equation 3.5.11, one gets:

$$2a + c + 2n - 2 = 2c + d \tag{3.5.12}$$

3.5.4 Integral Heat Transport Equation

Since Equation 3.5.4 is the same as Equation 3.4.4, the result of integrating Equation 3.5.4 with respect to y_* from $y_* = 0$ to $y_* = \infty$ could be reproduced from article 3.4 as:

$$\frac{d}{dx_*}\int_0^\infty (u_{s_*}\Delta T_{s_*} h_*)dy_* + \frac{I_7}{I_8}\int_0^\infty \frac{\partial}{\partial y_*}(v_{s_*}\Delta T_{s_*} h_*)dy_* = 0 \qquad (3.5.13)$$

Equation 3.5.13 reduces to:

$$\frac{d}{dx_*}\int_0^\infty u_{s_*}\Delta T_{s_*} h_* dy_* = 0 \qquad (3.5.14)$$

which could be further reduced to:

$$\frac{d}{dx_*} x_*^{a+c+d+n} = 0 \qquad (3.5.15)$$

from which:

$$a + c + d + n = 0 \qquad (3.5.16)$$

3.5.5 Solution for the Exponents

There are four unknown exponents a, b, c and d, but only three independent equations (Equations 3.5.7, 3.5.12 and 3.5.16) have so far been developed. Similarity analysis of Equations 3.5.2, 3.5.3 and 3.5.4 does not yield any new equation. As a result, one of the four

exponents will remain unknown. Let c be the unknown exponent. Solving Equations 3.5.7, 3.5.12 and 3.5.16, one gets:

$$a = -\left(\frac{2}{3} + c\right) \quad ; \quad d = -\left(\frac{2}{3} + c\right) \quad ; \quad n = \left(\frac{4}{3} + c\right) \tag{3.5.17}$$

If $c = 0$, then:

$$a = -\frac{2}{3} \quad ; \quad d = -\frac{2}{3} \quad ; \quad n = \frac{4}{3} \tag{3.5.18}$$

If $c = 1$, then:

$$a = -\frac{5}{3} \quad ; \quad d = -\frac{5}{3} \quad ; \quad n = \frac{7}{3} \tag{3.5.19}$$

3.6 Summary of Conclusions and Comments

In this chapter, the hydraulics of surface thermal discharges have been studied. By performing an order of magnitude study of the relevant equations of motion, it has been possible to divide the flow into three regimes referred to as small, moderate or large Richardson number (Ri) flows. Then assuming that the velocity and excess temperature profiles are similar in the depth (or z) direction, the reduced equations have been integrated in the z direction. These integral equations were analysed and were also further integrated in the lateral (or y) direction assuming similarity of the velocity and excess temperature profiles in that direction.

A similarity analysis of these equations has shown that for small Richardson number, the scales for velocity (u_m), excess temperature (ΔT_m), lateral width (b), and depth (h) are given as:

$$u_m \propto \frac{1}{x} \tag{3.6.1a}$$

$$\Delta T_m \propto \frac{1}{x} \tag{3.6.1b}$$

$$b \propto x \tag{3.6.1c}$$

$$h_m \propto x \tag{3.6.1d}$$

where x is the longitudinal distance from the outlet (or the relevant virtual origin).

For large Richardson numbers, assuming that $h \propto x^o$, it has been found that:

$$u_m \propto \frac{1}{x^{1/3}} \tag{3.6.2a}$$

$$\Delta T_m \propto \frac{1}{x^{2/3}} \tag{3.6.2b}$$

$$b \propto x \tag{3.6.2c}$$

For moderate Richardson number, the variation of h with longitudinal distance x could not be predicted. If $h_m \propto x^c$, then:

$$u_m \propto \frac{1}{x^{2/3 + c}} \quad ; \quad \Delta T_m \propto \frac{1}{x^{2/3 + c}} \quad ; \quad b \propto x^{4/3 + c} \qquad (3.6.3)$$

If $c = 1$, Equation 3.6.3 reduces to:

$$u_m \propto \frac{1}{x^{5/3}} \qquad (3.6.4a)$$

$$\Delta T_m \propto \frac{1}{x^{5/3}} \qquad (3.6.4b)$$

$$b \propto x^{7/3} \qquad (3.6.4c)$$

If $c = 0$, Equation 3.6.3 reduces to:

$$u_m \propto \frac{1}{x^{2/3}} \qquad (3.6.5a)$$

$$\Delta T_m \propto \frac{1}{x^{2/3}} \qquad (3.6.5b)$$

$$b \propto x^{4/3} \qquad (3.6.5c)$$

CHAPTER 4

LABORATORY EQUIPMENT AND METHODS

4.1 General

The laboratory experiments were performed in a model basin at the T. Blench Hydraulics Laboratory at the University of Alberta. The experimental objectives have been described in article 2.16.2.

4.2 Experimental Equipment

4.2.1 Model Basin and Flow System

The model basin was a 50 ft. long, non-circulating basin, 15'-0" wide and 2'-0" deep with a horizontal floor. A general view is shown in Figure 4.1. The basin walls were constructed from 6" wide hollow concrete blocks mortared to the floor. The thermal effluent was let into the basin by a head canal 5'-0" long, 1'-4" wide and 1'-4" deep. Different shaped outlets could be fixed in this head canal. The inlet to the canal was 2'-0" deep and water rose in it from the bottom and then passed over a V notch where the discharge could be measured accurately. A 2" diameter telescopic pipe for overflow was fixed in this chamber to maintain constant head over the V notch.

At the basin outlet, the water flowed over 3'-7" long and 8" deep tail gates. These were constructed from marine plywood and their height was adjustable. The tailgates rested on 8" high 6" wide concrete walls fixed to the floor. A 6" diameter pipe was fixed at the floor

FIGURE 4.1 GENERAL VIEW OF THE BASIN

below the tailgates to dewater the basin. The water over the tailgate or through the pipe passed on to the sump. The basin could be filled with water either from a laboratory sump through a 6" overhead pipe or from the city water supply.

Sometimes the plume was found to meander or veer to one side. To counter this and make the flow central, 1/2 inch diameter holes were made on the side wall of the basin 16 inches above the floor and 7 ft. and 9 ft. away from the inlet. These holes were connected to a copper pipe leading to the drain. The holes could be made to flow or not depending on the requirements of flow conditions.

4.2.2 Water Heater for Generating Thermal Effluent

The heated discharge was supplied from a water heater (Delta Hot Water Blast Cleaning System, Delta Manufacturing and Engineering Corporation, Deltas, Texas). This had a burner input of 900,000 Btu and, coupled with a pump, had a capacity of up to 60 gallons per minute of water at a constant temperature of up to 130°F. A flexible hose connected the water boiler to the inlet of the canal. A schematic diagram of the hot water discharge system is shown in Figure 4.2.

4.2.3 Cooling Water Supply

Without the supply of cooling water, steady state conditions could be attained only when the temperature of the entire lake, from inlet to outlet, becomes equal since the evaporation from the surface jet was negligibly small. Stolzenbach and Harleman (1971) passed a cold water discharge of 50 gallons/min in their tank, irrespective of the

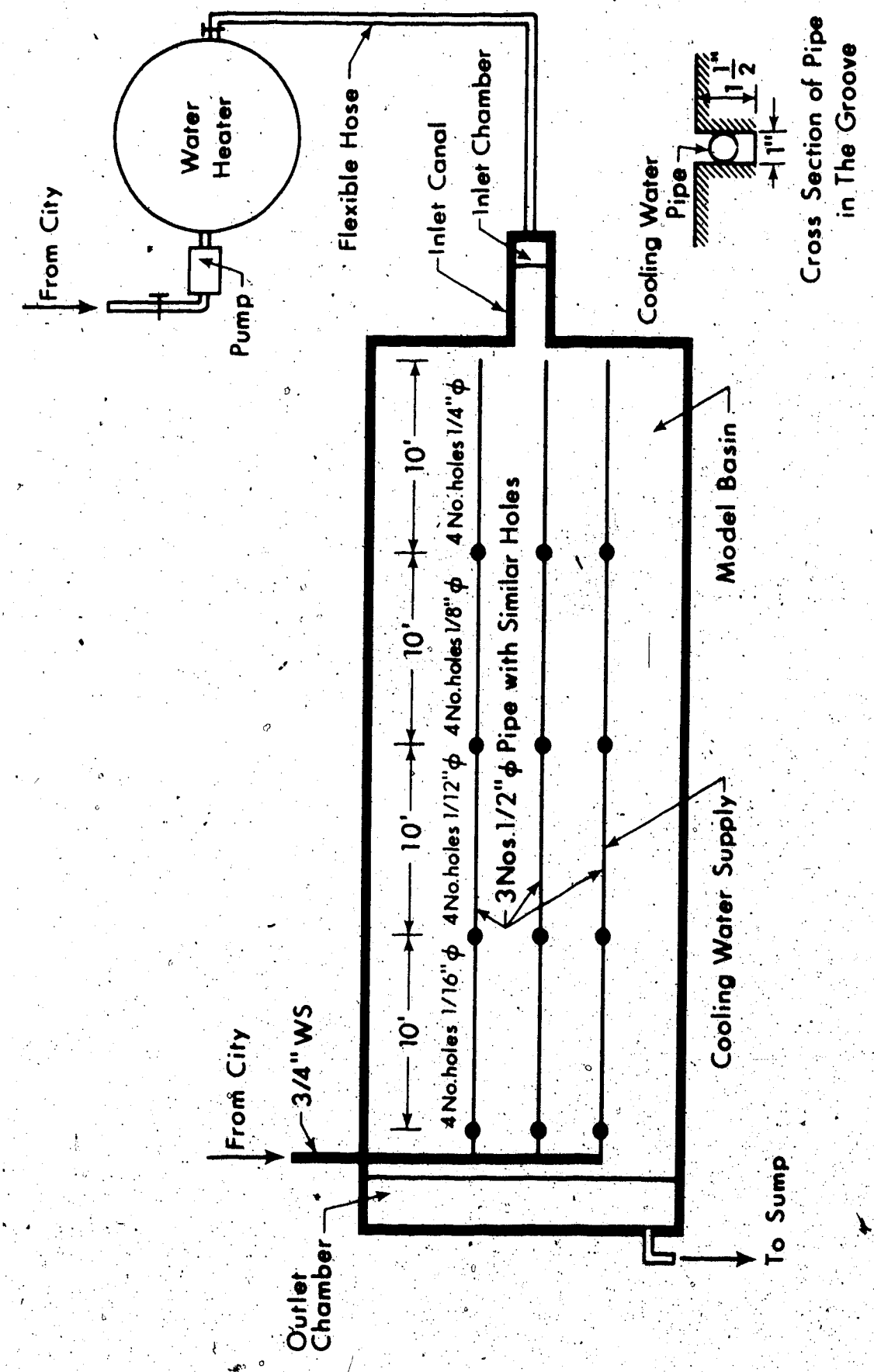

FIGURE 4.2 SCHEMATIC DIAGRAM OF HOT WATER DISCHARGE SYSTEM

inflow discharge of heated water. Stefan (1970) does not mention the quantity of cold water discharge passed through the tank. The amount of cold water to be discharged in the present case was obtained by doing preliminary experiments to establish steady state conditions in the flume. A dicharge of 0.05 cusecs of cold water satisfied this requirement for all the runs. This cold water was discharged through three copper pipes (1/2" diameter placed 4 ft. c/c) running along the length of the basin. These pipes were placed in 1.5" wide and 1" deep groove made in the floor, with the holes in the pipes pointing downwards. This arrangement is shown in Figure 4.2. The cooling water first flowed downwards, and then had to rise up and gently spread on the floor. The excess outlet temperature varied from 2.5°F for smaller discharges to 4.5°F for larger discharges through the inlet. Steady state conditions were obtained in all the runs. Experimental measurements were confined only to the first quarter length of the flume, and an injection of dye showed a clearly defined jet regime in this length.

4.2.4 Experimental Instrumentation

The instrumentation was developed for (1) simultaneous determination of temperature of water at various points, and (2) velocity of water at a given location

4.3 Instrumentation for Thermal Measurements

4.3.1 Thermistor Probes

The temperature of the heated jet was measured by an array of

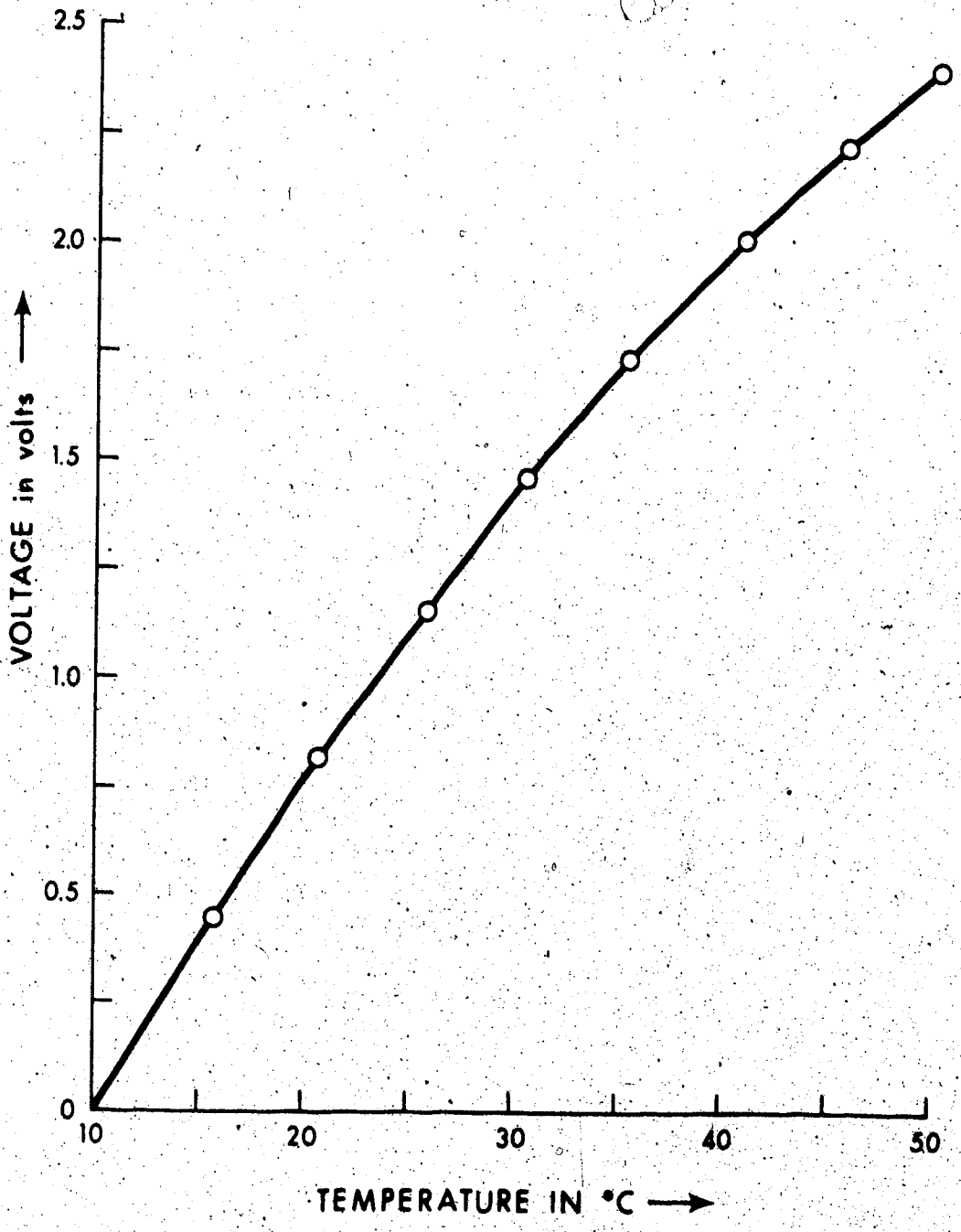

FIGURE 4.3 TYPICAL CALIBRATION CURVE

thermistor probes. Thermistors are resistors with a high negative temperature coefficient of resistance. As the temperature increases, the resistance goes down and vice versa. They are manufactured from semi-conductor materials made by sintering mixtures of metallic oxides such as manganese, nickel, cobolt, copper, iron and uranium.

The thermistors used in the present experiment were glass probe thermistors supplied by Fennel Electronics. The specifications for these are given in Appendix B.

4.3.2 Probe Calibration

Calibration was carried out in a water bath. The bath temperature was measured by a "Quartz thermometer", model HP-2801A. Such thermometers monitor the frequency changes of quartz crystal oscillation. Because the quartz thermometer converts temperature into frequency rather than into resistance or voltage, it was free of the problem of lead resistance and noise pickup inherent in other types of temperature measuring systems. The thermometer can read to a resolution of 0.001°C. A typical calibration curve for the thermistors is given in Figure 4.3.

4.3.3 Mounting of Thermistor Probes

Sixteen thermistor probes were used in the present experiments. Fourteen of these were mounted on a rake trolly. The remaining two were mounted at the inlet and outlet of the basin.

The rake trolly was powered by a D.C. electric motor and could be moved in the lateral and vertical directions. To allow positioning along the jet, this trolly was mounted on another trolly which could be shifted manually in the longitudinal direction. The location of the rake was sensed electronically and the coordinates x, y and z punched on the paper tape along with thermistor probe readings.

The probes were mounted on brass tubes spaced 3" c/c. Limit switches were installed in both lateral and vertical directions for safe operation of the thermistor probes mounted on rakes.

4.3.4 Data Acquisition System

The thermistor leads were connected to a thermistor conditioner which in turn was connected to the following elements:

1. 100 Channel Scanner - Digitec Model 635.
   (United Systems Corporation)
2. Scan Counter.
3. Integrating Digital Voltmeter.
   (Hewlett Packard 3480B Digital Voltmeter)
4. Punch Controller.
   (United Systems Corporation - Model 623)
5. Papertape Punch.
   (United Systems Corporation - Model 671)

A general view of the data acquisition system is shown in Figure 4.4a.

Each thermistor was assigned to a particular channel scanner. In addition x, y and z cordinates were also assigned a channel each. The scanner sequentially sampled from 0 to 19, routing the analogue signal to an analogue/digital converter where they were digitized and

FIGURE 4.4a

GENERAL VIEW OF DATA ACQUISITION SYSTEM

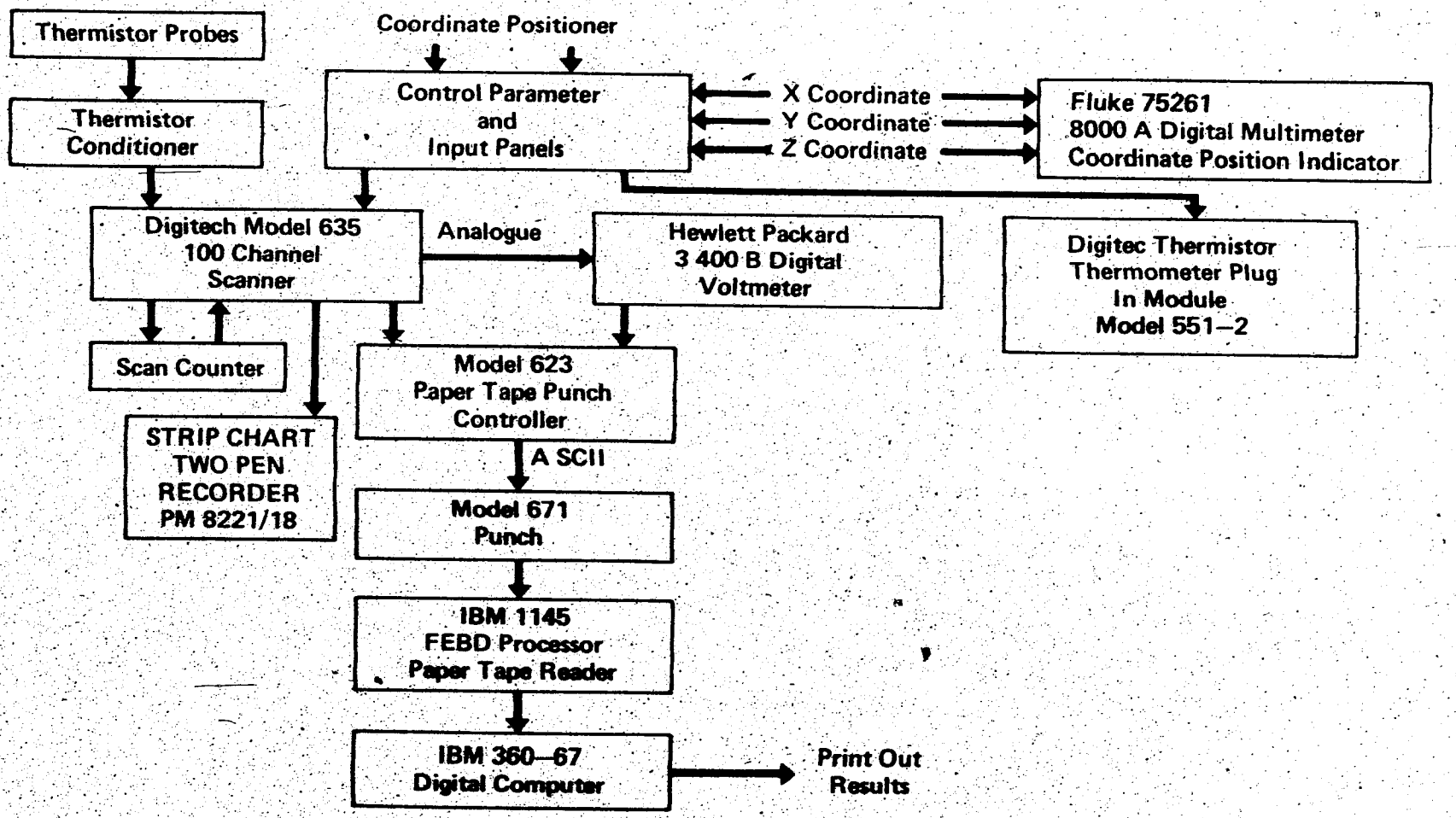

FIGURE 4.4(b) DATA ACQUISITION AND PROCESSING SYSTEM

converted to binary coded decimal (BCD) signals. The papertape punch controller formated the BCD signal to ASCII (American Standard Code for Information Interchange) and routed it to the papertape punch. The papertape was then read by 1145FEBD processor tape reader and data was recorded in a computer file.

The scan counter was set for 10 cycles. The scanner therefore went through all channels 10^0 times before each reading.

4.3.5 Reduction of Data to Temperature

An equation for the calibration curve was worked out by a nonlinear least square fit to the data. Each of the voltage readings was first converted into corresponding temperature and their mean and standard deviation determined thereafter. The error in measurement arising due to nonlinearity in calibration has thus been avoided.

4.3.6 Strip Chart Recorder

The first two thermistors on the rake were also connected to a Two Pen Strip Chart Recorder. The pen recorder used was type PM 8221/18. It had a range from 5 mv to 20v and a chart speed from 2 cm/hr to 18 cm/min. The recorder permits continuous recording of temperature at any point. Temperature fluctuation at a point can thus be easily measured by this recorder. Whether or not steady state conditions existed throughout the experiment could be verified by taking a continuous record at a given point. An example is shown in Figure 4.5. The recorder was manufactured by Phillips-Denmark.

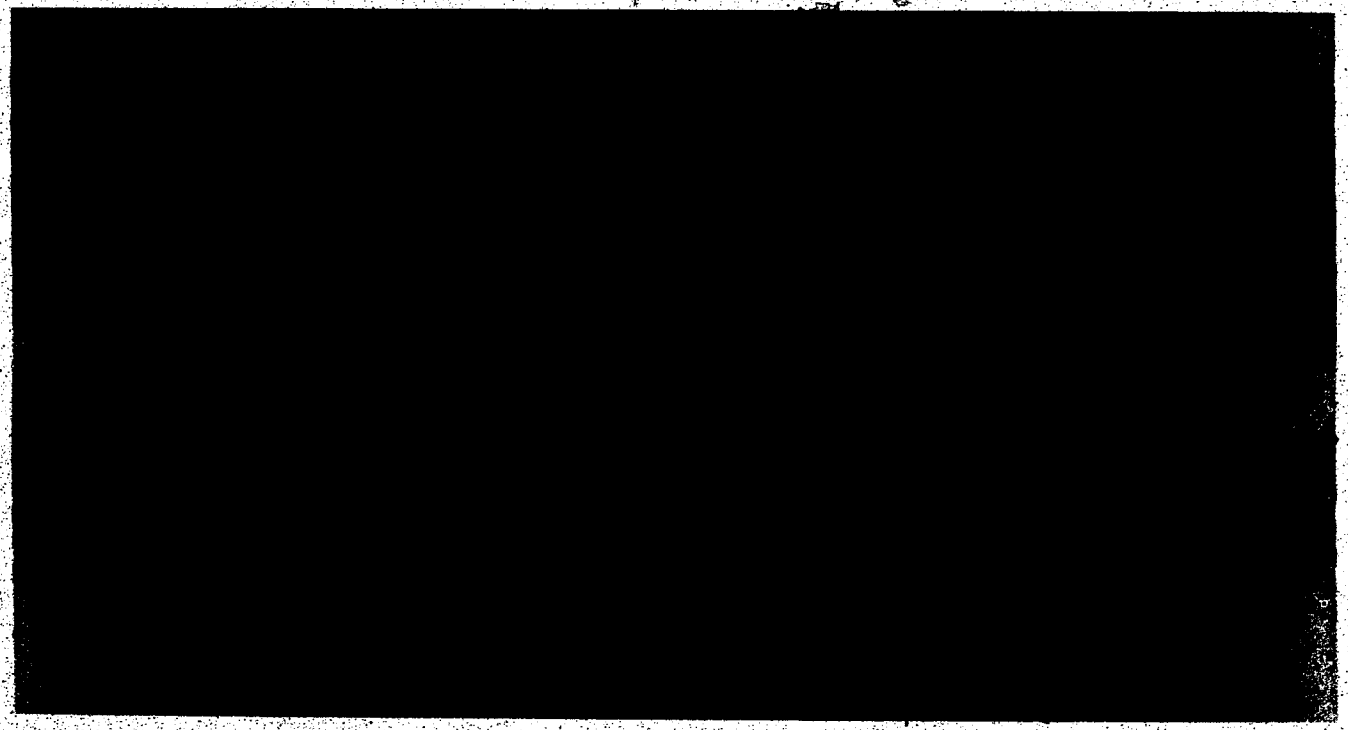

FIGURE 4.5 OUTPUT OF A STRIP CHART RECORDER FOR VERIFICATION OF STEADY STATE CONDITION

4.3.7 Digitec Thermistor Thermometer Plug-in Module

This thermistor thermometer gave a digital display of temperature in °C. The thermometer was capable of reading from -30.0°C to +100°C. The calibration was checked with the quartz thermometer. The instrument had connections for two probes and was used along with the other thermistor probes to maintain a check on thermistors performance.

4.4 Measurement of Velocity

4.4.1 Introduction

The experimental range of velocity was less than 0.325 ft/sec. Schraub, et al.'s (1965) detailed study of the hydrogen bubble technique suggested that this could satisfactorily be used for this range of velocity measurement.

The hydrogen bubble method is primarily a visual method similar to the observation of flow field with the aid of dye streaks. However, these generally provide only a qualitative interpretation. In an unsteady flow, therefore, the interpretation of the results becomes difficult. An improvement in this flow visualization technique was brought about by the introduction of the so-called time lines. The time lines give the time intervals between two locations but do not provide information about the trajectory of time lines. Thus the quantitative determination of velocity, especially in transient flow, is not possible by these methods.

Clutter, Smith and Brazier (1959) were pioneers in the

field to evolve the hydrogen bubble method into its present form. They, however, report that the hydrogen bubble method in its present form is a direct outcome of the method evolved by F.X. Wortman, who applied an electric current to a wire to release telerium for the generation of time lines.

Schraub, Kline, Henry, Rustadler and Little (1965) employed several variations of the hydrogen bubble method to provide different patterns of combined-time-streak-marker and have presented details of an uncertainty analysis of the method.

Davis and Fox (1967) gave an evaluation of the hydrogen bubble technique for the quantitative determination of fluid velocities. Nagib, et al. (1969) utilized the hydrogen bubble technique for calibration of thermistor probes for the measurement of low velocities. Jonys (1972) used the hydrogen bubble for velocity measurement in a sediment-carrying flume.

A review of the existing literature showed a wide variety of voltage supply, current supply, wire and lighting arrangements that have been used so far; these are given in Table 4.1.

4.4.2 General Description of the Method

The method utilises the electrolysis of water at a very fine wire to introduce hydrogen bubbles into the flow. The hydrogen produced at the wire is removed by the drag of the flowing water and breaks it into very small bubbles. These bubbles act as a tracer and can be made visible by lighting. If the negative electrode is subjected to

TABLE 4.1 DESCRIPTION OF ELECTRICAL EQUIPMENTS USED BY VARIOUS INVESTIGATORS

Investigators	Type and Size of Wire	Voltage Range	Current Range	Pulse Width	Pulse Frequency	Bubble Diameter	Type and Power of Light Illumination	Remarks
1. Clutter, Smith & Brazier a) Flow Visualization b) Quick Velocity Measurement	0.005" dia steel piano wire kinked by passing through old gear 0.001" dia platinum wire	15 to 600 (volts) 300 to 400 (volts)	0 - 0.6 amp	2.5 to 90 milli sec. duration 2.0 milli sec duration	1 to 30 per sec.	0.005" to 0.010"	Mercury vapour light source gives a plane 1/2" to 3/4" thick. Electronic flash light duration of 1 millisecond.	Life of wire limited to 15 to 20 runs because it was corroded by the electrolytic process.
2. Schraub, Kline et al.	0.0005" to 0.002" diameter platinum probe wire 6" long	10 to 250 Preferred 100 (volts)				0.00025" to 0.002"	750 watt projector light to light an area of 8". Angle of incidence of light 65° from vertical.	
3. Davis & Fox	Tungsten wire with 0.002" diameter	Cyclic reset generator produces voltage pulses of 20 volts			Repetition rate from 0.06 to 20 cycles per second		Angle of incidence less than 75°. Strobotac light, 7 million beam candle power, flash duration, 3 micro sec pulsed at a rate of 5 pulse/sec.	
4. Hegib et al	Annealed platinum-rhodium (10%) 0.0015" diameter straight wire. 0.004" diameter kinked wire.	DC power supply capable of supplying 500 volts	0.1 amp				Several 500 watt flood lamps.	
5. Jonys	0.[illegible]" diameter tungsten wire	Best Preferred 325 (volts)		10 milli sec.	10 cycles per sec.		650 watt movie light 35 mm camera with macro lens.	
6. Present Investigation	0.002" diameter tungsten wire	400 volts	0.1 to 0.3 amp	15 milli sec.	1 to 10 pulse/sec	0.001" Average	Fibre light	Life of wire has been found to be extraordinarily good.

pulsation, rows of hydrogen bubbles are produced. The distance between two rows on a photograph, corrected for scale factor and divided by the time between pulsation, gives the velocity of the point. The method possesses certain advantages as reported in the literature, namely:

1. Tracer particles are easily placed in the flow at any desired location and the quantity of tracer particles is easily controlled.
2. Hydrogen bubbles do not contaminate the water as much as dye, tellurium or other tracers.
3. Hydrogen bubbles do not lose their identity in wakes or turbulent flows as do filaments of dyes, tellurium, etc., because of diffusion.
4. The wires are of sufficiently small diameter so as not to create any noticeable wake effects.
5. It allows simultaneous measurements over a whole plane at an instant without appreciable flow disturbance.
6. It provides simultaneously the velocity field and a visual image of the flow structure.
7. The angle of divergence of the flow can be easily measured and as such the velocity v in the lateral direction can be easily determined.

Jonys (1972) reports that the method yields instantaneous rather than mean velocity of flow. However, Shraub, et al. (1965) report that the technique is unable to detect fluctuations whose physical scale is small compared to the distance over which averaging takes place and the bubbles are unable to respond to fluctuations whose physical scale

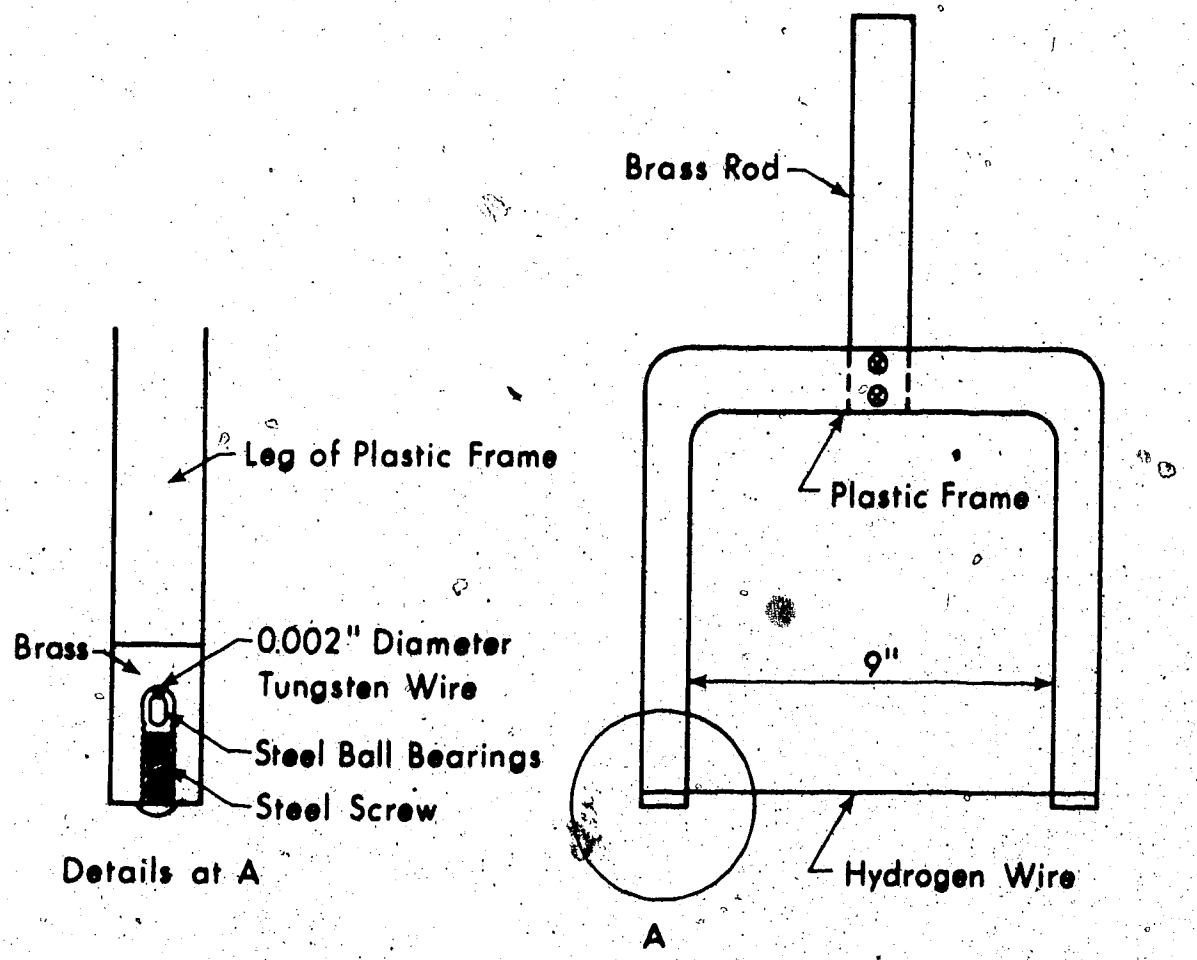

FIGURE 4.6 ARRANGEMENT FOR SUSPENDING HYDROGEN WIRE

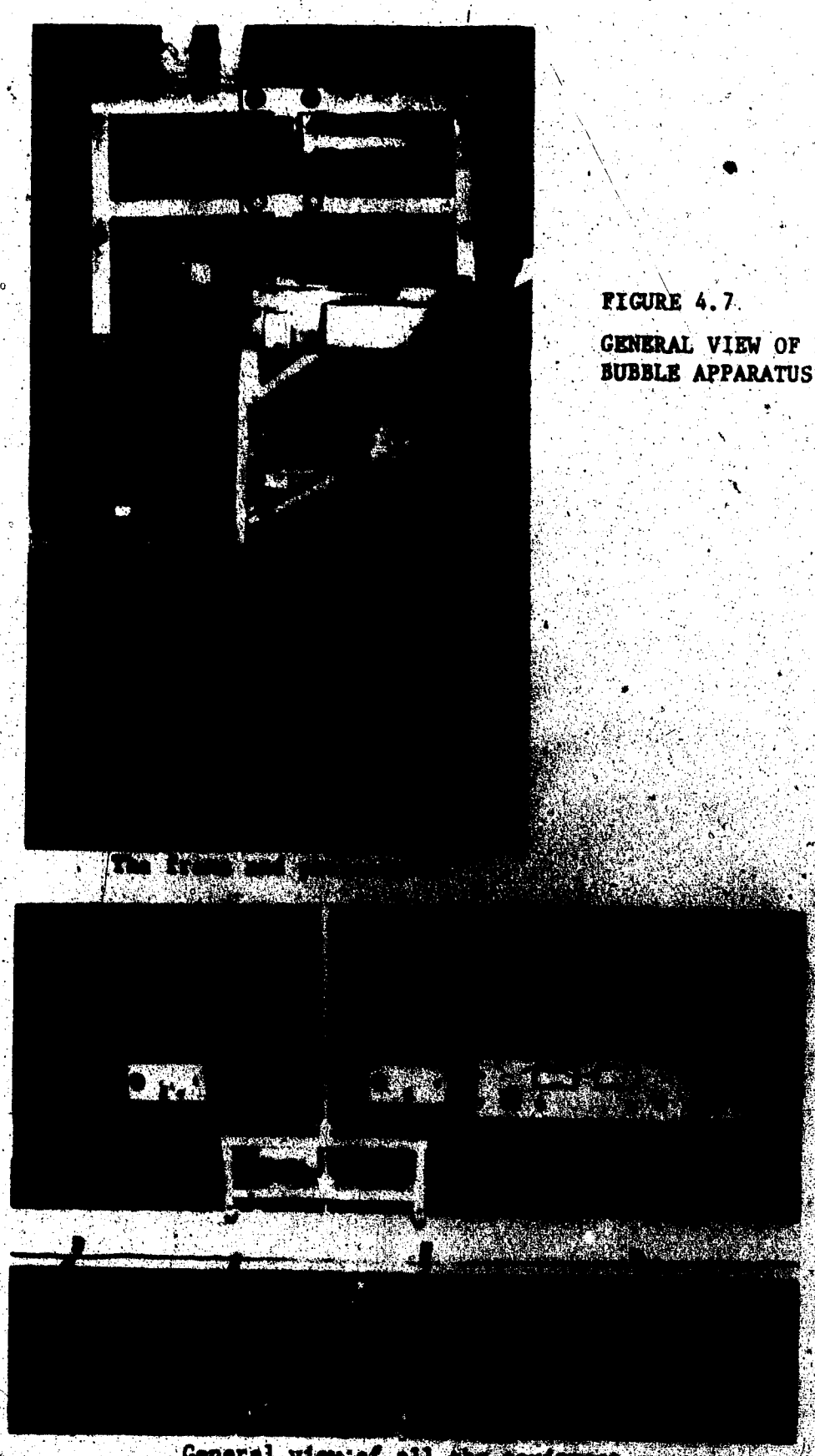

General view of all the equipment

FIGURE 4.7

GENERAL VIEW OF HYDROGEN BUBBLE APPARATUS

is small compared to their diameter. This point has been further clarified in the limitations of the method, wherein it has been inferred that the technique does not yield instantaneous velocity caused due to smaller eddies but does respond to fluctuations due to large eddies.

4.5 Description of the Apparatus

The apparatus consisted of the following equipment:

1. Bubble generating wire and frame.
2. Pulse generator unit.
3. Power supply unit.
4. Fiber light for illumination.
5. Polaroid and Pentax 35mm cameras for photography.

4.5.1 Bubble Generating Wire: The wire at which hydrogen bubbles were generated was made of 0.002" tungsten wire which acts as a cathode. The wire was insulated (By Rid Arc Spray Paint) at a few points to get streak lines. Haywood and Tory (1967), and Swanson (1967) advocated that the rise of bubbles due to buoyancy is appreciably lower if the wire is placed horizontally in the flow field. This appears to be due to the absence of cumulative effect of buoyancy in case of vertically suspended wire. Accordingly the wire was installed perpendicular to the direction of the flow in the horizontal plane. The wire was held tightly in position by the arrangement shown in Figure 4.6. The assembly of the wire and the plastic frame was mounted on the moving trolly. The frame could be moved vertically by an electric motor. The wire had a length of 9". The flume floor acted

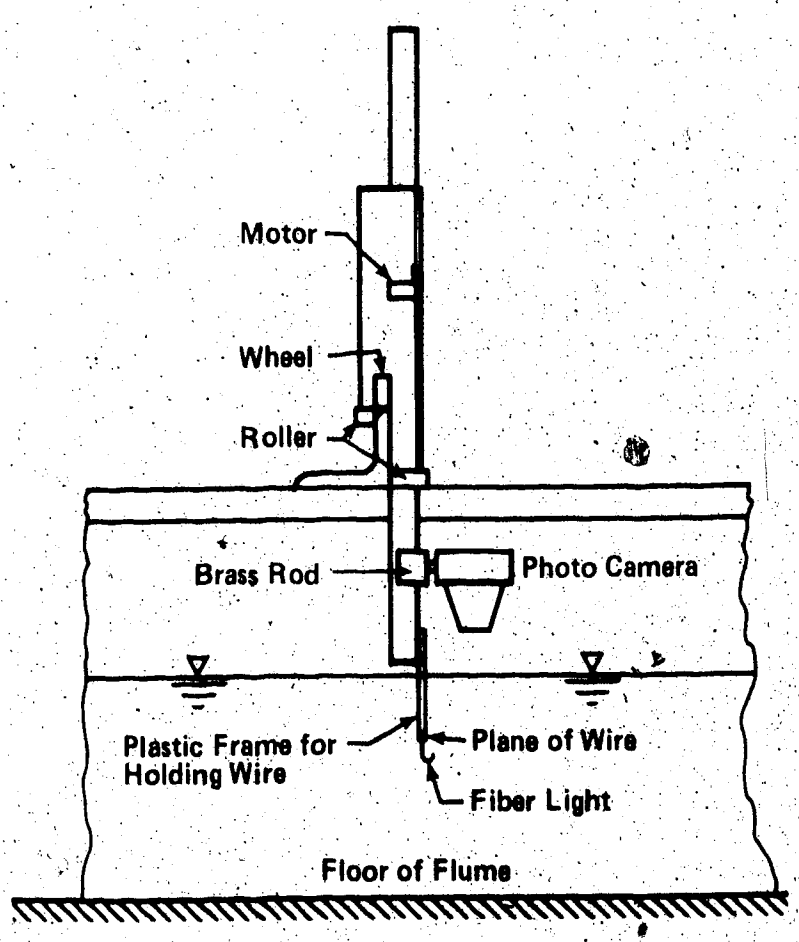

FIGURE 4.8(a) SCHEMATIC DIAGRAM FOR HYDROGEN BUBBLE APPARATUS

as the anode in these experiments. A general view of the hydrogen bubble apparatus is shown in Figure 4.7 and Figure 4.8a.

4.5.2 Pulse Generator Unit: A circuit that has worked satisfactorily in providing uniform bubble production is shown in Figure 4.9. Layout of electronic equipment is given in Figure 4.8b. The voltage required was about 400 volts. This voltage could be pulsed at a rate of 1 to 10 pulse/s with a pulse width of approximately 15 milliseconds.

4.5.3 Power Supply Unit: This unit supplies power at a variable working voltage from about 10 to 400 volts. The current obtained at 400 volts is less than 0.1 amperes.

4.5.4 Fiber Light for Illumination: Considerable time was spent in finding a suitable light source which could be suspended under water to provide sufficient light for photography, and which would not create any disturbance in the flow pattern. Fiber light ultimately provided the solution. The light source was suspended by the side of the frame carrying the wire and the light was then bent underneath so as to light the bubbles from under the plane of bubble generation. The light was thrown up at an angle approximately 65° to the vertical. The light source was a high intensity illumination (#150 supplied by Donald-Jenner Industries) and a projection lamp of 150 watt at 120 volts was used.

4.5.5 Photography: Two cameras, one pentax and the other polaroid, were used for photography. The polaroid camera had an advantage in that it gave photoprints immediately so that it could be

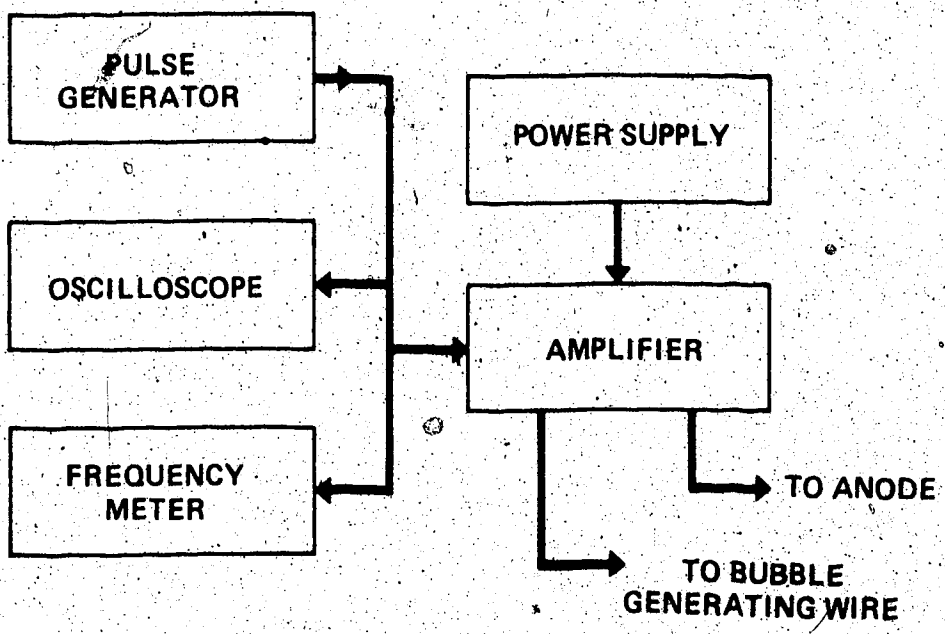

FIGURE 4.8(b) BLOCK DIAGRAM OF ELECTRONIC EQUIPMENT

VARIABLE PULSER FOR CYCLIC LOADING

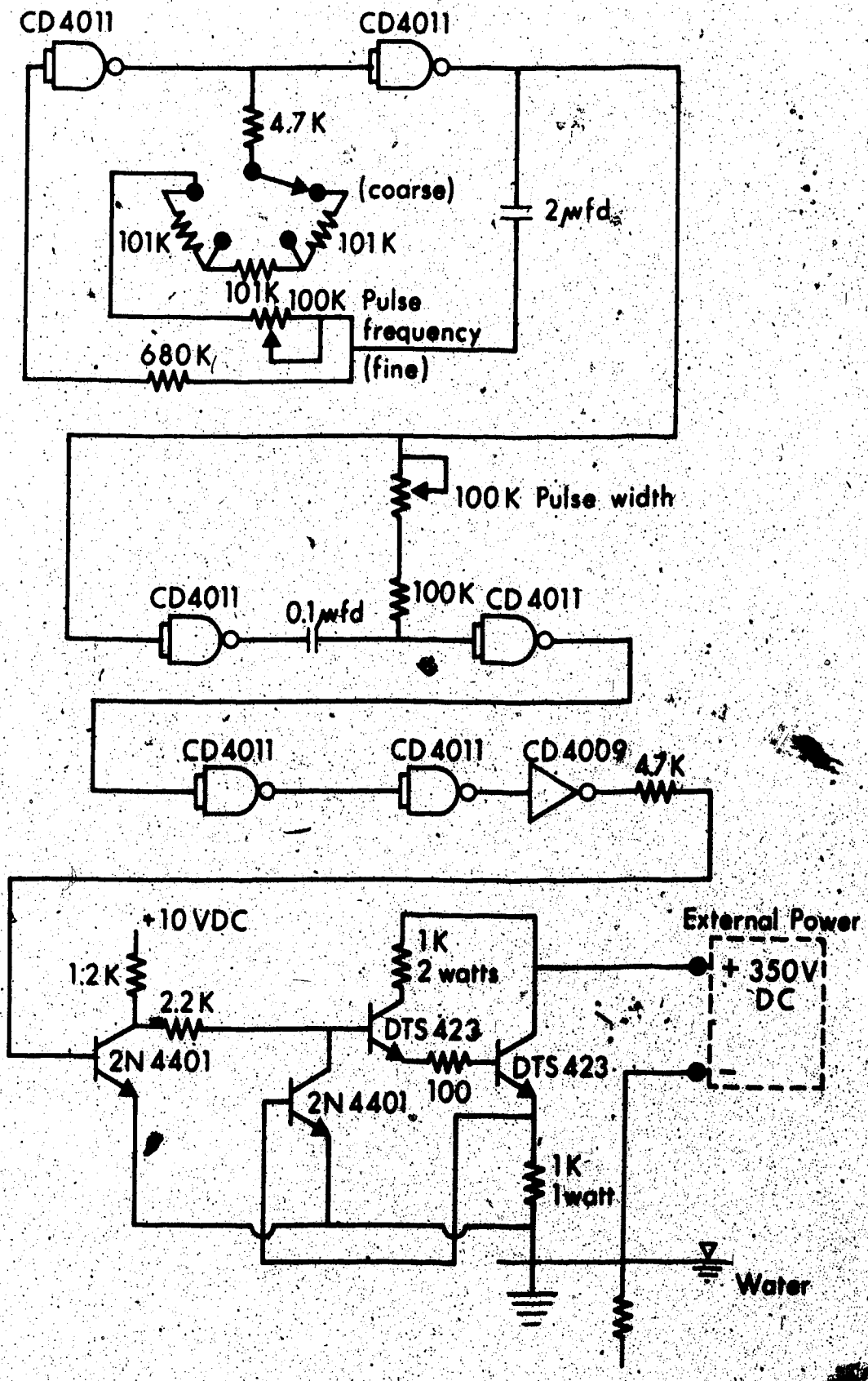

FIGURE 4.9 CIRCUIT OF VARIABLE PULSER FOR CYCLIC LOADING

determined if the bubbles appeared in the photograph. It had the disadvantage that the photographic record could not be taken in quick succession. On the other hand, the 35mm pentax camera gave better pictures and was used where photographs were required in quick succession. Polaroid type 47, ASA3000 and Tri-X Kodak 2475 with ASA1600 films were used with these cameras.

4.6 Details of Method and Operating Experience

The hydrogen bubbles were produced at a uniform rate by applying a constant voltage of 400 volts across the wire. In order to ensure good results, the wire was cleaned with a cotton swab dipped in legroine and acetone solutions. At the beginning of measurements, the voltage was applied by reversing the polarity for approximately 30 seconds and thereafter the electrolysis was started with proper polarity. Usually the wire required some time before the bubble production started at a uniform rate. This time lag between switching the circuit and the start of the uniform bubble production is known as aging time. As the wire became older, the aging time reduced.

The camera was mounted about 5" above the hydrogen bubble generating wire, and was triggered gently without disturbing the flow pattern. Sufficient time is allowed, for the decay of any disturbances created during the movement of the wire frame from one point to another, before taking any measurements.

Although the instrument used carried provisions for variable voltage supply, the voltage was usually kept constant at 400 volts

during operation. Such a high voltage has not been used by other investigators. Schraub, et al. (1967) recommended that the voltage be kept below 100 volts during operation as a safeguard against operational hazards. However, at a low voltage the bubble production was found to be nonuniform. The equipment supplying power was properly enclosed, hence there was no operational hazard experienced in the present case.

The current utilized for bubble production was always below 0.1 amperes and this did not create any problems with the density of bubble production.

The use of the tungsten wire proved quite successful. Jonys (1973) reports that a set of three wires was used for the entire experiment. The tungsten wire in the present case never corroded and generally behaved very well except for some breakage during cleaning. However, no continuous bubble production was ever attempted with these wires.

To facilitate photography of the hydrogen bubbles, all reflections were eliminated from the observational area. The bed of the flume in the region where photographs were taken was covered with a black plate in order to provide a black background for the photographs. Some typical photographs for hydrogen bubble rows are shown in Figure 4.10.

4.6.1 Measurement of Longitudinal Velocity

The longitudinal velocity u is given as:

$$u = \frac{\Delta x}{S f_x} \cdot \text{number of pulse/sec.} \qquad (4.6.1)$$

x = 7 y = 3.5 z = 0 P = 3.1/S Ri = 1.14

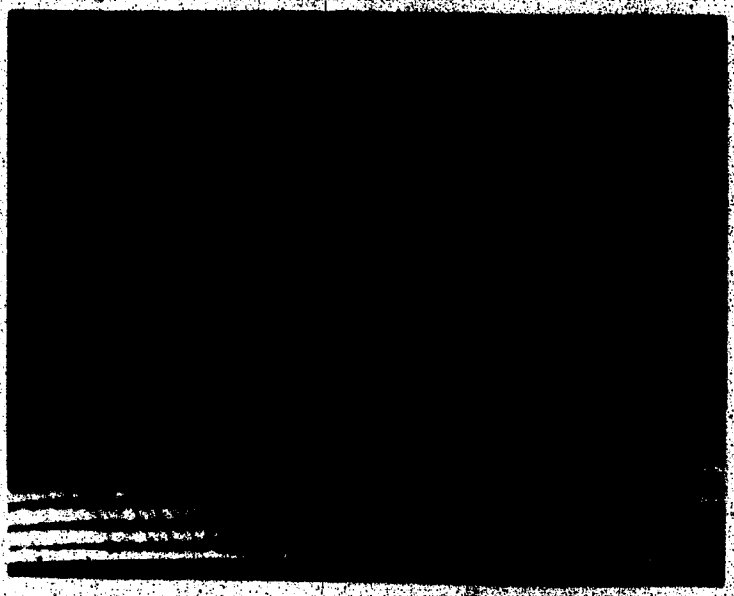

x = 7 y = 4.0 z = 0 P = 3.1/S Ri = 1.14

FIGURE 4.10 SOME TYPICAL PHOTOGRAPHS FOR HYDROGEN BUBBLE ROWS FOR VELOCITY MEASUREMENT (Continued)

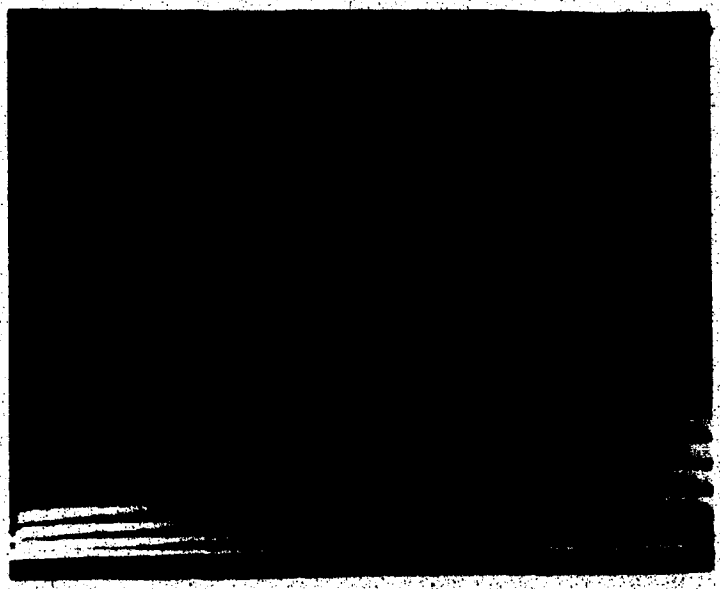

x = 6 y = 3.0 z = 0.025 P = 3.6/S Ri = 1.14

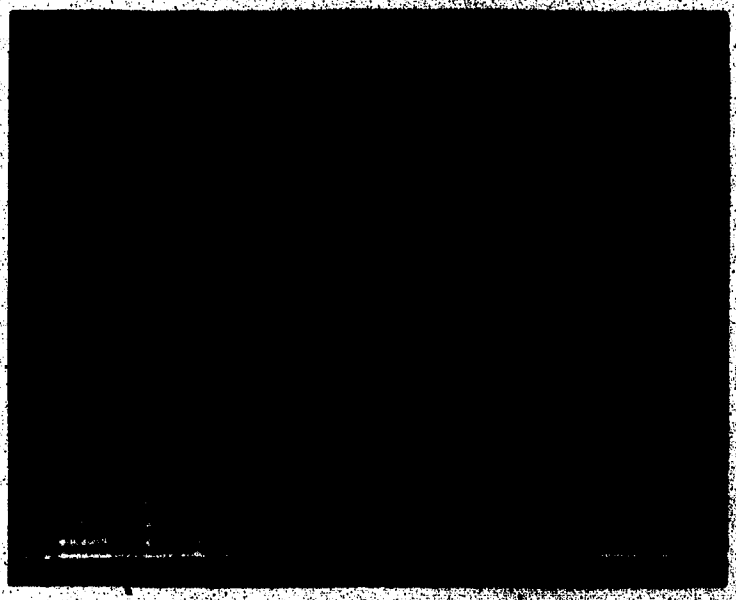

x = 3 y = 0 z = 0.025 P = 3/S Ri = 1.14

FIGURE 4.10 SOME TYPICAL PHOTOGRAPHS FOR HYDROGEN BUBBLE ROWS FOR VELOCITY MEASUREMENT

TABLE 4.2 TABULATION OF DISTANCES FOR CALCULATION OF SCALE FACTOR

Actual Distance in ft = B	Distance on the Film in mm = A					
	z = 0.0 ft	z = 0.025 ft	z = 0.05 ft	z = 0.075 ft	z = 0.01 ft	z = 0.0125 ft
0.01	2.25	2.30	2.30	2.30	2.30	2.30
0.02	4.40	4.50	4.60	4.65	4.70	4.55
0.03	6.60	6.75	6.90	7.00	7.10	6.90
0.04	8.75	8.95	9.15	9.25	9.40	9.30
0.05	10.95	11.20	11.45	11.60	11.75	11.65
0.06	13.05	13.40	13.75	13.85	14.0	14.05
0.07	15.20	15.65	16.15	16.20	16.25	16.45
0.08	17.40	17.95	18.45	18.50	18.60	18.80

Remark: $S_f = A/B$

where Δx = average distance in the longitudinal direction between two successive rows on the film in feet, and Sf_x = scale factor in the longitudinal direction where the scale factor Sf_x is defined as the ratio of average distance on the film between two rows to its actual distance in the water body. The scale factor takes into account the correction for refraction through water, any lens distortion, and size reduction on the film. It was determined by photographing a scale at various levels below water surface, coinciding with the plane of the wire. The scale factor for different depths is shown in Table 4.2.

4.6.2 Measurement of Lateral Velocity v

Due to the insulation of wire at different intervals, streak lines were obtained. The distance ΔS was measured along a streak line and then resolved into longitudinal and transverse directions. Then:

$$v = \frac{\Delta y}{Sf_y} \cdot \text{Number of pulses/sec} \qquad (4.6.2)$$

where Sf_y = scale factor in the lateral direction. The value of Sf_x and Sf_y were found to be the same in the present experiments. Typical photographs for velocity measurements are as given in Figure 4.10.

4.7 Limitations of the Method

Schraub, et al. (1965) listed the uncertainties that may be encountered in measuring velocity by this technique. These uncertainties are listed below:

1. Measurement of Δx on the photograph.
2. Averaging effects in changing velocity field.
3. Possible displacement of the bubble out of the horizontal plane of the wire due to bubble rise.
4. Response of the bubbles to fluctuations.
5. Resolution problems due to finite bubble size and due to finite averaging interval.
6. Velocity defect behind bubble generating wire.

Details of these are described in the following sections.

4.7.1 Measurement Uncertainty

In determining average distance between two rows, the error involved was reduced to a minimum by measuring the distance on the photograph through a magnifying lens of 10X magnification. This lens is fitted with an eye piece and a scale graduated to 0.1 mm which could be interpolated to .01 mm. A typical undertainty of about 2.5% in Δx from these measurements may be assumed.

4.7.2 Averaging Uncertainty

The velocity field in the jet is changing. Hence the velocity obtained at a point would be the average velocity over a region on which the measurement was made. A typical distance over which the averaging was recorded in this experiment was less than 0.1 ft. Consider, for the present, a case of submerged circular jet for analysis of uncertainty. The circular jet has been chosen as the decay of centerline velocity in this case is maximum. Assuming that the average centerline velocity over a region x_1 to x_o is $\bar{u}_m$ and a typical velocity anywhere is u_m, then:

$$(x_1 - x_o)\,\frac{\bar{u}_m}{U_o} = \int_{x_o}^{x_1} \frac{u_m}{U_o}\,dx$$

but let $u_m/U_o = k_1/x$, then:

$$(x_1 - x_o)\frac{\bar{u}_m}{U_o} = k_1 \ln \frac{x_1}{x_o}$$

Hence percentage uncertainty with respect to u_m at x_o represented as $u_{m(x_o)}$ is given as:

$$\frac{u_{m(x_o)} - \bar{u}_m}{u_{m(x_o)}} = \frac{\frac{k_1}{x_o} - \frac{k_1}{(x_1 - x_o)} \ln \frac{x_1}{x_o}}{k_1/x_o} \times 100\%$$

$$= \left(1 - \frac{x_o}{x_1 - x_o} \ln \frac{x_1}{x_o}\right) \times 100\% \qquad (4.7.1)$$

In a typical case like the present experimental setup with an inlet width of 2", the minimum length of potential core is 1'-0". Hence in this case $x_1 = 1.1'$ and $x_o = 1.0'$:

$$\% \text{ Uncertainty} = \left[1 - \frac{1}{(1.1 - 1)} \ln \frac{1.1}{1}\right] \times 100$$

$$= (1 - 10 \times .09531) \times 100$$

$$= 4.69\% \qquad (4.7.2)$$

The percentage uncertainty worked out is the maximum for cases of inlets having width 2" and higher and for any type of jet including the three dimensional jet being treated in the present case.

The error could be much larger if the bubbles go out of the

x-z plane due to predominant v velocity present. The analysis can be done similar to the one done previously. This is illustrated as follows. Referring to Figure 4.11, let the velocity in the direction of the streak line be U and this direction be represented as S. If $\bar{U}$ is the average velocity over S_1 to S_o, one can write:

$$\bar{U}\,(S_1 - S_o) = \int_{S_o}^{S_1} U\,dS \qquad (4.7.3)$$

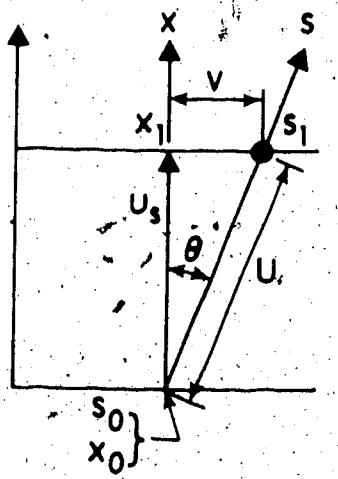

FIGURE 4.11 VELOCITY ALONG A STREAK LINE

Let: $u_s = u_m f_1(\eta)$

also $v = \bar{\alpha}\, u_m$ (as a rough approximation)

Then: $U = \sqrt{u_s^2 + v^2} = u_m \sqrt{\bar{\alpha}^2 + f_1^2}$

Substituting for U in Equation 4.7.3, it may be written that:

$$\bar{U}\,(S_1 - S_o) = \int_{S_o}^{S_1} u_m \sqrt{\bar{\alpha}^2 + f_1^2}\; dS$$

Since $u_m = k_1/x = k_1/S\cos\theta$, so:

$$\bar{U} = \frac{k_1 \sqrt{\bar{\alpha}^2 + f_1^2}}{(\cos\theta)(S_1 - S_o)} \ln \frac{S_1}{S_o} \qquad (4.7.4)$$

Hence, percentage uncertainty:

$$\frac{u_{s\,x_o} - \bar{u}}{u_{sx_o}} = \frac{U\cos\theta\big|_{x_o} - \bar{U}\cos\theta}{U\cos\theta\big|_{x_o}} = \frac{U_{(x_o)} - \bar{U}}{U_{(x_o)}}$$

and since $U_{(x_o)} = \dfrac{k_1 \sqrt{\bar{\alpha}^2 + f_{1x_o}^2}}{x_o}$

Therefore percentage uncertainty $= 1 - \dfrac{\bar{U}}{U_{(x_o)}}$

$$= 1 - \frac{x_o \sqrt{\bar{\alpha}^2 + f_1^2} \ln \frac{S_1}{S_o}}{[(S_1 - S_o) \cos \theta] \sqrt{\bar{\alpha}^2 + f_{1x_o}^2}}$$

Also $(S_1 - S_o) \cos \theta = x_1 - x_o$ and $S_1/S_o \simeq x_1/x_o$. Hence the percentage uncertainty:

$$= 1 - \left(\frac{x_o}{x_1 - x_o}\right)\left(\frac{\bar{\alpha}^2 + f_1^2}{\bar{\alpha}^2 + f_{1x_o}^2}\right)^{1/2} \ln \frac{x_1}{x_o} \qquad (4.7.5)$$

Because of a very small averaging distance, $f_{1x_o} \simeq f_1^2$ and Equation 4.7.5 reduces to Equation 4.7.1, or:

$$\text{Percentage Uncertainty} = 1 - \left(\frac{x_o}{x_1 - x_o}\right) \ln \frac{x_1}{x_o} \qquad (4.7.1)$$

4.7.3 Uncertainties Associated with Bubble Rise

The average size of the bubble determined by a microscope was found to be 0.001" in diameter. For bubbles of this size in water with kinematic viscosity of 10^{-5} ft^2/sec, the rising velocity works out to be 0.0012 fps, as approximated by Schraub, et al. (1965) on the basis of Stokes solution. The measurements were usually made over four or five rows of hydrogen bubbles. The frequency was 5 cycles/sec hence the time

interval between the first row and the sixth row was one second. The bubbles might have risen by 0.0012 ft during this time interval. The gradient of velocity $\partial w/\partial z$ is large, hence this could contribute a significant error.

In a typical case, let the half depth $h = 0.0425$ ft and the measurement of velocity be performed at 0.075 ft. Then let u_1 equal the velocity at $z = 0.075'$ and u_2 equal the velocity at $z = 0.0762$. The velocity distribution profile in vertical direction has been found to be closely represented by:

$$\frac{u}{u_m} = e^{-0.693\,(z/h)^2}$$

Hence:

$$u_1 = u_m\, e^{-0.693\,(.075/0.0425)^2} = 0.1155\, u_m$$

also:

$$u_2 = u_m\, e^{-0.693\,(.0762/0.0425)^2} = 0.1077\, u_m$$

$$\text{Average Velocity } u = \frac{1}{2}\,(u_1 + u_2) = 0.1116\, u_m$$

Thus percentage uncertainty equals:

$$\frac{u_1 - u}{u_1} \simeq 3.37\%$$

However, this uncertainty will go on reducing for the velocity measurement done above this level.

4.7.4 Uncertainty Caused Due to a Slip Between Bubbles and Surrounding Fluid

David and Fox (1967) make an approximate analysis of the slip of bubbles on the basis of virtual mass and deduce that bubbles are accelerated very rapidly to the fluid velocity. The response time for attaining 98% of fluid velocity by the bubbles was found to be 1 ms. Swanson (1967) points out that this value is 30 ms. However, because of the lubricated wire surface, the bubbles do not start with zero velocity, and this tends to reduce the calculated response time. Therefore, the error caused due to the slip is likely to be small and can be easily neglected.

4.7.5 Uncertainty Due to Turbulent Fluctuations

Schraub, et al. (1965) pointed out that the method cannot detect fluctuations whose physical scale is small compared to the distance over which averaging takes place and a bubble cannot respond to fluctuations whose physical scale is small compared to its diameter. Soo (1967) states that if the particle is large compared to the scale of turbulence, the main effect of the turbulence will be on the drag coefficient and the particle will follow the slower large scale turbulent motion of the fluid. If the particle is small compared to the smallest scale of turbulence, it will respond to all the turbulent components of the fluid.

In the present example, bubbles are of 0.001" diameter and the mean speed at source varies between 0.156 to 0.323 ft/sec. Hence, the minimum cycles of turbulent fluctuations to which the bubbles may start responding is:

FIGURE 4.12 TURBULENCE PATTERN IN THE JET

$$= \frac{0.0323 \times 12}{0.001} = 3876$$

It is obvious that this goes on reducing further as the centerline velocity decays.

Another factor which limits the frequency of fluctuations is the averaging time ΔT. If the velocity is averaged over time ΔT, fluctuations occurring in smaller times will not be observed even though the bubbles may follow faithfully to much higher frequencies.

The photograph in Figure 4.12 shows the turbulence pattern in the jet. The size of the largest eddy appears to be 0.062 ft. Thus the time scale of this eddy is:

$$t = \frac{\ell}{u} = \frac{0.062}{0.168} = 0.37 \text{ seconds}$$

Averaging was done over a period of one second in the present case and thus the measurement appears to represent a fairly good average.

Further, the centerline velocity was measured by taking an average of velocities obtained from five photographs, the velocities so obtained did not differ from each other by more than 5%. It is thus anticipated that the velocities obtained in the present case represented an average velocity.

4.7.6 Uncertainties Caused Due to Wake Effects

A hydrogen lubrication sheath tends to form around the wire, but is highly surface-tension-unstable and breaks up into bubbles very

close to the wire. This will decrease the drag coefficient because of very low viscosity of hydrogen. The decrease in drag would result in a smaller wire wake and "blockage" effect. Another effect that tends to reduce the wake effect is caused by the hydrogen circulation in the bubbles giving a flow regime such that the liquid flow around spherical bubbles can be considered somewhere between potential and Stoke's flow. Schraub, et al. report that the bubble velocity reaches the free stream velocity in less than 70 wire diameters for all cases tested. Thus the bubble displacement in the present case has been measured only after points greater than 70 wire diameters downstream from the wire.

4.7.7 Total Uncertainty

Total uncertainty can be obtained by taking the square root of the sum of the squares of individual uncertainties. Thus:

$$\text{Total Uncertainty} = [(\delta_{meas})^2 + (\delta_{avg})^2 + (\delta_{buoy})^2]^{1/2} \times 100$$

$$= [(0.025)^2 + (0.0469)^2 + (0.037)^2]^{1/2} \times 100$$

$$= 6.47\%$$

The results should thus be relied upon within 7 percent of the actual value.

4.7.8 Verification

To check for any unforeseen uncertainty, velocity measurements were made very close to the nozzle by hydrogen bubble technique and compared with average velocity calculated by dividing the volumetric

flow rate through the nozzle by the nozzle area. The results were found to be very close.

CHAPTER 5

PRESENTATION OF TEMPERATURE AND VELOCITY MEASUREMENTS AND DISCUSSIONS

5.1 General

The objectives of experimental investigations have already been described in Chapter 2. Five sets of experiments for a range of Richardson numbers Ri from 0.15 to 1.14 have been carried out. The details of the initial conditions are given in Table 5.1.

Detailed velocity and temperature measurements have been made both in lateral and vertical directions. The procedure for velocity measurements by hydrogen bubble technique and temperature measurements by thermistor probes have been described in Chapter 4. Two sizes of rectangular inlets have been used. The first series of three experiments (Run Nos. 3 to 5) were carried out with an inlet having $b_o/h_o = 3.16$, whereas the last series of two experiments (Run Nos. 1 and 2) were carried out with $b_o/h_o = 1.06$. The values of Reynolds number in these experiments remained approximately in the range of 7000 to 7500.

5.2 Velocity Measurements

Velocity profile measurements were made at nine cross-sections separated by one foot from each other. Surface velocity was also measured close to the nozzle, approximately 0.3 feet away. This surface velocity was found to be almost equal to the average inlet velocity for Run Nos. 1 to 3; but for Run Nos. 4 and 5 with Ri = 0.79 and 1.14

TABLE 5.1 EXPERIMENTAL DETAILS

Run No.	Inlet Details		Velocity at Inlet U_o in ft/sec	Inlet Temperature T_o		Ambient Temperature T_a		$(\Delta\rho)_o$ gm/cc	$\frac{(\Delta\rho_o)}{\rho_a}$	Ri	F_{rD}	$\nu \times 10^5$	R_e
	Depth h_o in ft	Width b_o in ft		in °C	in °F	in °C	in °F						
1	0.1515	0.161	0.322	27.50	81.50	13.50	56.30	0.00317	0.00317	0.15	2.56	0.895	7588
2	0.1515	0.161	0.2635	33.90	93.02	13.00	55.40	0.0051	0.0051	0.35	1.67	0.799	6980
3	0.158	0.5	0.172	30.27	86.48	16.25	61.25	0.00331	0.003311	0.56	1.32	0.862	7727
4	0.155	0.5	0.156	31.11	88.00	15.00	59.00	0.003813	0.003806	0.79	1.13	0.847	7049
5	0.155	0.5	0.156	36.00	96.80	14.00	57.20	0.005524	0.005528	1.14	0.94	0.767	7784

R_e = Reynold's number = $\frac{4U_o b_o h_o}{\nu(b_o + 2h_o)}$

the difference was significant due to the formation of floating plumes as discussed in Section 5.4.1.

For some of the runs, the jet tended to meander. Measurements were recorded only when the jet centerline followed a straight line trajectory coincident with flume centerline. The velocity profiles measured on the surface had a maximum velocity at center and minimum towards the edges. The profile in the vertical plane showed the same trend with the maximum velocity at the surface or close to it and reducing to smaller values at increasing depths below water surface. Typical velocity profiles for Run No. 2 are shown in Figures 1 to 5. The shape of velocity profiles for other Richardson numbers were of the same nature and the corresponding data are tabulated in Appendix C (Tables C-1 to C-4).

5.3 Velocity Distribution on the Surface (Transverse Plane)

For all runs, the velocity profiles on the surface were checked for similarity by plotting u_s/u_m versus η_u where $\eta_u = y/b_u$ and b_u is the half velocity width of the jet. These profiles have been found to be similar for all Richardson numbers tested. A typical plot of similarity for two values of Richardson numbers, large (0.79) and moderate (0.35), are shown in Figures 5.6 and 5.7. The length of potential core has been found to be small and the velocity distribution similar all along the length of measurement from approximately 6.5 times the inlet depth. Similarity plots for other Richardson numbers are given in Appendix C (Figures C-1 to C-3).

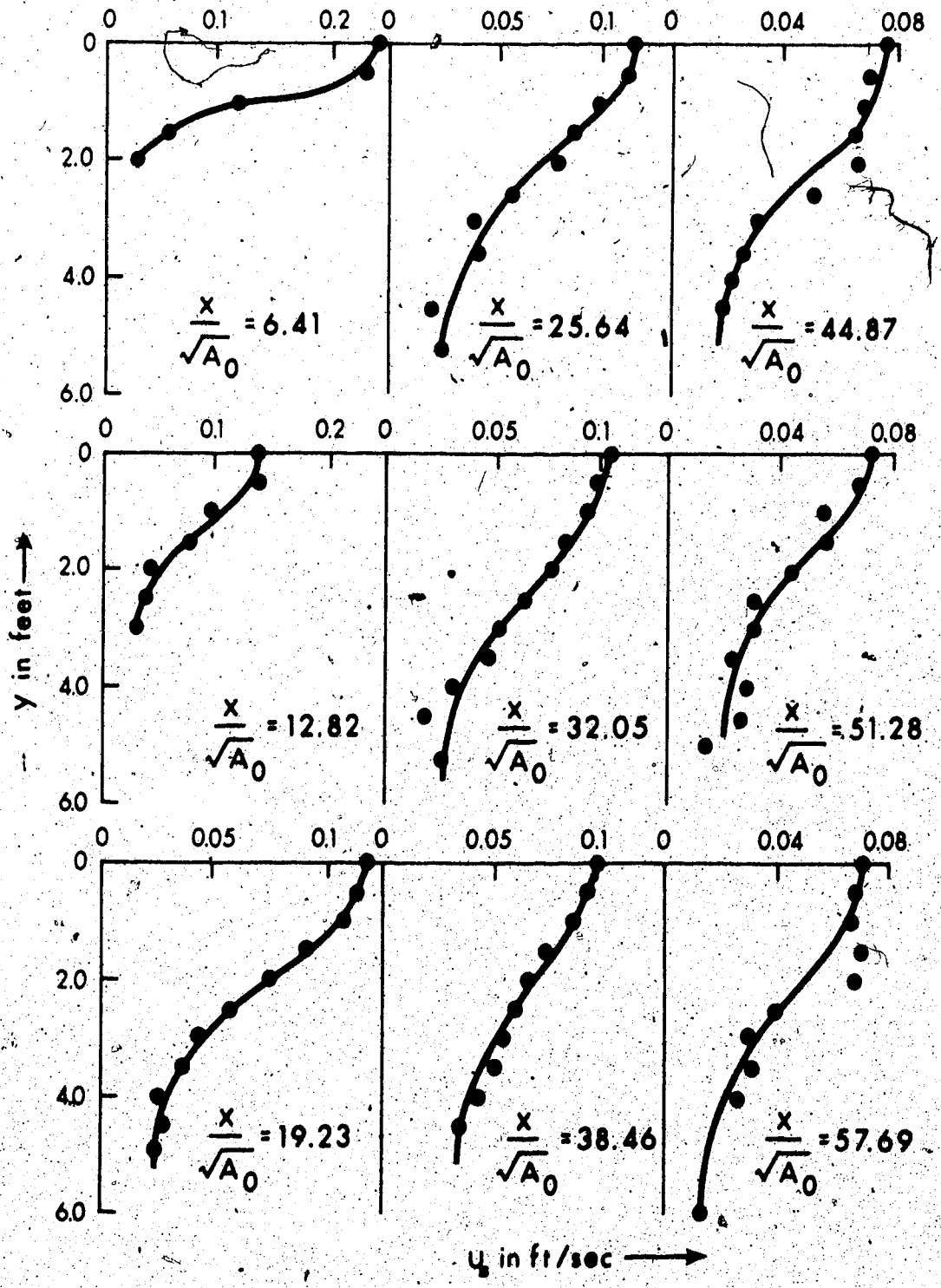

FIGURE 5.1 LATERAL DISTRIBUTION OF LONGITUDINAL VELOCITY AT SURFACE ($z/\sqrt{A_0} = 0$), Ri = 0.35

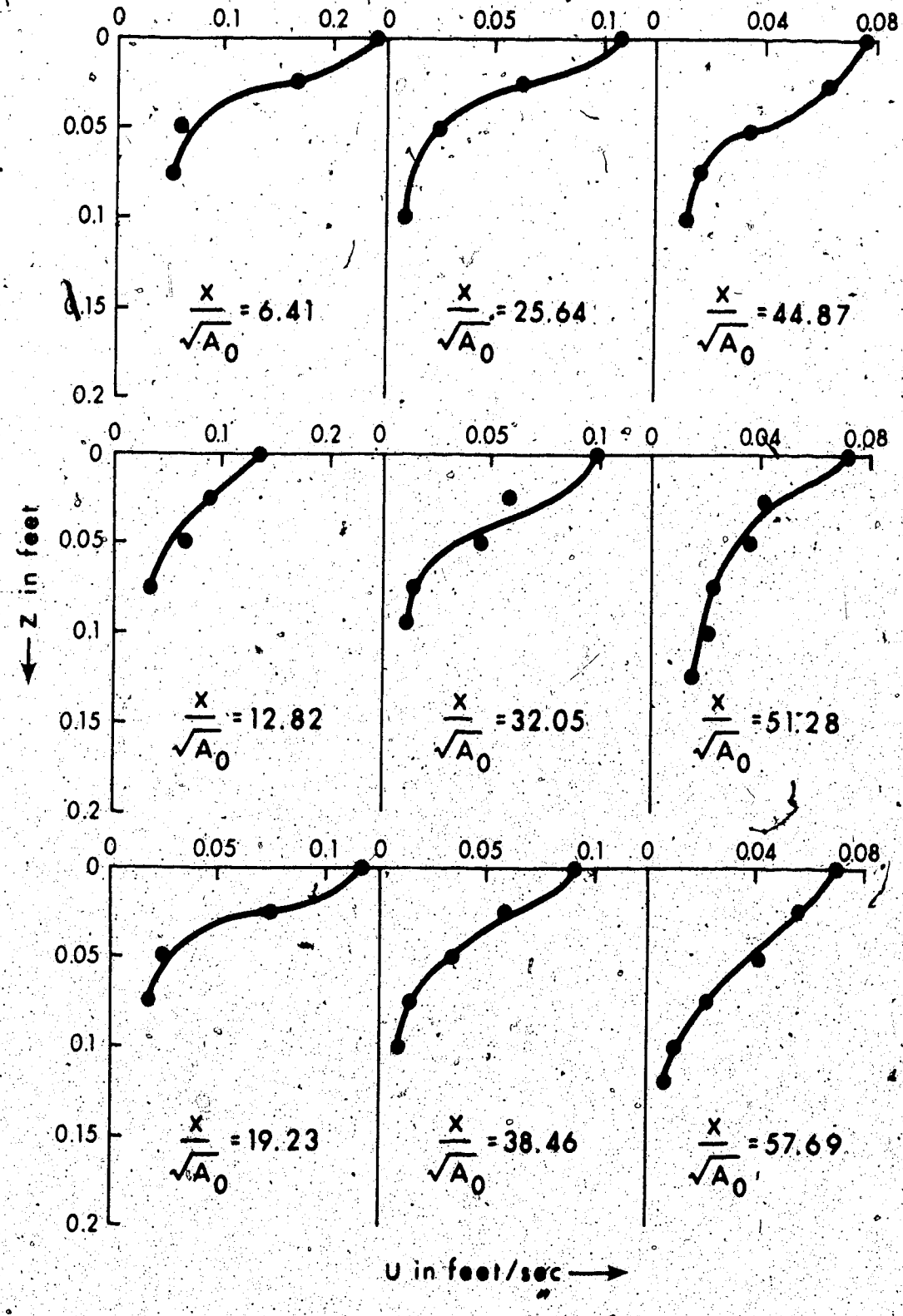

FIGURE 5.2 VERTICAL DISTRIBUTION OF LONGITUDINAL VELOCITY AT CENTRAL PLANE ($y/\sqrt{A_0} = 0$) , Ri = 0.35

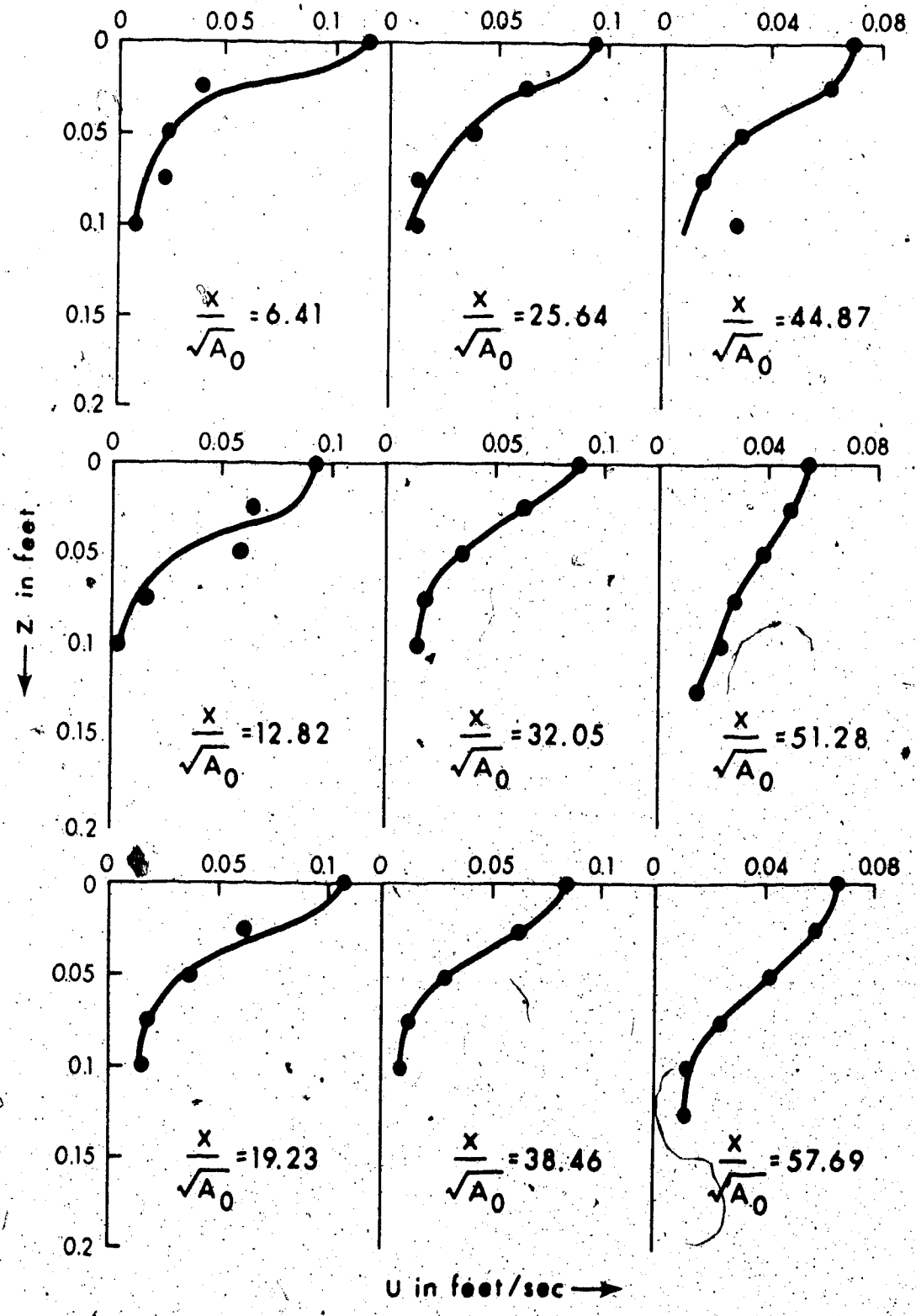

FIGURE 5.3 VERTICAL DISTRIBUTION OF LONGITUDINAL VELOCITY
SECTION $y/\sqrt{A_0}$ = .6.41 , Ri = 0.35

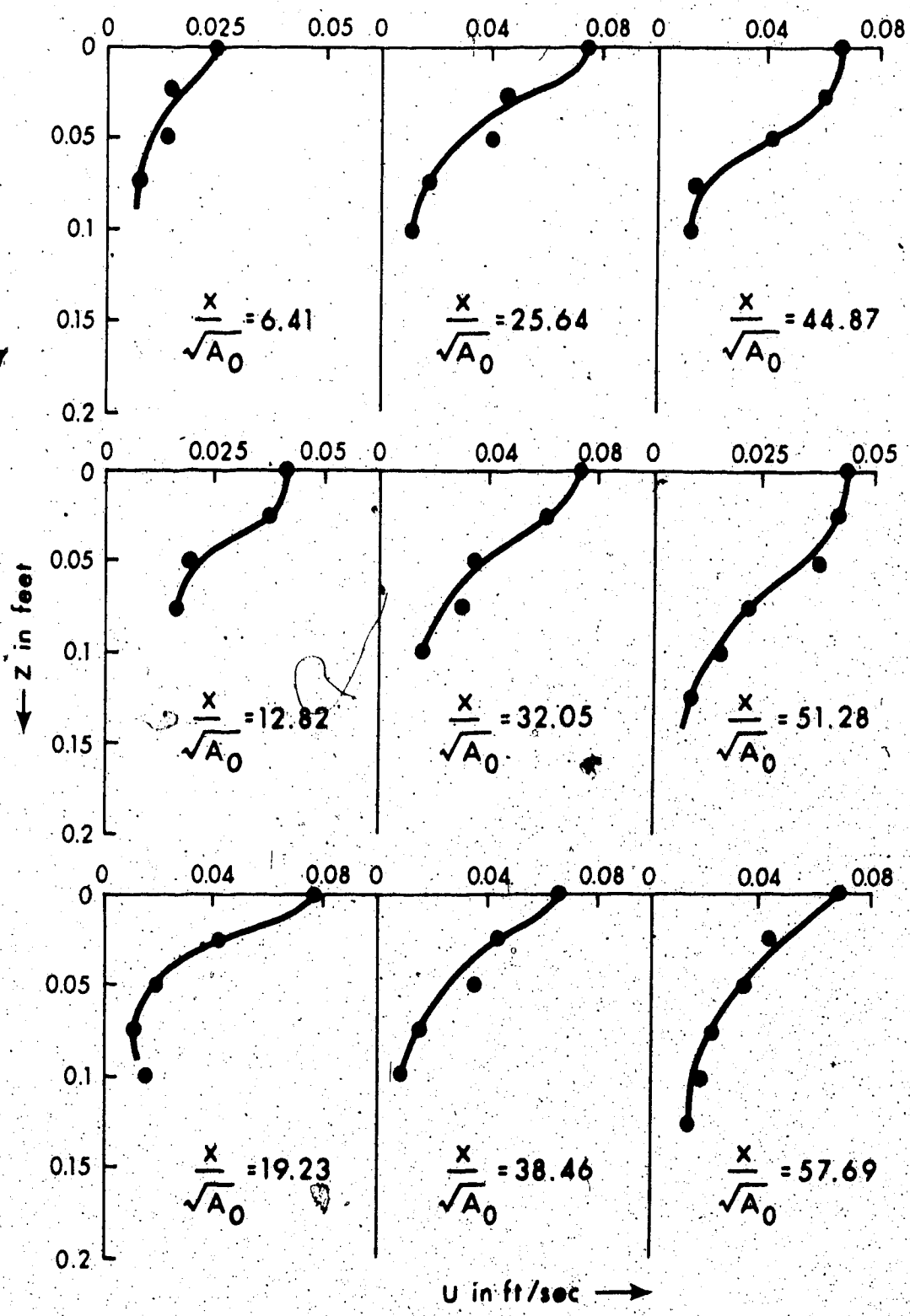

FIGURE 5.4 VERTICAL DISTRIBUTION OF LONGITUDINAL VELOCITY
SECTION $y/\sqrt{A_0}$ = 12.82 , Ri = 0.35

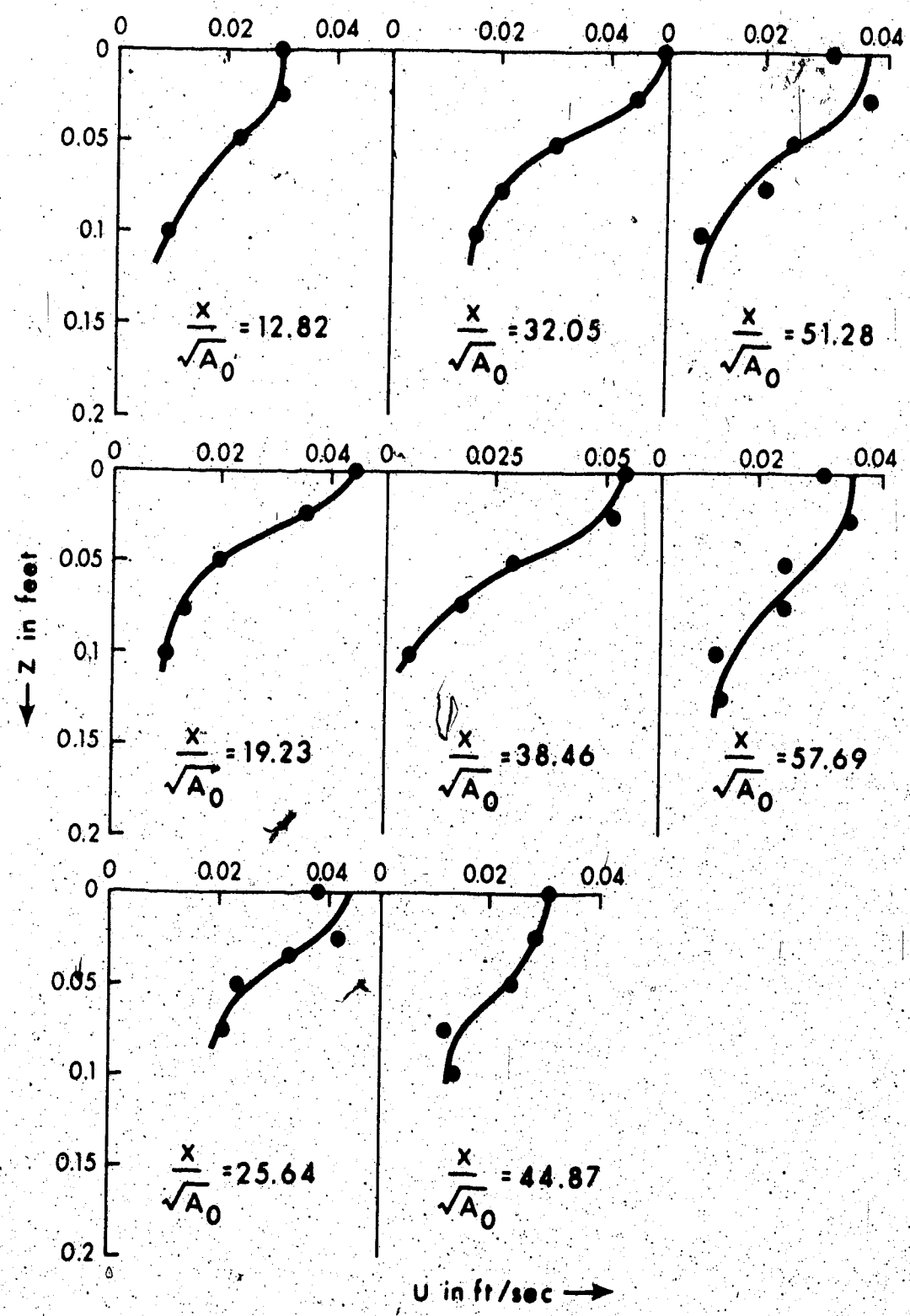

FIGURE 5.5 VERTICAL DISTRIBUTION OF LONGITUDINAL VELOCITY
SECTION $y/\sqrt{A_0}$ = 19.23 , Ri = 0.35

Various forms of similarity functions have been used by different investigators in the jet regime. These are listed in Table 5.2.

TABLE 5.2 FORMS OF VELOCITY DISTRIBUTION

Type of Distribution	Equation
Tollmien's Equation for Axisymmetric Jet	Numerical solution available. Coordinates of similarity profile are taken from Abramovich (1963)
Schlichting's Type Solution [1] for Turbulent Axisymmetric Jet	$u_s/u_m = [1 + 0.41\ (y/b_u)^2]^{-2}$
Exponential Distribution [2]	$u_s/u_m = \text{Exp}\ [-\ 0.693\ (y/b_u)^2]$
Abramovich's Wake Solution Used by Stolzenbach and Harleman.	$u_s/u_m = [1 - (y/\bar{b}_u)^{3/2}]^2$
Distribution used by Anwar (72b)	$u_s/u_m = 3/2\ (y/\bar{b}) - 1/2\ (y/\bar{b}_u)^3$
Exponential Distribution Used by Motz and Benedict	$u_s/u_m = \text{Exp}\ [-\ (y/b_u)^2]$

[1] This solution for turbulent axisymmetric jets was obtained by Goertler by applying Prandtl's new theory of turbulence, however, the solution was identical to that of Schlichting's solution for axisymmetric laminar jets.

[2] Also popularly known as Gaussian distribution.
Note $\bar{b}_u$ is the full velocity width of the jet from centerline to the edge where $u \triangleq 0$.

5.3.1 Similarity Profile for Large Richardson Number

As discussed in a later section, Ri = 0.79 and 1.14 have been found to belong to large Richardson number range. The first three forms of the similarity function as listed in Table 5.2 have been com-

pared with the present data as shown in Figure 5.6 for $Ri_o = 0.79$. The comparison indicates that any of these forms is suitable up to $\eta = 1.0$; but for the value of $\eta > 1.0$, the exponential distribution given by $\exp(-0.693\,\eta^2)$ is more suitable than the other two. This exponential distribution is definitely more preferable to that used by Motz and Benedict.

Abramovich's wake solution can be modified by assuming $\bar{b}_u$ to be proportional to b_u and evaluating the proportionality constant so as to yield u_s/u_m equal to 0.5 when η equals 1.0. The modified equation can be written as:

$$u_s/u_m = (1 - 0.293\,\eta^{3/2})^2 \qquad (5.3.1)$$

This equation lies close to the Tollmien's curve up to $\eta < 1.0$ and close to the exponential distribution for $\eta > 1.0$ and hence is not shown in Figure 5.6. Similarly the distribution used by Anwar can be changed to:

$$u_s/u_m = 1 - \left(\frac{3}{5.76}\,\eta - \frac{1}{47.75}\,\eta^3\right) \qquad (5.3.2)$$

which suggests that $\bar{b} = 2.88\,b_u$. The distribution lies much below the data up to $\eta < 1.0$ and much above the data for $\eta > 1.0$ and thus does not provide a good fit.

5.3.2 Forms of Similarity for Moderate Richardson Number

The similarity forms for moderate Richardson numbers shown in

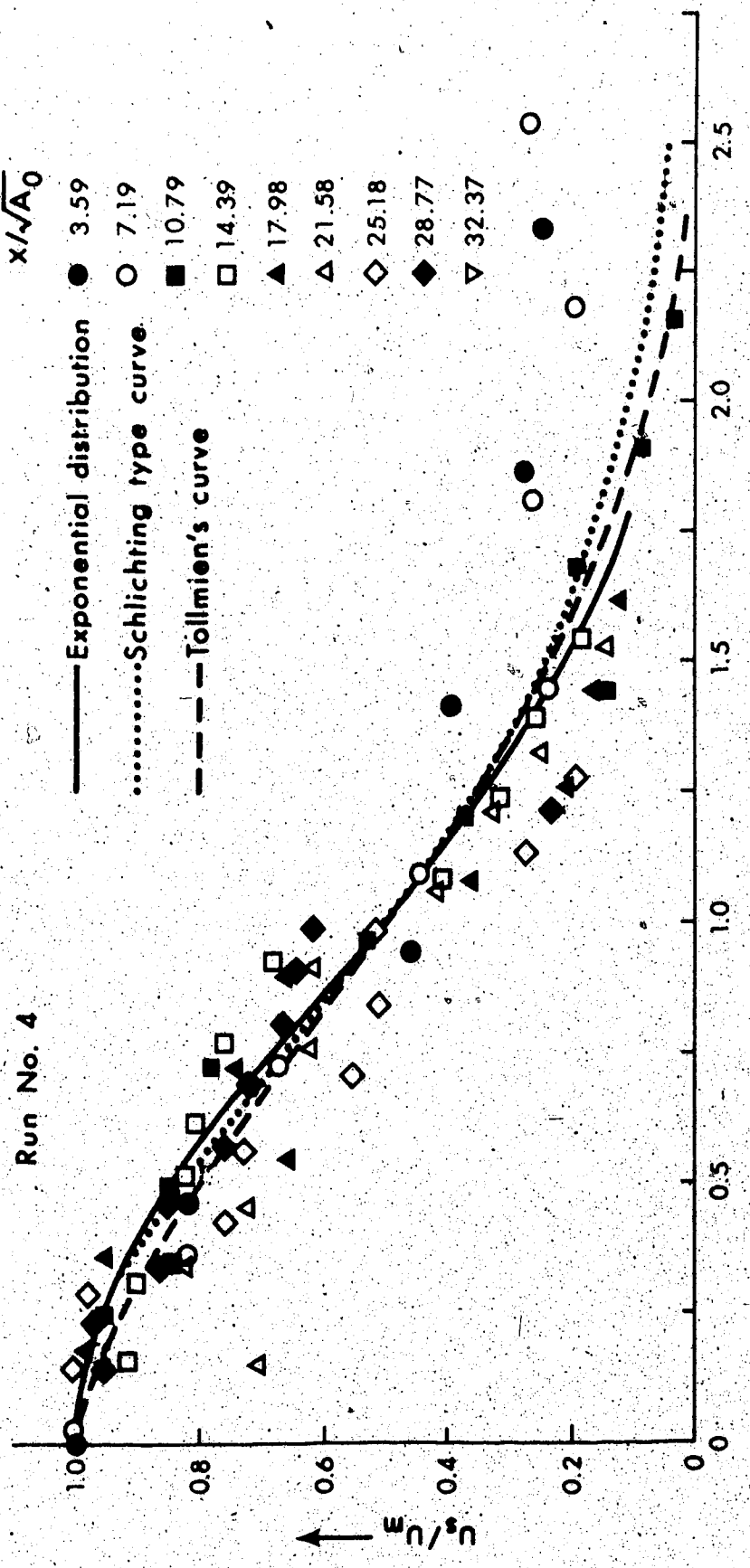

FIGURE 5.6 NON-DIMENSIONAL LONGITUDINAL VELOCITY PROFILE ON THE SURFACE $z/\sqrt{A_0} = 0$, Ri = 0.79

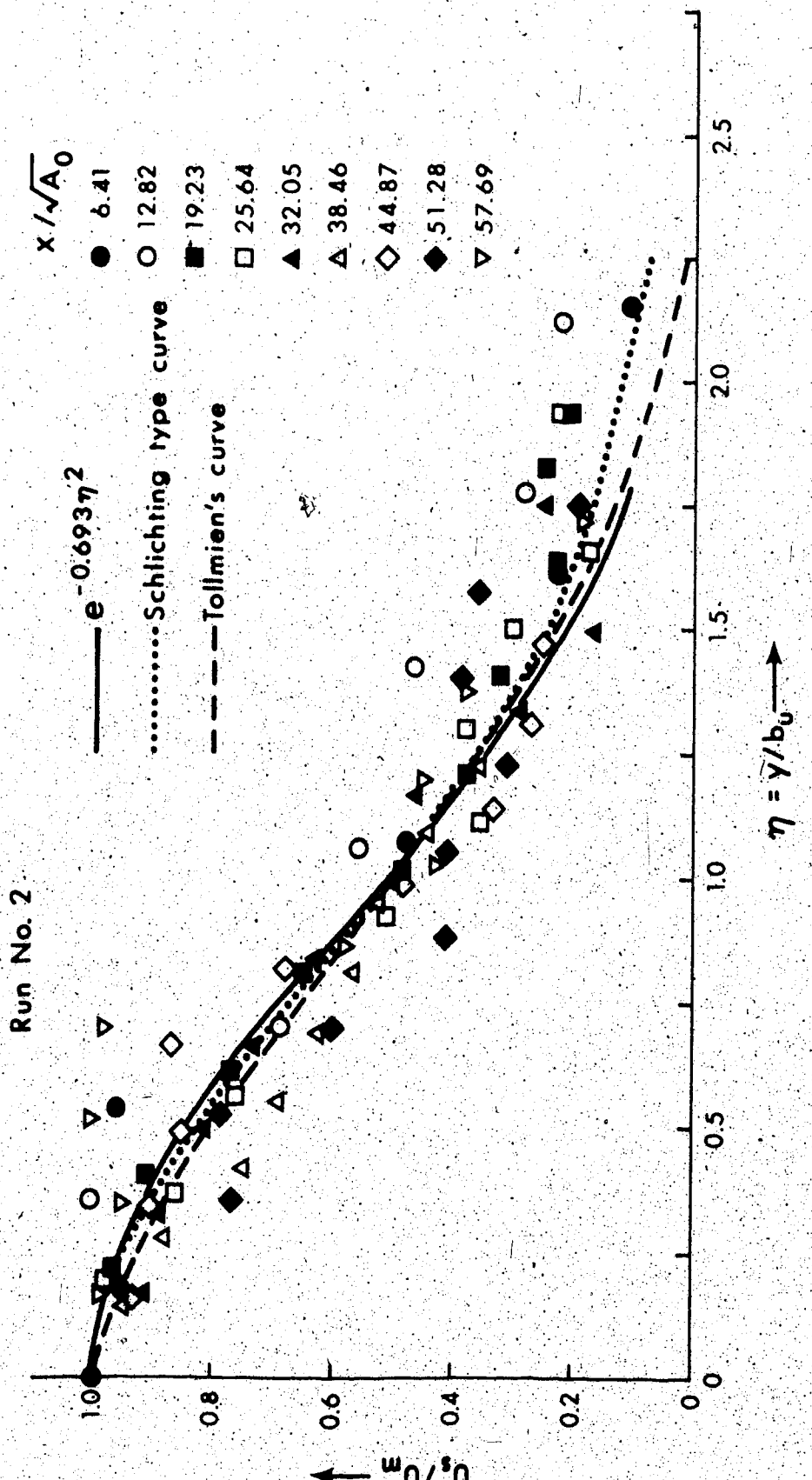

FIGURE 5.7 NON-DIMENSIONAL LONGITUDINAL VELOCITY PROFILE ON THE SURFACE $z/\sqrt{A_0} = 0$, Ri = 0.35

Figure 5.7 are practically the same as those for large Richardson numbers with a small difference towards the tail end. The similarity form for moderate Ri near the tail end is closer to that of a three dimensional nonbuoyant jet than that of large Ri. Although any of the profiles can be taken as a good approximation, Schlichting's type curve fits the data better towards the tail end. However, exponential distribution is simpler to use in practice.

5.4 Velocity Distribution in the Central Vertical Plane

5.4.1 Large Richardson Number

The velocity distribution in the vertical plane for large Richardson number is shown in Figure 5.8. The distribution has been found to be similar along parallel vertical planes over the whole length of measurement. This distribution has been compared with the Schlichting's type curve and the exponential distribution given by $e^{-0.693(z/h_u)^2}$. The exponential distribution no longer fits the data closely as it lies above the experimental data up to $z/h_u < 1.0$ and below the data for $z/h_u > 1.0$, whereas the agreement with Schlichting's type curve is much better.

5.4.2 Moderate Richardson Number

The distribution for vertical velocity variation is shown in Figure 5.9. There is some scatter in the data, however, the plot clearly shows that the profiles are similar and have approximately the same form as for large Ri. The data could be closely approximated by

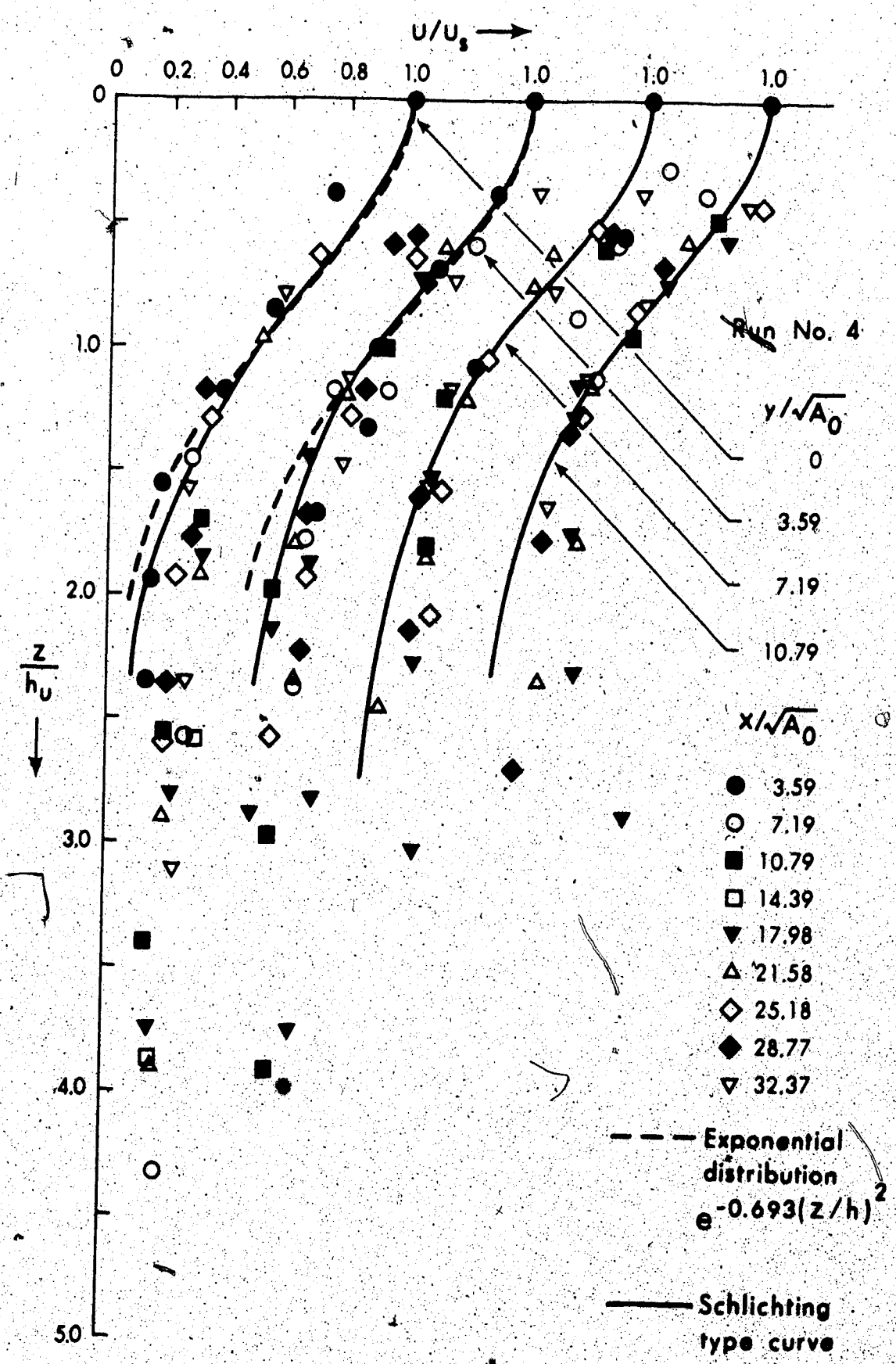

FIGURE 5.8 NON-DIMENSIONAL LONGITUDINAL VELOCITY PROFILES IN VERTICAL PLANES, SECTION $y/\sqrt{A_0}$ = 0 TO 10.79, Ri = 0.79

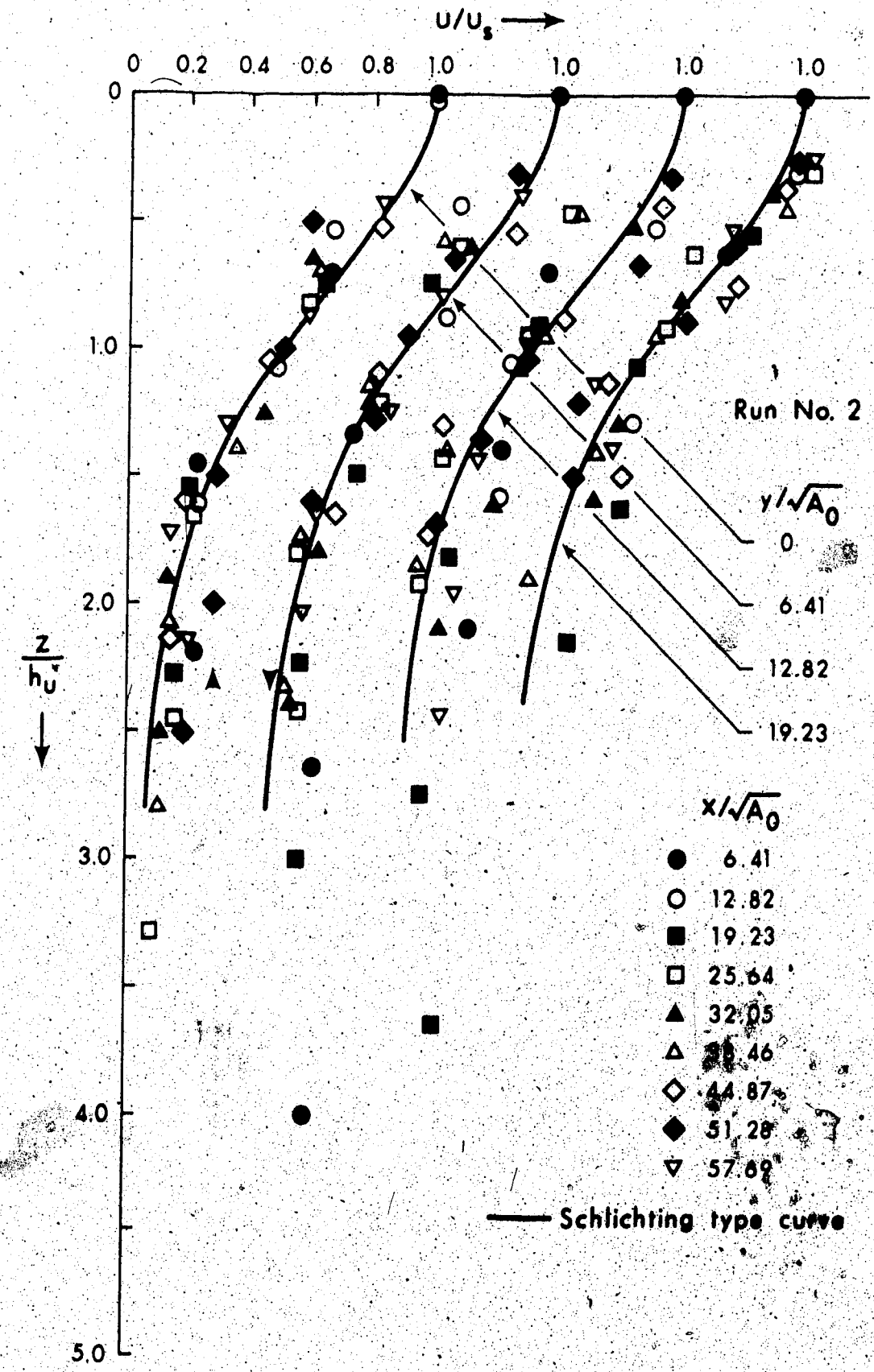

FIGURE 5.9 NON-DIMENSIONAL LONGITUDINAL VELOCITY PROFILES IN VERTICAL PLANES, SECTION $y/\sqrt{A_0}$ = 0 TO 19.23, R1 = 0.35

Schlichting's type curve.

5.5 Decay of Maximum Velocity

Maximum velocity has been found to be on the centerline of the jet. Pani (1972) showed that decay of the centerline velocity for a jet should be plotted as u_m/U_o versus $x/\sqrt{A_o}$ in order to eliminate the effect of aspect ratio h_o/b_o. A plot of u_m/U_o versus $x/\sqrt{A_o}$ is shown in Figure 5.10(a). The data show some systematic variation with Richardson numbers. For Run Nos. 1 to 3, the surface velocities observed near inlet U_{os} were the same as the calculated average velocity out of the inlet U_o ; but for Run Nos. 4 and 5, the surface velocities observed near inlet U_{os} were higher than the average velocities. A plot of u_m/U_{os} versus $x/\sqrt{A_o}$ is shown in Figure 5.10(b). The data still show the systematic variation with Richardson numbers. At this stage it is not clear whether various values of source Richardson numbers used in the experiments pertain to a moderate or a large Richardson number range. The theoretical analysis for moderate Richardson number (for $c = 0$) shows that $u_m \propto (1/x)^{2/3}$, as given by Equation 3.6.5a. Therefore, all the runs have been plotted as $(U_{os}/u_m)^{3/2}$ versus $x/\sqrt{A_o}$ and the slope of the straight lines so obtained have been determined. These plots are shown in Figure 5.11(a) and Figure 5.11(b). The value of these slopes are shown in Figure 5.12. The plot shows that the slope first decreases and then increases with an increase in Richardson number. A discussion on this change of behaviour is given in the next paragraph. This change occurs near $Ri = 0.84$. The

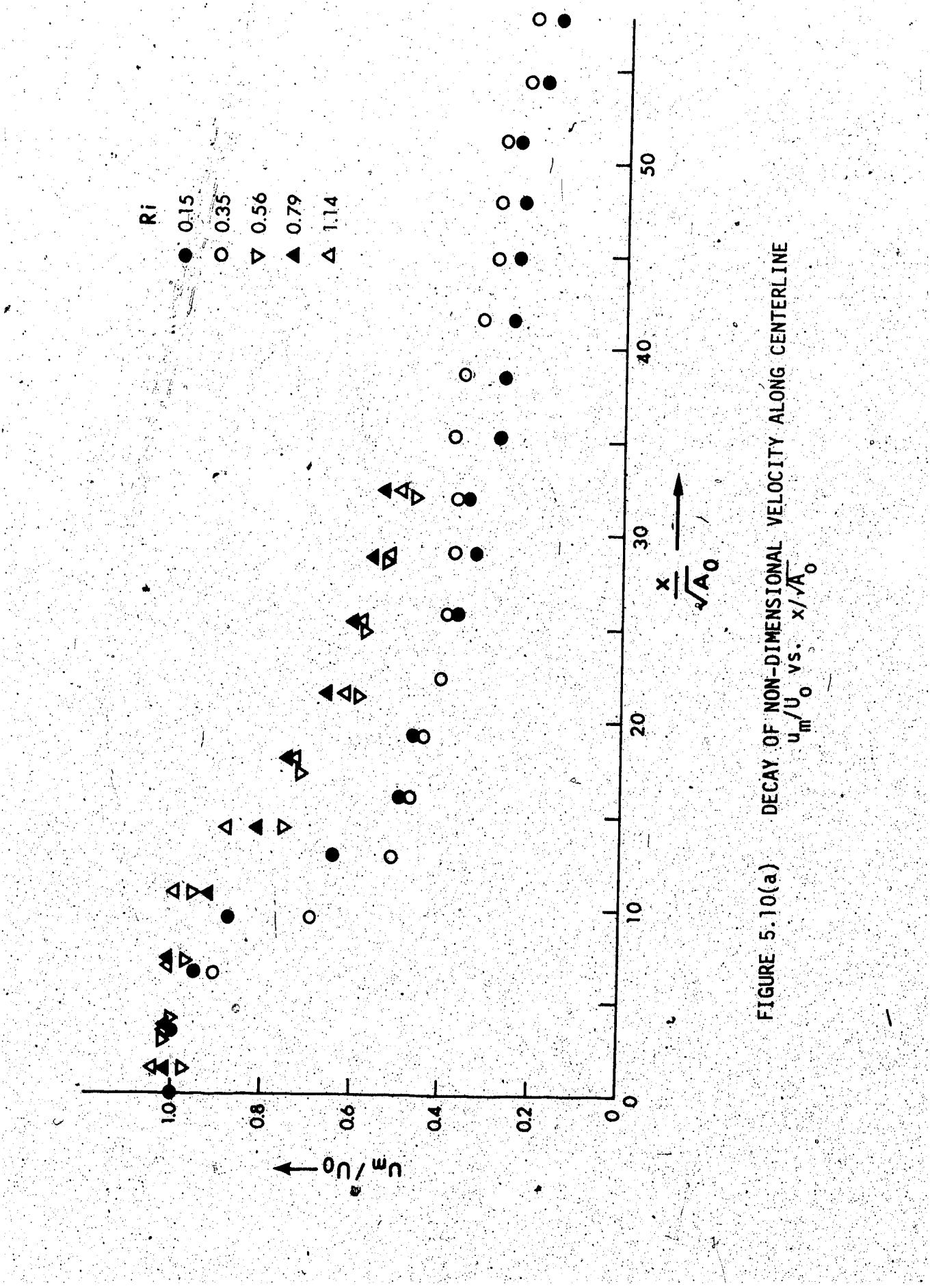

FIGURE 5.10(a) DECAY OF NON-DIMENSIONAL VELOCITY ALONG CENTERLINE
u_m/U_o vs. $x/\sqrt{A_o}$

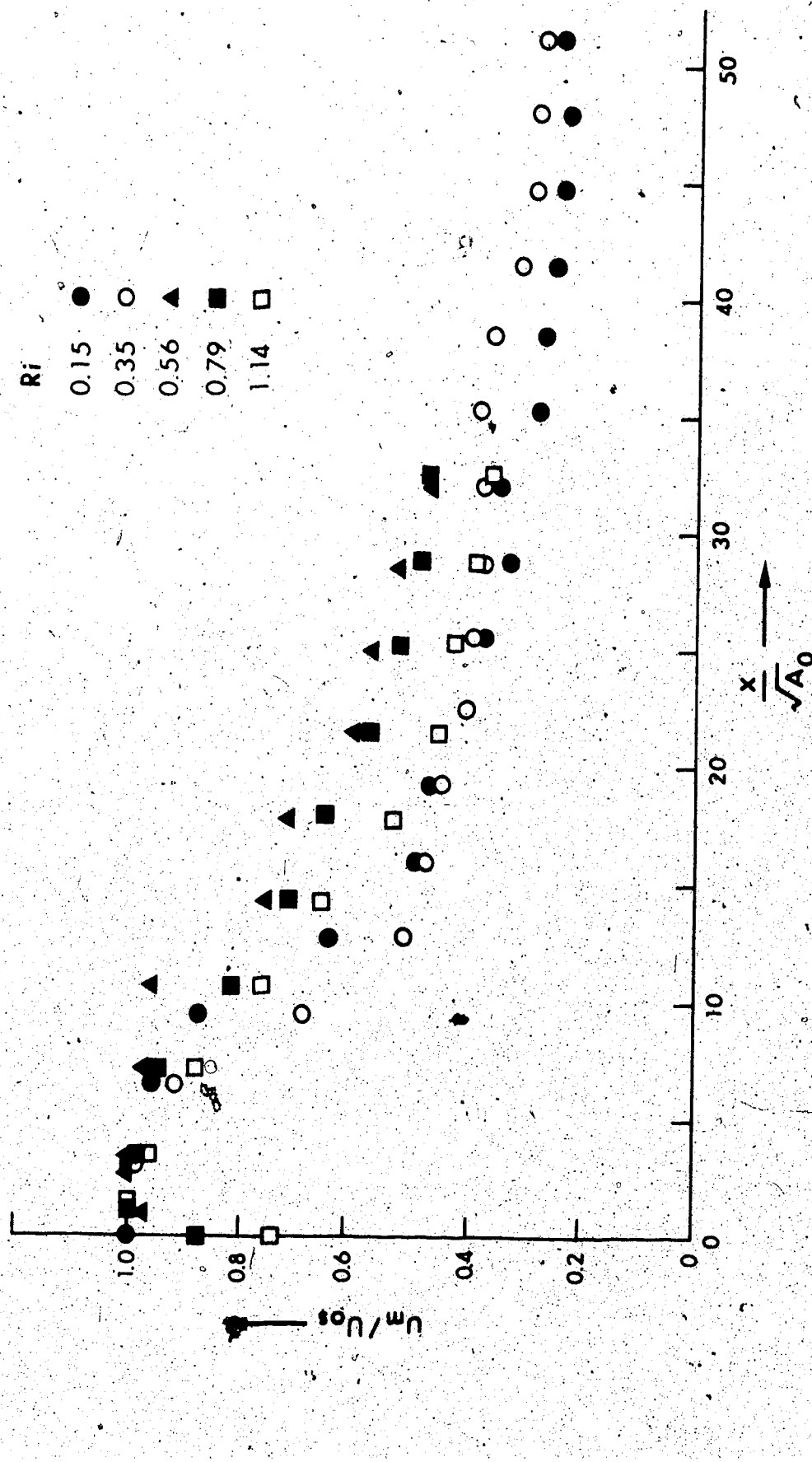

FIGURE 5.10(b) DECAY OF NON-DIMENSIONAL VELOCITY ALONG CENTERLINE u_m/U_{os} versus $x/\sqrt{A_o}$

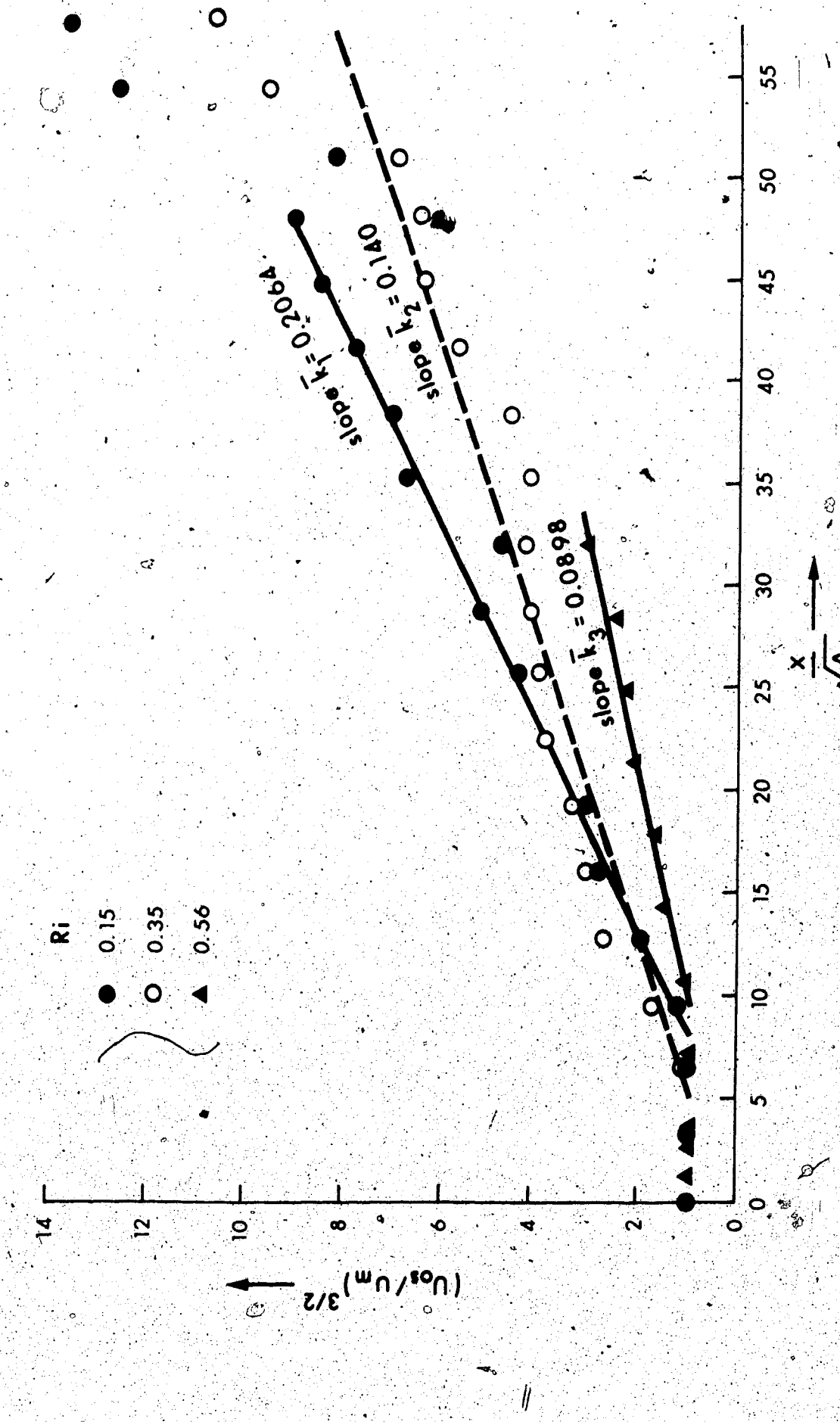

FIGURE 5.11(a) SLOPE OF VELOCITY SCALE FOR Ri 0.15 TO 0.56

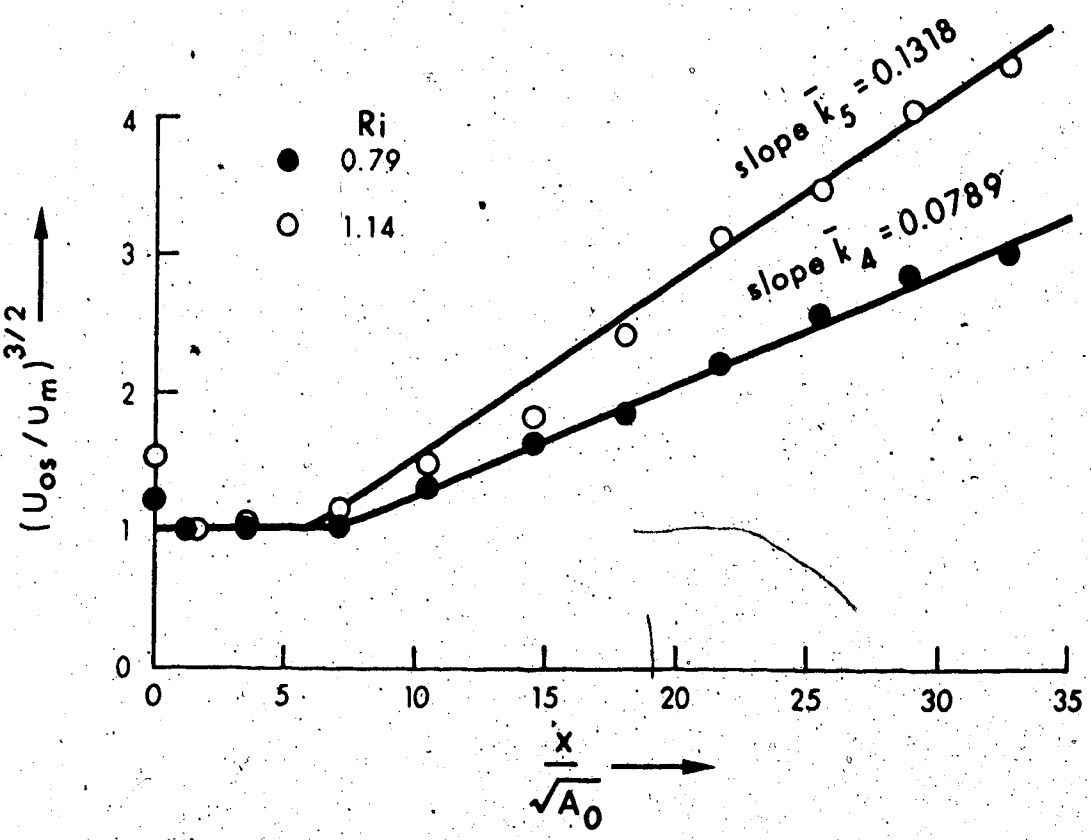

FIGURE 5.11(b) SLOPE OF VELOCITY SCALE FOR Ri 0.79 AND 1.14

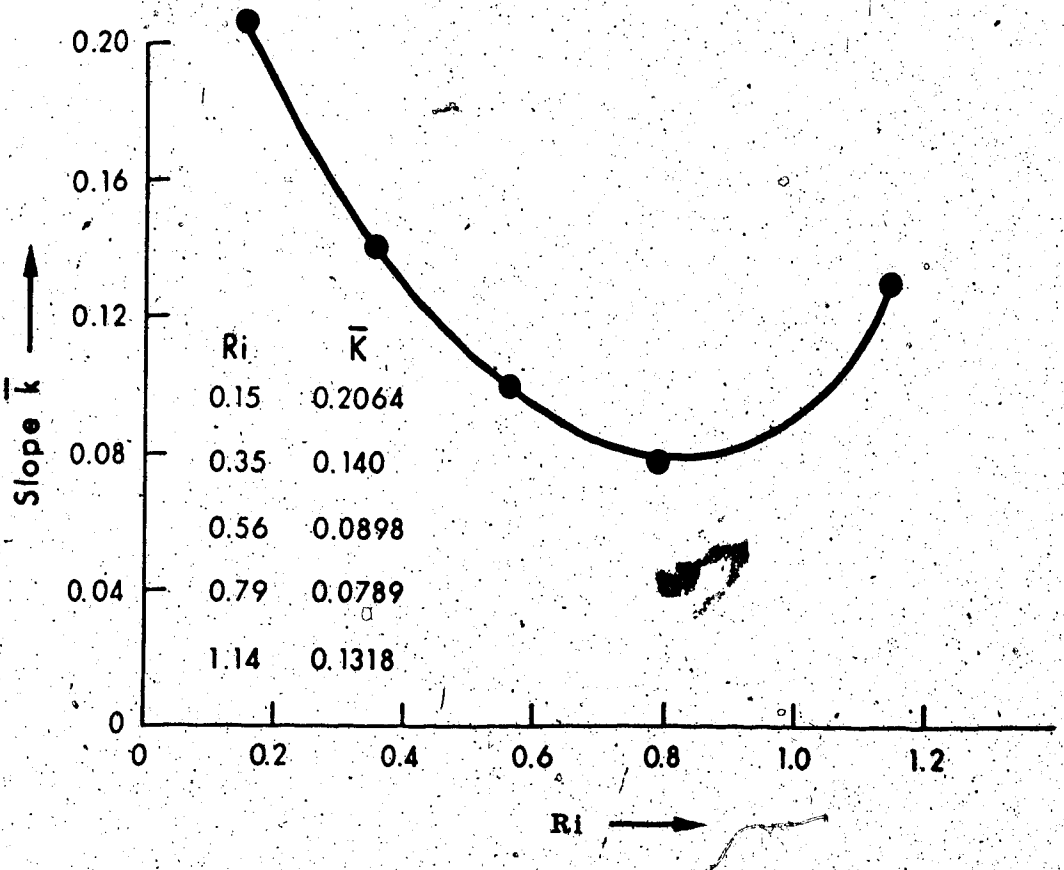

FIGURE 5.12 VARIATION OF SLOPE OF VELOCITY SCALES WITH RICHARDSON NUMBERS

Richardson number Ri = 1.14 is thus considered to belong to a different group, whereas, Ri = 0.79 appears to be a border case. Half widths of temperature and velocity for Ri = 0.79 plotted with respect to x (Figure 5.13) yield a straight line with practically no scatter in the data. As discussed in Equation 3.6.2b, the value of b for high Ri is linearly proportional to x. Hence the values of Ri = 0.79 and higher are classified as large Richardson number and the lower values are treated as moderate Ri. This has been further discussed in the section dealing with centerline decay of temperature.

The reason for change of the behaviour of the slope variation cannot be stated very precisely. It appears that for moderate Richardson number the jet goes on thining as the Richardson number increases and so the decay of centerline velocity reduces. As the Richardson number approaches 0.8, the formation of a floating plume starts whereby the surface velocity near the inlet becomes larger than average velocity from the inlet. This provides a larger velocity gradient for diffusion in lateral direction, further this increased surface velocity considerably increases the lateral entrainment ($v_e = \alpha u_m$), and thus leads to a rapid decay of velocity as Richardson number increases.

5.5.1 Decay of Maximum Velocity for Moderate Ri

The theoretical analysis for moderate Richardson numbers, in fact, indicates the value of u_m as follows:

$$u_m \propto \frac{1}{x^{2/3 + c}} \qquad (3.6.3)$$

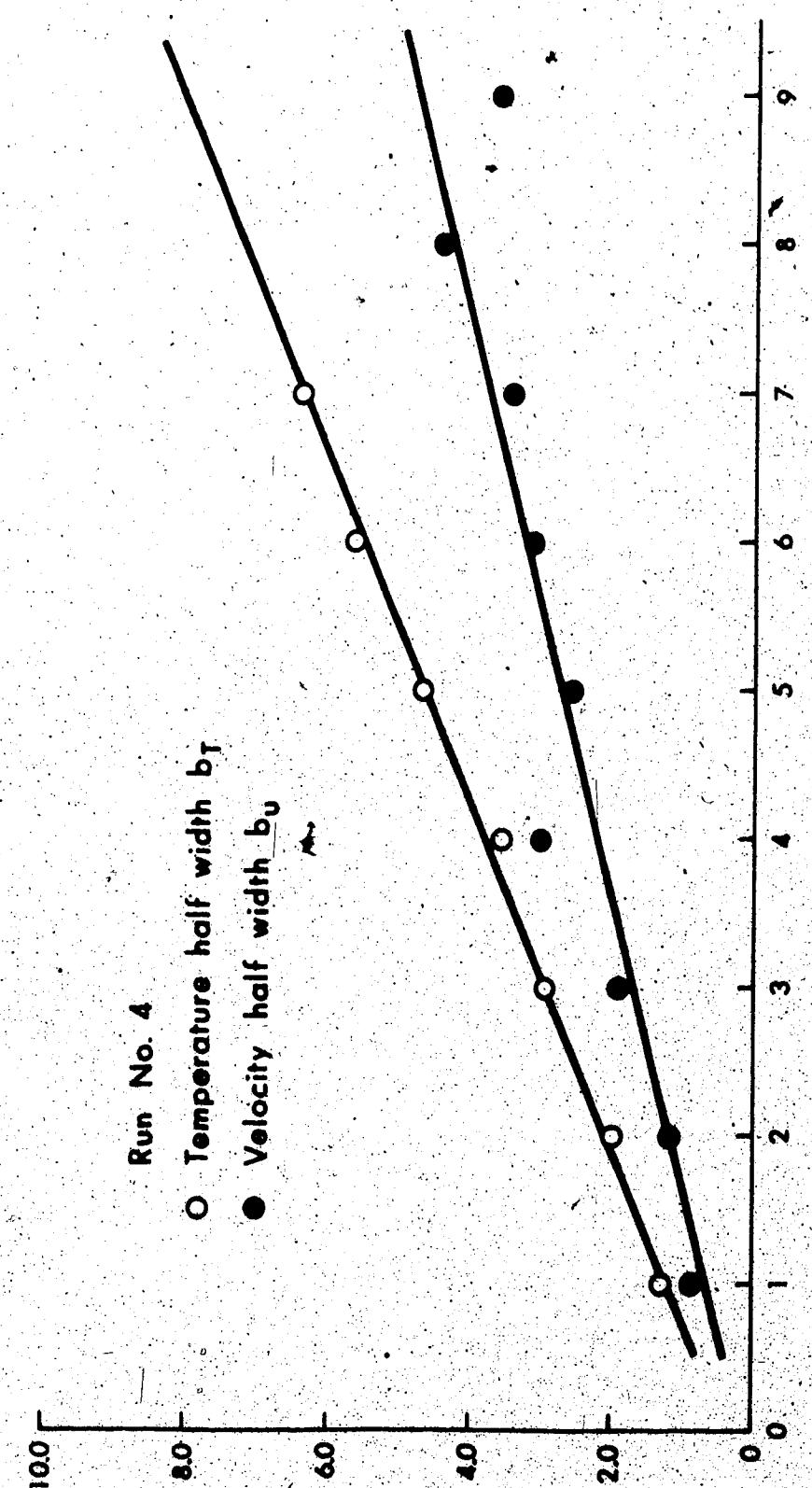

FIGURE 5.13 VARIATION OF HALF WIDTH OF JET FOR Ri = 0.79

The value of c is the exponent of x for variation of h_{mu} in the longitudinal direction. The variation of h_{mu} is shown in Figure 5.16(b). The variation of h_{mu} for moderate range from $Ri = 0.15$ to 0.56 cannot be considered anything but constant, hence $c = 0$. Thus, Equation 3.6.3 becomes:

$$u_m \propto \frac{1}{x^{2/3}} \qquad (3.6.5a)$$

A study of dimensional analysis of the problem indicates the same result.

Experimental data have been plotted as per Equation 3.6.5a. The constant of proportionality in Equation 3.6.5a has been found to be a function of Ri as shown in Figure 5.11(a). The experimental data can be merged together by plotting $(U_o/u_m)^{3/2}\ Ri^{m_1}$ versus $x/\sqrt{A_o}$ for several values of m_1. The value of m_1 that yields the best fit to the data works out to be 1/2. There could be various other forms as well to represent this variation of Ri but it has to be empirically chosen. A polynomial variation of Ri to merge the scatter in the data seems to be convenient and hence has been adopted in all further formulations.

The above equation of mean straight line passing through the data is as shown in Figure 5.14:

$$u_m/U_o = 5.678\ Ri^{1/3}(x/\sqrt{A_o} + 1)^{-2/3} \qquad (5.5.1)$$

The above equation can also be reduced to the simpler form as:

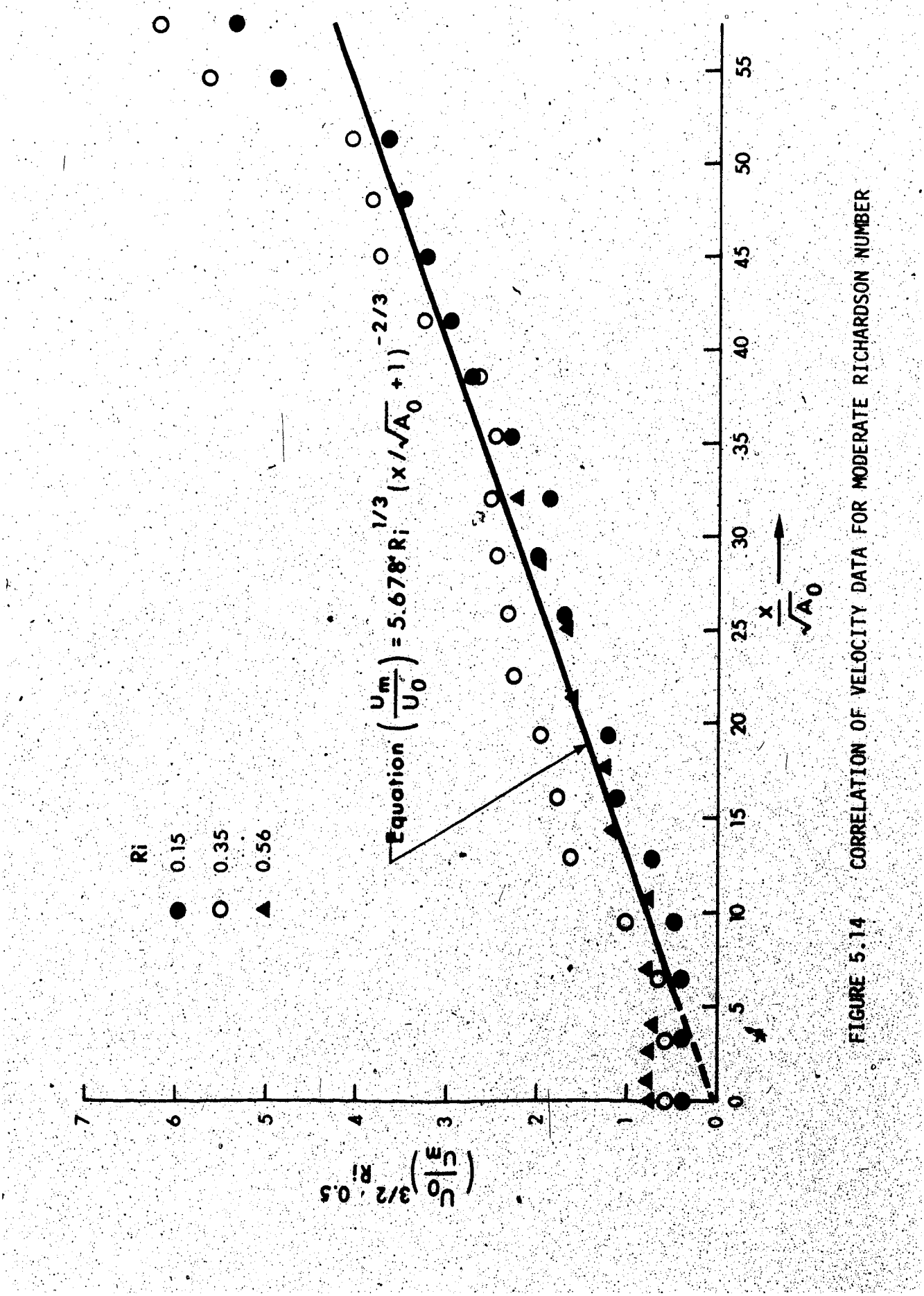

FIGURE 5.14 CORRELATION OF VELOCITY DATA FOR MODERATE RICHARDSON NUMBER

$$u_m/U_o = \frac{5.678\,(Ri)^{1/3}}{(x/\sqrt{A_o})^{2/3}} \qquad (5.5.2)$$

where $x/\sqrt{A_o}$ is measured from virtual origin, or, if measured from the inlet, should be true for large distances from the outlet.

5.5.2 Decay of Maximum Velocity for Large Ri

The theoretical analysis for large Richardson number range indicates the value of u_m as:

$$u_m \propto \frac{1}{x^{1/3}} \qquad (3.6.2a)$$

The constant of proportionality in the case of moderate Richardson number depended on Ri. In the case of Equation 3.6.2a, the proportionality constant should also depend upon Ri. The experimental results have therefore been plotted as:

$$\left(\frac{U_o}{u_m}\right)^3 Ri^{m_1} \sim (x/\sqrt{A_o})$$

The value of m_1 that suits the data best equals $-1/2$ and the plot of $(U_o/u_m)^3\, Ri^{-1/2}$ versus $(x/\sqrt{A_o})$ is shown in Figure 5.15.

The equation of a mean straight line passing through the data is:

$$\left(\frac{u_m}{U_o}\right) = 1.434\, Ri^{-1/6}\, (x/\sqrt{A_o} - 10.5)^{-1/3} \qquad (5.5.3a)$$

applicable for $x/\sqrt{A_o} > 12.5$ and:

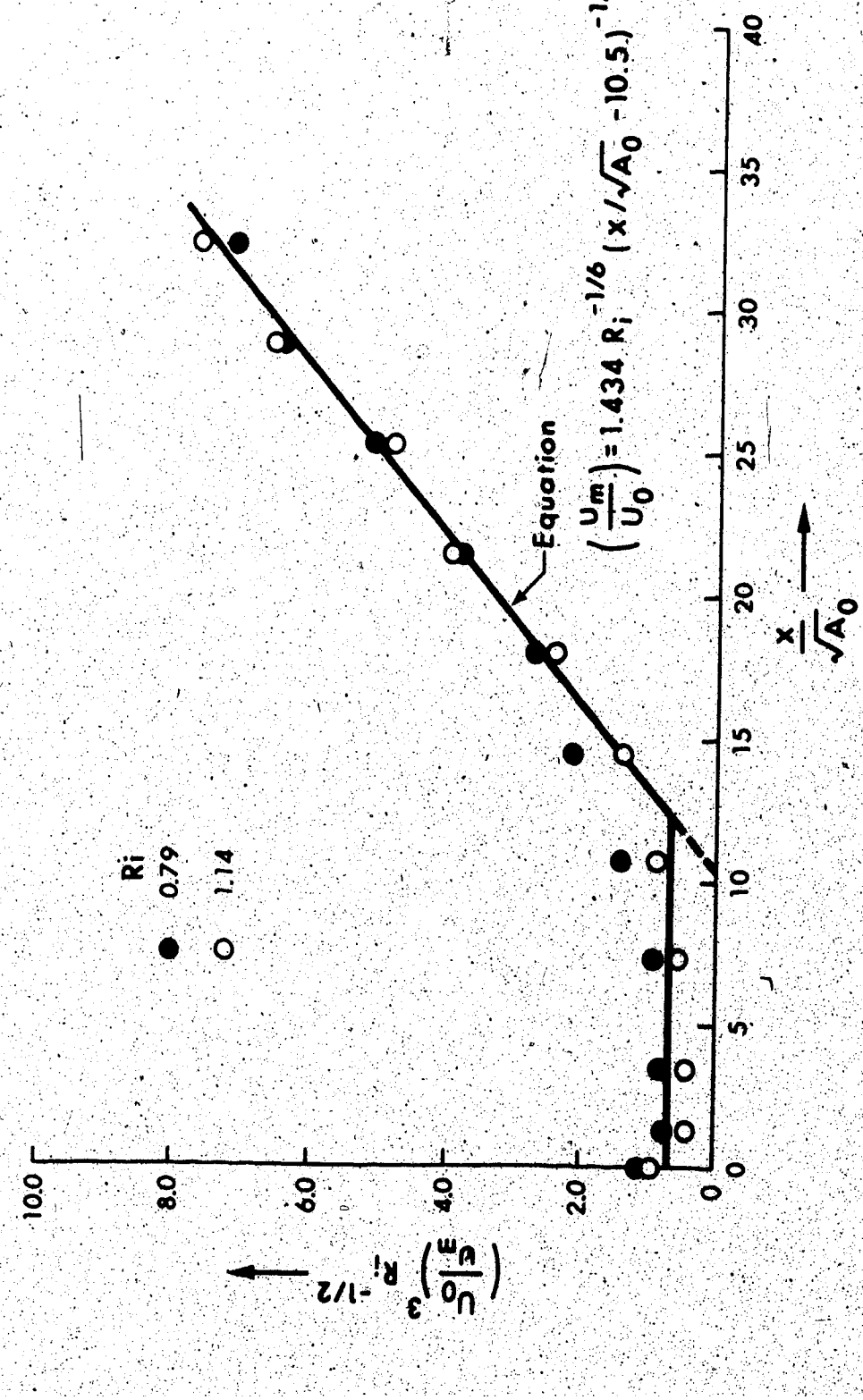

FIGURE 5.15 CORRELATION OF VELOCITY DATA FOR HIGH RICHARDSON NUMBER

$$\left(\frac{u_m}{U_o}\right) = 1.154\ Ri^{-1/6} \qquad (5.5.3b)$$

applicable for $x/\sqrt{A_o} \leq 12.5$

Equation 5.5.3a indicates a large virtual origin correction in this case. Such a large virtual origin correction perhaps can be explained as resulting from the formation of the floating plume as described earlier in Section 5.5. Due to this, the surface velocities near the inlet exceeded the average by 14.1% for $Ri = 0.79$ and 34.4% for $Ri = 1.14$. This formation of a floating plume presumably leads to a large origin correction. Such an increase in velocity has also been observed in the field. Paddock, et al. (1973, page 69) measured velocities as high as 60% above outfall velocities at the Point Beach outfall.

5.6 Length Scale

5.6.1 Variation of Half Velocity Depth of the Jet in Lateral Cross-sections

Vertical spread of the jet is produced essentially by turbulent mixing which is in turn affected by buoyancy. The buoyancy force not only inhibits vertical mixing, but the gravity current caused by it may reduce the depth at the center and increase it on the sides, as shown in Figure 2.7(c). Variation of half velocity depth for run No. 4 is shown in Figure 5.16(a). Variation for other runs follows the same pattern and their values are given in Appendic C (Tables C-5 to C-8).

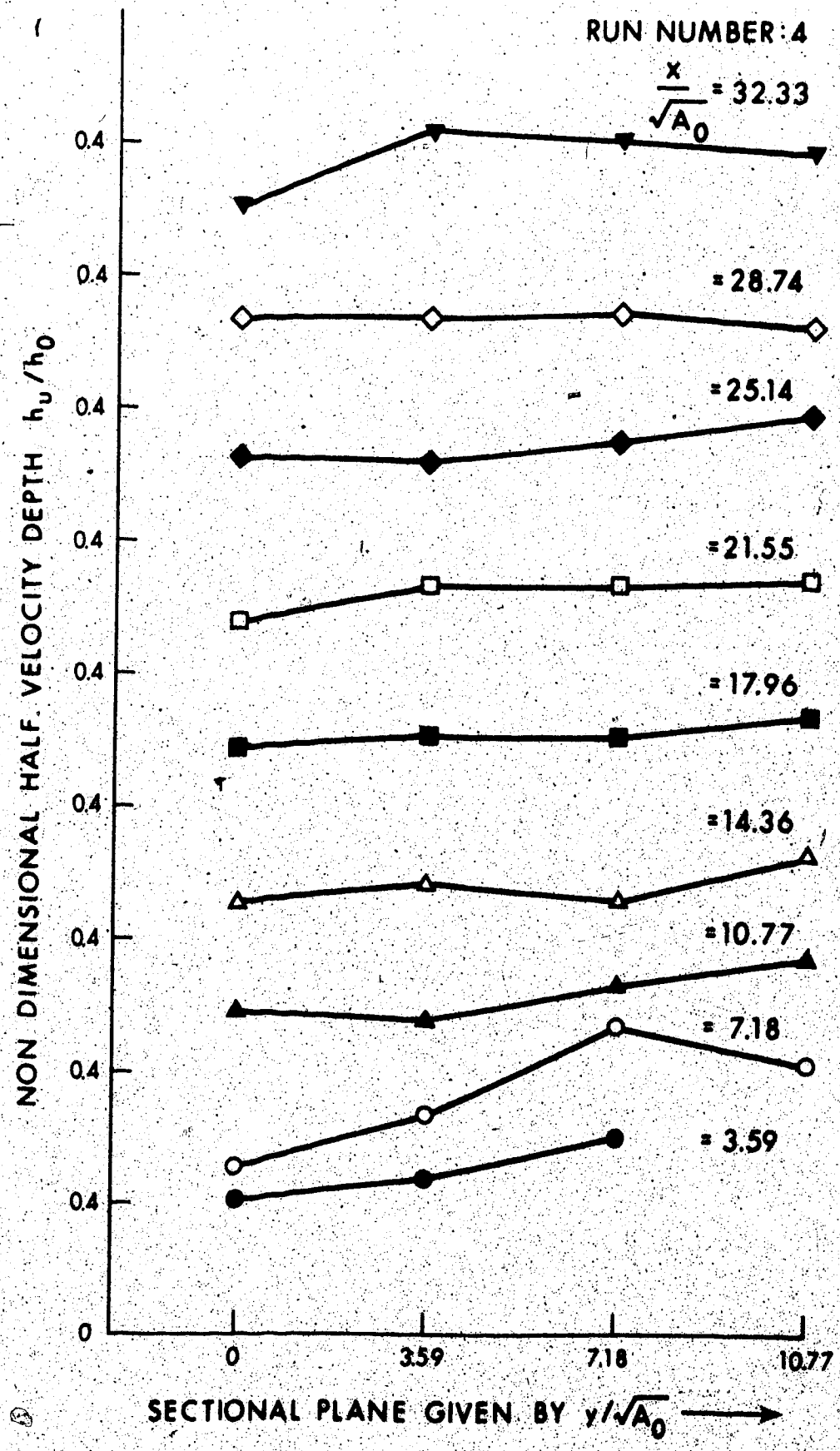

FIGURE 5.16(a) LATERAL VARIATION OF HALF VELOCITY DEPTH FOR R1 = 0.79

The half depth of the jet remains approximately constant after $x/\sqrt{A_o} > 14.36$. For $x/\sqrt{A_o} < 14.36$, the half velocity depth of the jet on the side appears to be thicker than that at the center. It appears that the buoyancy force at the central plane neat the inlet is much higher than that at parallel planes in the lateral direction away from the center. Due to this uneven distribution of buoyancy force, the reduction of half depth seems to be maximum in the center. Hence, the depth on the side planes becomes more as stated earlier. As one moves downstream along the length of the flume, the buoyancy force decreases and its difference between the central plane and side planes becomes less pronounced, therefore, the half depth tends to become more uniform.

5.6.2 Variation of Half Velocity Depth in the Longitudinal Direction

The variation of half velocity depth is shown in Figure 5.16 (b). The value of centerline half depth is more or less constant for Ri = 0.15 and 0.35. For Ri = 0.56, the parameter shows a slight increase after an initial abrupt decrease. The same trend continues in the case of large Richardson number as well. The behaviour however is not very systematic.

Values of average half depth, as shown in Figure 5.17, are found to be remarkably constant all along the length measured. Logically, one would expect significant vertical mixing to occur at such a low value of Richardson number, Ri of 0.15, but even for that value average half depth has been found to be relatively constant. A similar observation has been made by Paddock, et al. (1973, page 125). They

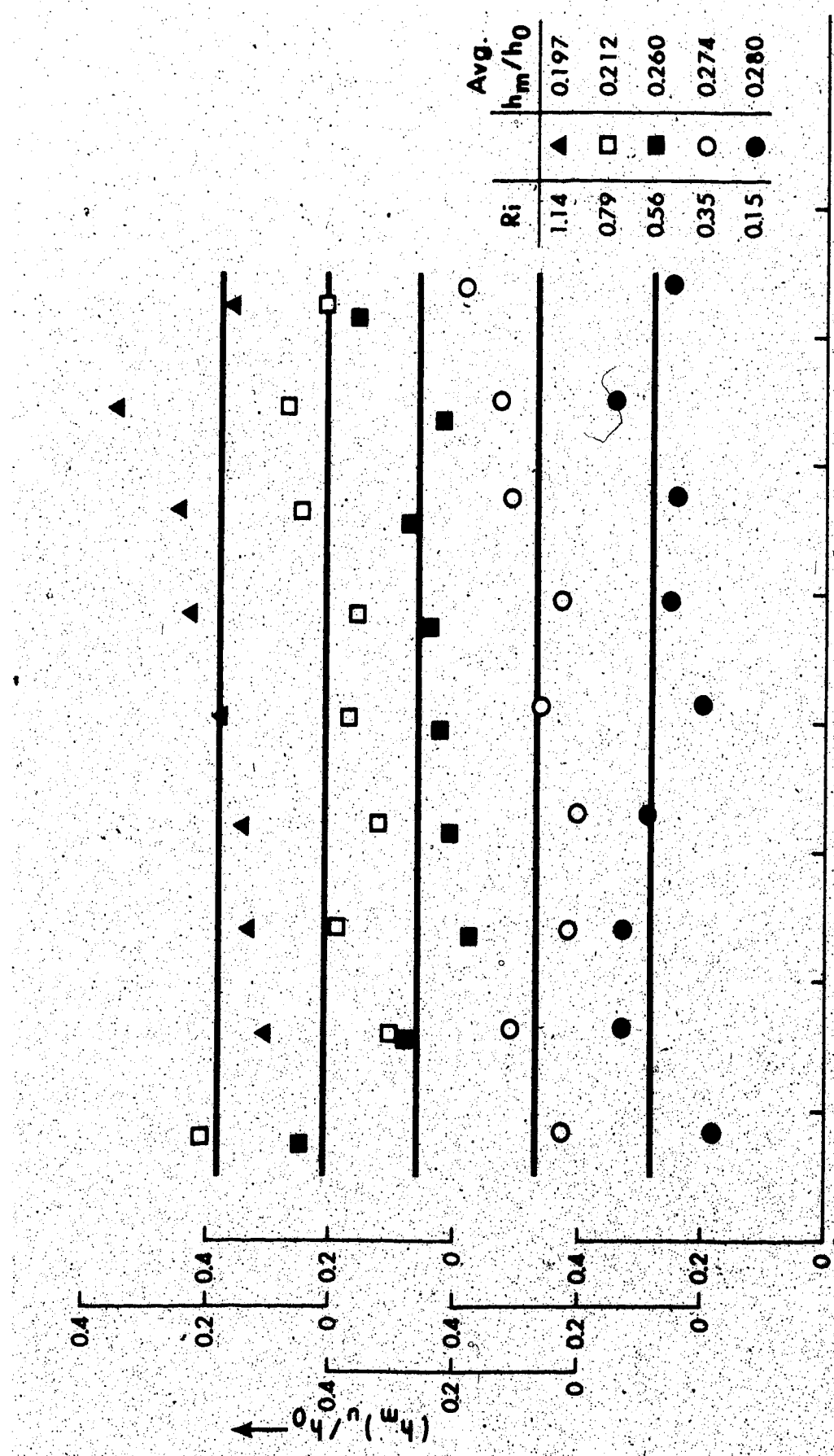

FIGURE 5.16(b) VARIATION OF CENTERLINE HALF VELOCITY DEPTH WITH DISTANCE

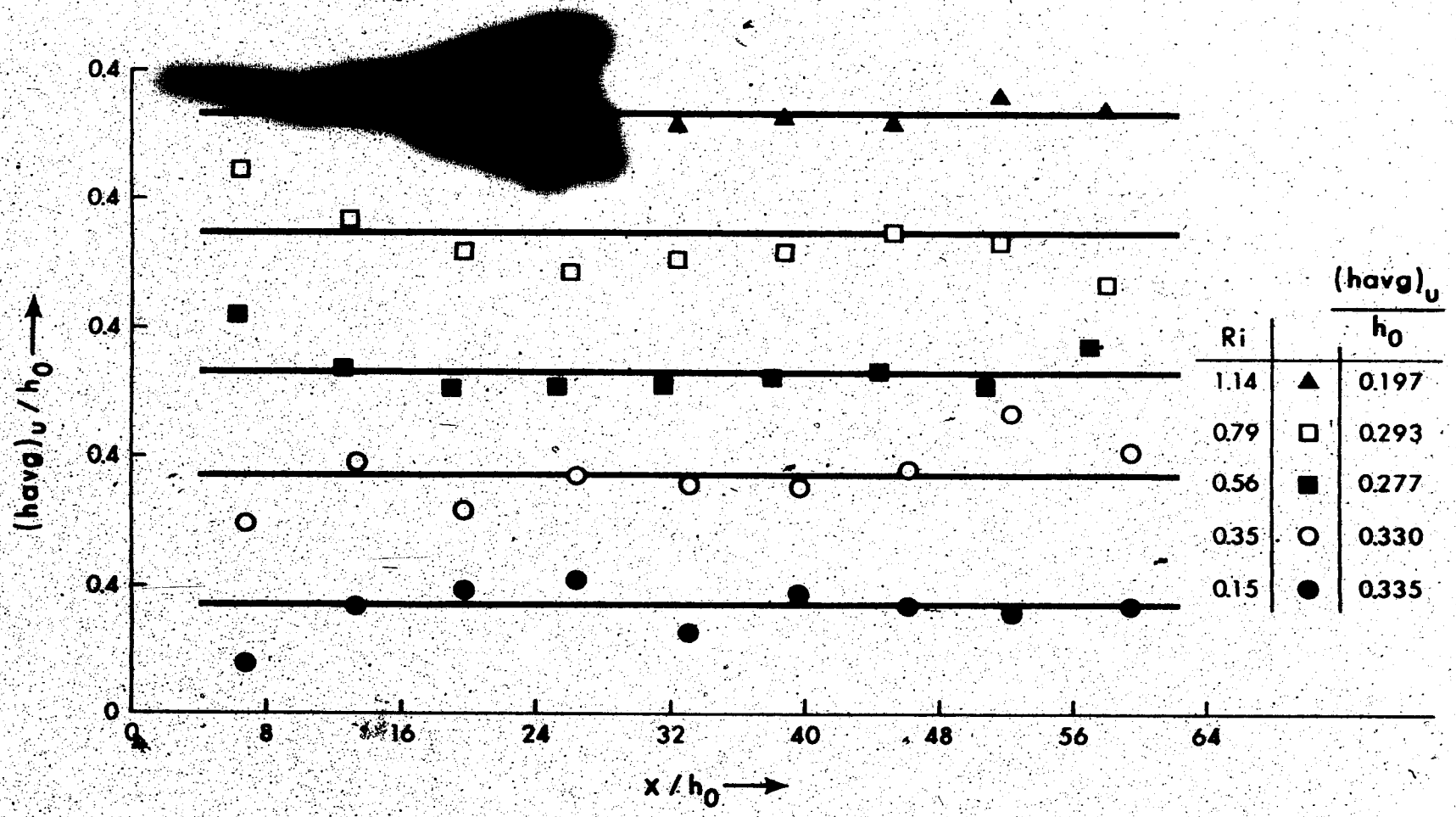

FIGURE 5.17 VARIATION OF AVERAGE HALF DEPTH OF JET WITH DISTANCE

state that for Richardson number greater than 0.25 buoyant spreading is quite important; only for Richardson number lower than 0.04 could a substantial amount of vertical entrainment be expected.

It may be pointed out that there is an initial decrease in depth then the jet becomes constant in depth. The value of $(h_{avg})/h_o$ also decreases as the Richardson number increases. The data thus has been correlated by treating Ri as a variable. The value of $(h_{avg}/h_o)\ Ri^{1/8}$ versus x/h_o is plotted in Figure 5.18. A mean line can be drawn through the curve and its equation is:

$$(h_{avg\ u}/h_o)\ Ri^{1/8} = 0.26 \qquad (5.6.1)$$

5.6.3 Variation of Half Velocity Width of Jet

The variation of half width of jet plotted as b_u/b_o versus x/b_o is shown in Figure 5.19. Near the end of length of measurement approximately 9 feet away from the inlet, the side effect seems to affect the growth of the jet as the rate of growth of half jet seems to decrease near this point. The data have been segregated for large and moderate Richardson numbers and plotted separately in Figure 5.19(a) and Figure 5.19(b). The data show a very small effect of Richardson number on widths which can normally be neglected, but an increase in source Richardson number leads to an increase in the buoyancy force in the jet with a corresponding increase in lateral pressure thus causing a greater spread. Therefore, the value of half width for temperature and velocity should increase as Richardson number increases although

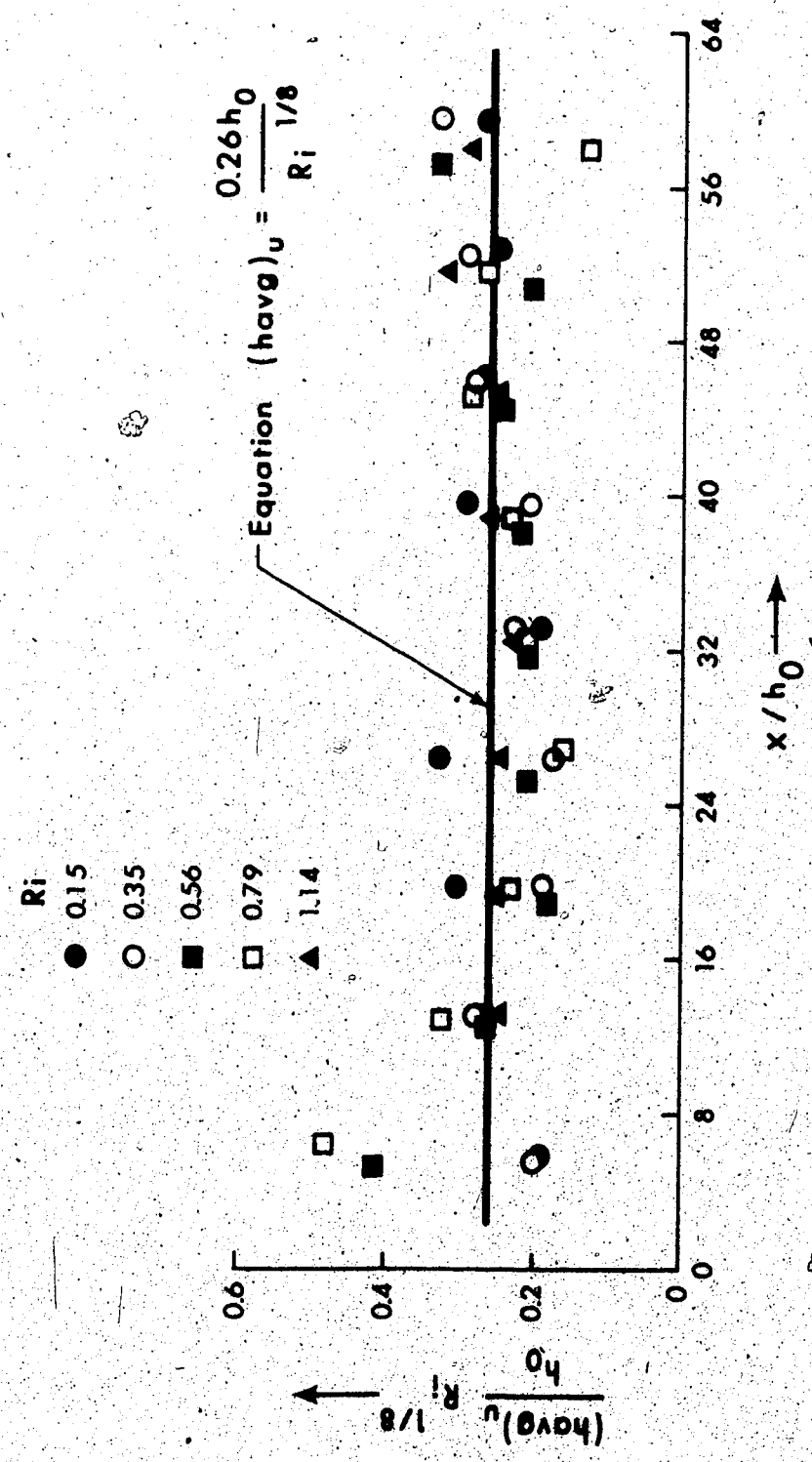

FIGURE 5.18 CORRELATION OF AVERAGE HALF DEPTH FOR VELOCITY FOR VARIOUS Ri

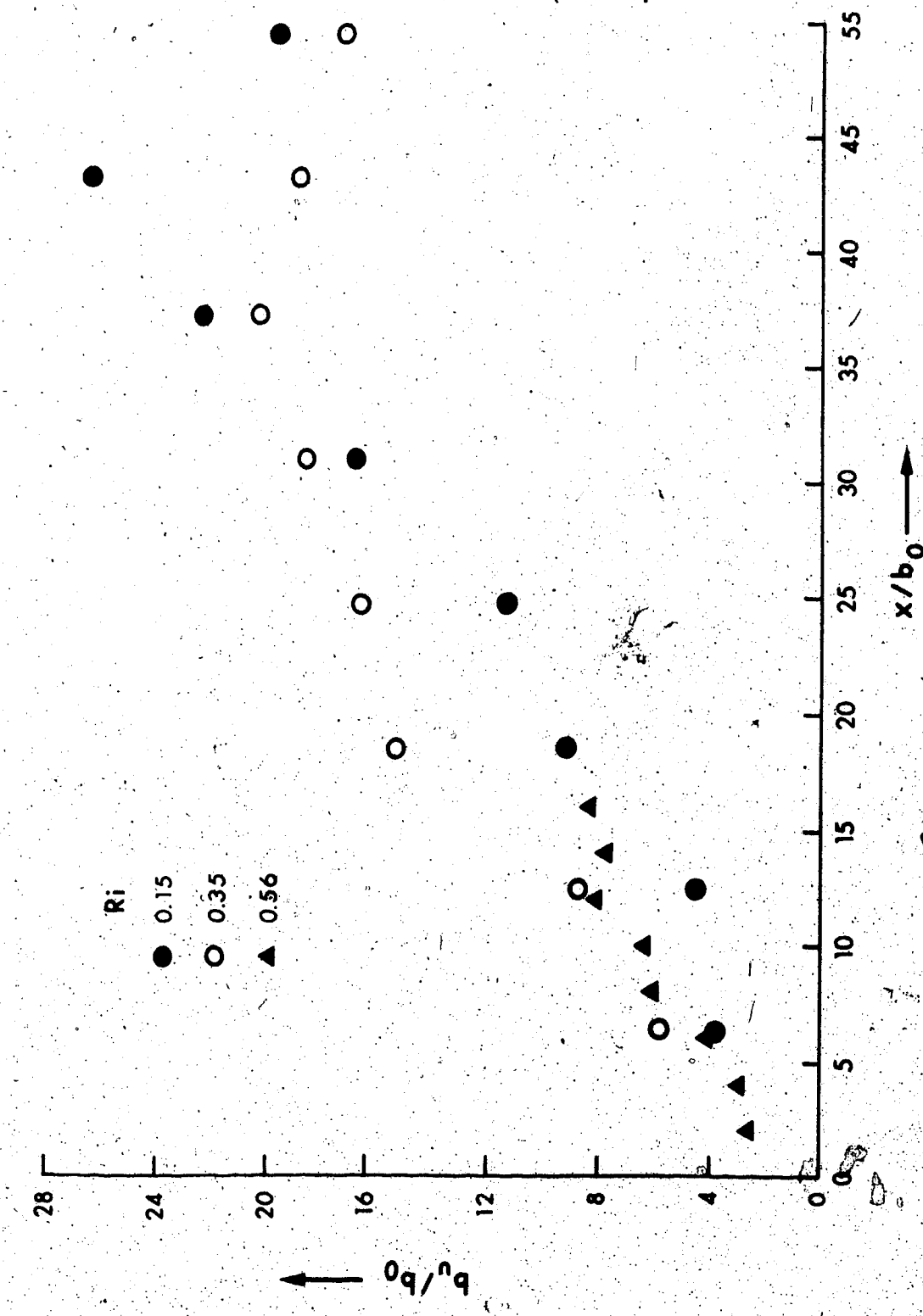

FIGURE 5.19(a) VARIATION OF NON-DIMENSIONAL HALF VELOCITY WIDTH WITH LONGITUDINAL DISTANCE FOR MODERATE Ri

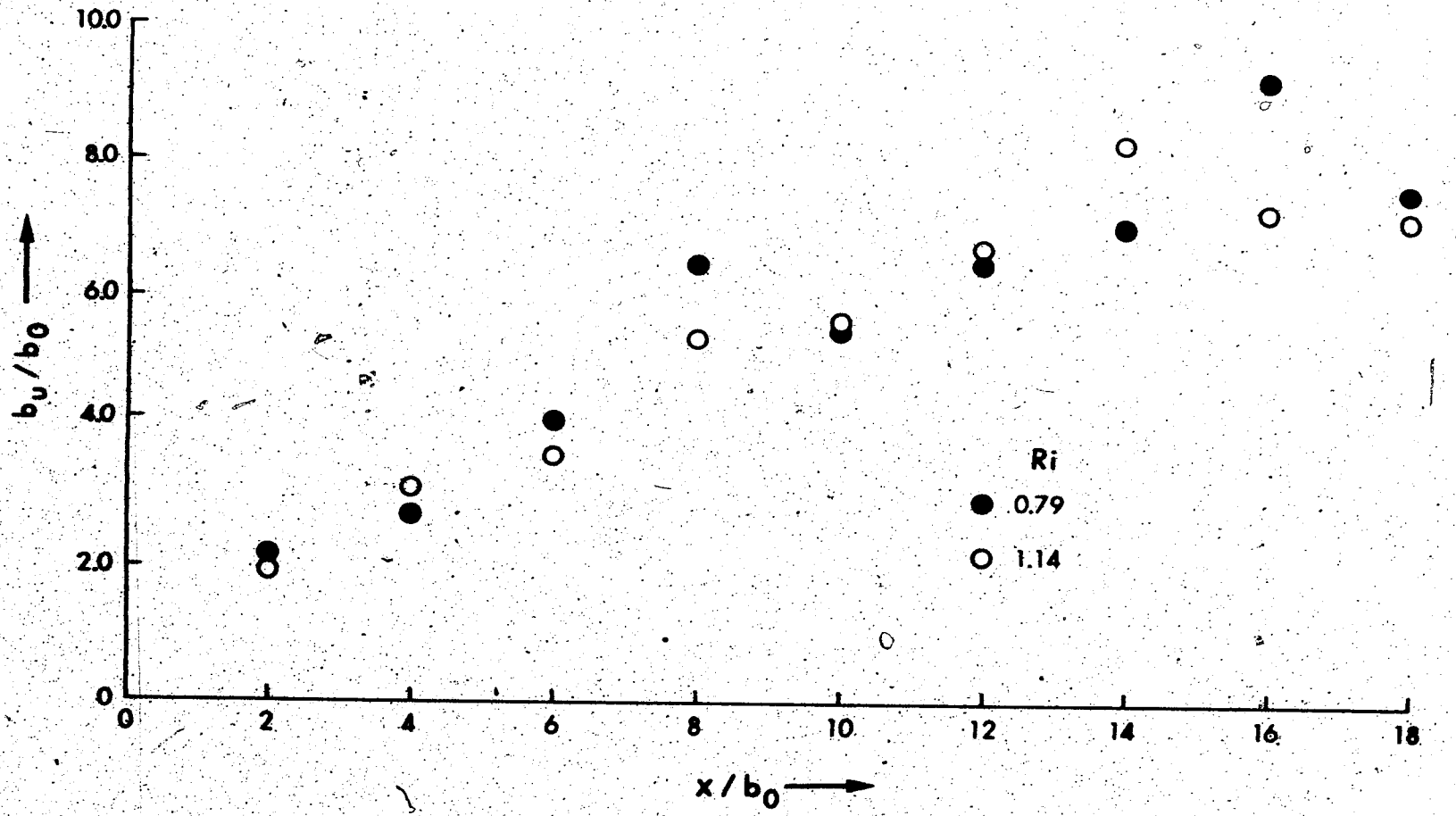

FIGURE 5.19(b) VARIATION OF NON-DIMENSIONAL HALF VELOCITY WIDTH WITH LONGITUDINAL DISTANCE FOR LARGE Ri

its effect could be small.

For moderate Richardson number the theoretical analysis gives $b \propto x^{4/3}$ when $c = 0$, as given by Equation 3.6.5c. The influence of Richardson number can be considered to be contained in the proportionality constant. Accordingly the experimental data has been plotted as $(b_u/b_o)\ Ri^{-m_1}$ versus x/b_o and the value of m_1 which gives a better fit with the data is found to be 1/8. The data are shown in Figure 5.20. The equation of mean straight line passing through the data is given by:

$$b_u/b_o = 0.206\ [Ri^{1/8}(x/b_o + 3.5)]^{4/3} \qquad (5.6.2)$$

For large Richardson number, the theoretical analysis gives $b \propto x$ as given by Equation 3.6.2b. The constant of proportionality here should contain the influence of Richardson number. A plot of $(b_u/b_o)^{3/4}\ Ri^{-1/8}$ versus x/b_o is shown in Figure 5.21. The correlation of data appears satisfactory. The equation of mean straight line passing through the experimental data is given by:

$$b_u/b_o = 0.4935\ Ri^{1/8}(x/b_o + 1.7) \qquad (5.6.3)$$

5.7 Measurement of Lateral Velocity v

The lateral velocity, v, has been measured in most of the experimental runs. The value of v component follows a distribution similar to that of nonbuoyant jets. A few typical plots for run No. 3

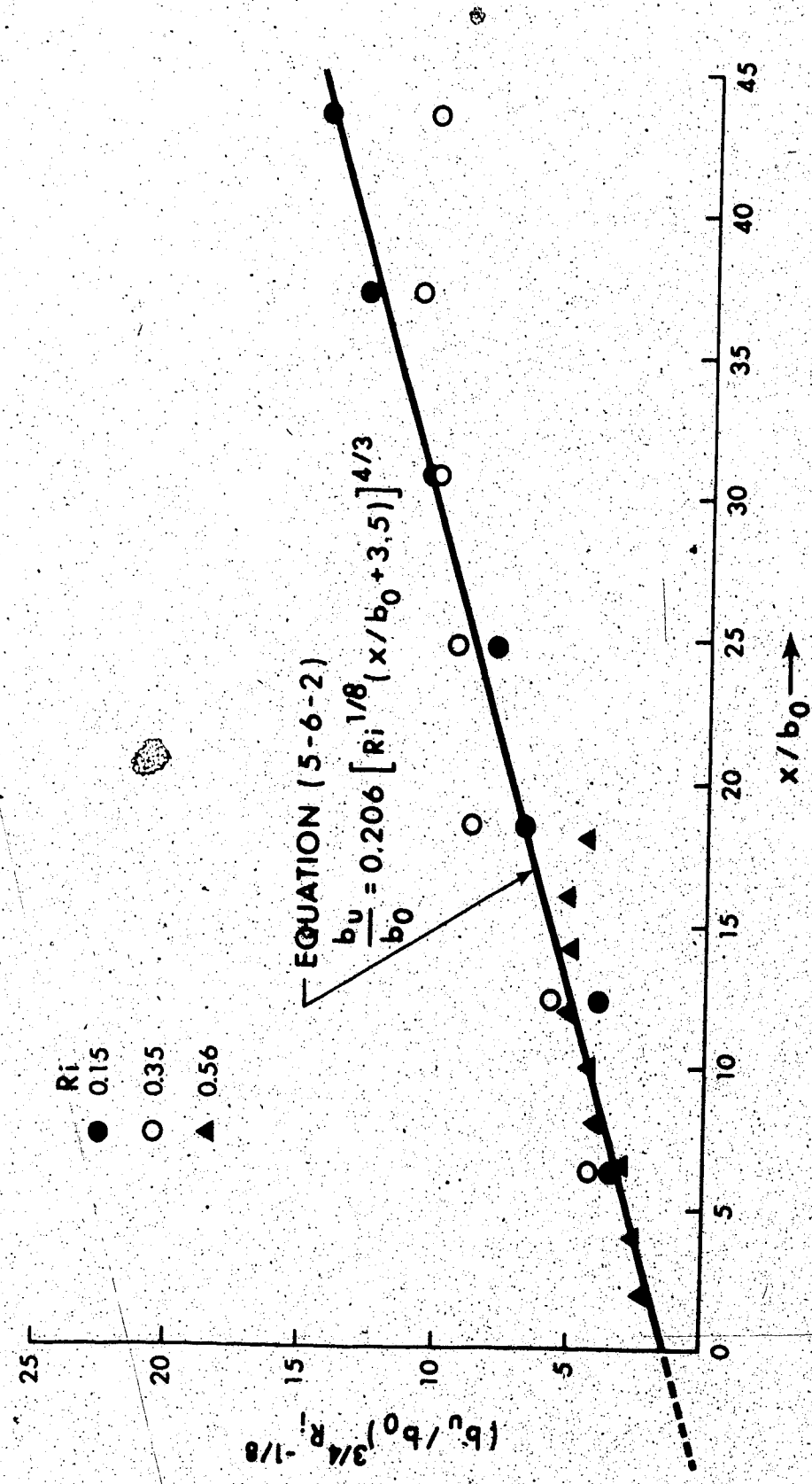

FIGURE 5.20 CORRELATION OF DATA FOR HALF VELOCITY WIDTH FOR MODERATE Ri

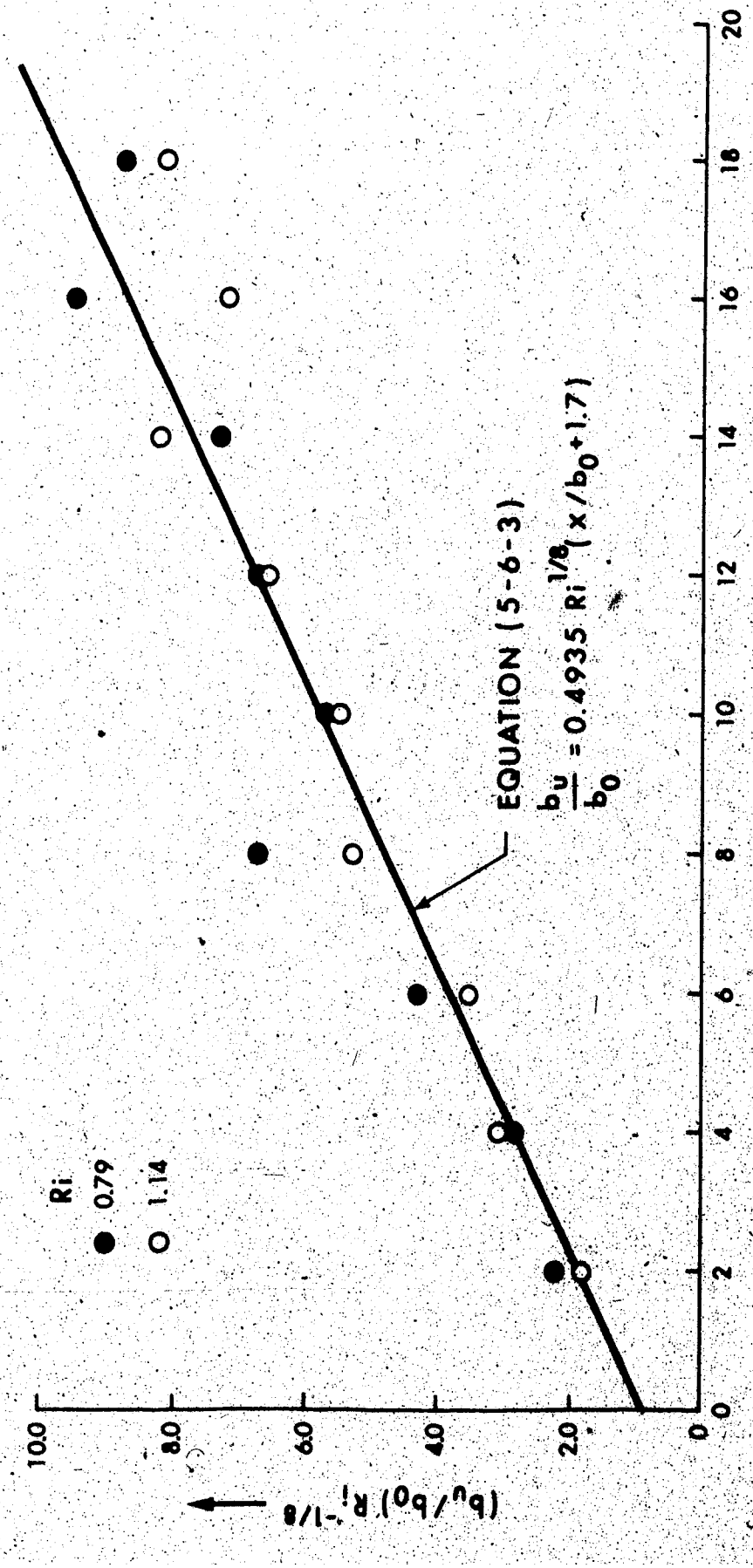

FIGURE 5.21 CORRELATION OF DATA FOR HALF VELOCITY WIDTH FOR LARGE Ri

are shown in Figure 5.22. The value of lateral velocity observed in the early regions of measurement has been found to be large. For this run, v_{max}/u_m was found to be about 0.5 as compared to 0.019 for non-buoyant circular jets. This substantial difference in spread appears to be induced by stratification and buoyancy. This value of v/u_m rises as Ri increases reaching 0.576 for Ri 1.14. Stefan (1972) finds this value as 0.40 in his experiments. Values of lateral velocity v measured for other runs are given in Appendix C (Figure C-9 and Figure C-10).

5.7.1 Entrainment Coefficient α

Fluid jets have the characteristics of "entraining" the surrounding fluid. Several different methods have been used to determine the value of α, defined as the ratio of v_e/u_m. Albertson (1950) determined α by calculating the mass flow rate by integration of the velocity profiles obtained at different axial stations. The principal difficulty with this method lies in the measurements of low velocities near the jet edge particularly at large axial distances. Ricou and Spalding (1961) measured the entrained flow instead of the jet flow. The jet was surrounded by a concentric chamber, closed at one end except for the jet nozzle and open to the atmosphere at the other end. The chamber was double walled with a porous inner wall through which measured entrainment air was supplied to the jet. When the pressure inside the jet, but remote from jet centerline, was equal to the atmospheric pressure, the rate of entrainment air supply was presumed to be equal to that which would occur naturally in the abscence of the

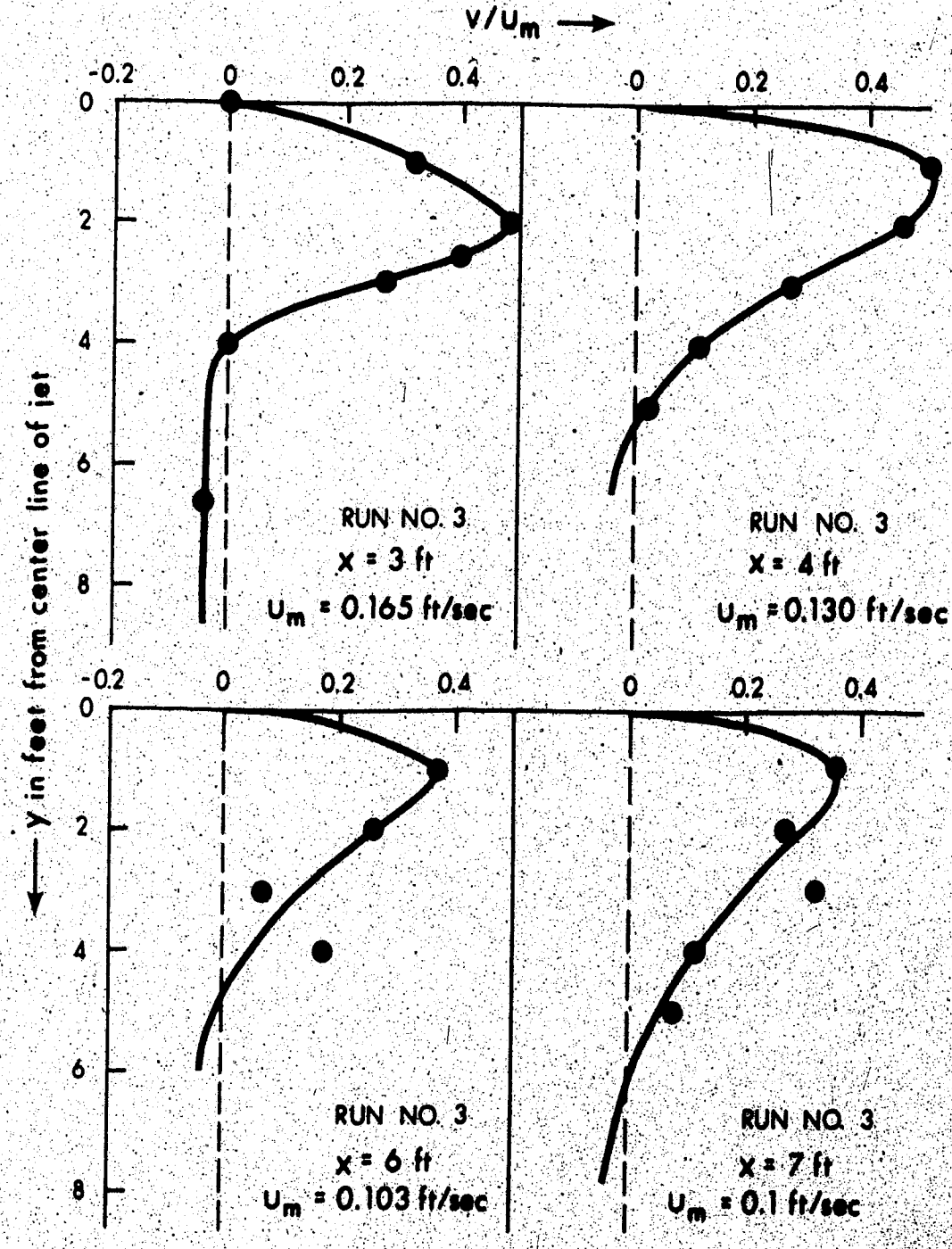

FIGURE 5.22 TYPICAL PLOT FOR LATERAL VELOCITY (v) DISTRIBUTION FOR Ri = 0.56

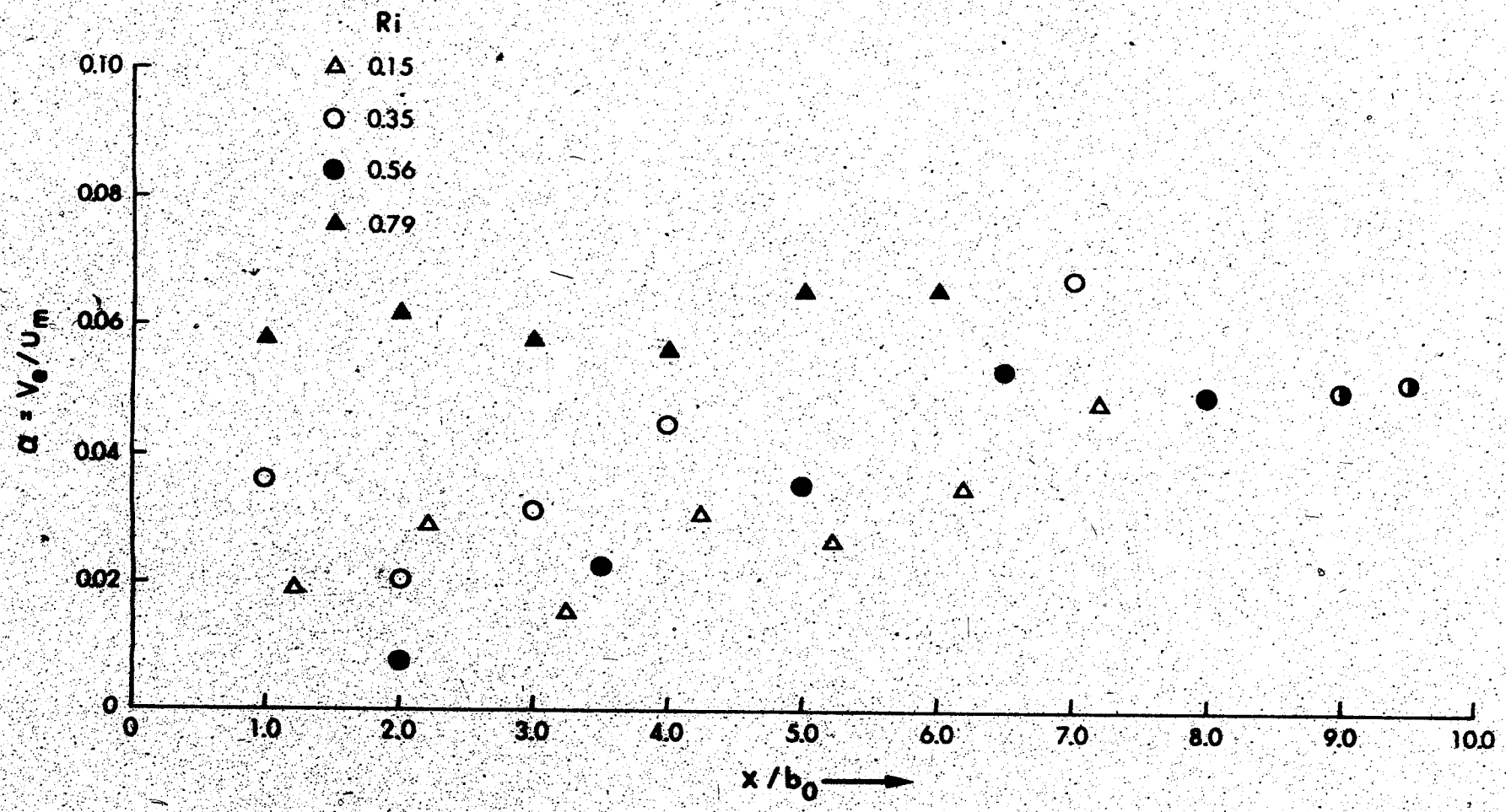

FIGURE 5.23. VARIATION OF COEFFICIENT OF ENTRAINMENT VELOCITY WITH DISTANCE

chamber.

The entrainment velocity in the present experiment was measured directly by means of the hydrogen-bubble technique. The value of α thus obtained for Ri = 0.79 varied from 0.056 to 0.065. This is equivalent to the value obtained for a plane jet. For Ri = 0.56, α obtained starts from a lower value in the beginning and rises to 0.052 after $x/b_o = 8.0$. This tendency of entrainment coefficient rising from lower to higher values are exhibited by axisymmetric jets as found by Hill (1972). The value of α measured for Ri = 0.35 rose from 0.02 to 0.067 at $x/b_o = 21.67$ and α for Ri = 0.15 could be measured only up to 0.048 at $x/b_o = 22.29$. The experimental results are shown in Figure 5.23. The data shows some scatter which is difficult to explain at the present time.

5.8 Temperature Measurements

Taking temperature measurements proved to be easier and quicker than taking velocity measurements. As in velocity measurements, temperature measurements were also made at nine cross-sections, separated by a distance of 1 foot from each other, for every test run. The temperature excess profile measured on the surface yielded a jet-like character with maximum temperature excess at the center and decreasing towards the edges. The profile in the vertical plane shows the same trend with maximum temperature excess on the surface or close to it and then decreasing towards the bottom. The values of temperature excess at surface are shown in Figure 5.24 for Ri = 0.79. The

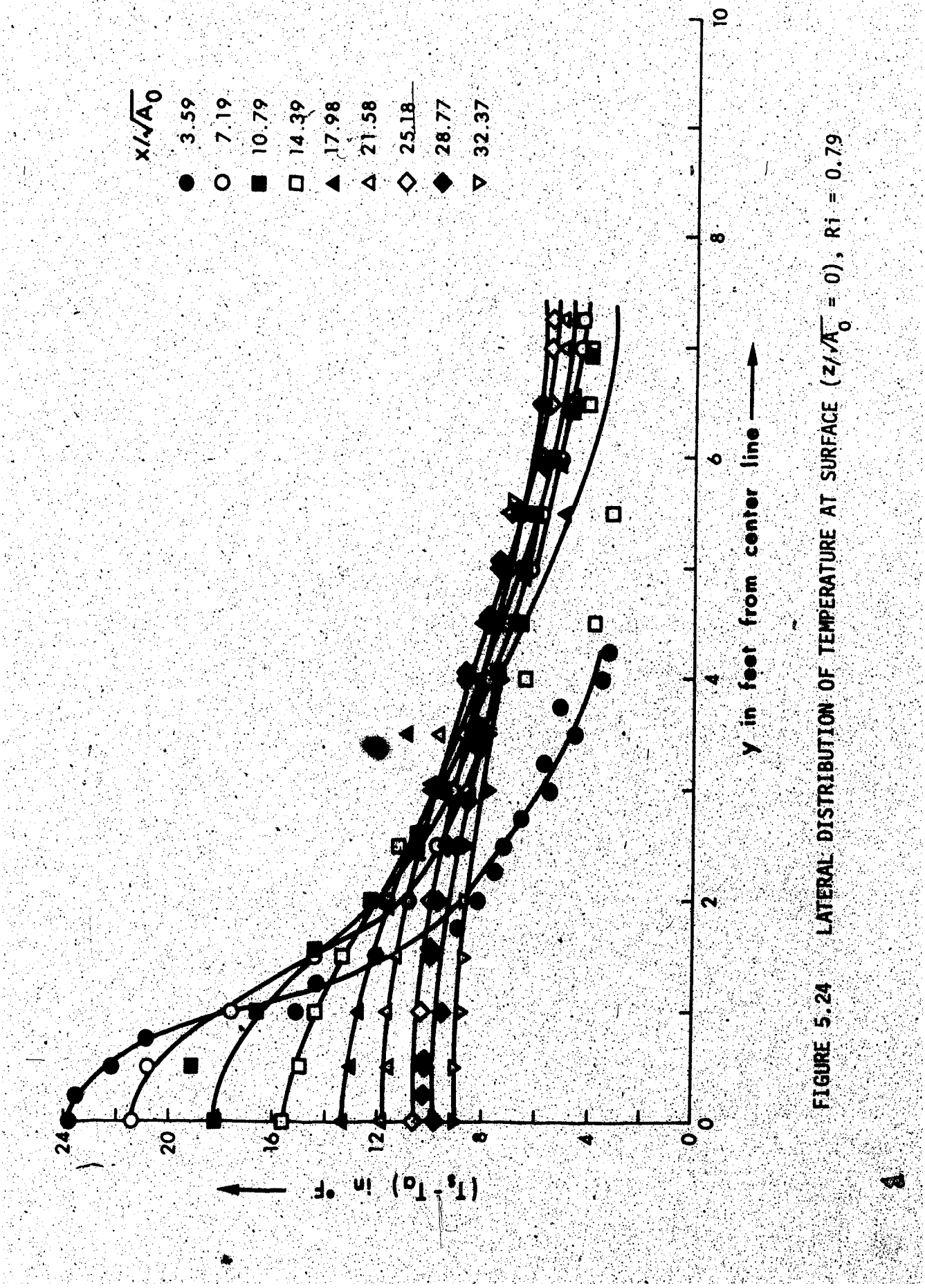

FIGURE 5.24 LATERAL DISTRIBUTION OF TEMPERATURE AT SURFACE ($z/\sqrt{A_0} = 0$), Ri = 0.79

temperature excess for other Richardson numbers follow a similar pattern and corresponding data are tabulated in Appendix C (Table C-9 to C-12). The variation of temperature excess in vertical planes for the same run is shown in Figures 5.25 to 5.28. The data for other values of Ri are given in Appendix C (Tables C-13 to C-16).

5.8.1 Temperature Distribution on the Surface

For all the runs, the temperature excess profiles on the surface were checked for similarity by plotting $\Delta T_s/\Delta T_m$ versus η. The profile has been found to be similar for all the Richardson numbers tested all along the length of measurement. A typical plot of similarity for large Ri is shown in Figure 5.29. The similarity plot for moderate Ri is shown in Figure 5.30; the plots for the remaining Richardson numbers are given in Appendix C.

The forms of similarity functions used by different investigators for temperature distribution are given in Table 5-3. Tollmien's equation and Schlichting's type equation for the velocity distribution were derived on the basis of Prandtl's old and new theories of turbulence, respectively. Prandtl's theories of turbulence, both new and old, yield no difference between velocity and temperature distributions; this is not in conformity with experimental results. In the present case, the temperature distribution has been found to be wider than the velocity distribution, hence the value of b_u in some of the distributions given in Table 5.2 has been changed to b_T and included in Table 5.3 for temperature distribution.

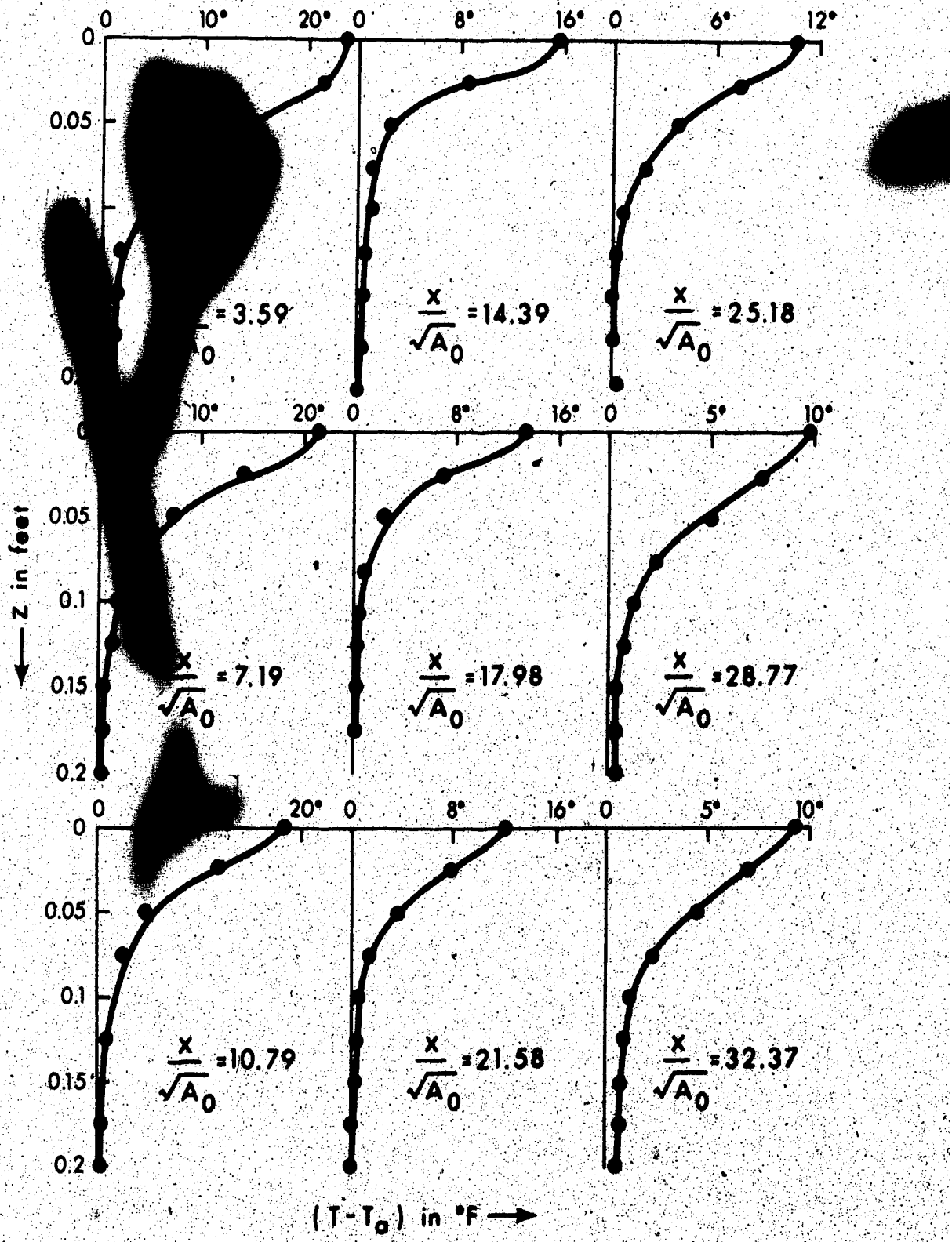

FIGURE 5.25 VERTICAL DISTRIBUTION OF TEMPERATURE AT CENTRAL PLANE ($y/\sqrt{A_0} = 0$), RI = 0.79

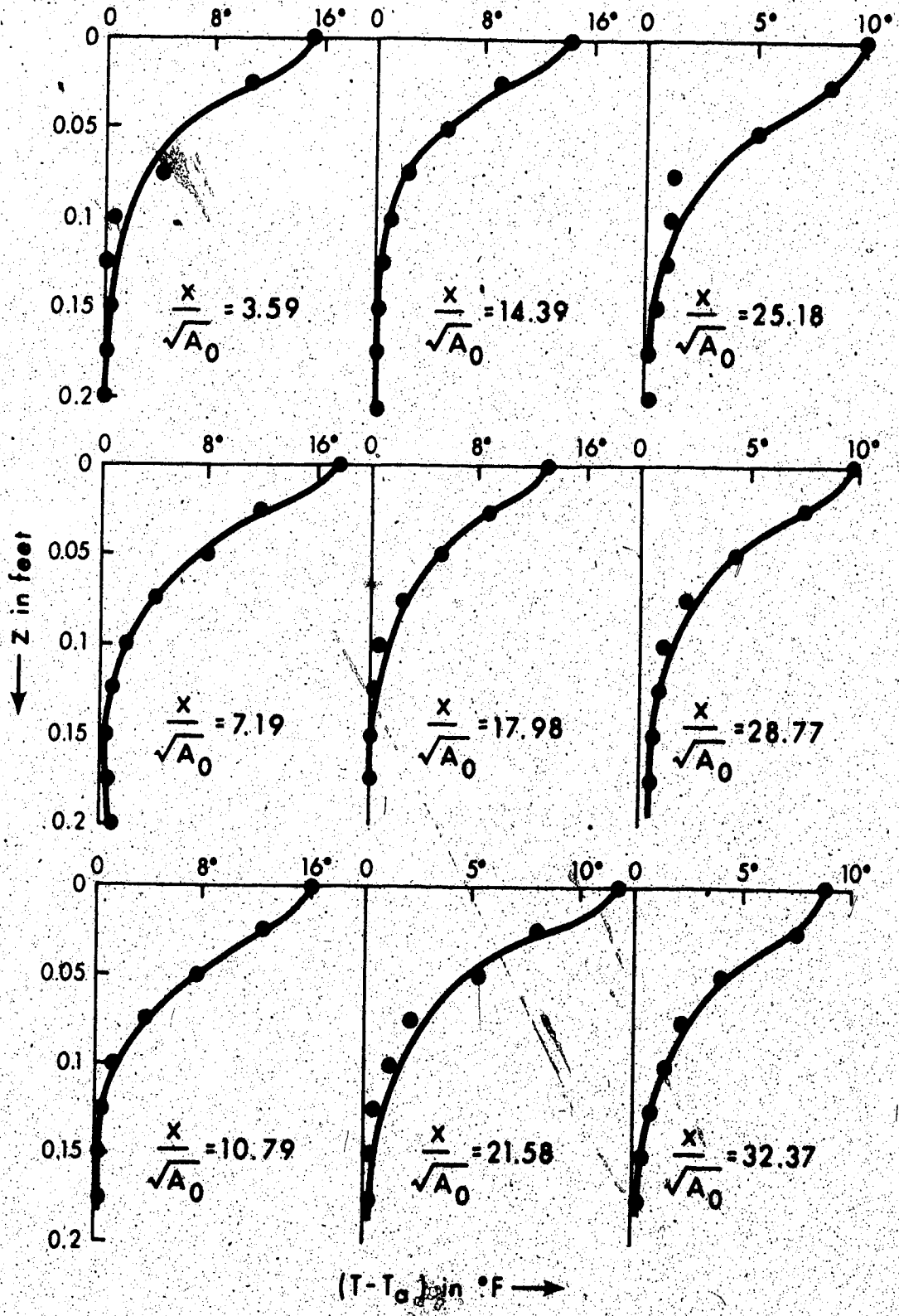

FIGURE 5.26 VERTICAL DISTRIBUTION OF TEMPERATURE SECTION
$y/\sqrt{A_0}$ = 3.59, Ri = 0.79

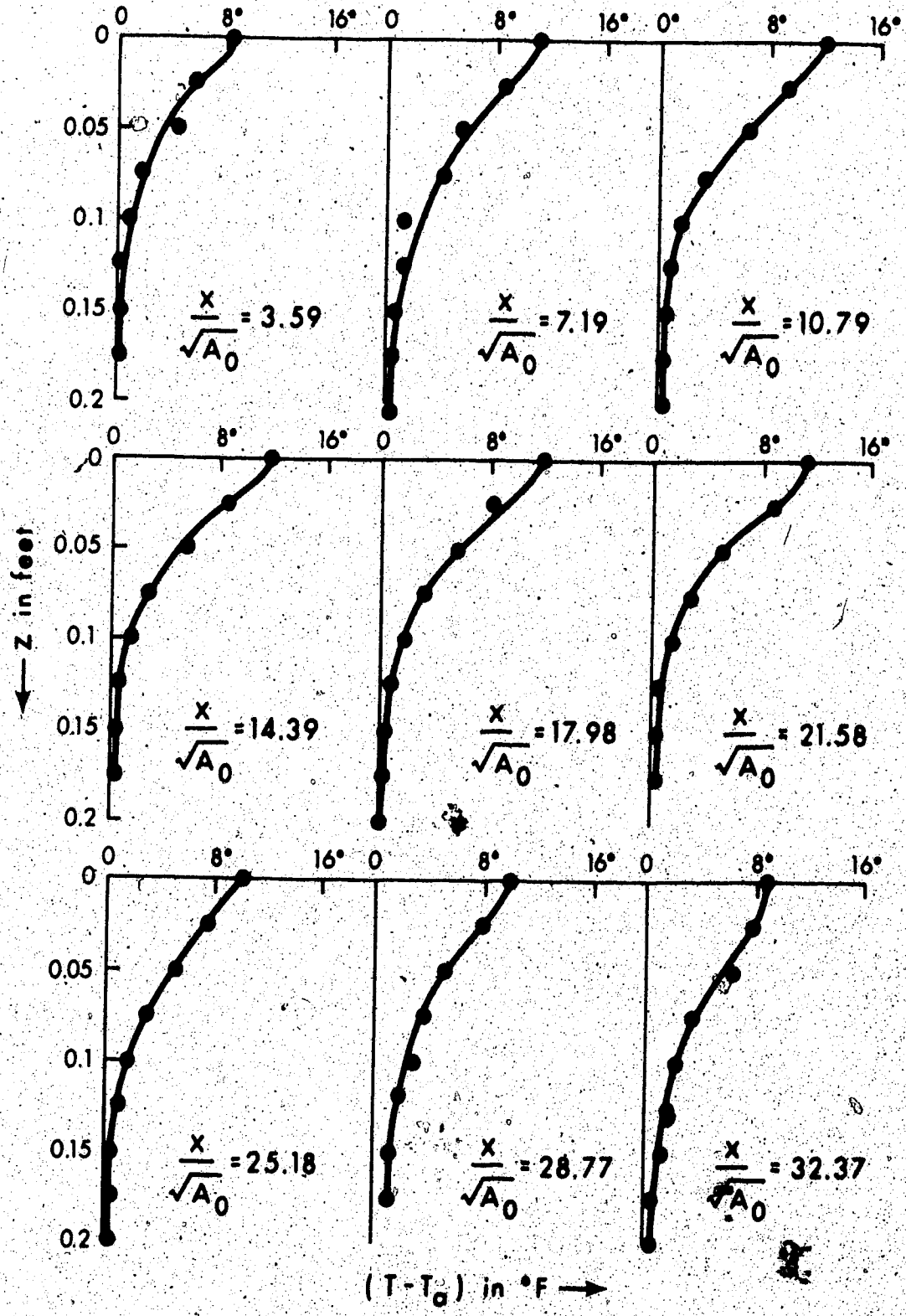

FIGURE 5.27 VERTICAL DISTRIBUTION OF TEMPERATURE
SECTION $y/\sqrt{A_0} = 7.19$, Ri = 0.79

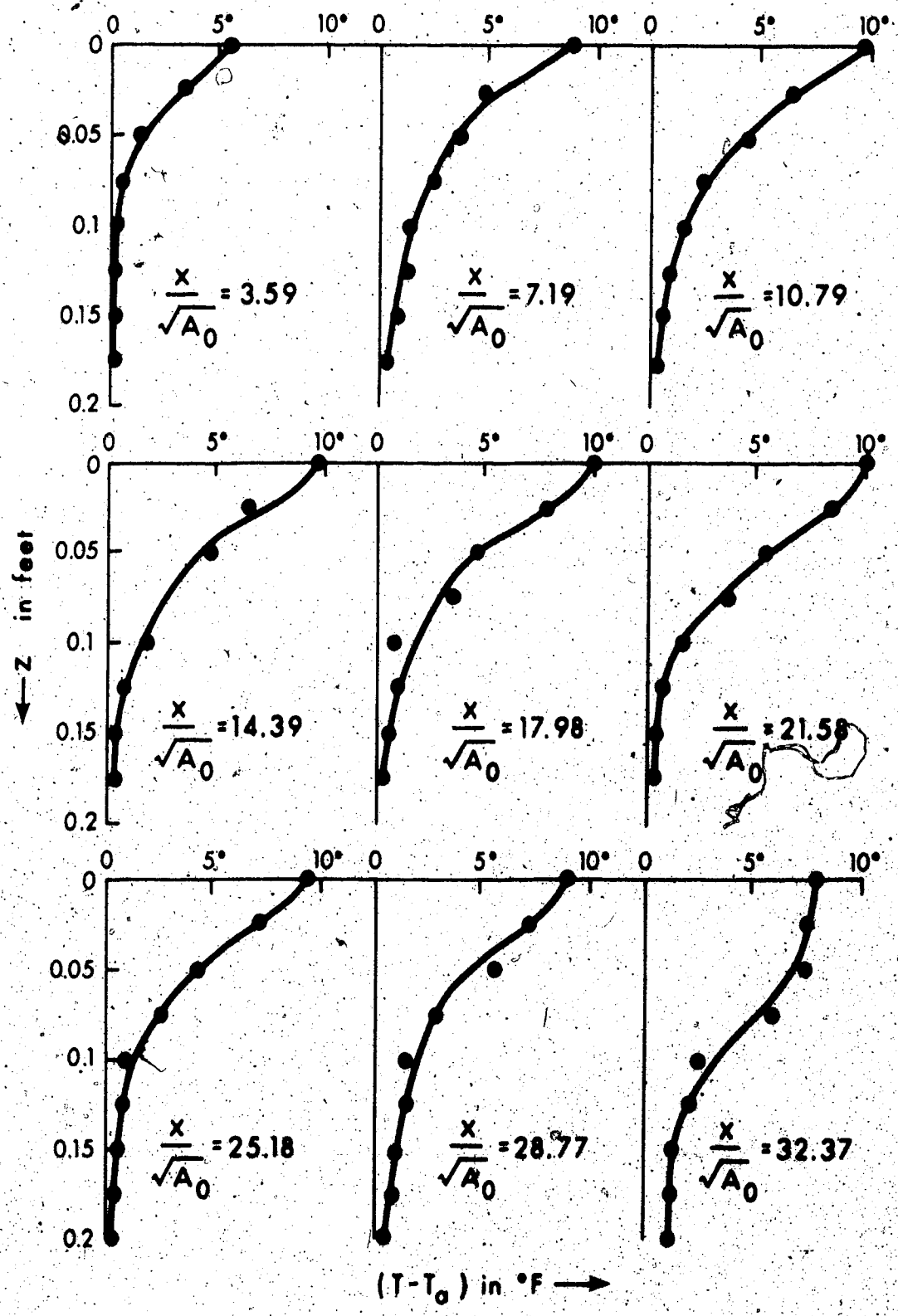

FIGURE 5.28 VERTICAL DISTRIBUTION OF TEMPERATURE
SECTION $y/\sqrt{A_0}$ = 10.79, Ri = 0.79

TABLE 5.3 FORMS OF TEMPERATURE DISTRIBUTIONS

Name of Distribution	Form of Similarity
Exponential Distribution	$\Delta T_s/\Delta T_m = \text{Exp}\ [-\ 0.693\ (y/b_T)^2]$
Abramovich's Wake Solution (Used by Stolzenbach and Harleman	$\Delta T_s/\Delta T_m = [1 - (y/\bar{b}_T)^{3/2}]$
Exponential Distribution Used by Motz and Benedict	$\Delta T_s/\Delta T_m = \text{Exp}\ (-\ y/b_T)^2$
Schlichting's Type Equation	$\Delta T_s/\Delta T_m = [1 + 0.41\ (y/b_T)^2]^{-2}$
Distribution Obtained in the Present Theory	$\Delta T_s/\Delta T_m = [1 + 7.0\ (y/b_T)^2]^{-1/3}$
Note that b_T is the half temperature width and $\bar{b}_T$ is the full temperature width of the jet.	

Abramovich's wake solution can again be modified, as was done for Equation 5.3.1, by assuming $\bar{b}_T$ to be proportional to b_T and evaluating the proportionality constant so as to yield $\Delta T_s/\Delta T_m$ equal to 0.5 when η equals 1.0. The modified equation can be written as:

$$\frac{\Delta T}{\Delta T_s} = [1 - 1/2\ (y/b_T)^{3/2}] \qquad (5.8.1a)$$

and: $$\bar{b} = 1.59\ b_T \qquad (5.8.1b)$$

These equations have been compared with the data. Only three curves, exponential distribution, Schlichting type curve and the distribution

developed in the present theory, are plotted for comparison in Figure 5.29 showing the similarity profile for large Ri. The exponential distribution and Schlichting type distribution developed in the present theory, are plotted for comparison in Figure 5.29 showing the similarity profile for large Ri. The exponential distribution and Schlichting type distribution show good fit up to $\eta = 1.0$ but, of the two, the Schlichting type curve shows a better fit. Abramovich's wake solution Equation 5.8.1a (not shown in the figures) lies inbetween Schlichting type curve and exponential distribution up to $\eta = 1.0$. Beyond this, all these curves lie considerably lower than the experimental data. On the other hand, the function developed in the present theory for large Ri (Equation 3.4.40) fits the data for $\eta > 1.0$ but lies somewhat below for $\eta < 1.0$. The value of k_2^2 in Equation 3.4.40 is chosen as 7.0 so that the value of $f_3(\eta) = 0.5$ when $\eta = 1.0$. The same findings hold good for the similarity profile for moderate Ri (Ri = 0.56), as shown in Figure 5.30. Equation 3.4.40 fits somewhat better here even though 0.56 is not really a large Richardson number.

5.8.2 Similarity for Temperature Profiles in Vertical Planes

Temperature distribution has been found to be similar in vertical planes. These are shown in Figure 5.31 for Ri = 0.79 and Ri = 1.14, and Figure 5.32 for Ri = 0.35. The experimental plot has been compared with Exp $[- 0.693 (z/h_T)^2]$ plotted as dotted lines and Schlichting's curve plotted as a full line on both the curves. Although the fit of experimental data with exponential distribution

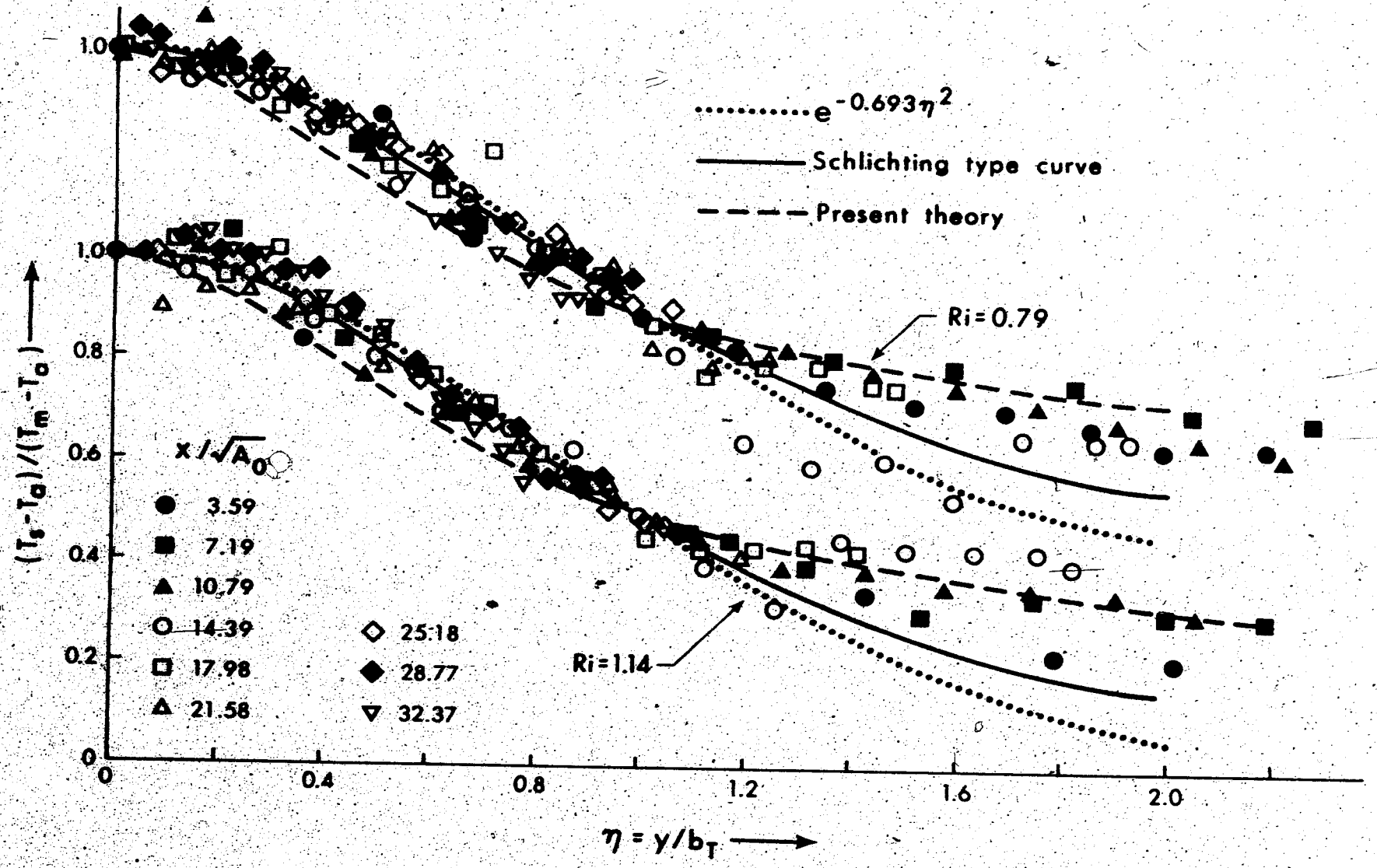

FIGURE 5.29 NON-DIMENSIONAL TEMPERATURE PROFILE ON THE SURFACE $z/\sqrt{A_0} = 0$, Ri = 0.79 AND 1.14

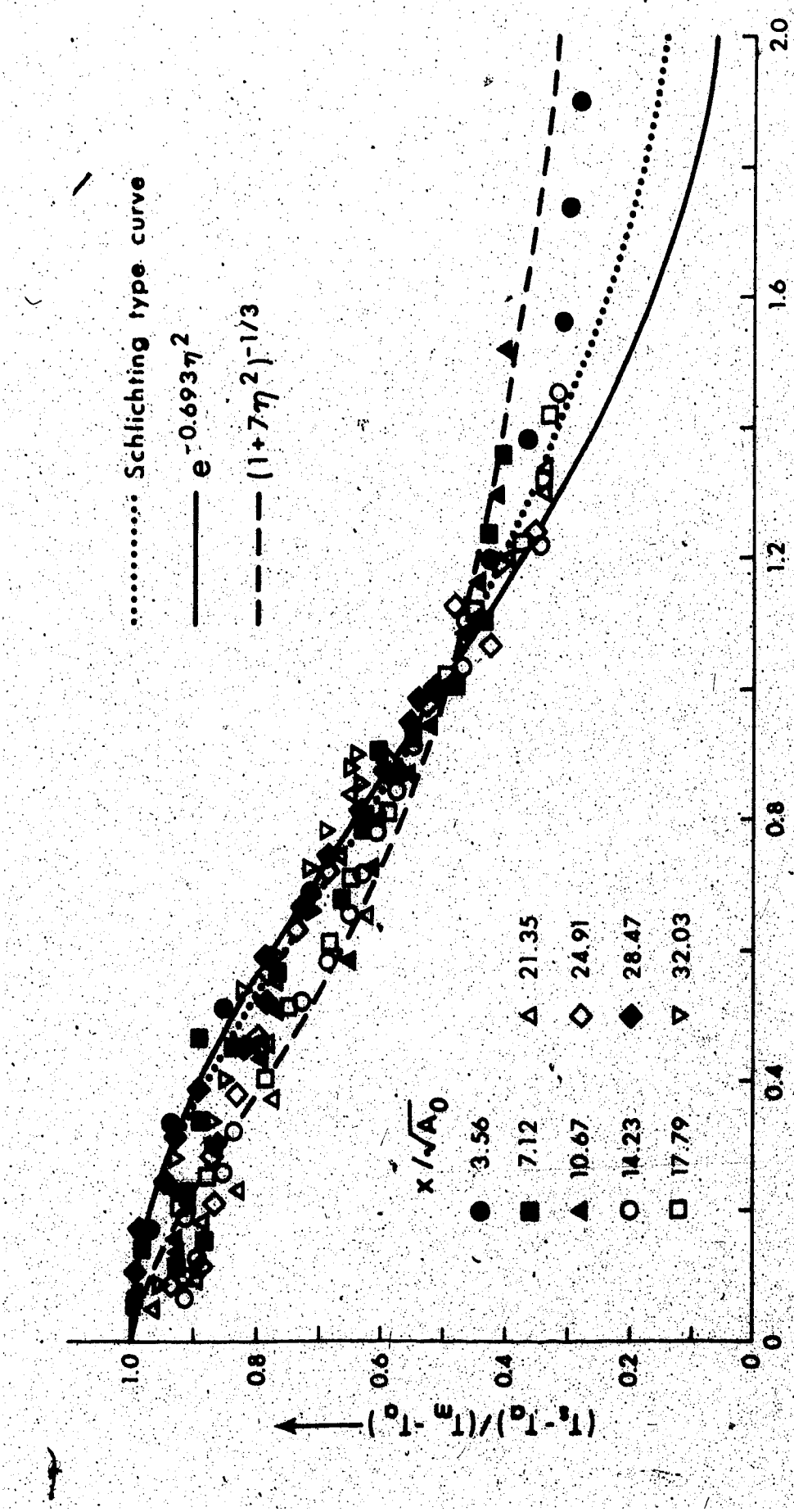

FIGURE 5.30 NON-DIMENSIONAL TEMPERATURE DISTRIBUTION ON THE SURFACE
$z/\sqrt{A_o} = 0$, $Ri = 0.56$

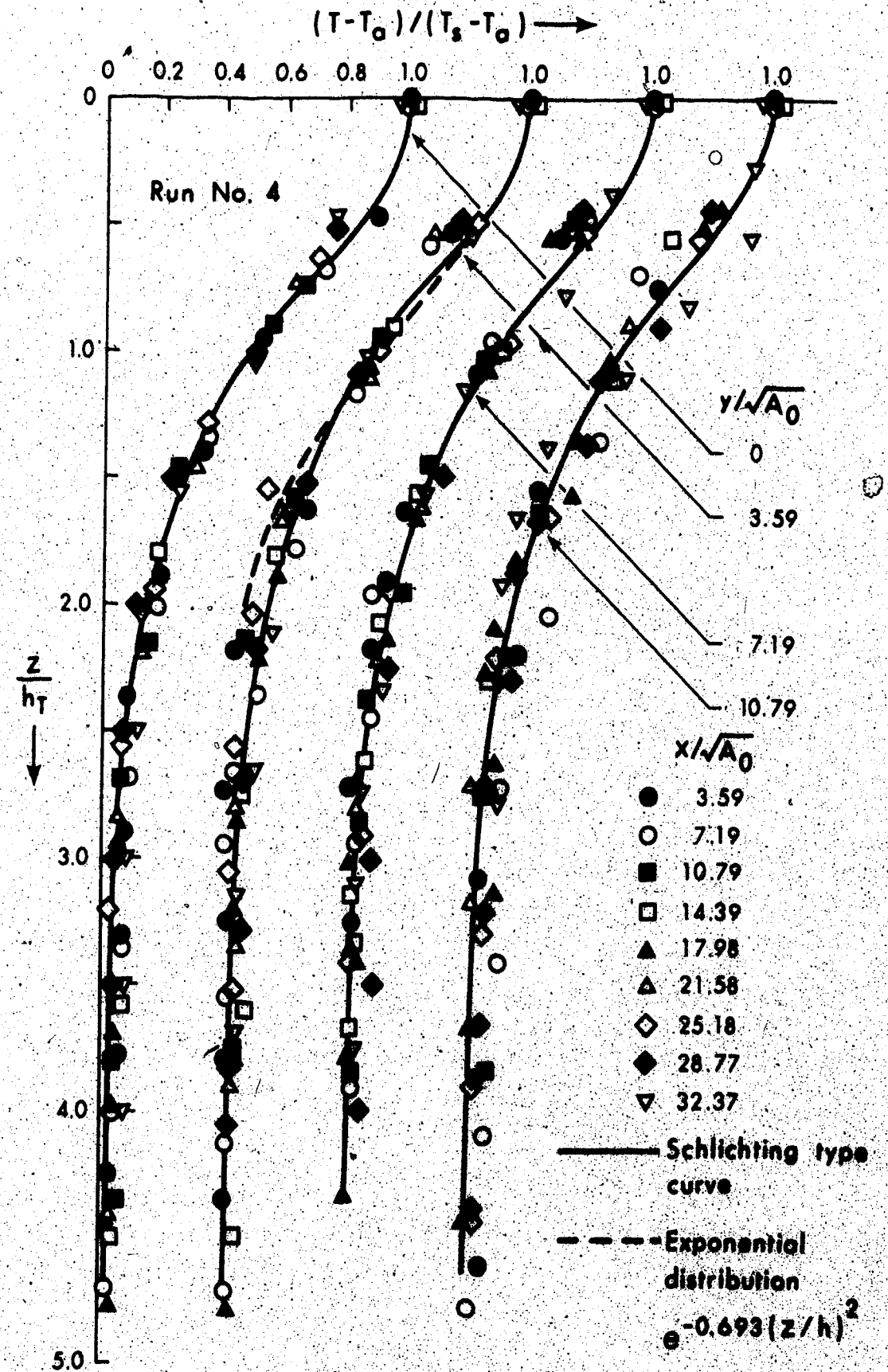

FIGURE 5.31 NON-DIMENSIONAL TEMPERATURE PROFILES IN VERTICAL PLANES, SECTION $y/\sqrt{A_0}$ = 0 TO 10.79, R1 = 0.79

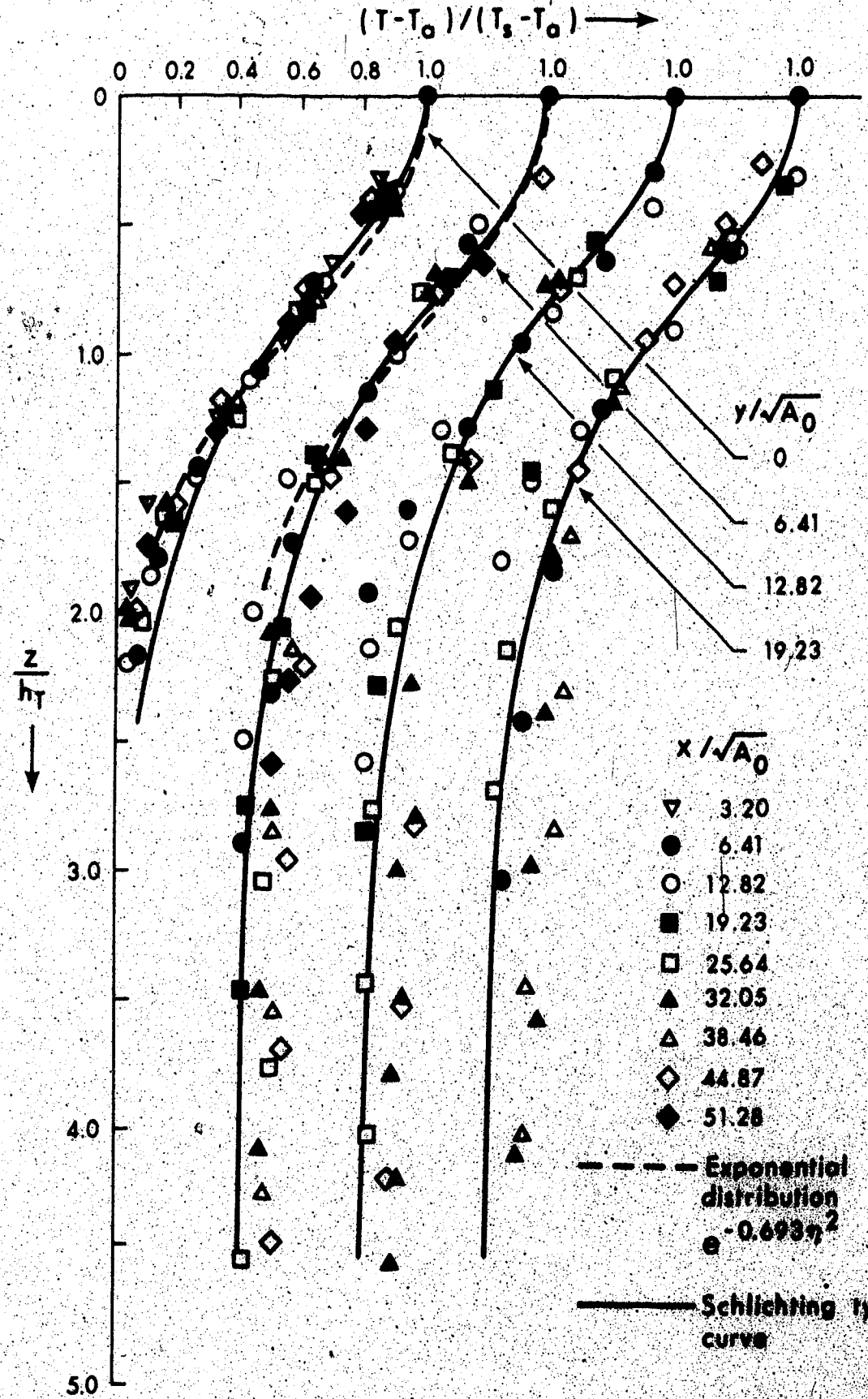

FIGURE 5.32 NON-DIMENSIONAL TEMPERATURE PROFILES IN VERTICAL PLANES, SECTION $y/\sqrt{A_0}$ = 0 TO 19.23, R1 = 0.35

is not bad, Schlichting's curve seems to fit the data better.

5.9 Decay of Maximum Excess Temperature

The centerline temperature excess has been plotted as $(\Delta T_m/\Delta T_o)$ versus $x/\sqrt{A_o}$ and plots for all the runs are shown in Figure 5.33. The data do not fall on any one line and the scatter indicates the influence of other factors such as Richardson number. Stolzenbach and Harleman (1971) carried out a dimensional analysis to show that:

$$\left(\frac{u_m}{U_o}, \frac{\Delta T_m}{\Delta T_o}, \frac{b}{\sqrt{A_o}}, \frac{h}{\sqrt{A_o}}\right) = \text{fun}\left(Ri, A_s, \frac{x}{\sqrt{A_o}}\right)$$

where A_s equals aspect ratio h_o/b_o. They predict a large influence of aspect ratio on the flow pattern. According to their findings, a large aspect ratio provides a large available area for lateral entrainment and the temperature drops more rapidly. On the contrary, the influence of aspect ratio is lost immediately due to sudden increase in the width of the jet. Thus the influence of aspect ratio, if any, on the dilution should be minor and should normally be accounted for by plotting $\Delta T_m/\Delta T_o$ versus $x/\sqrt{A_o}$ as was done in the case of the velocity plots.

5.9.1 Decay of Maximum Excess Temperature for Moderate Ri

The theoretical analysis for moderate Ri indicates that the integral momentum and buoyancy flux remains constant and the decay of

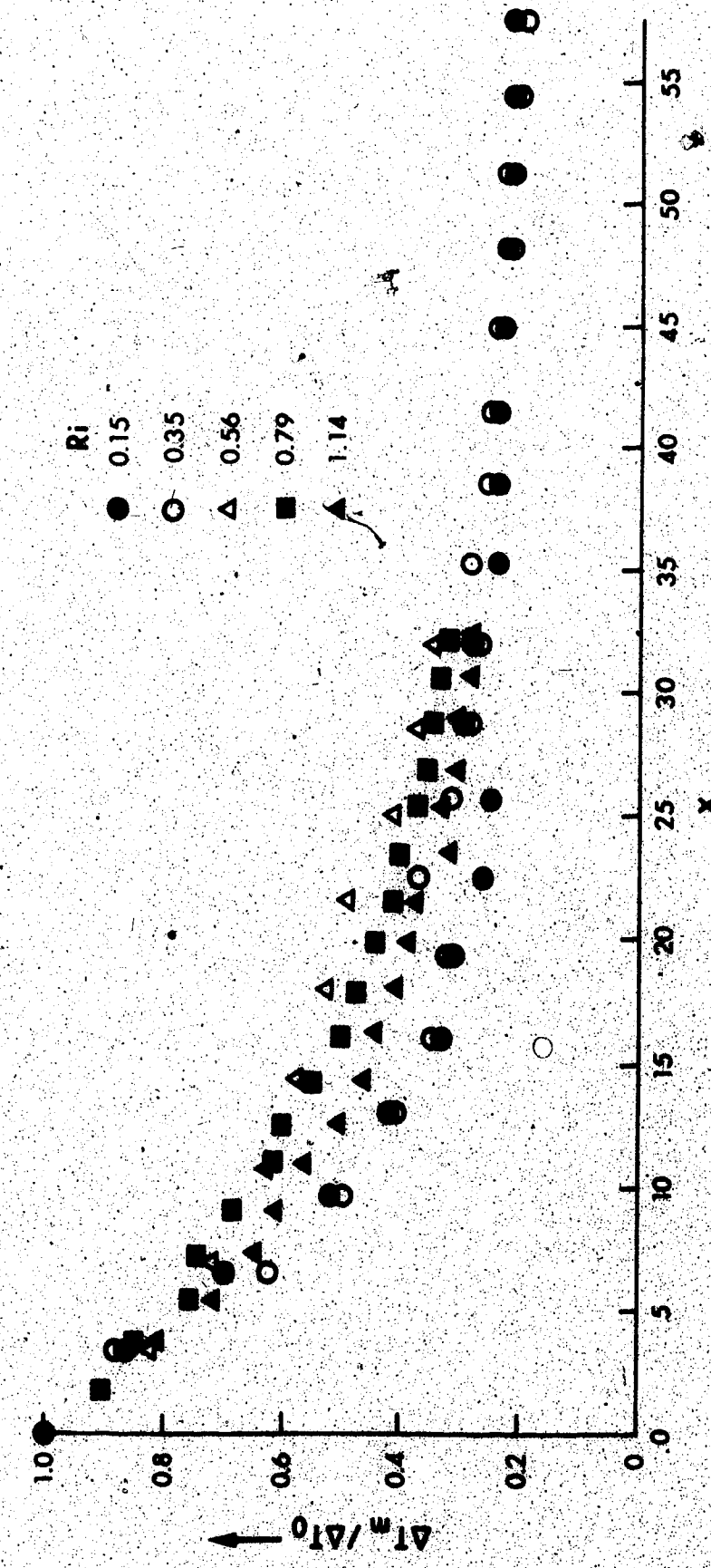

FIGURE 5.33 DECAY OF NON-DIMENSIONAL MAXIMUM TEMPERATURE EXCESS ALONG CENTRAL PLANE

maximum temperature is given by:

$$\Delta T_m \propto \frac{1}{x^{2/3 + c}} \qquad (3.6.3)$$

The value of c, as given in Section 3.3.4, is the exponent for the variation of h in the longitudinal direction. This value for velocity was shown to be zero as shown in Section 5.6.2. Thus Equation 3.6.3 becomes:

$$\Delta T_m \propto \frac{1}{x^{2/3}} \qquad (3.6.5b)$$

A study of dimensional analysis of the problem indicates the same result.

As discussed in the previous section, the experimental data show some kind of systematic variation with Ri. This influence of Ri can be considered to be contained in the proportionality constant. Adopting the polynomial variation of Ri, as done earlier, all the data were plotted as $(\Delta T_o/\Delta T_m)^{3/2}\ Ri^{m_1}$ versus $x/\sqrt{A_o}$ for several values of m_1. The value of m_1 that shows the best fit works out to be 1/2. The plot is shown in Figure 5.34.

The equation of mean straight line passing through this data is:

$$\frac{\Delta T_m}{\Delta T_o} = 4.4178\ Ri^{1/3}(x/\sqrt{A_o} + 1.795)^{-2/3} \qquad (5.9.1a)$$

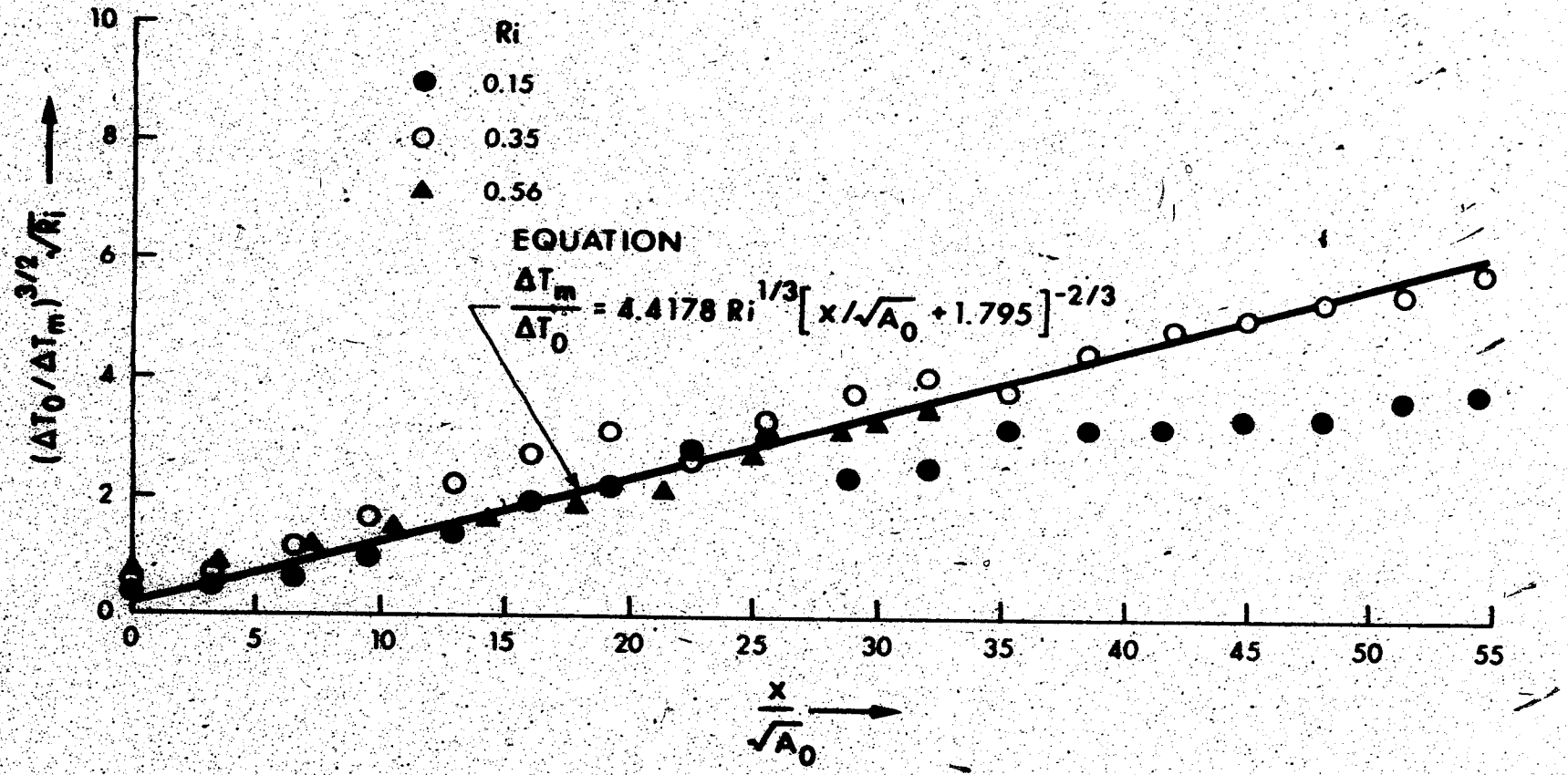

FIGURE 5.34 CORRELATION OF TEMPERATURE EXCESS DATA ON THE CENTERLINE FOR MODERATE Ri

5.9.2 Decay of Maximum Excess Temperature for Large Ri

The value of centerline temperature excess for this range of Ri is also predicted by Equation 3.6.2b to decay as:

$$\Delta T_m \propto \frac{1}{(x^{2/3} + c)}$$

The value of h_{mu} for Ri = 0.79, as shown in Figure 5.16, can be treated as approximately constant but for Ri 1.14 it first decreases considerably and then slowly increases. The value of $h_{avg\ u}$ for both of these runs, as shown in Figure 5.17, remains quite constant, as shown in Section 5.6.2. Hence the value of c for this range of Richardson number can be considered to be zero. This was also logically derived under Section 3.4.5. Thus the value of ΔT_m is given by Equation 3.4.26 as:

$$\Delta T_m \propto \frac{1}{x^{2/3}}$$

Figure 5.33 shows that the values of $(\Delta T_m/\Delta T_o)$ for Ri = 0.79 are higher than the values of $(\Delta T_m/\Delta T_o)$ for Ri 1.14. This indicates that the value of $(\Delta T_m/\Delta T_o)$ reduces as Ri increases. The same behaviour was observed for the velocity plot as given in Section 5.5.2. The data was thus again plotted as $(\Delta T_o/\Delta T_m)^{3/2}\ Ri^{m_1}$ versus $x/\sqrt{A_o}$ for several values of m_1. The value of m_1 that shows the best fit is -1/2. The plot is shown in Figure 5.35. The equation of mean straight line passing through the data is given by:

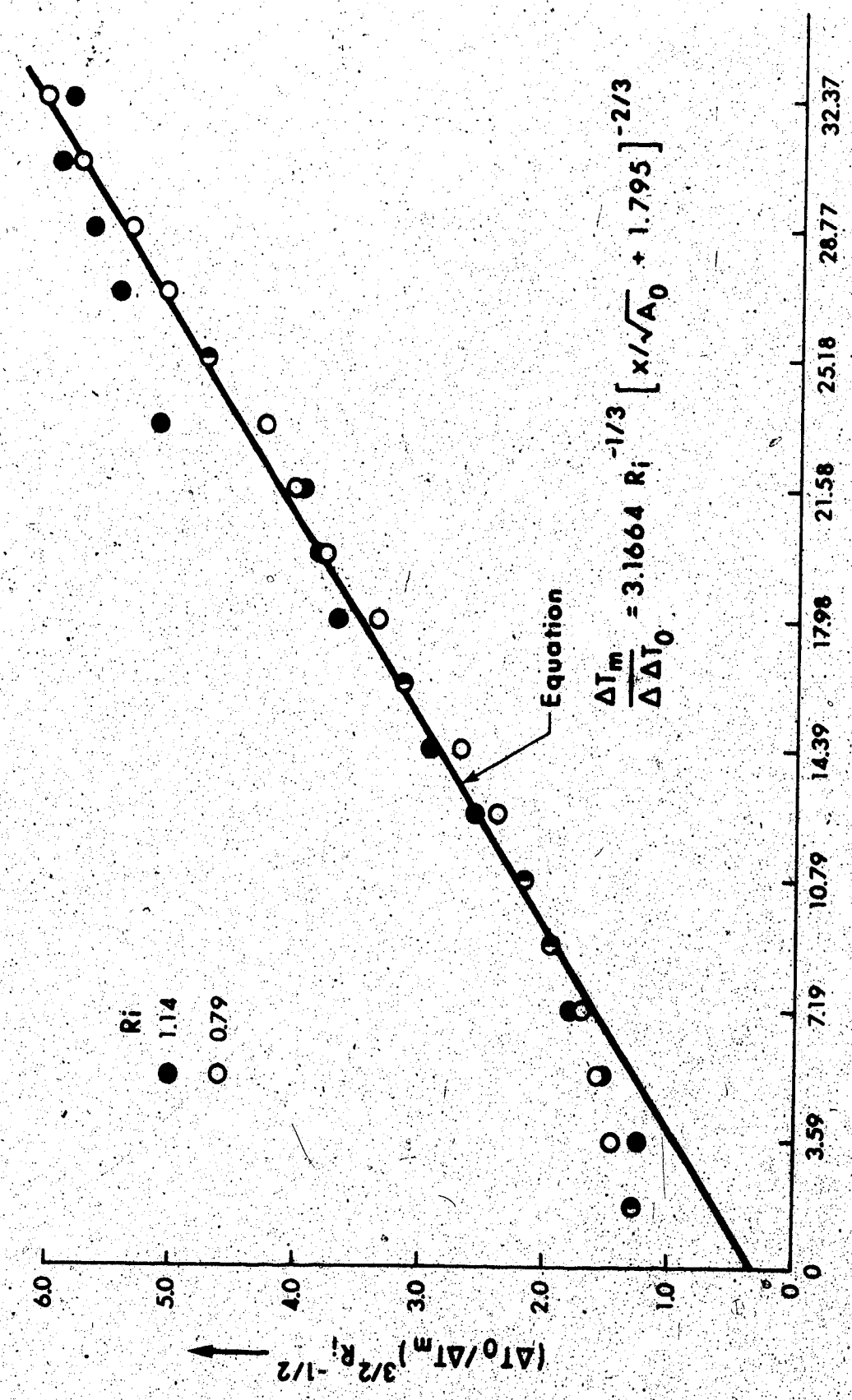

FIGURE 5.35 CORRELATION OF TEMPERATURE EXCESS DATA ON THE CENTERLINE FOR LARGE Ri

$$\frac{\Delta T_m}{\Delta T_o} = 3.1664\ Ri^{-1/3}\ (x/\sqrt{A_o} + 1.795)^{-2/3} \qquad (5.9.2)$$

The difference between Equation 5.9.1 and Equation 5.9.2 may be noted. The constant in Equation 5.9.1 is multiplied by $Ri^{1/3}$ whereas in Equation 5.9.2, it is multiplied by $Ri^{-1/3}$. This change of behaviour from moderate to large Ri has already been discussed under Section 5.5. Although the correlation of data to formulate these equations is purely empirical, yet it appears as though the floating plume formation at large Richardson numbers leads to a greater transverse diffusion and lateral entrainment, and the temperature excess starts dropping faster as Richardson number further increases.

5.9.3 Determination of Limiting Ri Between Moderate and Large Richardson Number

The virtual origin for both sets of data lies close to the inlet and is the same. Equations 5.9.1 and 5.9.2 can be compared to get a value of Richardson number which is the border case. This can be written as:

$$4.4178\ Ri^{1/3} = 3.1664\ Ri^{-1/3}$$

hence: $Ri = 0.61$ (5.9.3)

Thus we find that $Ri = 0.79$ indeed can be taken as large Richardson number. The limiting value at which Richardson number changes from

moderate to large, therefore, lies in the range $0.61 < Ri < 0.86$.

5.10 Variation of Half Depth of the Jet

5.10.1 Variation of Half Temperature Depth in Lateral Cross-Sections

Variation of half temperature depth for Run No. 4 is shown in Figure 5.36. Variation of half temperature depths for other runs follows the same pattern and their values are given in Appendix C (Tables C-13 to C-16). The trend shown for temperature half depth are quite similar to those for velocity. Half depth on central planes has been found to be somewhat less than on side planes. This appears to be due to the presence of a higher buoyancy force at the central plane and has already been discussed in Section 5.6.1. Half depth for temperature appear to be more uniform along the cross-section and are in general thicker than those of velocity.

5.10.2 Variation of Half Temperature Depth in the Longitudinal Direction

The variation of half depth of jet for temperature on the central plane for $Ri = 0.35$, as shown in Figure 5.37(a), remains fairly constant. For other runs, the value first decreases and then increases. It keeps on continuously decreasing for $Ri = 0.15$. The value of h_{mu} was shown as constant in Section 5.6.1 and the same form of similarity function, namely Schlichting type, satisfies both velocity and temperature distributions hence the constancy of h_{mu} implies constancy in h_{mT}. The variation in the value of h_{mT} also, after

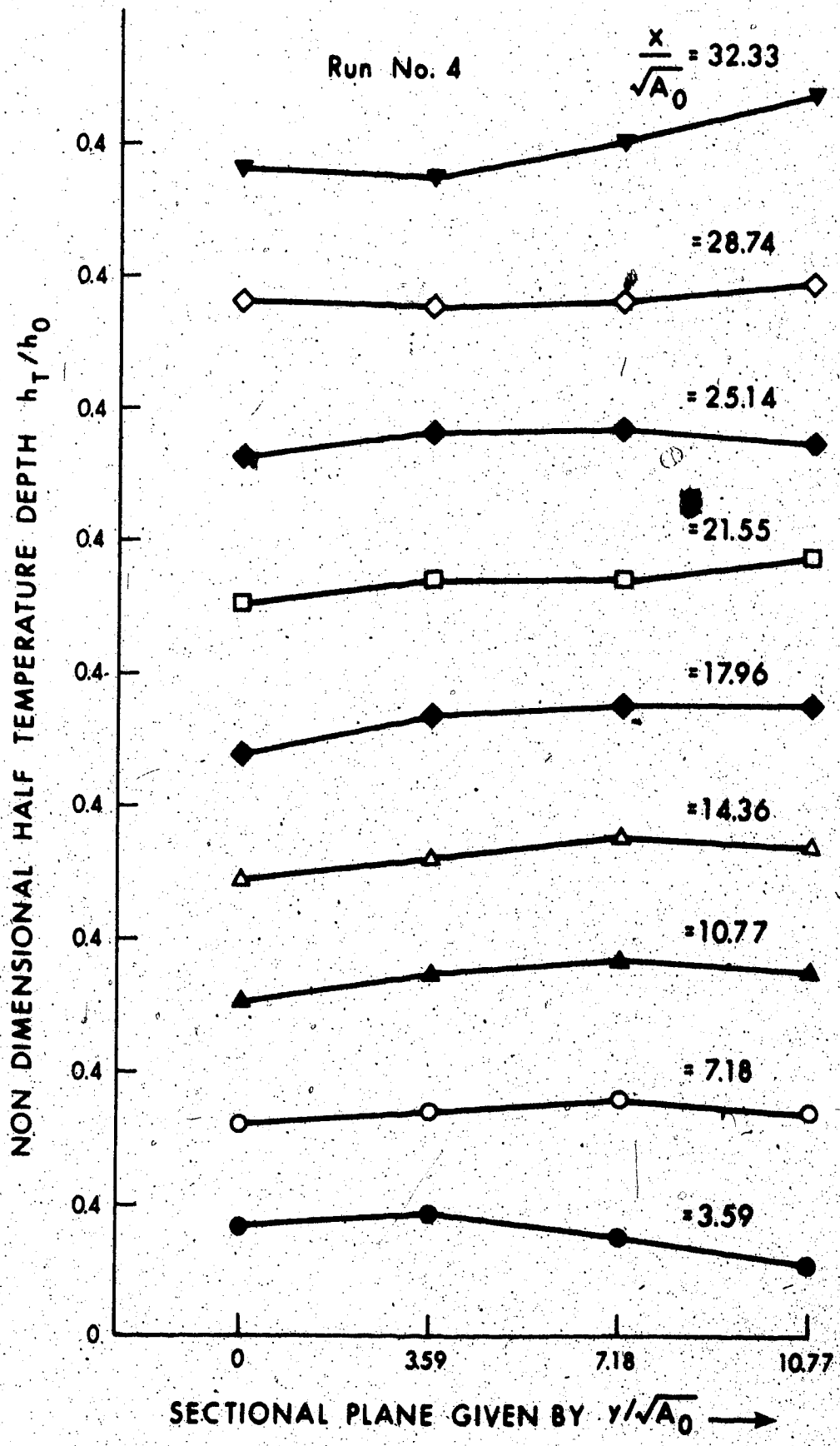

FIGURE 5.36 LATERAL VARIATION OF HALF TEMPERATURE DEPTH FOR Ri = 0.79

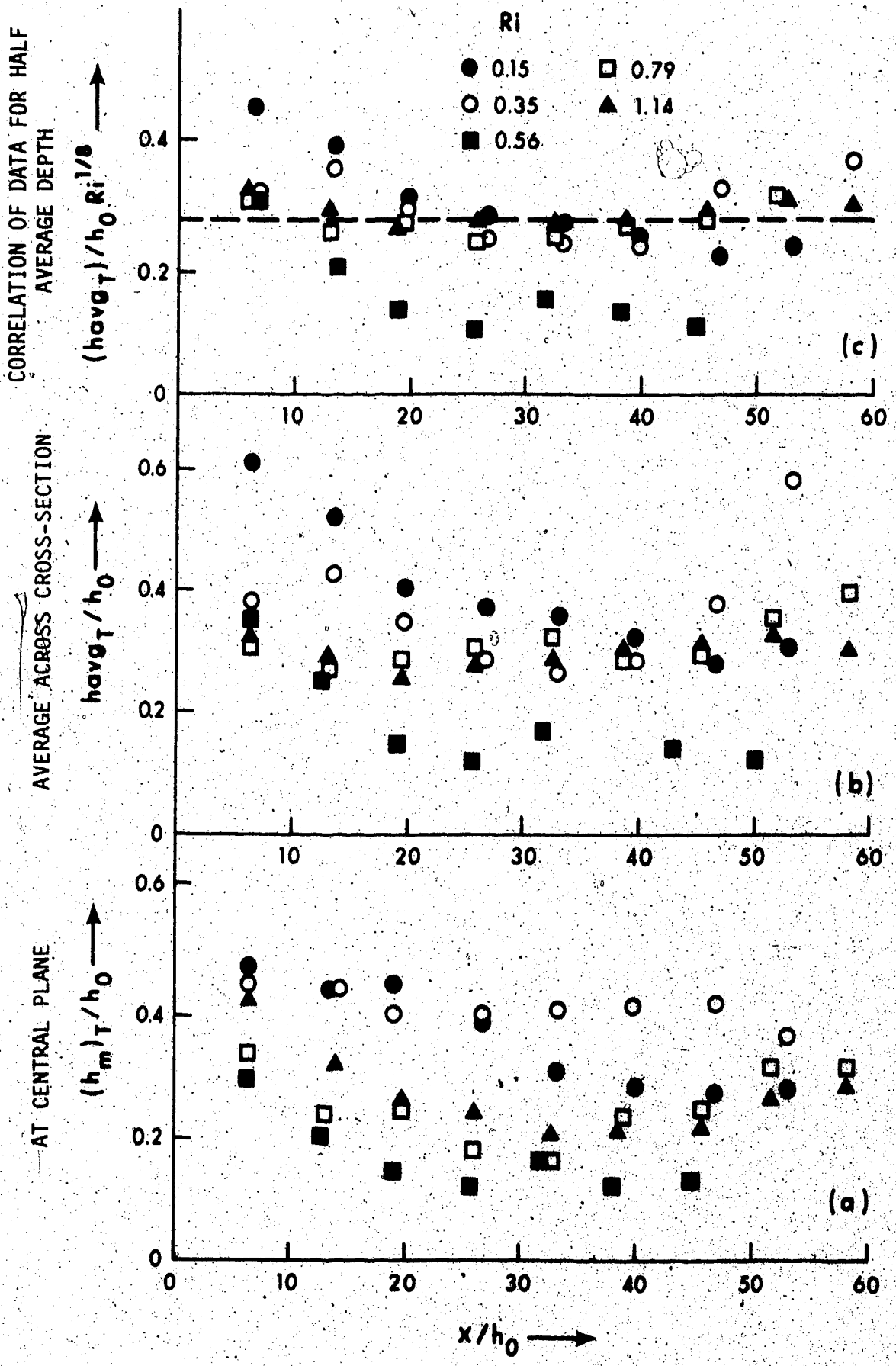

FIGURE 5.37 VARIATION OF HALF TEMPERATURE DEPTH

$x/h_o > 20$, cannot be considered to be large and may thus be treated as approximately constant. The value of $h_{avg\ T}/h_o$ shows that it remains fairly constant with distance for $x/h_o > 20$, this is shown plotted in Figure 5.37(b). The scatter in the data shows a trend of its dependence on Ri. The value of $(h_{avg\ T}/h_o)\ Ri^{1/8}$ versus x/h_o is plotted in Figure 5.37(c). All the experimental data, except for Ri = 0.56, cluster around a mean line whose equation is given as;

$$h_{avg\ T}/h_o = 0.29\ Ri^{-1/8} \qquad (5.10.1)$$

The experimental data for Ri = 0.56 lie lower than other experimental data which fit Equation 5.10.1. The discrepancy cannot be explained at this stage. The deviation could as well be a result of experimental error in measuring vertical profiles as this was the first set of experimental runs carried out in the series.

5.11 Variation of Half Width of Jet for the Temperature

The variation of half width of the jet plotted as b_T/b_o versus x/b_o is shown in Figure 5.38(a) (for $x/b_o < 20$) and in Figure 5.38(b) (for $x/b_o > 20$). Data for Ri = 0.56 to 1.14 can be grouped together whereas the data for Ri = 0.15 and 0.35 show a different type of variation. The effect of Richardson number is not quite obvious, but the width should go on increasing as Ri increases because of the greater buoyancy force in the center. The width obtained for Ri = 0.35 is higher than Ri = 1.14. This shows the influence

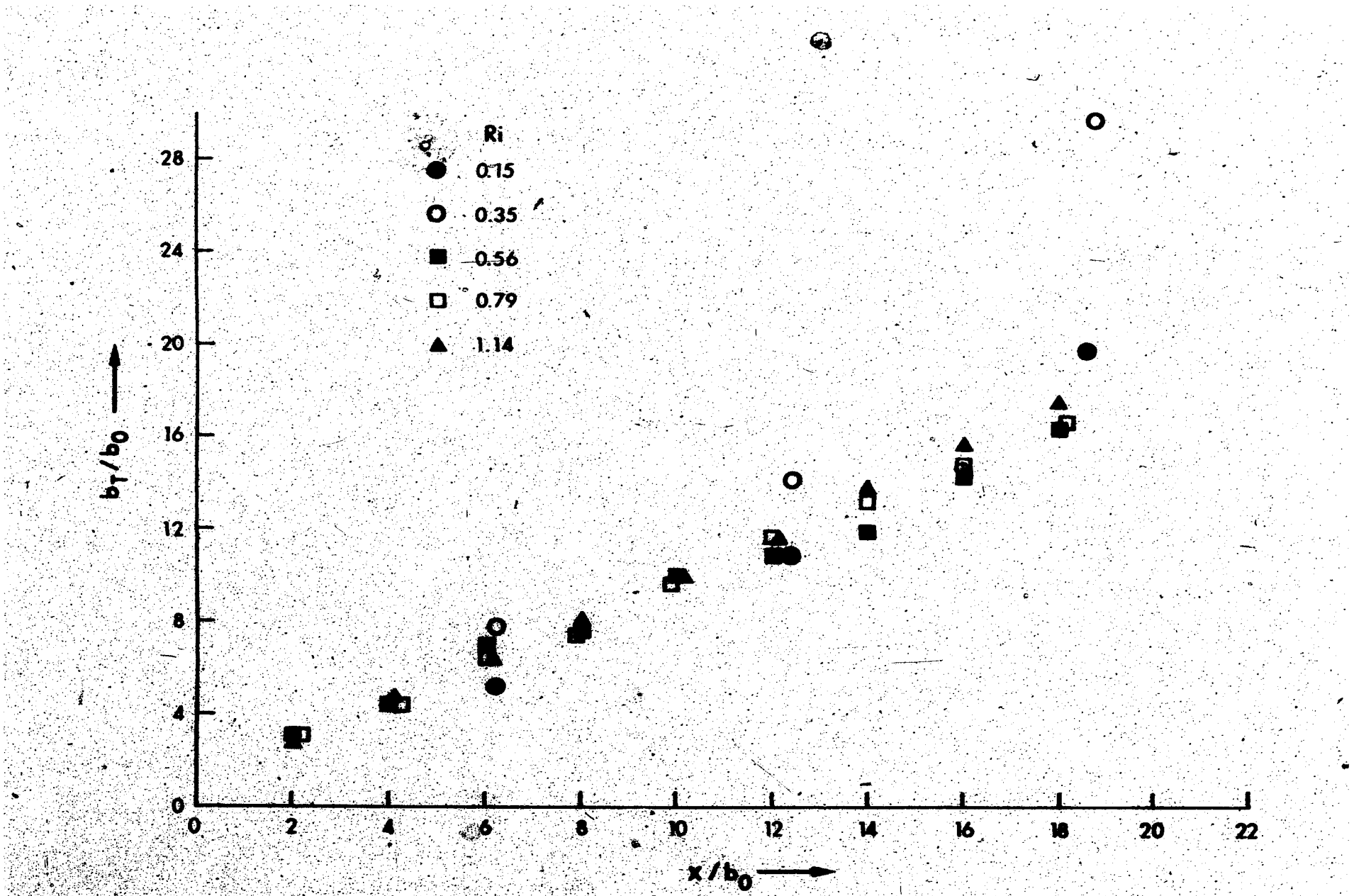

FIGURE 5.38(a) VARIATION OF HALF TEMPERATURE WIDTH OF THE JET FOR ALL RUNS WITH DISTANCE FOR x/b_o = 0 TO 20

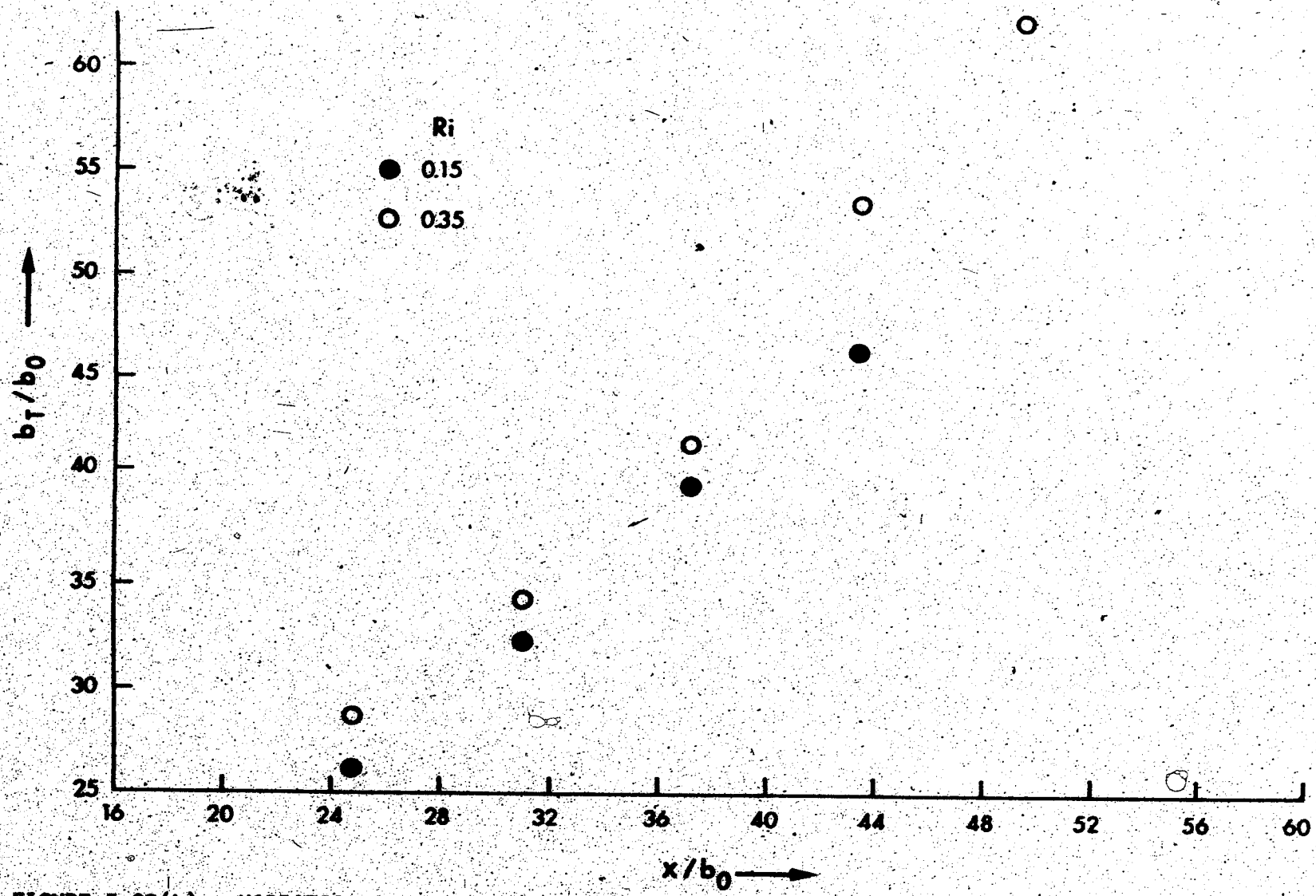

FIGURE 5.38(b) VARIATION OF HALF TEMPERATURE WIDTH OF THE JET FOR ALL RUNS WITH DISTANCE FOR x/b_0 = 20 TO 50

of the aspect ratio. However, before drawing any firm conclusion, the data for moderate and large Ri are segregated and are plotted according to variations given by Equation 3.6.5c and Equation 3.6.2c.

The half width varies as x for large Richardson numbers and as $x^{4/3}$ for moderate Richardson numbers. Data for moderate Richardson numbers are plotted in Figure 5.39 as $(b_T/b_o)^{3/4}\ Ri^{-1/8}$ versus x/b_o. The exponent of Ri is empirically fitted which shows a very small effect of Ri on the width. The plot shows that the data for all the runs of moderate Richardson numbers can be grouped together. The equation for mean straight line passing through the data is given by:

$$\frac{b_T}{b_o} = 0.404\ Ri^{1/6}(x/b_o + 2)^{4/3} \qquad (5.11.1)$$

Data for large Ri are plotted as $(b_T/b_o)\ Ri^{-1/8}$ versus x/b_o in Figure 5.40. The plot of experimental data follows a straight line, the equation for which works out to be:

$$\frac{b_T}{b_o} = 0.9146\ Ri^{1/8}\ (x/b_o + 1) \qquad (5.11.2)$$

Since the data could be correlated without bringing in the aspect ratio as a parameter, it is concluded that the effect of aspect ratio on flow, if any, should be minimal.

5.12 Comparison of Similarity Profile for Temperature and Velocity Distribution

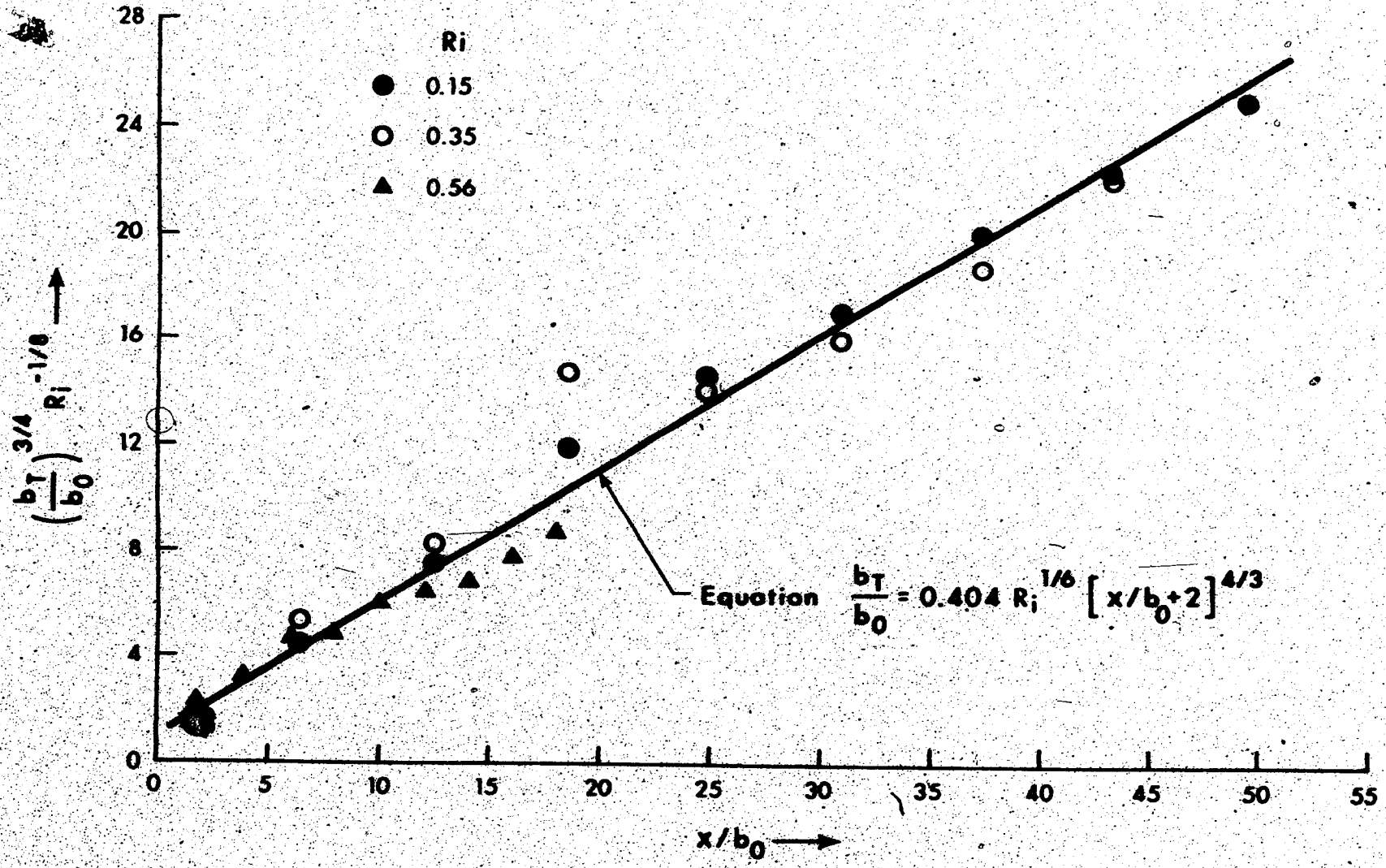

FIGURE 5.39 CORRELATION OF DATA FOR HALF TEMPERATURE WIDTH FOR MODERATE Ri

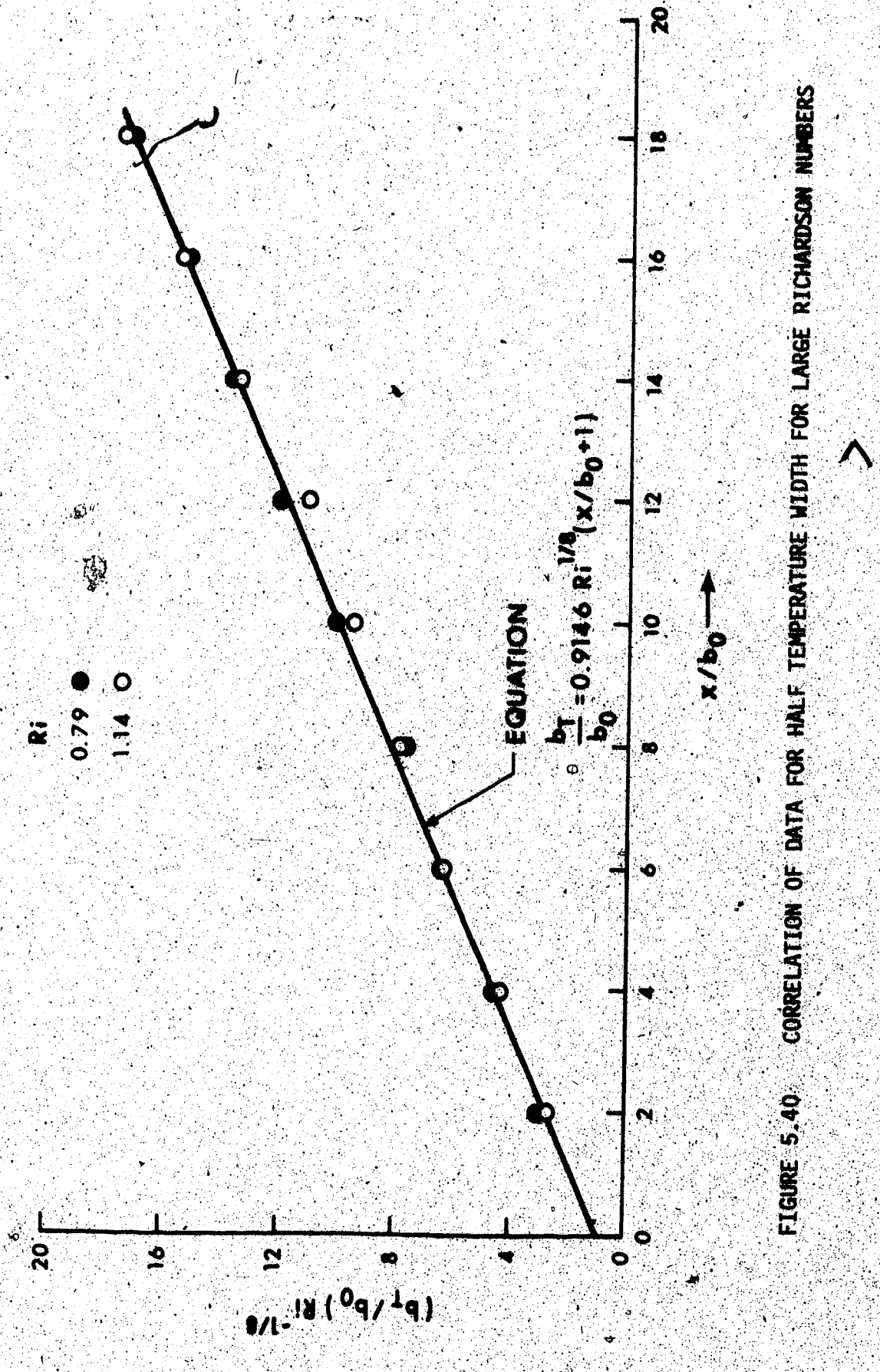

FIGURE 5.40 CORRELATION OF DATA FOR HALF TEMPERATURE WIDTH FOR LARGE RICHARDSON NUMBERS

A comparison of similarity profile for temperature and velocity distribution on surface, for Ri = 0.79, is shown in Figure 5.41. The temperature profile is found to be wider than the velocity profile. The data prove that the assumption of the same similarity function for temperature and velocity distributions is not proper.

The exponential distribution, Exp $[- 0.693 (y/b_T)^2]$ satisfies the similarity for temperature excess as an upper envelope. The equation of exponential curve for temperature distribution can be worked out in terms of y/b_u. For large Ri, as shown in Equation 5.14.2, $b_T = 1.85\, b_u$ hence $y/b_T = y/1.85 b_u$. Thus the equation for temperature distribution can be written as:

$$\frac{\Delta T_s}{\Delta T_m} = \text{Exp}\,[- 0.693\,(y/b_T)^2]$$

$$= \text{Exp}\,[- 0.20248\,(y/b_u)^2] \qquad (5.12.1)$$

Equation 5.12.1 is plotted in Figure 5.41 and satisfies the temperature distribution very well.

A comparison of similarity profile in central vertical plane, shown in Figure 5.42 indicates no distinct difference between velocity and temperature profiles.

5.13 Comparison of Decay of Maximum Velocity and Temperature

For moderate Richardson number:

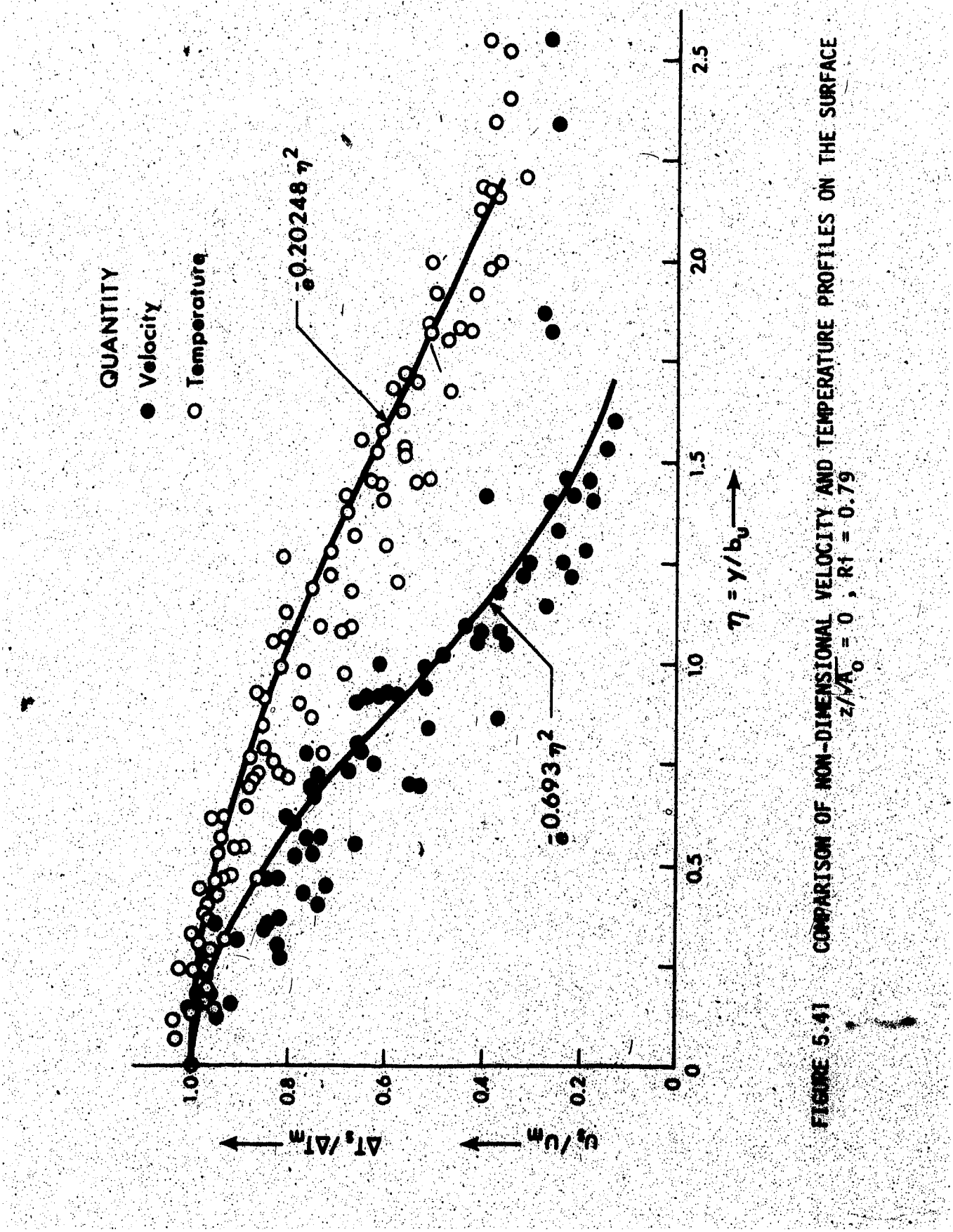

FIGURE 5.41 COMPARISON OF NON-DIMENSIONAL VELOCITY AND TEMPERATURE PROFILES ON THE SURFACE
$z/A_o = 0$, $R_f = 0.79$

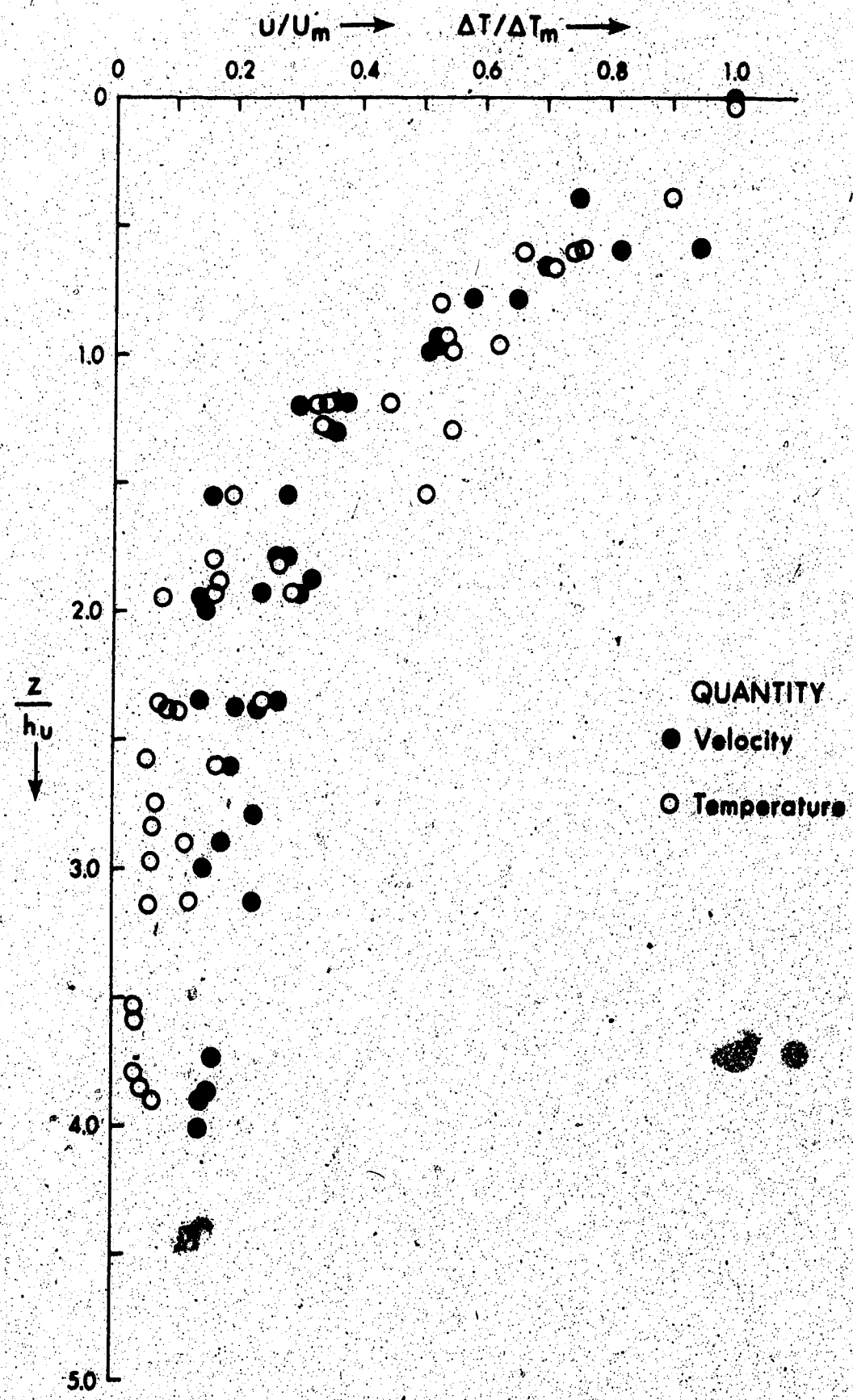

FIGURE 5.42 COMPARISON OF SIMILARITY PROFILES FOR VELOCITY AND TEMPERATURE ALONG CENTRAL VERTICAL PLANE $y/\sqrt{A_o} = 0$, Ri = 0.79

$$\frac{u_m}{U_o} = 5.678\ Ri^{1/3}\ (x/\sqrt{A_o} + 1)^{-2/3} \qquad (5.5.1)$$

and:

$$\frac{\Delta T_m}{\Delta T_o} = 4.4178\ Ri^{1/3}\ (x/\sqrt{A_o} + 1.795)^{-2/3} \qquad (5.9.1)$$

Taking the distances to be measured from virtual origin and neglecting the small differences from the origin, we can determine:

$$(u_m/U_o)\ /\ (\Delta T_m/\Delta T_o) = 1.285 \qquad (5.13.1)$$

This ratio for circular submerged nonbuoyant jets is 1.371 and for plane nonbuoyant jets it is 1.153 (Abramovich, 1963). Thus the present ratio lies inbetween a plane and a circular submerged nonbuoyant jet. This seems to be logical as the jet is not fully three dimensional due to a considerable inhibition of vertical mixing for the range of Richardson number considered in the present case. Equation 5.13.1 also shows that the temperature and velocity are affected in the same order by an increase in buoyancy. The comparison cannot be done for large Ri as the exponents of variation for temperature and velocity are different.

5.14 Comparison of Half Width for Velocity and Temperature

For moderate Ri the value of half width of temperature is given as:

$$\frac{b_T}{b_o} = 0.404\ Ri^{1/6}\ (x/b_o + 2)^{4/3} \qquad (5.11.1)$$

This value for velocity is given by:

$$\frac{b_u}{b_o} = 0.206\ Ri^{1/6}\ (x/b_o + 3.5)^{4/3} \qquad (5.6.3)$$

Neglecting the virtual origin correction, we get:

$$\frac{b_T}{b_u} = 1.96 \qquad (5.14.1)$$

For large Ri , the value of half width of temperature is given as:

$$\frac{b_T}{b_o} = 0.9146\ Ri^{1/8}\ (x/b_o + 1) \qquad (5.11.2)$$

and:

$$\frac{b_u}{b_o} = 0.4935\ Ri^{1/8}\ (x/b_o + 1.7) \qquad (5.6.2)$$

Neglecting again the virtual origin correction, we get:

$$\frac{b_T}{b_u} = 1.85 \qquad (5.14.2)$$

These results agree with the field results of Paddock and Policastro (1973) who found that, on the average, the temperature half width is twice as wide as the velocity half width.

5.15 Comparison of Half Depth for Velocity and Temperature

The value of h_{avg} for velocity is given by:

$$(h_{avg})_u = 0.26\ h_o/Ri^{1/8} \qquad (5.6.1b)$$

and that for temperature by:

$$h_{avg\ T} = 0.29\ h_o/Ri^{1/8} \qquad (5.10.1)$$

Thus the ratio:

$$(h_{avg\ T}) / (h_{avg\ u}) = 1.115 \qquad (5.15.1)$$

Hence, although the temperature half width becomes much wider than that for velocity, the ratio of half depths generally remains small as the vertical mixing is inhibited.

5.16 Explanation for a Wider Temperature Half Width than Velocity Half Width

At this stage a discussion as to why heat or tracer disperses more than momentum in a fluid is appropriate. This question cannot be answered in a definite way. Many investigators, e.g., Townsend (1956), Schubauer and Tchen (1961), Abraham (1963), Lumley and Tennekes (1972) have tried to explain the phenomenon and these are summarised as follows.

According to Abraham: "Collision occurs between lumps of fluid in a turbulent motion which affects the momentum of the lumps involved while the lumps may retain their indentity. Thus the difference in mean concentration of a tracer or temperature are less pro-

nounced than the corresponding differences in a momentum". Why should momentum alone be affected by collision and not the concentration of a tracer is not clear in his argument.

Schubauer and Tchen explain it in a more logical manner. They argue that any property that has been in the flow for a considerable length of time should be mixed to a fair degree of uniformity when it has arrived at a particular cross-section. Dilution occurs at the sharp boundaries and also new fluid has recently become turbulent there. Therefore, one should not expect complete uniformity everywhere within sharp boundaries. Experiments show that turbulent energy, temperature in the case of heated jets or wakes and concentration of a tracer in a jet, are nearly uniform over the fully turbulent core and decrease gradually in the turbulent bulges as the boundary is approached. The overall average decrease towards the boundaries is faster than that in turbulent parts alone due to the abscence of any contribution from nonturbulent parts.

The foregoing behaviour does not apply in the same degree to axial momentum. The mean velocity difference decreases considerably across the core and continues to decrease in the protruding turbulent bulges. This is obviously why the mean velocity distribution is less braod than the mean temperature distribution, but it is only a superficial explanation since it leaves unexplained why the momentum should have been given preferential treatment in the mixing process.

Lumley and Tennekes' explanation to the phenomenon is as follows: "Some molecules travelling faster than average carry more

thermal energy with them and make more collisions per unit time. Energetic molecules thus do more than a proportionate share in transporting heat. Further, buoyancy generated eddies cause relatively little momentum transport but they are quite effective in transporting heat".

Perhaps a better explanation of the phenomena can be offered with the help of "Double Structure of The Flow" enumerated by Townsend. The fully turbulent fluid is bounded by a contorted surface, creating a large surface area for entrainment. This contorted surface is so large as to approach centeral plane of the flow in some cases. The variation of intermittency in a jet shows that it is equal to 1.0 only in a very thin zone near the central plane, the flow being turbulent and nonturbulent elsewhere. At a particular section where a large amount of fluid has become turbulent at one instant, heat is spread all over. At another instant, the extend of fluid encompassed by the turbulence is smaller but a part of heat which has been spread on the previous extent is retained there, possibly due to conduction over a length of time due to repetitive processes. The momentum or vorticity could not be retained in the part of fluid which has now become non-turbulent.

This gives rise to a large diffusion for heat than momentum. The temperature gradient thus becomes smaller and smaller. Gradient type transfer requires that the diffusing movements shall be small compared to the distance over which gradient changes. The condition is satisfied by smaller eddies but not by larger eddies. According to

Townsend, the total rate of transport is a combination of gradient diffusion by smaller eddies which contain most of the turbulent energy, and bulk convection by large eddies. Since the gradient in scalar quantities like heat and matter have been reduced, it would appear that these quantities have been transported laterally more by bulk convection than by gradient diffusion. On the other hand, prospect for gradient diffusion for momentum is better.

5.17 Equation of Isotherm

The equation of isotherm can be easily worked out for various stages of Richardson number if the form of similarity and temperature decay scale are known. This is shown separately for the three ranges in the following sections.

5.18 Equation of Isotherm for Small Richardson Number

Experimental data of Jen and Wiegel are utilized here to work out the equation of isotherms. The temperature decay scale and form of similarity, from Chapter 2, are:

$$\frac{\Delta T_s}{\Delta T_m} = \text{Exp}\left[-3(y/x)^2(1/Ri^{1/4})\right] \qquad (5.18.1a)$$

$$\frac{\Delta T_m}{\Delta T_o} = 7.0\, d_o/x \qquad (5.18.1b)$$

and:

$$\frac{b_T}{b_o} = 0.57\, x/b_o\, Ri^{1/8} \qquad (5.18.1c)$$

Equation 5.18.1a and Equation 5.18.1b can be combined and written in a more general form as:

$$\Delta T_* = \frac{7.0\sqrt{A_o}}{x} \text{ Exp } [-3(y/x)^2(1/Ri^{1/4})] \qquad (5.18.2)$$

Jen and Wiegel's Equation 5.18.1a reduces to a more familiar form which can be written as:

$$\frac{\Delta T_s}{\Delta T_m} = \text{Exp } [-0.9747\ (y/b_T)^2] \qquad (5.18.3)$$

This equation does not satisfy the boundary condition when $y = b_T$, $\Delta T_s = \frac{1}{2}\ \Delta T_m$. Therefore, their experimental data (shown in Figure 5.43) has been compared with the equation that satisfies the boundary conditions. This is the general equation:

$$\frac{\Delta T_s}{\Delta T_m} = \text{Exp } [-0.693\ (y/b_T)^2]$$

The comparison has been found to be satisfactory. Thus the coefficient 0.9747 in Equation 5.18.3 is changed to 0.683 and Equation 5.18.2 changes to:

$$\Delta T_* = \frac{7.0\sqrt{A_o}}{x} \text{ Exp } [-2.133\ (y/x)^2\ Ri^{-1/4}] \qquad (5.18.4)$$

Rearrangement of Equation 5.18.4 yields the equation of isotherm:

$$\frac{y}{\sqrt{A_o}} = \frac{x}{\sqrt{A_o}} \left(\frac{Ri^{1/8}}{1.46}\right) \left(\ln \frac{7.0\sqrt{A_o}}{x} \frac{1}{\Delta T_*}\right)^{1/2} \qquad (5.18.5)$$

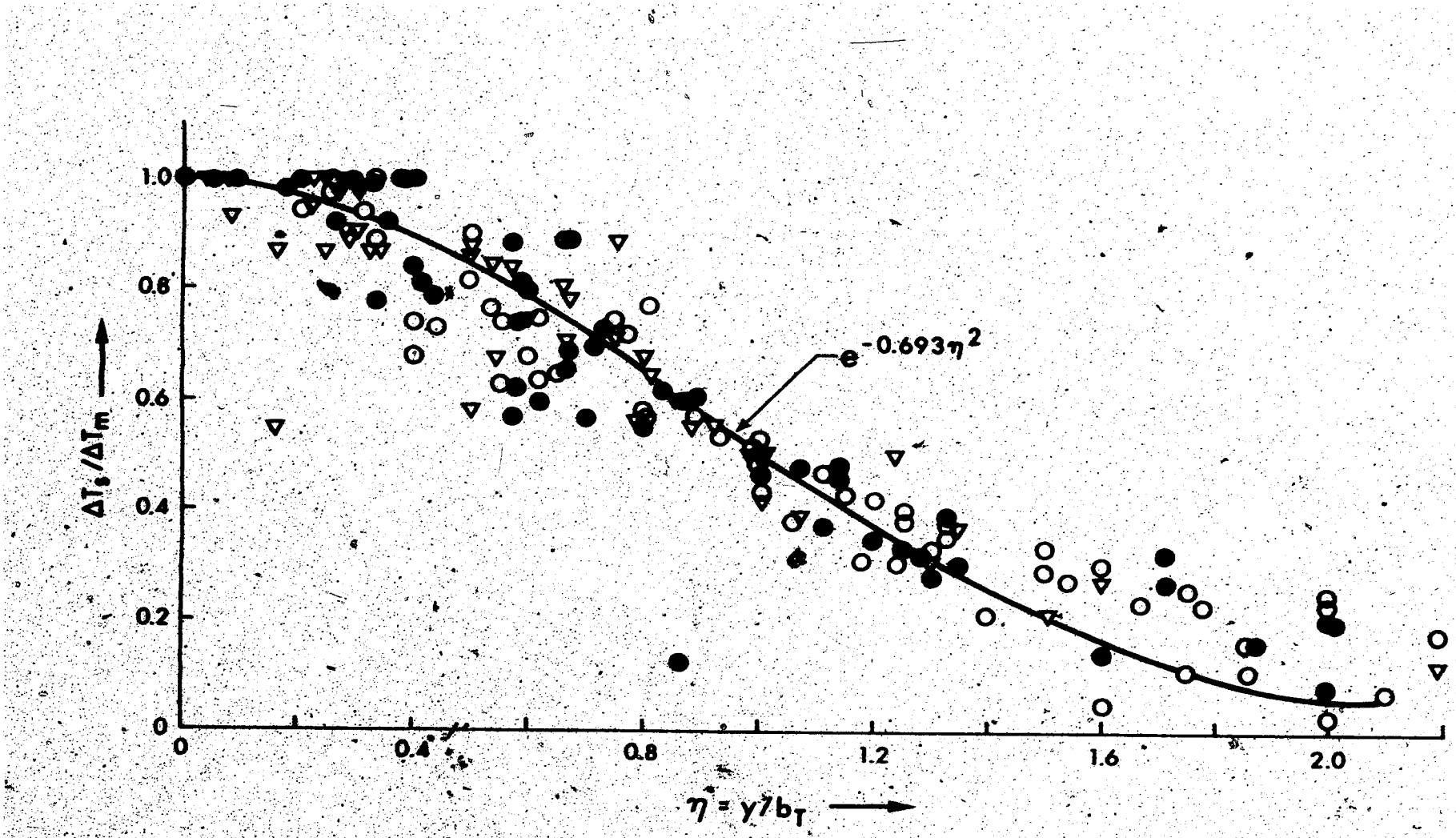

FIGURE 5.43 SIMILARITY OF TEMPERATURE PROFILE FOR SMALL Ri (JEN AND WIEGEL'S EXPERIMENTAL DATA)

5.18.1 Location of Maximum Spread of the Isotherm

The location of the maximum spread of the isotherm can be easily obtained by differentiating Equation 5.18.5 with respect to x. The algebraic manipulation thereafter yields:

$$(\bar{x}_1/\sqrt{A_o}) = 4.245/\Delta T_* \qquad (5.18.6)$$

The location where isotherm intercepts x axis can be obtained by putting y = 0 in Equation 5.18.5, so that:

$$(\bar{x}_2/\sqrt{A_o}) = 7.0/\Delta T_* \qquad (5.18.7)$$

5.18.2 Area Contained Within the Isotherm

If A_y is the area contained within the isotherm, then:

$$\frac{A_y}{2} = \int_o^{\bar{x}_2} y\,dx$$

$$= \int_o^{(7.0\sqrt{A_o})/\Delta T_*} \frac{x\,Ri^{1/8}}{1.46} \cdot \left[\ln 7.0 \left(\frac{\sqrt{A_o}}{x}\right) \frac{1}{\Delta T_*}\right]^{1/2} dx \qquad (5.18.8)$$

Integrating the above equation by the use of a Gamma function, one gets:

$$\Delta T_* = 4.58\ Ri^{1/6}\ (A_y/A_o)^{-0.5} \qquad (5.18.9a)$$

It appears more practical to represent the above equation as:

$$A_y/A_o = 21.03\ Ri^{1/8}\ (\Delta T_*)^{-2} \qquad (5.18.9b)$$

5.18.3 Equation of Isotherm in Vertical Planes

The similarity form of vertical profile for all our range of experiments has been approximated as:

$$\frac{\Delta T}{\Delta T_s} = \text{Exp}\left[-0.693\ (z/h_T)^2\right] \qquad (5.18.10)$$

As reported in Jen and Wiegel's experiments, the slope of the bottom of mixing jets beneath the axis of the jet is between 1/8 and 1/5.5. Taking an average slope to 1/6.75 and considering that the full depth of the jet is larger than the half jet by a factor of 2.25, one can write:

$$h_T = \frac{x}{15.2} \qquad (5.18.11)$$

Substituting Equation 5.18.11 in Equation 5.18.10 and rearranging:

$$\frac{z}{\sqrt{A_o}} = \frac{x}{12.66\sqrt{A_o}} \left(\ln \frac{\Delta T_s}{\Delta T}\right)^{1/2} \qquad (5.18.12)$$

Equations 5.18.12 and 5.18.4 can be combined and rearranged to yield:

$$\frac{y}{\sqrt{A_o}} = \frac{Ri^{1/8}}{1.46}\left[\frac{x^2}{A_o} \ln\left(\frac{7.0\sqrt{A_o}}{x}\right)\left(\frac{\Delta T_o}{\Delta T}\right) - 160.11\frac{z^2}{A_o}\right]^{1/2} \qquad (5.18.13)$$

On the central plane y = 0, hence:

$$\frac{z}{\sqrt{A_o}} = \frac{x}{12.66\sqrt{A_o}}\left[\ln\left(\frac{7.0\sqrt{A_o}}{x}\right)\left(\frac{\Delta T_o}{\Delta T}\right)\right]^{1/2} \qquad (5.18.14)$$

The isotherm intercepts x axis at:

$$\frac{\bar{x}_{2z}}{\sqrt{A_o}} = 7.0 \left(\frac{\Delta T_o}{\Delta T}\right) \qquad (5.18.15)$$

Derivation similar to Equation 5.18.9a leads to:

$$\frac{\Delta T}{\Delta T_o} = 1.10 \ (A_z/A_o)^{-0.5} \qquad (5.18.16a)$$

or:
$$\frac{A_z}{A_o} = 1.212 \ (\Delta T_o/\Delta T)^2 \qquad (5.18.16b)$$

A plot of Equations 5.18.5, 5.18.9b, 5.18.14 and 5.18.16b are shown in Appendix D.

5.19 Equation of Isotherm for Moderate Richardson Numbers

For the development of the equation of isotherm for moderate and large Richardson numbers, exponential distribution for similarity of temperature profiles in both horizontal and vertical planes has been chosen as it is convenient to use, and its agreement with data is satisfactory. Characteristic equation needed for the development of isotherms are:

$$\frac{\Delta T_m}{\Delta T_o} = 4.4178 \ Ri^{1/3} \ (x/\sqrt{A_o} + 1.795)^{-2/3} \qquad (5.9.4)$$

$$\frac{\Delta T_s}{\Delta T_m} = \text{Exp} \ [- 0.693 \ (y/b_T)^2]$$

$$\frac{b_T}{b_o} = 0.404 \; Ri^{1/6} \; (x/b_o + 2)^{4/3} \qquad (5.11.1)$$

The above three equations can be combined and rearranged to yield:

$$\frac{y}{b_o} = 0.4853 \; Ri^{1/6} \; (x/b_o + 2)^{4/3} \cdot \left\{ \ln \left[\frac{4.4178 \; Ri^{1/3}}{\Delta T_* \left(\frac{x}{\sqrt{A_o}} + 1.795 \right)^{2/3}} \right] \right\}^{1/2} \qquad (5.19.1)$$

5.19.1 Location of Maximum Spread of the Isotherm

This can be obtained by differentiating Equation 5.19.1 and equating $\partial y/\partial x$ to zero. The final solution has been obtained by assuming $x + 2\,b_o = x + 1.795\,\sqrt{A_o}$. The solution then, is:

$$\frac{\bar{x}_1}{\sqrt{A_o}} = \frac{5.64\,\sqrt{Ri}}{(\Delta T_*)^{3/2}} - 1.795 \qquad (5.19.2)$$

The location at which the isotherm cuts the centerline is found by putting $y = 0$ in Equation 5.19.1. This gives:

$$\frac{\bar{x}_2}{\sqrt{A_o}} = \frac{9.296\,\sqrt{Ri}}{(\Delta T_*)^{3/2}} - 1.795 \qquad (5.19.3)$$

5.19.2 Area Contained Within the Isotherm

$$A_y = 2 \int_0^{\bar{x}_2} y \, dx$$

Substituting for y from Equation 5.19.1, varying the limits of integration from $[(x/\sqrt{A_o}) + 1.795] = 0$ to $\bar{x}_2/\sqrt{A_o}$, simplifying it considerably, and using Gamma function, one gets:

$$\frac{A_y}{A_o} = 35.71\ (\sqrt{A_o}/b_o)^{1/3}\ \frac{Ri^{4/3}}{(\Delta T_*)^{7/2}} \qquad (5.19.4a)$$

or:
$$(\Delta T_*) = 2.777\ (\sqrt{A_o}/b_o)^{0.095}\ Ri^{0.381}\ (A_y/A_o)^{-0.2857} \qquad (5.19.4b)$$

5.19.3 Equation of Isotherm in Vertical Planes

According to the present series of experiments:

$$\frac{\Delta T}{\Delta T_s} = \text{Exp}\ [-\ 0.693\ (z/0.29\ h_o)^2\ Ri^{1/4}] \qquad (5.19.5)$$

Equations 5.19.5 and 5.19.1 can be combined and then simplified to yield a general equation of isotherm given by:

$$z = \frac{h_o Ri^{-1/8}}{2.87} \left\{ \ln \left[\frac{\Delta T_o}{\Delta T} \cdot \frac{4.4178\ Ri^{1/3}}{\left(\frac{x}{\sqrt{A_o}} + 1.795\right)^{2/3}} \right] - \frac{4.24\ (y/b_o)^2\ Ri^{-1/3}}{\left(\frac{x}{b_o} + 2\right)^{8/3}} \right\}^{1/2} \qquad (5.19.6a)$$

At the central plane $y = 0$, so that:

$$z = \frac{h_o Ri^{-1/8}}{2.87} \left\{ \ln \left[\frac{\Delta T_o}{\Delta T} \cdot \frac{4.4178\ Ri^{1/3}}{\left(\frac{x}{\sqrt{A_o}} + 1.795\right)^{2/3}} \right] \right\}^{1/2} \qquad (5.19.6b)$$

The location where the isotherm intercepts the x axis can be obtained by putting $z = 0$ in the above equation. This yields:

$$\frac{\bar{x}_2}{\sqrt{A_o}} = 9.28 \sqrt{Ri}\ (\Delta T_o/\Delta T)^{3/2} - 1.795 \qquad (5.19.7)$$

5.19.4 Area Contained Within the Isotherm

As in the case of Section 5.19.3, the value:

$$A_z = \int_0^{\bar{x}_2} z\,dx$$

Substituting for z from Equation 5.19.6b, simplifying and using Gamma function, one gets:

$$\frac{A_z}{h_o \sqrt{A_o}} = (1.78\ Ri^{1/4})^{3/2}\ (\Delta T/\Delta T_o)^{-1.5} \qquad (5.19.8a)$$

or: $$(\Delta T/\Delta T_o) = 1.78\ Ri^{1/4}\ (A_z/h_o\sqrt{A_o})^{-2/3} \qquad (5.19.8b)$$

A plot of Equations 5.19.1, 5.19.4b, 5.19.6b and 5.19.8b are shown in Appendix D.

5.20 Equation of Isotherm for Large Richardson Number

The equations needed to develop the equation of isotherm are:

$$\frac{\Delta T_m}{\Delta T_o} = 3.1664\ Ri^{-1/3}\ (x/\sqrt{A_o} + 1.795)^{-2/3} \qquad (5.9.5)$$

$$\frac{\Delta T_s}{\Delta T_m} = Exp\ [-\ 0.693\ (y/b_T)^2] \qquad (5.20.1)$$

and:

$$\frac{b_T}{b_o} = 0.9146\ Ri^{1/8}\ (\frac{x}{b_o} + 1) \qquad (5.11.2)$$

These can be combined and rearranged to yield:

$$\frac{y}{b_o} = 1.098\ (\frac{x}{b_o} + 1)\ Ri^{1/8} \left\{ \ln \left[\frac{3.164}{\Delta T_*} Ri^{-1/3}\ (\frac{x}{\sqrt{A_o}} + 1.795)^{-2/3} \right] \right\}^{1/2} \qquad (5.20.2)$$

5.20.1 Location of Maximum Spread of the Isotherm

This can be obtained by differentiating Equation 5.20.2 and equating $\partial y/\partial x$ to zero. The final solution, obtained by assuming $x + b_o = x + 1.795\ \sqrt{A_o}$ is:

$$\bar{x}_1 = \frac{3.414}{\Delta T_*^{3/2}} (Ri/A_o)^{-1/2} - 1.795\ \sqrt{A_o}$$

5.20.2 Location Where Isotherm Cuts x Axis

This can be found by equating y to zero in Equation 5.20.2. Thus:

$$\bar{x}_2 = (3.1644/\Delta T_*)^{3/2}(Ri/A_o)^{-1/2} - 1.795\sqrt{A_o} \qquad (5.20.4)$$

5.20.3 Area Under the Isotherm

$$A_y = 2\int_0^{\bar{x}_2} y\,dx$$

Substituting for y from Equation 5.20.2, varying the limits of integration $x/\sqrt{A_o} + 1.795 = 0$ to $\bar{x}_2/\sqrt{A_o}$, simplifying it considerably, assuming $(x + b_o) = (x + 1.795\sqrt{A_o})$, and using Gamma function, one can derive:

$$\Delta T_* = 2.61\ Ri^{-0.291}(A_y/A_o)^{-0.3334} \qquad (5.20.5a)$$

or:
$$A_y/A_o = 17.80\ Ri^{-0.873}(\Delta T_*)^{-3} \qquad (5.20.5b)$$

5.20.4 Equation of Vertical Isotherm

According to the present series of experiments:

$$\frac{\Delta T}{\Delta T_s} = \text{Exp}\left[-0.693\left(\frac{z}{0.29\ h_o}\right)^2 Ri^{1/4}\right] \qquad (5.19.5)$$

Equation 5.19.5, 5.20.1 and 5.9.5 can be combined and to yield:

$$\frac{\Delta T}{\Delta T_o} = 3.166\ Ri^{-1/3}\left(\frac{x}{\sqrt{A_o}} + 1.795\right)^{-2/3} \cdot \text{Exp}\left[-0.693\ (y/b_T)^2 - \frac{8.24\ z^2\ Ri^{1/4}}{h_o^2}\right]$$

Further simplification yields:

$$z = \frac{h_o}{2.87} Ri^{-1/8} \left\{ \ln \left[3.1664\ Ri^{-1/3} (\Delta T_o/\Delta T) \right. \right.$$

$$\left. \left. (\frac{x}{\sqrt{A_o}} + 1.795)^{-2/3} \right] - 0.828\ Ri^{-1/4} \left(\frac{y/b_o}{x/b_o + 1} \right)^2 \right\}^{1/2} \qquad (5.20.6a)$$

On the central plane $y = 0$ so:

$$z = \frac{h_o}{2.87} Ri^{-1/8} \left\{ \ln \left[3.1664\ Ri^{-1/3} (\Delta T_o/\Delta T) \right. \right.$$

$$\left. \left. (\frac{x}{\sqrt{A_o}} + 1.795)^{-2/3} \right] \right\}^{1/2} \qquad (5.20.6b)$$

The location where the isotherm intercepts x axis is given by:

$$\bar{x}_2/\sqrt{A_o} = 5.63\ Ri^{-1/2} (\Delta T_o/\Delta T)^{3/2} - 1.795 \qquad (5.20.7)$$

5.20.5 Area Within the Vertical Isotherm

$$A_z = \int_o^{\bar{x}_2} z\,dx$$

Following the procedures described earlier, one gets:

$$\frac{\Delta T}{\Delta T_o} = 1.268\ Ri^{-10/24} \left(\frac{A_z}{h_o \sqrt{A_o}} \right)^{-2/3} \qquad (5.20.7a)$$

or:

$$\frac{A_z}{h_o \sqrt{A_o}} = 1.43\ Ri^{-5/8} (\Delta T/\Delta T_o)^{-1.5} \qquad (5.20.7b)$$

A plot of Equations 5.20.2, 5.20.5b, 5.20.6b and 5.20.7b are shown in Appendix D.

5.21 Measurement of Length of Zone of Flow Establishment

Various investigators have calculated the length of the zone of flow establishment; notable amongst them are Shirazi and Davis, and Stefan (1975). Their formulations are listed below:

Shirazi and Davis Formula:

$$\frac{x_p}{h_o} = 5.4\, A_s^{-2/3} Ri^{1/6} \qquad (5.21.1a)$$

or:

$$\frac{x_p}{\sqrt{A_o}} = 5.4\, (Ri/A_s)^{1/6} \qquad (5.21.1b)$$

Stefan's Formula:

$$\frac{x_p}{h_o} = 6.05\, A_s^{-0.46} \left(1 + \frac{0.50\, Ri^{-1/2} - 1.50}{0.4\, Ri^{-1/2}}\right) e^{-0.9\, R} \qquad (5.21.2a)$$

where R is the cross flow velocity ratio. This equation can be modified for jet flows with R = 0 as:

$$\frac{x_p}{\sqrt{A_o}} = 6.05 \left(1 + \frac{0.50\, Ri^{-1/2} - 1.50}{0.4\, Ri^{-1/2}}\right) \qquad (5.21.2b)$$

The length of the zone of flow establishment can also be derived from

the present analysis as given in Equation 5.9.4 and 5.9.5. Taking $\Delta T_m/\Delta T_o = 1.0$ we get the length of the zone of flow establishment as:

$$\frac{x_p}{\sqrt{A_o}} = 9.285\ Ri^{1/2} - 1.795 \qquad (5.21.3)$$

for moderate Ri, and:

$$\frac{x_p}{\sqrt{A_o}} = 5.634\ Ri^{-1/2} - 1.795 \qquad (5.21.4)$$

for large Ri.

All these formulas are compared with the actual length of the flow establishment measured in the experiment for a centerline temperature decay of 90%. The comparison is shown in Table 5.4.

TABLE 5.4 LENGTH OF FLOW ESTABLISHMENT

Ri	Length of Flow Establishment Obtained in Expt.	Length Given by Present Theory	Length Obtained From Shirazi's Formula	Length Obtained From Stefan's Formula
	$x_p/\sqrt{A_o}$	$x_p/\sqrt{A_o}$	$x_p/\sqrt{A_o}$	$x_p/\sqrt{A_o}$
0.15	3.20	1.80	3.93	5.60
0.35	3.20	3.69	4.53	4.03
0.56	4.34	5.15	5.88	3.10
0.79	2.60	4.54	6.23	2.43
1.14	3.52	3.48	6.62	1.75

It appears, therefore, that the determination of the zone of flow establishment by the present theory may be satisfactory beyond Ri = 0.35.

CHAPTER 6

SUMMARY, CONCLUSIONS AND RECOMMENDATIONS

6.1 Summary and Conclusions

The discharge of thermal effluents into natural water bodies is an important engineering problem due to the enormous ecological effects that might follow. The waste heat is usually discharged into a lake as a three dimensional heated surface jet. Such a heated surface jet flowing into a quiescent lake was considered for theoretical and experimental study in this thesis.

The theoretical work started with an order of magnitude study of the equations of motion. This study was based on the argument that increments in the buoyancy force suppressed the production of turbulence terms due to density stratification and increased the importance of buoyancy terms in the equation of motion. The order of magnitude study of the Reynolds equation of motion (Section 3.1) indicated three regimes of flow characterised by small, moderate and large (source) Richardson number Ri. For each of these cases, the equation of motion and the heat transport equations were integrated, nondimensionalized and subjected to a similarity analysis.

6.1.1 Results for Small Ri

From the similarity analysis for small Ri , the centerline velocity, temperature excess and length scales were given by the following expressions:

$$\Delta T_m \propto x^{-1.0} \; ; \; u_m \propto x^{-1.0} \; ; \; b \propto x \; ; \; h \propto x \qquad (6.1.1)$$

Expressions for vertical entrainment velocity w_e and lateral velocity v were derived by combining the energy and continuity equations. The values of v and w_e were found to vary as:

$$v \propto \frac{1}{x} \; ; \quad w_e \propto \frac{1}{x} \qquad (6.1.2)$$

Experiments were carried out only for moderate and high Richardson numbers as such no experimental verifications for Equation 6.1.1 could be made. However, the results of Jen, et al. (1966) for this range of Ri were in agreement with these expressions.

6.1.2 Results for Large Ri

Similarity analysis on the governing equation of motion for large Richardson number gave various scales as follows:

$$u_m \propto x^{-1/3} \; ; \; \Delta T_m \propto x^{-2/3} \; ; \; b \propto x \; ; \; h \propto x^{o} \qquad (6.1.3)$$

Expressions for vertical entrainment velocity w_e and lateral velocity v were derived again and these are:

$$w_e \propto x^{-4/3} \quad ; \quad v \propto x^{-1/3} \qquad (6.1.4)$$

Temperature distribution in lateral direction was theoreti-

cally found to vary as:

$$\frac{\Delta T_s}{\Delta T_m} = [1 + 7\ (y/b_T)^2]^{-1/3} \qquad (6.1.5)$$

Experimental results for large Ri indicated that:

(i) Profiles of velocity and excess temperature distribution were similar in both lateral and vertical directions. The similarity profiles can be closely approximated either by Schlichting type curve given as:

$$(1 + 0.41\ \eta^2)^{-2} \qquad (6.1.6)$$

or by exponential distribution given as:

$$\text{Exp}\ (-\ 0.693\ \eta^2) \qquad (6.1.7)$$

where $\eta = y/b_u$ for lateral velocity profiles

$= z/h_u$ for vertical velocity profiles

$= y/b_T$ for lateral excess temperature profile

$= z/h_T$ for vertical excess temperature profile.

(ii) The similarity profile of excess temperature distribution in lateral direction could also be satisfactorily approximated with the theoretically predicted curve $[1 + 7\ (y/b_T)^2]^{-1/3}$.

(iii) Transition from moderate to large Richardson number occurred at

a value between 0.61 to 0.84.

(iv) Decay of the centerline velocity scale confirmed the theoretical deductions and u_m was found to vary as:

$$u_m/U_o = 1.436\ Ri^{-1/6}\ \left(\frac{x}{\sqrt{A_o}} - 10.5\right)^{-1/3}$$

(v) The value of average half depth of velocity for all Richardson numbers decreased very rapidly to about 26% of the outlet depth and then remained constant. The experimental result was given as $h_u = 0.26\ h_o/Ri^{1/8}$.

(vi) The value of half width scale of velocity also confirmed the theoretical analysis and was found as:

$$b_u/b_o = 0.4935\ Ri^{1/8}\ (x/b_o + 1.7)$$

(vii) Decay of the centerline temperature excess, ΔT_m, was given by:

$$\frac{\Delta T_m}{\Delta T_o} = 3.1664\ Ri^{-1/3}\ \left(\frac{x}{\sqrt{A_o}} + 1.795\right)^{-2/3}$$

which again confirmed the theoretical predictions.

(viii) The average half depth for temperature decreased rapidly to 0.29 times its value at the outlet and then remained constant. The experimental result gave $h_T = 0.29\ h_o/Ri^{1/8}$.

(ix) The half temperature width was found as:

$$\frac{b_T}{b_o} = 0.9146\ Ri^{1/8}\ \left(\frac{x}{b_o} + 1\right)$$

(x) The ratio of half width of temperature to that of velocity was found to be 1.86, which is quite significant.

6.1.3 Results for Moderate Ri

Similarity analysis on the governing equation of motion for moderate Ri indicated various scales as:

$$u_m \propto x^{-(\frac{2}{3} + c)} \quad ; \quad \Delta T_m \propto x^{(\frac{1}{3} + c)}$$

$$b \propto x^{\frac{4}{3} + c} \quad ; \quad h \propto x^{c} \qquad (6.1.8)$$

The expressions for vertical entrainment velocity w_e and lateral velocity v were derived as:

$$w_e \propto x^{-5/3} \quad ; \quad v \propto x^{-1/3} \qquad (6.1.9)$$

Experimental results for moderate Ri indicated that:

(i) There is no significant vertical mixing for a buoyant surface jet for $Ri > 0.15$. The value of c was found to be zero for the range of experiments done during the present investigation.

(ii) Profiles of velocity and temperature distribution in both the lateral and vertical directions were found to be similar and

the experimental data lie close to the similarity curves found for large Richardson number.

(iii) Decay of the centerline velocity, u_m, confirmed the theoretical deductions with $c = 0$ and was found to vary as:

$$\frac{u_m}{U_o} = 5.678\ Ri^{1/3}\left(\frac{x}{\sqrt{A_o}} + 1\right)^{-2/3}$$

and the value of half width of velocity:

$$\frac{b_u}{b_o} = 0.206\ Ri^{1/6}\left(\frac{x}{b_o} + 3.5\right)^{4/3}$$

(iv) Decay of the centerline temperature excess, ΔT_m, was found to vary as:

$$\frac{\Delta T_m}{\Delta T_o} = 4.4178\ Ri^{1/3}\left(\frac{x}{\sqrt{A_o}} + 1.795\right)^{-2/3}$$

and half temperature width as:

$$\frac{b_T}{b_o} = 0.404\ Ri^{1/6}\left(\frac{x}{b_o} + 2\right)^{4/3}$$

(v) Average half depth for both temperature and velocity varied in the same way as those for the large Richardson number.

All the above results confirmed the theoretical results for $c = 0$.

(vi) For moderate Ri the ratio $(u_m/U_o)/(\Delta T_m/\Delta T_o)$ was found to equal 1.285. This value lies between that for a circular non-buoyant and plane nonbuoyant jets.

(vii) The ratio of half width of temperature to that of velocity was found to be 1.96, which is quite significant.

(viii) The ratio of half depth of temperature to that of velocity was found equal to 1.115 for all Richardson numbers.

6.1.4 Isotherm Equations and Their Areas

The Equations of isotherms were worked out for all three regimes of flow based on the results described in previous articles. Areas of the isotherms were then worked out from these equations. Some of the siginficant results were as follows:

For Small Ri: $\Delta T_* \propto (A_y/A_o)^{-1/2}$

$$\Delta T/\Delta T_o \propto (A_z/A_o)^{-1/2}$$

For Moderate Ri: $\Delta T_* \propto (A_y/A_o)^{-2/7}$

$$\Delta T/\Delta T_o \propto (A_z/h_o\sqrt{A_o})^{-2/3}$$

For Large Ri: $\Delta T_* \propto (A_y/A_o)^{-1/3}$

$$(\Delta T/\Delta T_o) \propto (A_z/h_o\sqrt{A_o})^{-2/3}$$

6.1.5 Lengths of the Zone of Flow Establishment

The lengths of the zone of flow establishment were worked out

on the basis of the results derived earlier. These are:

For Moderate Ri: $$\frac{x_p}{\sqrt{A_o}} = 9.285\ Ri^{1/2} - 1.795 \quad \text{for} \quad Ri > 0.35$$

For Large Ri: $$\frac{x_p}{\sqrt{A_o}} = 5.634\ Ri^{-1/2} - 1.795$$

6.2 Recommendations for Further Study

The present investigation dealt with all the regimes of flow in the near field region for the surface discharge in a water body with stagnant surroundings. Future studies may consider:

(i) Surface discharges with cross flows and wind shear acting on the system. The work done on this subject so far deals only with very small cross flows, the results of which might as well be approximated by the present analysis without any cross flow. The equations of motion should therefore be written in the curvilinear coordinate system and the present analysis then extended to this situation.

(ii) Transition region or intermediate region with surface heat loss from the plume surface. A large amount of work has already been done in the far field region but the transition between this and the near field considered here has been largely ignored. Further work is required to fill this gap.

REFERENCES

Abbott, M.B. "On the Spreading of One Fluid Over Another". Part I, La Houille Blanche, Paris, France, No. 5, 1961, pp. 622-628. Part II, La Houille Blanche, No. 6, 1961, pp. 827-836.

Abraham, G. "Jet Diffusion in Stagnant Ambient Fluid". Publication No. 29, Delft Hydraulics Laboratory, July 1963.

Abramovich, G.N. "The Theory of Turbulent Jets". M.I.T. Press, Cambridge, Massachusetts, (English Translation) 1963.

Albertson, M.L., Dai, Y.B., Jensen, R.A. and Rouse, H. "Diffusion of Submerged Jets". Trans. ASCE, Volume 115, 1950, pp. 639-697.

An Energy Policy for Canada, Volume I. Analysis issued under the authority of the Ministry of Energy, Mines and Resources, Information Canada, Ottawa, 1973.

Anwar, H.O. "Behaviour of Buoyant Jets in Calm Fluid". Journal of the Hydraulics Division, ASCE, Volume 95, No. HY4, Proc. Paper 6688, July 1969, pp. 1289-1303.

Anwar, H.O. "Appearance of Unstable Buoyant Jets". Journal of the Hydraulics Division, ASCE, Volume 98, No. HY7, Proc. Paper 9012, July 1972a, pp. 1143-1156.

Anwar, H.O. "The Radial Spreading as a Free Surface Layer of a Vertical Buoyant Jet". Journal of Engineering Mathematics, Volume 6, No. 3, Wolters-Noordhoff Publications, Netherlands, July 1972b, pp. 257-272.

Asbury, J.G. and Frigo, A.A. "A Phenomenological Relationship for Predicting the Surface Areas of Thermal Plumes in Lakes". ANL/ES-5, April 1971.

Barr, D.I.H. "Some Observations of Small Scale Thermal Density Currents". Proceedings, 8th Congress of the International Association for Hydraulic Research, Montreal, Canada, 1959, pp. 6-C-1 to 6-C-22.

Barr, D.I.H. "Spread Characteristics of a Buoyant Discharge". Proceedings, 10th Congress of the International Association for Hydraulic Research, London, England, Volume 1, 1963, pp. 153-160.

Barr, D.I.H. "A Hydraulic Model Study of Heat Dissipation at Kincardine Power Station". Institution of Civil Engineers, Proceedings, Volume 10, Paper No. 6289, July 1968, pp. 305-320.

Bauer, D.P., Jobson, H.E., Jennings, M.E. "Generalized Stream Temperature Analysis System". Proceedings, 21st Annual Hydraulics Division Speciality Conference, Montana State University, ASCE, August 1973, pp. 167-178.

Brown, T.L. "Energy and the Environment". Charles E. Merril Publishing Company (A Bell & Howell Company), Columbus, Ohio, 1971, pp. 71-106.

Bryce, J.B., Elliott, R.V. "Thermal Plume Measurements in Lake Ontario and Resulting Phenomenological Model". International Symposium on Stratified Flows, Novosibirsk, 1972, Published by ASCE (1973), pp. 145-160.

Carter, H.H. " A Preliminary Report on the Characteristics of a Heated Jet Discharged Horizontally into a Transverse Current". Part I. Constant Depth, Technical Report No. 61, Chesapeake Bay Institute, The John Hopkins University, Baltimore, November 1969.

Clutter, D.W., Smith, A.M.O. and Brazier, J.G. "Techniques of Flow-Visualization Using Water as a Working Medium". Douglas Air Craft Division, Report No. ES-29075, April 1959.

Davis, W. and Fox, R.W. "An Evaluation of the Hydrogen Bubble Technique for the Quantitative Determination of Fluid Velocities Within Clear Tubes". Journal of Basic Engineering, Trans. ASME, Series D, Volume 87, December 1967, pp. 771-771.

Edinger, J.E. and Geyer, J.C. "Heat Exchange in the Environment". EEI Publication No. 65-902, John Hopkins University, June 1965.

Elliot, R.V. and Harkness, D.G. "A Phenomenological Model for the Prediction of Thermal Plumes in Large lakes". Proceedings, 15th Conference on Great Lakes & Reservoirs, International Association of Great Lakes and Reservoirs, 1972, pp. 544-564.

Ellison, T.H. and Turner, J.S. "Turbulent Entrainment in Stratified Flow". Journal of Fluid Mechanics, Volume 6, Part 3, October 1959, pp. 423-448.

Engelund, F. and Pedersen, F.B. "Surface Jet at Small Richardson Numbers". Journal of the Hydraulics Division, ASCE, Volume 99, No. HY3, Proc. Paper 9588, March 1973, pp. 405-416.

Fan, L.N. "Turbulent Buoyant Jets into Stratified or Flowing Ambient Fluids". W.W. Keck Laboratory of Hydraulics & Water Resources, Report No. KM-R-15, California Institute of Technology, 1967.

Fox, D.G. "Forced Plumes in Stratified Fluid". Journal of Geophysical Research, Volume 75, No. 33, November 1970, pp. 6818-6835.

Frazer, W., Barr, D.I.H. and Smith, A.A. "A Hydraulic Model Study of Heat Dissipation at Longannet Power Station". Institution of Civil Engineers, Proceedings, Volume 39, Paper No. 7039, January 1968, pp. 23-44.

Harleman, D.R.F. "Stratified Flow". Section 26, Handbook of Fluid Dynamics, Edited by V.L. Streeter, McGraw-Hill Book Company, 1961.

Harleman, D.R.F. "Thermal Stratification Due to Heated Discharges". International Symposium on Stratified Flows, Novosibirsk, 1972, Published by ASCE (1973).

Hayashi, T. and Shuto, N. "Diffusion of Warm Water Jets Discharged Horizontally at the Water Surface". Proceedings, 12th Congress of the International Association for Hydraulic Research, Colorado State University, Volume 4, September 1967, pp. 47-59.

Haywood, K.H. and Tory, C. Discussion on "Evaluation of Hydrogen Bubble Technique for the Quantitative Determination of Fluid Velocities Within Clear Tubes". Journal of Basic Engineering, Trans. ASME, Series D, Volume 87, December 1967, pp. 777-778.

Heinz, J.O. "Turbulence". McGraw-Hill Book Company, 1959.

Hill, B.J. "Measurement of Local Entrainment Rate in the Initial Region of Axisymmetric Turbulent Air Jets". Journal of Fluid Mechanics, Volume 51, Part 4, 1972, pp. 773-779.

Hirst, E.A. "Analysis of Round, Turbulent, Buoyant Jets Discharged to Flowing Stratified Ambients". Report No. ORNL-4685, Oak Ridge National Laboratory, June 1971.

Hirst, E.A. Discussion on "Two Dimensional Surface Warm Jets". Journal of the Hydraulics Division, ASCE, Volume 98, No. HY1, January 1972, pp. 299-301.

Hodges, L. "Environmental Pollution". Holt, Rinehart and Winston, Inc., New York, 1973, pp. 229-242.

Hopfinger, E.J. "Development of a Stratified Turbulent Shear Flow". International Symposium on Stratified Flows, Novosibirsk, 1972, Published by ASCE (1973), pp. 553-566.

Hoopes, J.A., Zeller, R.W. and Rohlich, G.A. "Heat Dissipation and Induced Circulations from Condenser Cooling Water Discharges into lake Monona". Report No. 35, Department of Civil Engineering, the University of Wisconsin, February 1968.

Hoult, D.P., Fay, J.A. and Forney, L.J. "A Theory of Plume Rise Compared with Field Observations". Journal of Air Pollution and Control Association, Volume 19, September 1969, pp. 585-590.

Jen Yuan, Wiegel, R. and Mobarek, I. "Surface Discharge of Horizontal Warm Water Jets". Journal of Power Division, ASCE, Volume 92, PO2, April 1966, pp. 1-30.

Jonys, C.K. "An Experimental Study of Bed Form Mechanics". Ph.D. Thesis (1973), The University of Alberta, Edmonton, Canada.

Kenny, B.C. "The Physical Effects of Waste Heat Input to the Great lakes". Scientific Series No. 28, Inland Waters Directorate, Canada Centre for Inland Waters, Burlington, Ontario, 1973.

Koh, R.C.Y. "Tow Dimensional Surface Warm Jets". Journal of the Hydraulic Division, ASCE, Volume 97, No. HY6, Proc. Paper 8186, June 1971, pp. 819-836.

Kolflat, T.D. "Cooling Tower Practices". Power Engineering, Volume 76, January 1974, pp. 32-39.

Lau, Y.L. and Dick, T.M. "Dimensional Analysis of Thermal Plumes". Hydraulics Division, Canada Centre for Inland Waters, Burlington, Ontario, Unpublished Report, December 1973.

Lumley, J.L. and Tennekes, H. "A First Course in Turbulence". M.I.T. Press, Cambridge, Massachusetts, 1972.

Mahajan, B. and John, J. "The Mixing of Shallow Submerged Heated Water Jets with An Ambient Reservoir". AIAA Journal, Volume 9, No. 11, November 1971, pp. 2135-2140.

Mahajan, B. and John, J. "Jet Mixing Studies Associated with Thermal Pollution". Proceedings, Institute of Environmental Sciences, 1971, pp. 210-218.

Maxwell, W.H. and Pazwash, H. "Boundary Effect on Jet Flow Patterns Related to Water Quality and Pollution Problems". Completion Report to Office of Water Resources Research, Department of the Interior, Washington D.C., January 1970.

Maxwell, W.H. and Pazwash, H. "Axisymmetric Shallow Submerged Turbulent Jets". Journal of the Hydraulics Division, Proc. Paper 9675, No. HY4, April 1973, pp.637-652

Morton, B.R., Taylor, G.I. and Turner, J.S. "Turbulent Gravitational Convection from Maintained and Instantaneous Sources". Proceedings, Royal Society of London, London, England, Series A, Volume 234, 1956, pp. 1-23.

Morton, B.R. "On a Momentum Mass Flux Diagrams for Turbulent Jets, Plumes and Wakes". Journal of Fluid Mechanics, Volume 10, 1961, pp. 101-112.

Motz, L.H. and Benedict, B.A. "Heated Surface Jet Discharged into a Flowing ambient Stream". Department of Environmental and Water Resources Engineering, Vanderbilt University, Nashville, Tennessee, Report No. 4, August 1970.

Nagib, H.M., Ludwig, W. Jr., Lavan, Z. and Fejer, A.A. "Experimental Investigation of the Hydrodynamic Stability of Flow in Rotating Pipes Using Thermistors". Proceedings, Sumposium on Turbulence Measurements in Liquids, September 1969, pp. 140-146.

Nichol, C.I.H. "Some Dynamical Effects of Heat on Turbulent Boundary layer". Journal of Fluid Mechanics, Volume 40, 1970, pp. 361-384.

Paddock, R.A., Policastro, A.J., Frigo, A.A., Frye, D.E. and Tokar, J.V. "Temperature and Velocity Measurements and Predictive Model Comparisions in the Near-Field Region of Surface Thermal Discharges". ANL/ES-25.

Palmer, M.D. "Estimate of the Physical Extent of Thermal Plumes at Lakeview, 1969-70". Water Quality Branch, Ontario Ministry of Environment, Toronto, 1972, (Information taken from Lau and Dick, 1973).

Pani, B.S. "Three Dimensional Wall Jets". Ph.D. Thesis, The University of Alberta, 1972.

Parker, F.L. and Krenkel, P.A. "Engineering Aspects of Thermal Pollution". Vanderbilt University Press, 1969.

Platten, J.L. and Keffer, J.F. "Entrainment in Deflected Axisymmetric Jets at Various Angles to the Stream". Technical Report, 6808, Department of Mechanical Engineering, University of Toronto, June 1968.

Policastro, A.J. and Tokar, J.V. "Heated Effluent Dispersion in Large Lakes: State of the Art of Analytical Modelling. Critique of Model Formulations". Argonne National Laboratory, ANL-ES-11, Center for Environmental Studies, 1972.

Pritchard, D.W. "Design and Siting Criteria for Once-Through Cooling Systems". American Institute of Chemical Engineers, 68th. Annual Meeting, Texas, 1971 (Review taken from Policastro, et al. 1972).

Prych, E.A. "A Warm Water Effluent Analyzed as a Buoyant Surface Jet", Notiser och Preliminara Rapporter Serie Hydrologi, NR 21, Sveriges Meterologiska och Hydrologiska Institut, Stockholm, 1972.

Rajaratnam, N. and Pani, B.S. "Three Dimensional Turbulent Wall Jets". Technical Report, Department of Civil Engineering, The University of Alberta, Edmonton, Canada, 1971.

Ricou, F.P. and Spalding D.B. "Measurements of Entrainment by Axisymmetric Turbulent Jets". Journal of Fluid Mechanics, Part I, Volume 11, August 1961, pp. 21-32.

Schraub, F.A., Kline, S.J., Henry, J., Runstadler, J.W. Jr. and Little, A. "Use of Hydrogen Bubbles for Quantitative Determination of Time Dependent Velocity Field in Low Speed Water Flows". Journal of Basic Engineering, Trans. ASME, Series D, Volume 85, June 1965, pp. 429-444.

Schubauer, G.B. and Tchen, C.M. "Turbulent Flow". Princeton Aeronautical Paperbacks, Princeton University Press, New Jersey, 1961.

Schlichting, H. "Boundary Layer Theory". McGraw Hill Book Company, New York, 1968.

Silberman, E. "Heated Surface Discharges Into Flowing Ambient Streams and Lakes". Chapter 10 of River Mechanics, Volume III, (Proceedings, 2nd Institute of River Mechanics, July-August 1972, Colorado State University, Fort Collins).

Silberman, E. "Warm Water Discharges Into Lakes and Reservoirs". International Symposium on Stratified Flows, Novosibirsk, 1972, Published by ASCE (1973).

Silberman, E. Discussion on "Surface Discharge of Horizontal Warm Water Jets". Journal of Power Division, Proceedings of ASCE, Volume 93, No. PO1, March 1967.

Singer, S.F. "Environmental Quality and Economics of Cooling". Power Generation and Environmental Change, Symposium of the Committee on Environmental Alterations for the Advancement of Science, December 1969, Published by M.I.T. Press, 1971.

Soo, S.L. "Fluid Dynamics of Multiphase Systems". Waltham, Massachusetts, Blaisdell Publishing Co., 1967.

Stolzenbach, K.D. and Harleman, D.R.F. "An Analytical and Experimental Investigation of Surface Discharges of Heated Water". Ralph M. Parson's Laboratory, M.I.T., Cambridge, 1971.

Stolzenbach, K.D., Adams, E.E. and Harleman, D.R.F. "A User's Manual for Three Dimensional Heated Surface Discharge Computations". Ralph M. Parson's Laboratory, Report No. 156, M.I.T., Cambridge, September 1972.

Stefan, H. "Modelling Spread of Heated Water Over Lakes". Journal of the Power Division, ASCE, Volume 96, No. PO3, Proc. paper 7375, June 1970, pp. 469-482.

Stefan, H. "Stratification of Flow From Channel Into Deep Lake". Journal of the Hydraulics Division, ASCE, Volume 96, No. HY7, Proc. Paper 7401, July 1970, pp. 1417-1434.

Stefan, H. and Schiebe, F.R. "Heated Discharge from Flume Into Tank". Journal of the Sanitary Engineering Division, ASCE, Volume 96, No. SA6, Proc. Paper 7762, December 1970, pp.1415-1453.

Stefan, H. "Dilution of Buoyant Two Dimensional Surface Discharges". Journal of the Hydraulics Division, ASCE, Volume 98, No. HY1, Proc. Paper 8653, January 1972, pp. 71-86.

Stefan, H. and Vaidyaraman, P. "J[illegible] Type Model for the Three Dimensional Thermal Plume in a Cross Current and Under Wind". St. Anthony Falls Hydraulic Laboratory, Water Resources Research, Technical Paper No. 58, Series A, Volume 8, No. 4, August 1972, pp. 998-1014.

Stefan, H., Chu, C.S. and Wing, H. "Impact of Cooling Water on Lake Temperatures". Journal of the Power Division, ASCE, Volume 98, No. PO2, Proc. Paper 9241, October 1972, pp. 253-272.

Stefan, H., Bergstedt, L. and Mrosla, E. "Flow Establishment and Initial Entrainment of Heated Water Surface Jets". Ecological Research Series, Report No. EPA-660/3-75-014, May 1975.

Stewart, R.W. "The Problem of Diffusion in Stratified Fluids". Advances in Geophysics, Volume 6, 1959, pp. 146-

Sundaram, T.R., Easterbrook, P. and Rundinger, G. "An Investigation of the Physical Effects of Thermal Discharges into Cayuga Lake". Report VT-2616-O-2, Thermal Plume Model, Cornell Aeronautical Laboratory, November 1969.

Swanson, W.M. Discussion on "Evaluation of the Hydrogen Bubble Technique for the Quantitative Determination of Fluid Velocities Within Clear Tubes". Journal of Basic Engineering, Trans. ASME, Series D, Volume 87, December 1967, pp. 780.

Tamai, N., Weigel, R.L. and Tornberg, G.F. "Horizontal Surface Discharges of Warm Water Jets". Journal of the Power Division, ASCE, Proc. Paper 6847, Volume 95, No. PO2, October 1969, pp. 253-276.

Townsend, A.A. "The Structure of Turbulent Shear Flow". Cambridge University Press, Cambridge, England, 1956.

Townsend, A.A. "Turbulent Flow in a Stabily Stratified Atmosphere". Journal of Fluid Mechanics, Volume 3, 1957, pp. 361-372.

Turner, J.S. "Buoyancy Effects in Fluids". Cambridge University Press, Cambridge, England, 1973.

Umrath, E. "Thermal Pollution - What is it, How can it be Measured". Institute of Environmental Sciences, Proceedings, 1972, pp. 415-419.

Vaisilev, V.I.K. and Chernyshova, R.T. "Mathematical Modelling of Surface Pollution of Water Body". Proceedings, 15th Congress of the International Association for Hydraulic Research, Turkey, Volume 2, 1973, pp. 129-136.

Wood, I.R. and Wilkinson, D.R. Discussion of "Surface Discharge of Horizontal Warm Water Jets". Journal of the Power Division, ASCE, Volume 93, No. PO1, Proc. Paper 5140, March 1967, pp. 149-151.

Wu, J. "Wind Stress and Surface Roughness at Air-Sea Interface". Journal of Geophysical Research, Volume 74, 1969, pp. 444-455.

Zeller, R.W., Hoopes, Z.A. and Rohlich, G.A. "Heated Surface Jets in Steady Cross Current". Journal of the Hydraulics Division, ASCE, Volume 97, No. HY9, Proc. Paper 8385, September 1971, pp. 1403-1426.

APPENDIX - A

LIST OF FUNCTIONS, SCALE VARIATIONS AND INTEGRALS

$$\frac{u}{u_s} = f_1(\xi) \qquad I_1 = \int_0^\infty f_1(\xi)\,d\xi$$

$$\frac{u_s}{u_m} = f_1(\eta) \qquad I_2 = \int_0^\infty f_2(\xi)\,d\eta$$

$$\frac{v}{v_s} = f_2(\xi) \qquad I_3 = \int_0^\infty f_1^{\,2}(\xi)\,d\xi$$

$$\frac{\Delta T}{\Delta T_s} = f_3(\xi) \qquad I_4 = \int_0^\infty f_1(\xi) f_2(\xi)\,d\xi$$

$$\frac{\Delta T_s}{\Delta T_m} = f_3(\eta) \qquad I_5 = \int_0^\infty \left[\int_0^\infty f_3(\xi)\,d\xi \right] d\xi$$

$$\frac{h}{h_m} = f_4(\eta) \qquad I_6 = \int_0^\infty f_2^{\,2}(\xi)\,d\xi$$

$$\frac{w_e}{w_{em}} = f(\eta) \qquad I_7 = \int_0^\infty f_2(\xi) f_3(\xi)\,d\xi$$

$$\frac{\tau_{xy}}{\rho_a U_m^{\,2}} = \bar{g}(\eta, \xi) \qquad I_8 = \int_0^\infty f_1(\xi) f_3(\xi)\,d\xi$$

$$u_{m_*} = k_1 x_*^{\,a} \qquad I_9 = \int_0^\infty f(\eta) f_1^{\,2}(\eta)\,d\eta$$

$$b_* = k_2 x_*^{\,n} \qquad I_{10} = \frac{1}{I_3} \int_0^\infty \left[\int_0^\infty \bar{g}(\eta,\xi)\, \frac{k_1}{k_2}\, f_1'(\eta) f_4(\eta)\,d\xi \right] d\eta$$

$$\Delta T_{m_*} = k_3 x_*^{\,d}$$

$$h_{m_*} = k_4 x_*^{\,c}$$

$$I_{11} = \int_0^\infty f_1^{\,3}(\eta) f_4(\eta) k_1 a d\eta$$

$$I_{12} = \int_0^\infty f_1^{\,2}(\eta) f_4(\eta) f_1'(\eta) k_1 n\eta d\eta$$

$$I_{13} = \left(\frac{I_4 I_1}{2 I_2 I_3} - 1\right) \int_0^\infty f_1^{\,3}(\eta) f_4(\eta) c k_1 d\eta$$

$$I_{14} = \left(\frac{I_4 I_1}{2 I_2 I_3} - 1\right) \int_0^\infty f_1^{\,3}(\eta) f_4(\eta) f_1 a d\eta$$

$$I_{15} = \left(\frac{I_4 I_1}{2 I_2 I_3} - 1\right) \left\{ \int_0^\infty f_1^{\,2}(\eta) k_1 n \left[f_1'(\eta) f_4(\eta) + f_4'(\eta) f_1(\eta) \right] \eta d\eta \right\}$$

$$I_{16} = -\frac{2 I_2 I_3 I_{10}}{I_1 I_4 I_9}$$

$$I_1' = \int_0^\infty f_1(\eta) d\eta$$

$$I_{17} = \frac{(I_{11} - I_{12} - I_{13} + I_{14} - I_{15})}{I_1 I_4 I_9} 2 I_2 I_3$$

$$I_{18} = \int_0^\infty f_1^{\,2}(\eta) f_4(\eta) d\eta$$

$$I_2' = \int_0^\infty f_1^{\,2}(\eta) d\eta$$

$$I_{19} = \int_0^\infty f_3(\eta) f_4^{\,2}(\eta) d\eta$$

$$I_3' = \int_0^\infty f_1(\eta) f_3(\eta) d\eta$$

$$I_{20} = \int_0^\infty f_1(\eta) f_3(\eta) f_4(\eta) d\eta$$

$$\bar{I}_1 = \int_{-1}^{+1} e^{-(n/b)^2} d(n/b)$$

$$I_{21} = \int_0^\infty f_1(\eta) f_3(\eta) f_4(\eta) d\eta$$

$$\bar{I}_2 = \int_{-1}^{+1} e^{-2(n/b)^2} d(n/b)$$

$$I_{22} = \int_0^{\infty} f_3(\eta) f_4^{\,2}(\eta) f_1(\eta) d\eta$$

$$I_{23} = \frac{I_5}{I_3} \, Ri \, k_1 k_2 k_3 \, [(a + d + n + 2c) \, I_{21} - I_{22} - n]$$

$$F_1(\eta) = \left[\int_0^{\eta} f_1(\eta) f_4(\eta) c k_1 d\eta + \int_0^{\eta} f_1(\eta) f_4(\eta) k_1 a d\eta - \int_0^{\eta} k_1 n (f_1 f_4)' \eta d\eta \right]$$

$$F_2(\eta) = - \frac{k_2}{f_4(\eta)} \, \frac{I_{16}}{I_2} \int_0^{\eta} f(\eta) d\eta$$

$$F_3(\eta) = - \frac{k_2}{f_4(\eta)} \left[\frac{I_{17}}{I_2} \int_0^{\eta} f(\eta) d\eta - I_{18} \right]$$

$$F_4(\eta) = k_1 k_3 \, (a+c+d) \, f_1(\eta) f_3(\eta) f_4(\eta) - \eta k_1 k_3 \, [f_1(\eta) f_3(\eta) f_4(\eta)]'$$

$$F_5(\eta) = \frac{I_7}{I_8} \, k_1 k_3 \, [F_3(\eta) f_3(\eta) f_4(\eta)]'$$

$$F_6(\eta, \xi) = \frac{1}{I_8} \, k k_1 \sqrt{k_2 k_4} \sqrt{L_o h_o} \, \Delta T_o \int_0^{\infty} [F_3(\eta) f_3(\xi) f_4(\eta)]'' d\xi$$

$$F_7(\eta) = \left[\left(I_{17} + \frac{I_{14}}{I_9 k_1 k_2} \right) \frac{1}{I_2} \frac{k_2}{k_4} \frac{1}{f_4(\eta)} \int_0^{\eta} f d\eta - \frac{k_1 k_2 I_1}{I_2} \frac{1}{f_4(\eta)} \int_0^{\eta} f_1(\eta) f_4(\eta) d\eta \right]$$

$$J_1(\eta) = \int_0^{\eta} f_1(\eta) d\eta$$

APPENDIX - B

TABLE B-1 DETAILS OF THERMISTOR PROBES

	Item	Detail
	1. Length of glass probes	2 inches
	2. Lead diameter	0.012"
	3. Lead material	'Dumet'
*	4. R_o at 25°C	2000 ± 20% Ω
	5. Code number	GB 32 P2 (Glass coated bead, 2 x 10^3 Ω resistance at 25°C, probe mounted, individual unit No. 2)
	6. $\frac{\text{Resistance at } 0°C}{\text{Resistance at } 50°C}$	7.3
**	7. Dissipation constant	1.0
***	8. Time constant T_c	25 seconds

Note:

* R_o : Resistance measured at approximately zero power.

** Dissipation constant: Amount of power in milliwatts which will raise the thermistor 1°C above its surroundings.

*** Time constant: Time required in seconds for the thermistor to change its own temperature 63% of the way from its original value to the value impressed upon it in a step change. It will take 5 times the time constant to change its value to 98%.

APPENDIX - C

VELOCITY PLOTS AND EXPERIMENTAL DATA

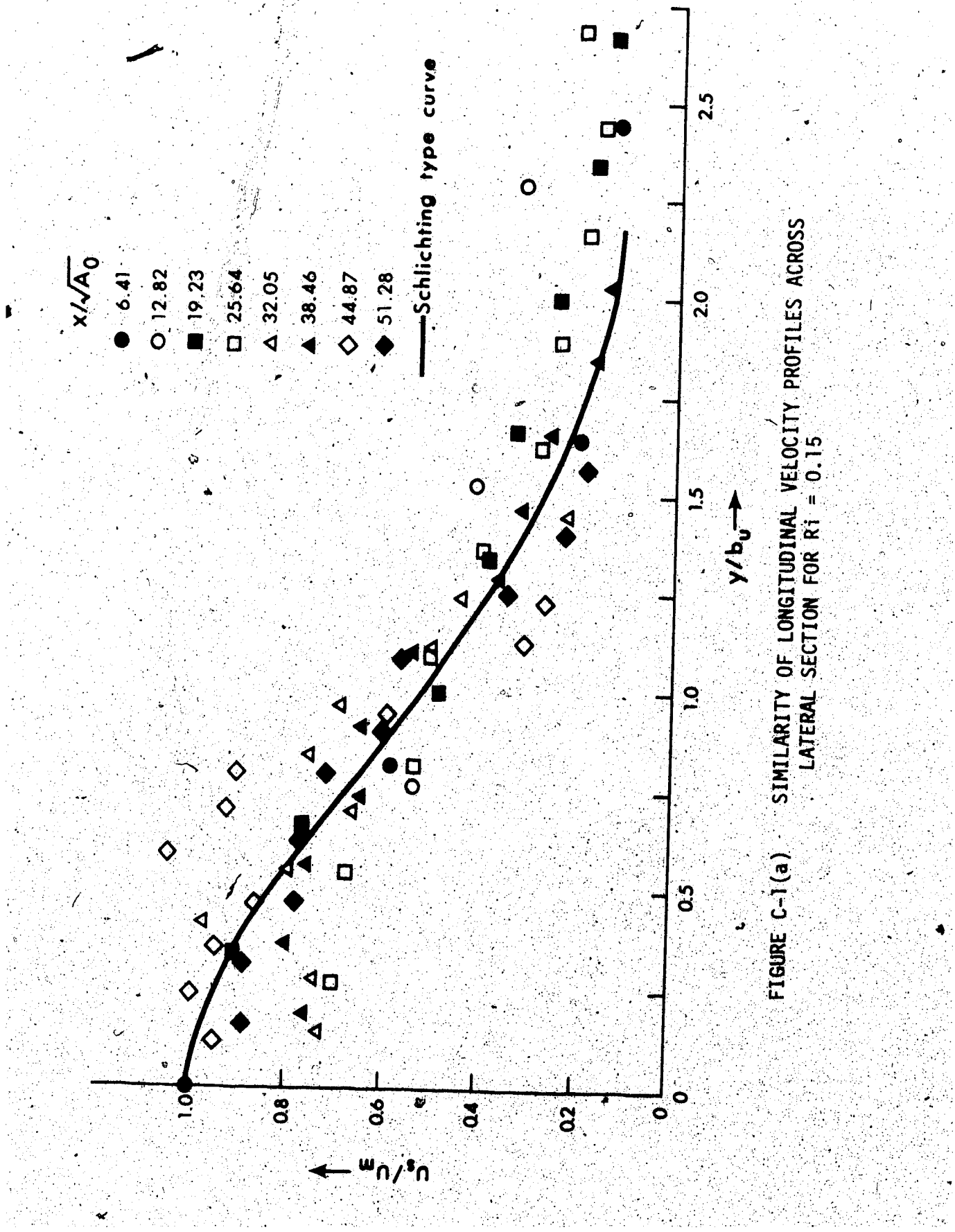

FIGURE C-1(a) SIMILARITY OF LONGITUDINAL VELOCITY PROFILES ACROSS LATERAL SECTION FOR Ri = 0.15

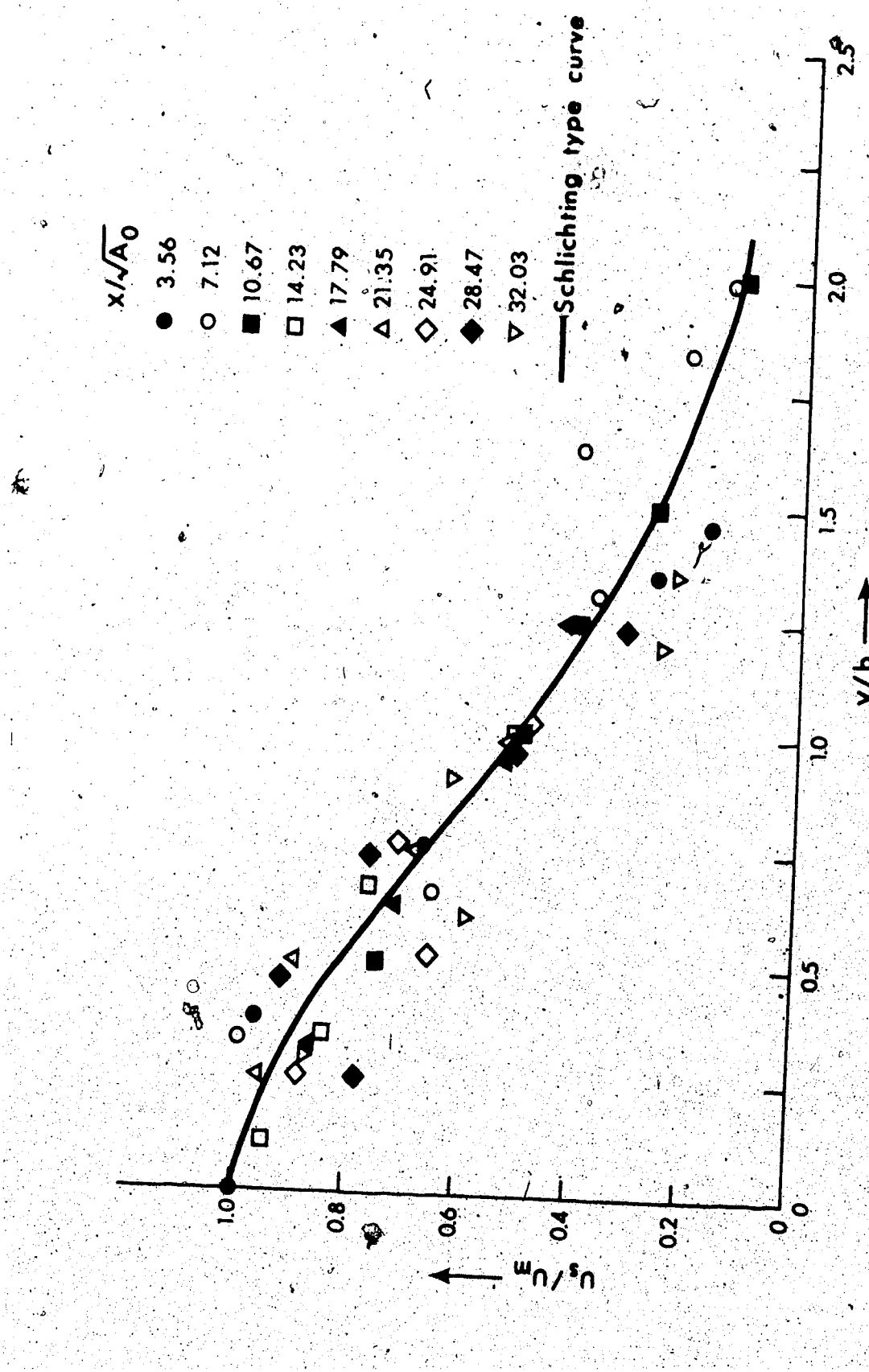

FIGURE C-1(b) SIMILARITY OF LONGITUDINAL VELOCITY PROFILES ACROSS LATERAL SECTION FOR Ri = 0.56

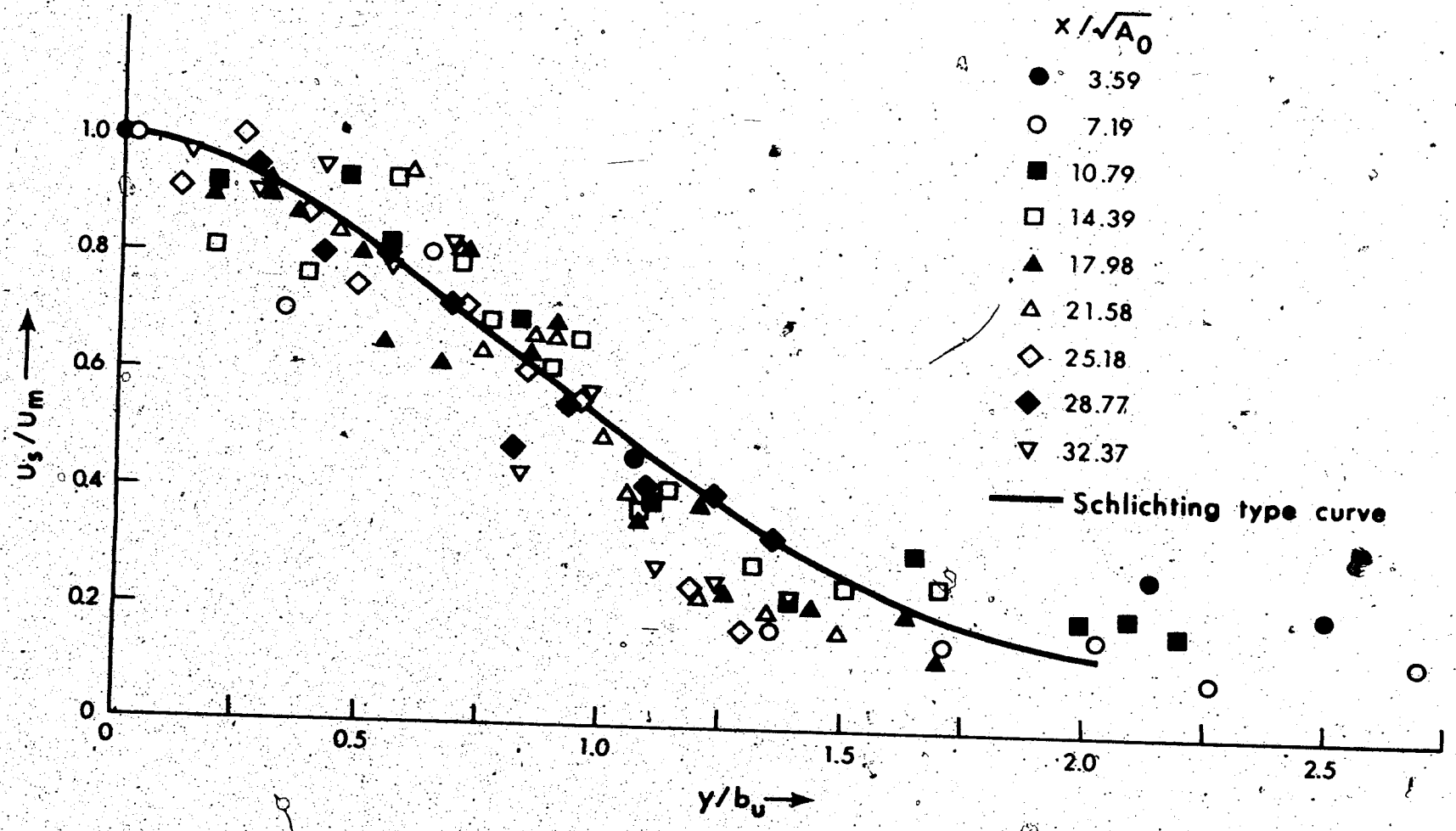

FIGURE C-1(c) SIMILARITY OF LONGITUDINAL VELOCITY PROFILES ACROSS LATERAL SECTION FOR Ri = 1.14

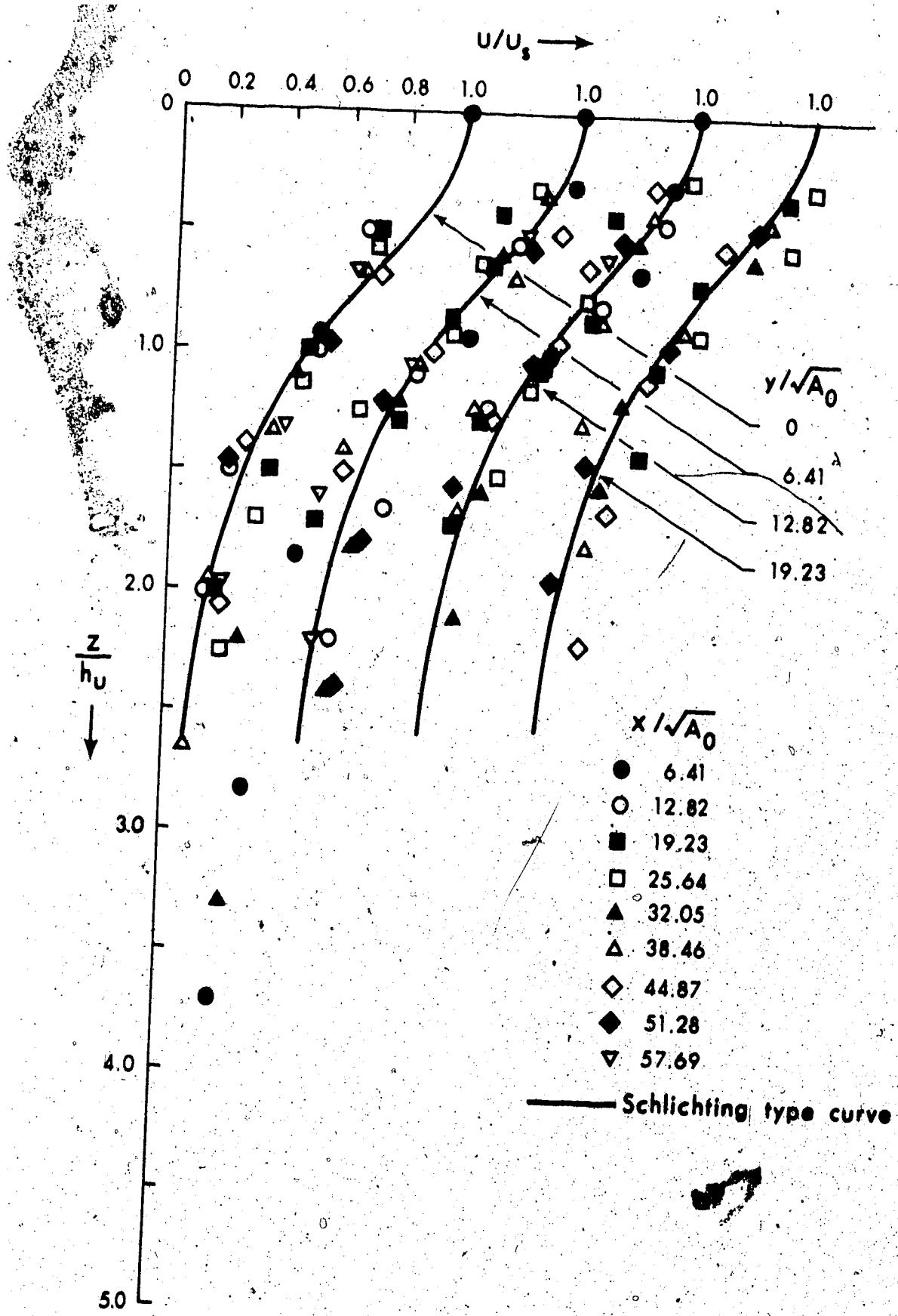

FIGURE C-2(a) SIMILARITY OF LONGITUDINAL VELOCITY PROFILES ACROSS VERTICAL SECTIONS FOR Ri = 0.15

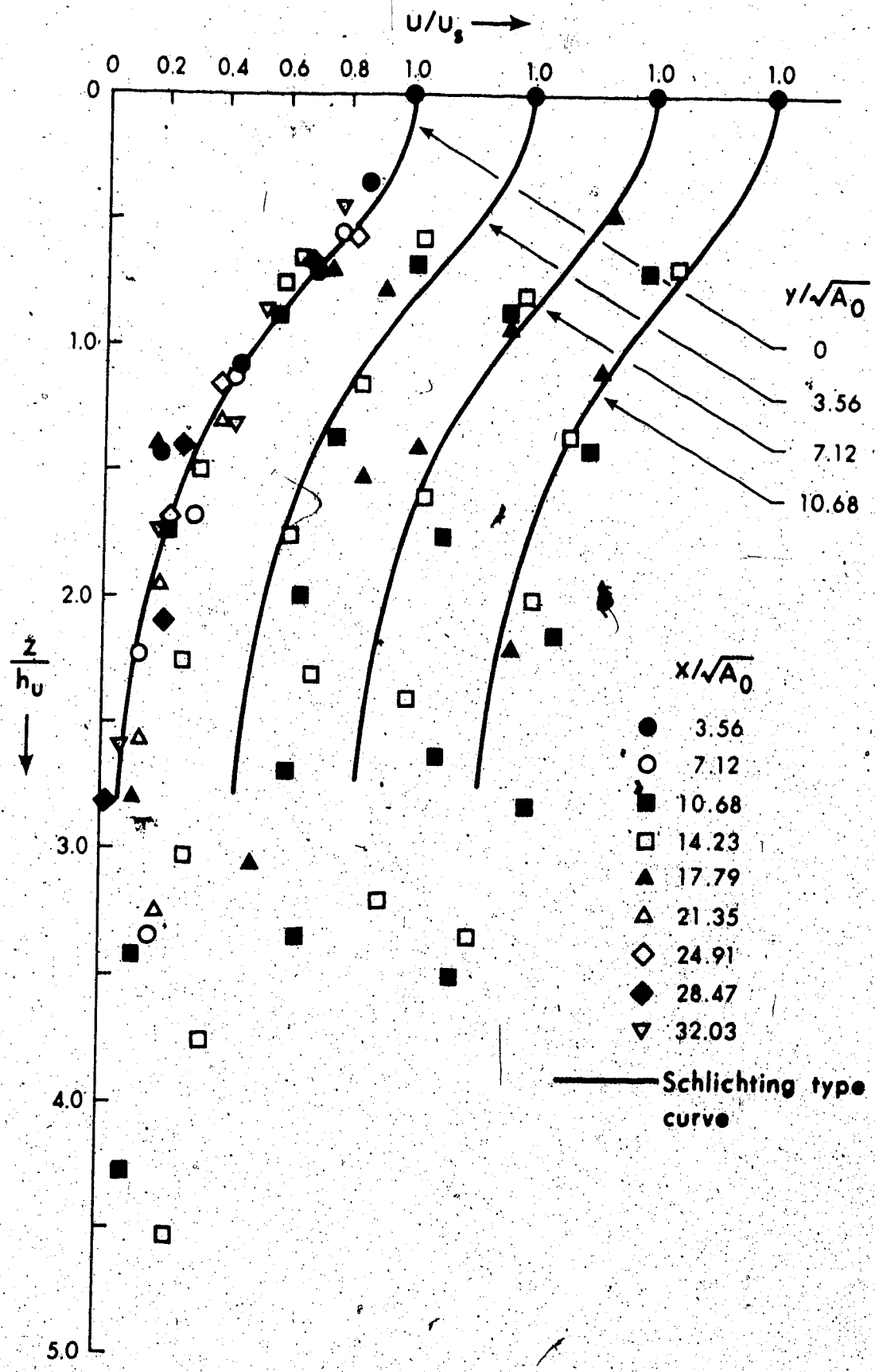

FIGURE C-2(b) SIMILARITY OF LONGITUDINAL VELOCITY PROFILES ACROSS VERTICAL SECTIONS FOR Ri = 0.56.

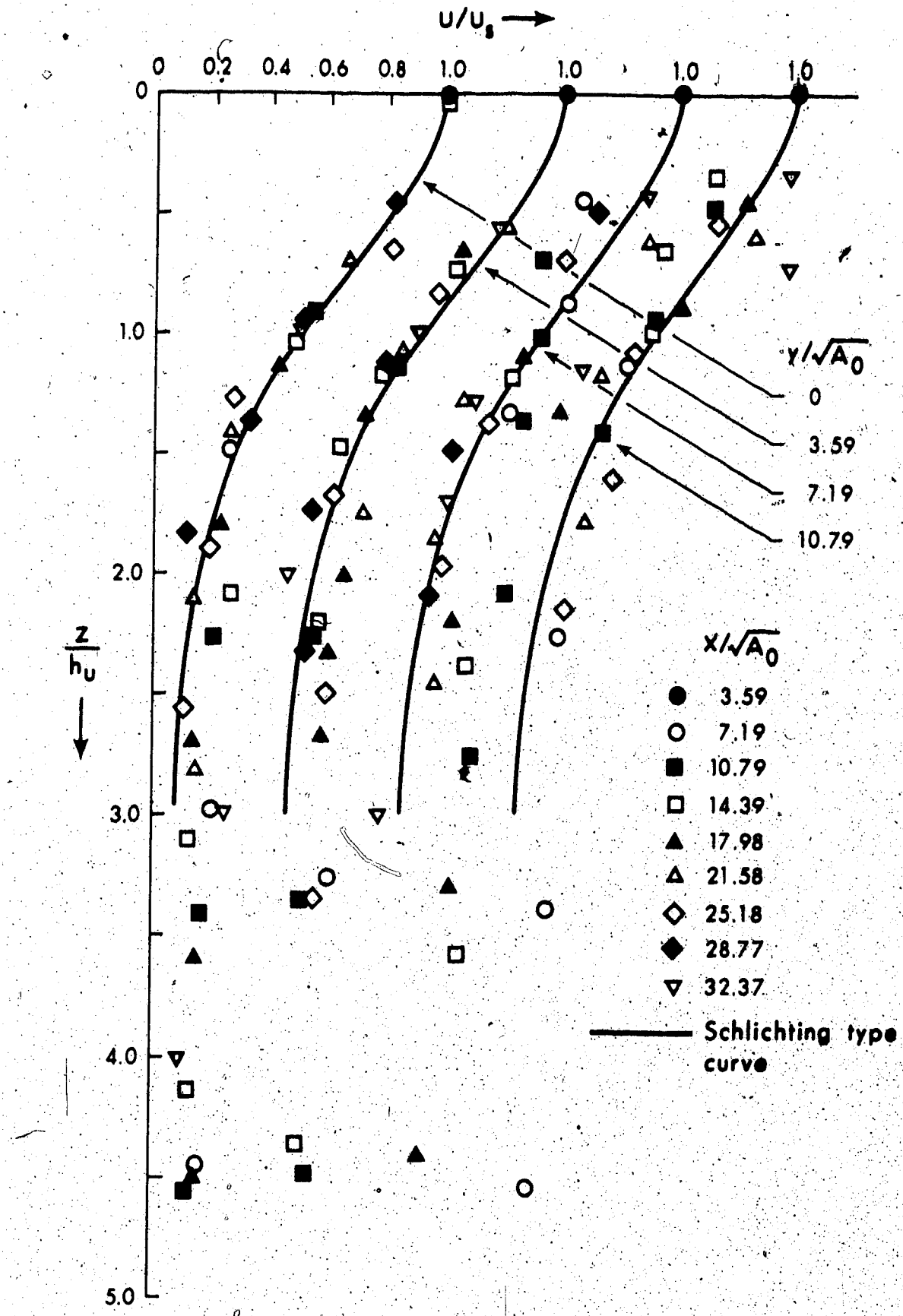

FIGURE C-2(c) SIMILARITY OF LONGITUDINAL VELOCITY PROFILES ACROSS VERTICAL SECTIONS FOR Ri = 1.14

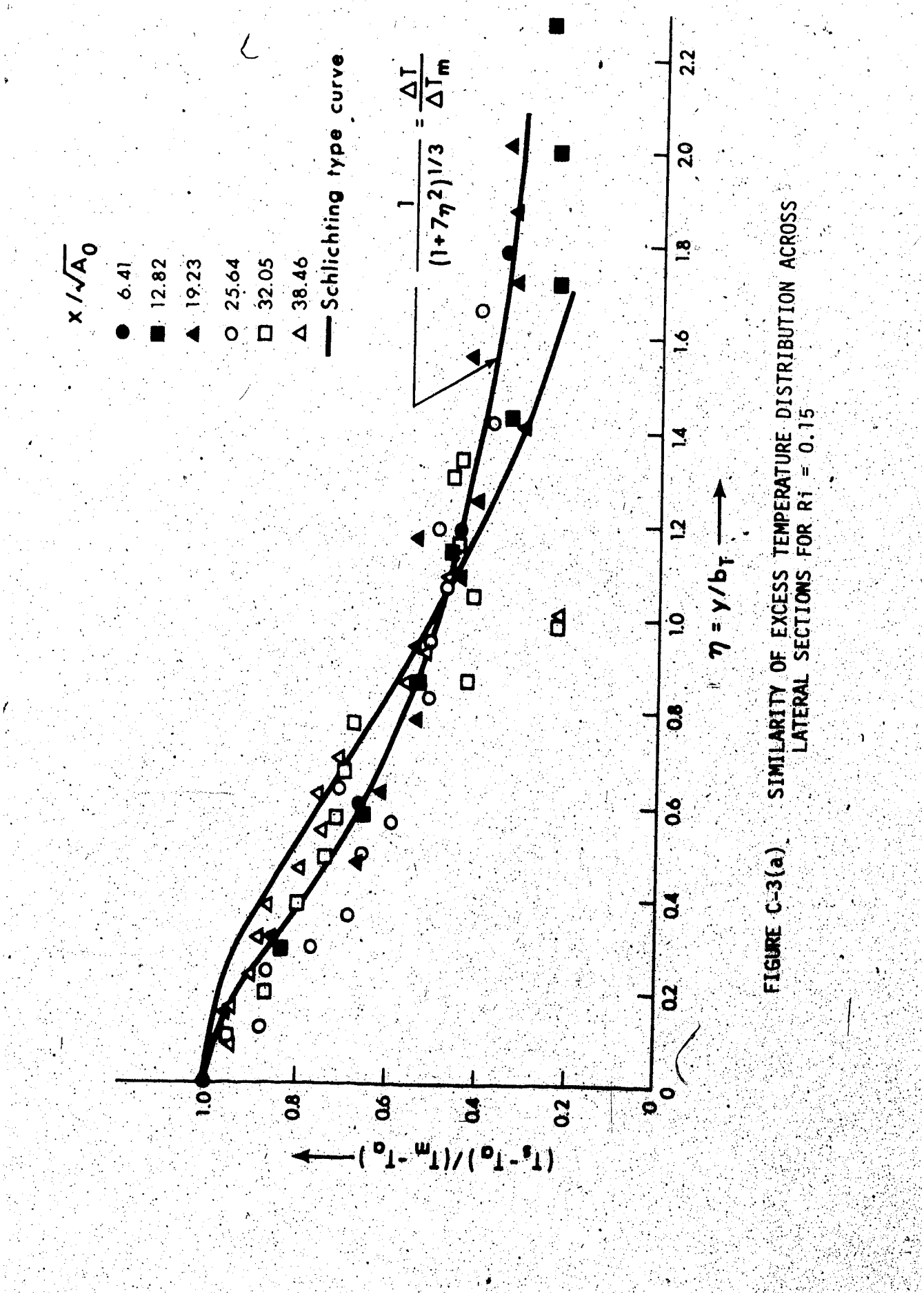

FIGURE C-3(a). SIMILARITY OF EXCESS TEMPERATURE DISTRIBUTION ACROSS LATERAL SECTIONS FOR Ri = 0.15

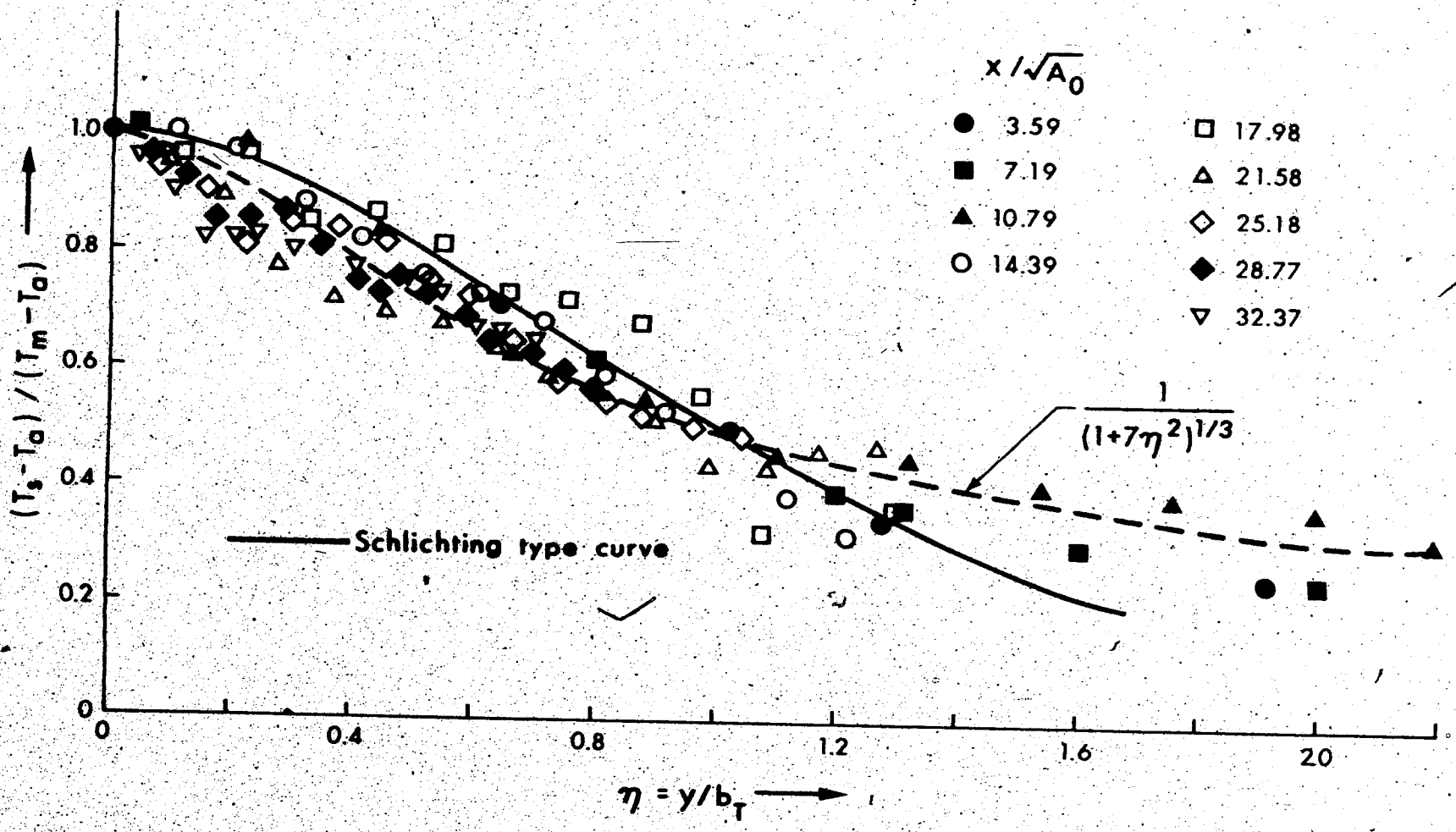

FIGURE C-3(b) SIMILARITY OF EXCESS TEMPERATURE DISTRIBUTION ACROSS LATERAL SECTIONS FOR Ri = 0.35

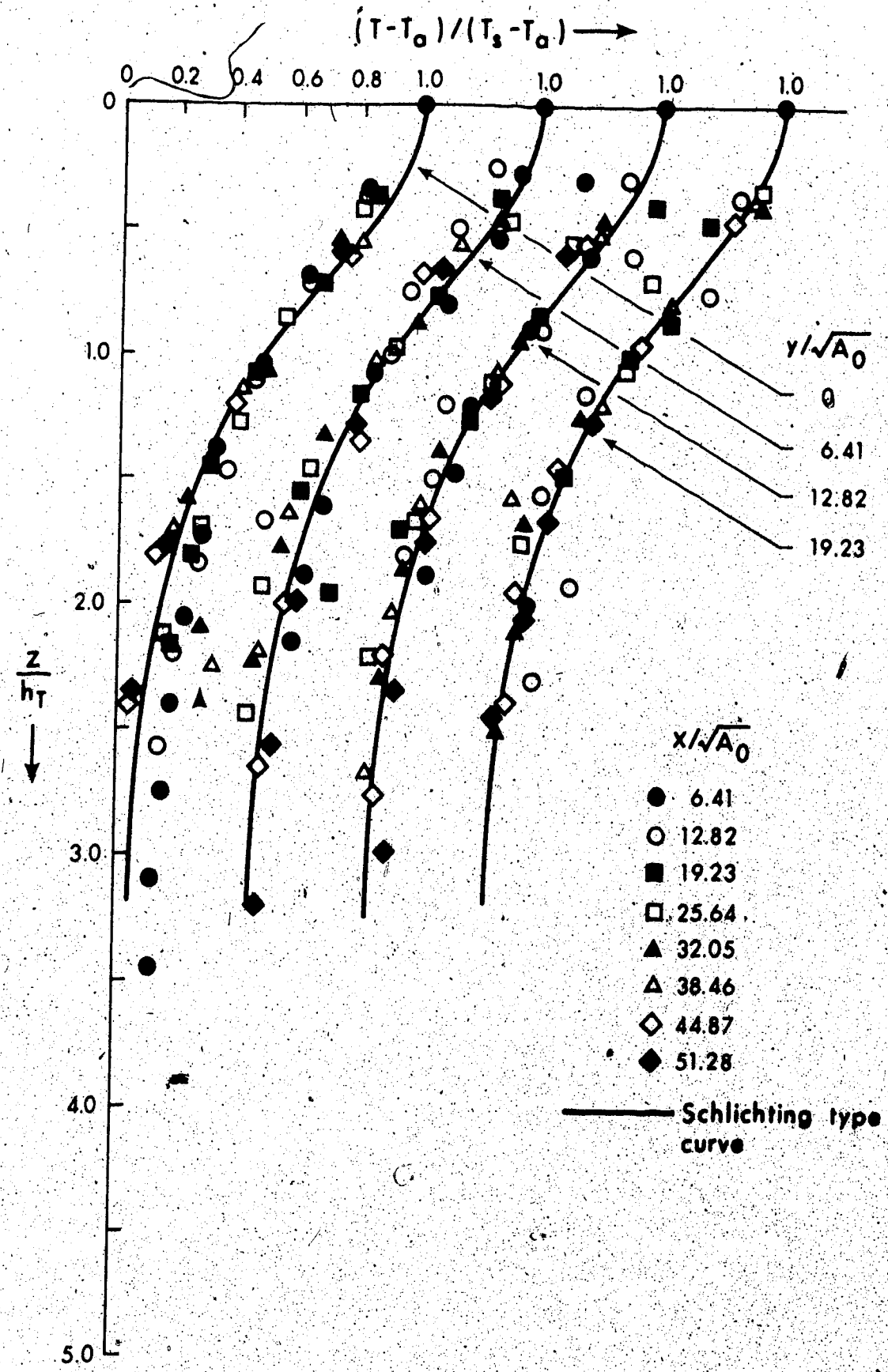

FIGURE C-4(a) SIMILARITY OF EXCESS TEMPERATURE DISTRIBUTION ACROSS VERTICAL SECTIONS FOR Ri = 0.15

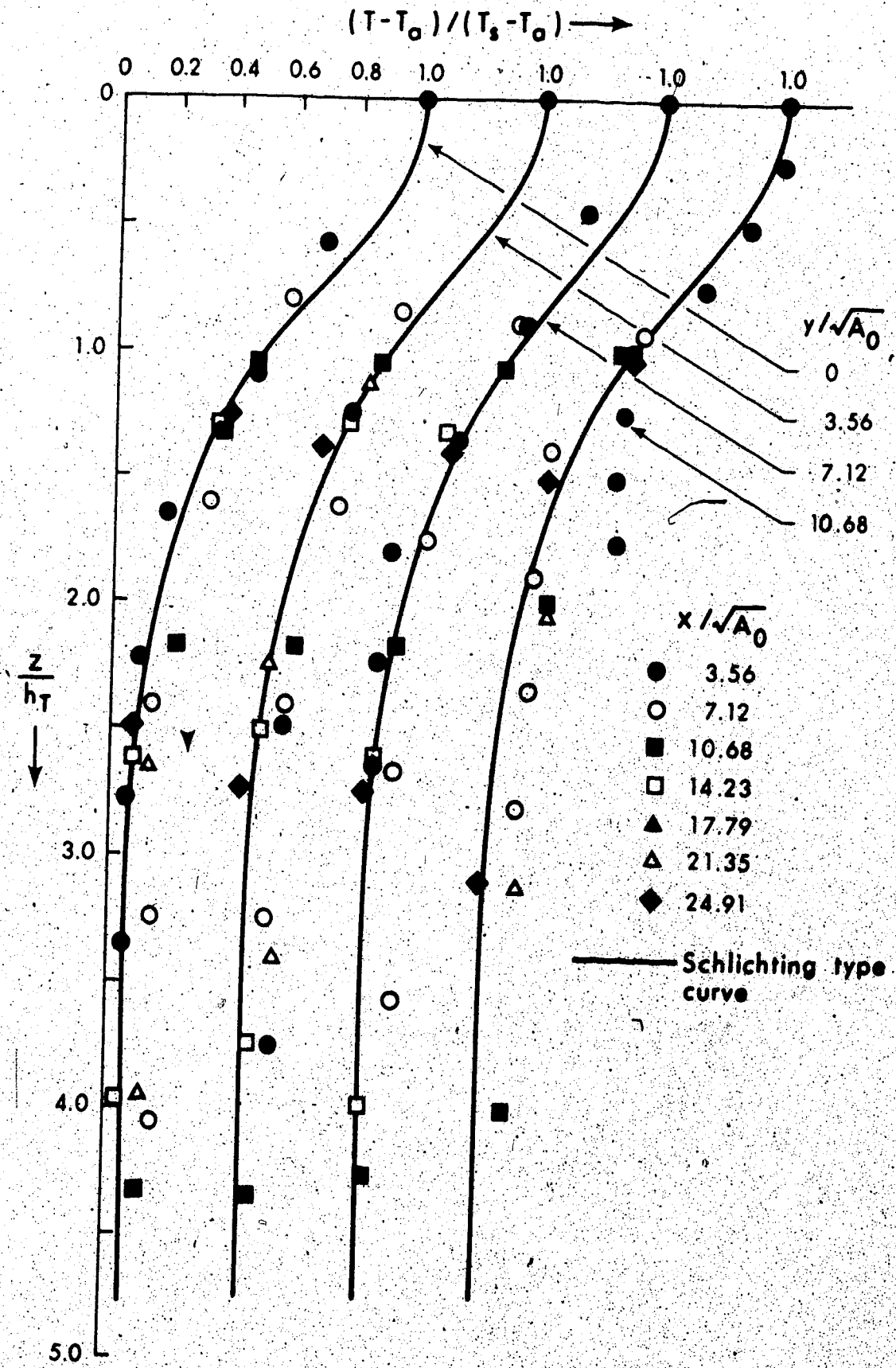

FIGURE C-4(b) SIMILARITY OF EXCESS TEMPERATURE DISTRIBUTION ACROSS VERTICAL SECTIONS FOR R1 = 0.56

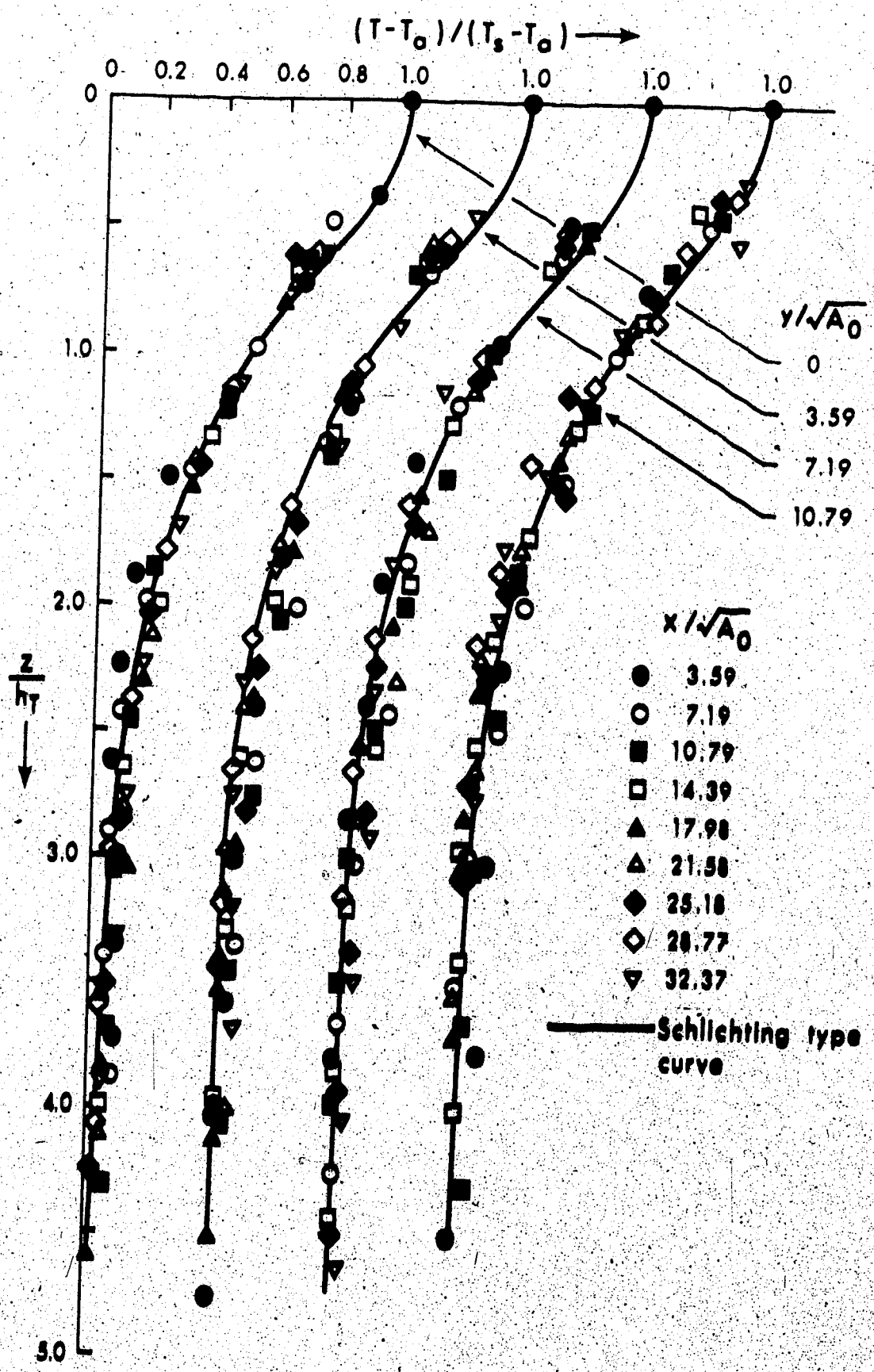

FIGURE C-4(c) SIMILARITY OF EXCESS TEMPERATURE DISTRIBUTION ACROSS VERTICAL SECTIONS FOR R1 = 1.14

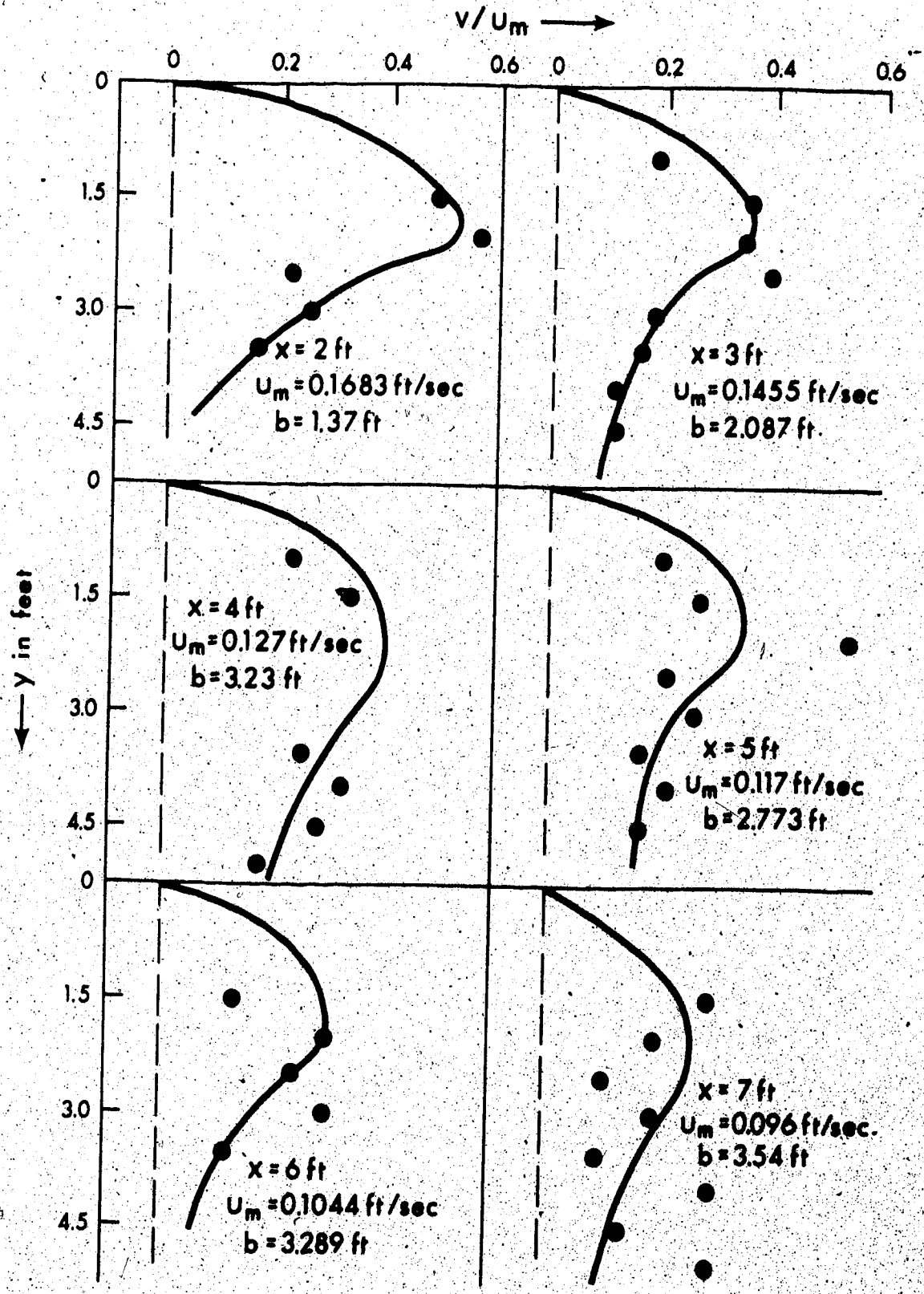

FIGURE C-5(a) LATERAL VELOCITY PROFILES FOR Ri = 0.79

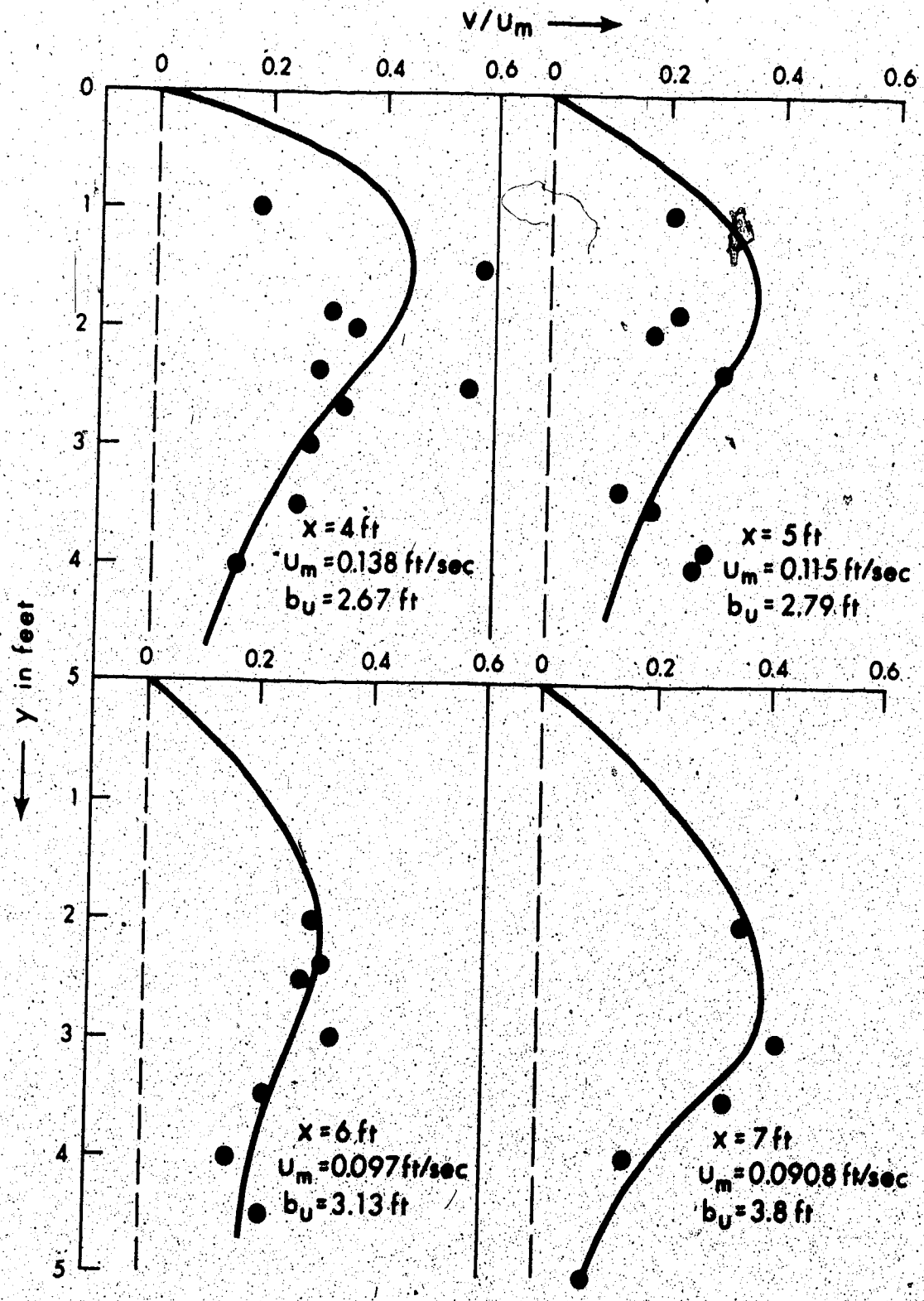

FIGURE C-5(b) . LATERAL VELOCITY PROFILES FOR Ri = 1.4

TABLE C-1 MEASURED LONGITUDINAL VELOCITY DISTRIBUTIONS IN HORIZONTAL PLANE

RUN NUMBER 1 h_o = 0.1515 ft. b_o = 0.161 ft. U_o^* = 0.3.3 ft/sec. Ri = 0.152 R = 7588

Distance from Center-line y in ft.	Longitudinal Velocity u_s in ft/sec at Surface (at x distance from outlet)								
	x = 1.0'	x = 2.0'	x = 3.0'	x = 4.0'	x = 5.0'	x = 6.0'	x = 7.0'	x = 8.0'	x = 9.0'
0	0.309	0.2074	0.153	0.1194	0.113	0.08786	0.0779	0.0802	0.0592
0.5	0.182	0.1109	0.139	0.0838	0.0885	0.0641	0.0739	0.0715	0.0596
1.0	0.062	0.0878	0.118	0.0818	0.0900	0.0657	0.0801	0.0715	0.0575
1.5	0.039	0.069	0.0739	0.0662	0.0862	0.0863	0.0739	0.0628	0.0468
2.0	0.0263	0.0332	0.0596	0.0612	0.074	0.0698	0.0676	0.0622	0.0394
2.5		0.0228	0.0501	0.0485	0.0739	0.0583	0.0826	0.0579	0.053
3.0		0.0268	0.039	0.033	0.0623	0.0669	0.0727	0.0476	0.0435
3.5		0.0237	0.0278	0.0292	0.0404	0.062	0.0702	0.0453	0.0373
4.0		0.0237	0.0215	0.0231	0.0365	0.0452	0.0468	0.0277	0.0365
4.5			0.0215	0.0194	0.0292	0.0391	0.0243	0.0186	
5.0			0.0198	0.0252	0.0190	–	0.021	0.0151	
5.25					–	0.020			
5.5					0.0164	–			

TABLE C-2 MEASURED LONGITUDINAL VELOCITY DISTRIBUTIONS

RUN NUMBER 3 h_o = 0.158 ft. b_o = 0.5 ft. U_o = 0.172 ft/sec. Ri = 0.56 R = 7727

Distance from Center-line y in ft.	Longitudinal [redacted] u in ft/sec at Surface (x = distance from outlet)								
	x = 1.0'	x = 2.0			x = 5.0'	x = 6.0'	x = 7.0'	x = 8.0'	x = 9.0'
0	0.174	0.168	0.165	0.130	0.124	0.103	0.10	0.915	0.0808
0.5	0.168	0.168	–	0.120	–	–	–	–	–
1.0	0.1166	0.109	0.123	0.109	0.108	0.099	0.0883	0.069	0.0704
1.5	–	–	–	–	–	–	–	–	–
1.8	0.0452	–	–	–	–	–	–	–	–
1.95	0.0283	–	–	–	–	–	–	–	–
2.0	–	0.0615	0.083	0.101	0.0891	0.099	0.0628	0.087	0.0459
2.5	–	0.0697	0.066	–	–	–	–	–	–
2.8	–	0.0354	–	–	–	–	–	–	–
3.0	–	0.0238	0.0448	0.0661	0.065	0.0702	0.071	0.0702	0.0505
3.5	–	–	–	–	–	–	–	–	–
4.0	–	–	0.0199	0.0228	0.0501	0.0531	0.049	0.0463	0.0202
4.5	–	–	–	–	–	–	–	–	0.0182
5.0	–	–	–	0.0041	–	–	0.0154	0.0291	–

TABLE C-3 MEASURED LONGITUDINAL VELOCITY DISTRIBUTIONS

RUN NUMBER 4 h_o = 0.155 ft. b_o = 0.5 ft. U_o = 0.156 ft/sec. Ri = 0.79 R = 7049

Distance from Centerline y in ft.	Longitudinal Velocity u in ft/sec at Surface (at x distance from outlet)								
	x = 1.0'	x = 2.0'	x = 3.0'	x = 4.0'	x = 5 ft	x = 6 ft	x = 7 ft	x = 8 ft	x = 9 ft
0	0.175	0.1683	0.1455	0.127	0.117	0.1044	0.096	0.0876	0.0845
0.5	0.189	0.1375	0.140	0.116	0.116	0.0739	0.0972	0.0833	0.0840
1.0	0.091	0.1136	0.123	0.115	0.112	0.0858	0.094	0.0856	0.0692
1.5	0.069	0.0742	0.114	0.105	0.078	0.0750	0.0739	0.0748	0.0627
2.0	0.0485	0.0391	0.0769	0.102	0.087	0.0828	0.07	0.0740	0.0635
2.5	0.04375	0.044	0.0536	0.097	0.078	0.065	0.0531	0.067	0.063
3.0	0.0284	0.0334	0.0225	0.074	0.0425	0.06445	0.0495	0.0663	0.0552
3.5	–	0.0456	0.03	0.0513	0.0239	0.04338	0.05	0.0582	0.0504
4.0	–	0	0.013	0.039	0.0205	0.0342	0.026	0.0564	0.0411
4.5	–	–	0.0567	0.033	0.0150	0.026	0.0182	0.053	0.0313
5.0	–	–	–	0.015	–	0.0152	0.0205	–	–
5.25	–	–	–	–	–	–	–	0.0205	0.015

TABLE C-4 MEASURED LONGITUDINAL VELOCITY DISTRIBUTIONS

RUN NUMBER 5 h_o = 0.155 ft. b_o = 0.5 ft. U_o = 0.156 ft/sec. Ri = 1.14 R = 7784

Distance from Center-line y in ft.	Longitudinal Velocity u in ft/sec at Surface (at x distance from outlet)								
	x = 1.0'	x = 2.0'	x = 3.0'	x = 4.0'	x = 5.0'	x = 6.0'	x = 7.0'	x = 8.0'	x = 9.0'
0	0.203	0.186	0.161	0.13865	0.1147	0.097	0.0908	0.0819	0.0777
0.5	-	0.131	0.148	0.113	0.1027	0.1088	0.0821	0.08847	0.0760
1.0	0.0951	0.150	0.1318	0.1067	0.1002	0.0898	0.0912	0.07419	0.0707
1.5	-	-	0.1118	0.130	0.0753	0.0822	0.0789	0.06579	0.0751
2.0	0.0547	0.0507	0.0624	0.097	0.0947	0.0929	0.0673	0.0668	0.0651
2.5	0.043	0.0273	-	0.0918	0.0799	0.0787	-	0.0594	0.0637
3.0	-	0.0317	0.05	0.056	0.04109	0.0645	0.0648	0.0304	0.0340
3.5	-	0.0175	0.034	0.03895	0.0265	0.0397	0.055	0.04529	0.0445
4.0	-	0.025	0.02925	0.035	0.02465	0.0231	0.0509	0.0343	0.0212
4.5	-	-	-	0.0355	0.0237	0.0194	0.021	0.033	0.0198
5.0	-	-	-	-	0.0148	0.0164	0.0159	0.0279	0.0179

TABLE C-5 MEASURED LONGITUDINAL VELOCITY DISTRIBUTION IN VERTICAL PLANES

RUN NUMBER 1 h_o = 0.1515 ft. b_o = 0.161 ft. U_o = 0.323 ft/sec. Ri = 0.152 R = 7588

Distance from Outlet x in ft.	Distance from Central Plane y in ft.	Longitudinal Velocity u in ft/sec in Vertical Planes (at z distance below the surface)					
		z = 0.0 ft	z = 0.025 ft	z = 0.05 ft	z = 0.075 ft	z = 0.10 ft	Half Velocity Depth h_u in Feet.
1.0	0	0.309	0.0156	0.142	0.0862	0.0557	0.027
	1	0.062	0.0619	0.0436	0.0388	–	0.08
	2	0.0263	0.0241	0.0214	0.0129	–	0.075
	3	–	–	–	–	–	–
2.0	0	0.2074	0.137	0.104	0.0399	0.0247	0.05
	1	0.0878	0.0687	0.0382	0.0301	0.014	0.0453
	2	0.0332	0.0301	0.0227	0.0096	0	0.0616
	3	0.0268	0.0271	0.0220	0.0165	0.0163	–
3.0	0	0.153	0.1085	0.0752	0.0523	0.0239	0.05
	1	0.118	0.0841	0.066	0.0454	0.0112	0.0584
	2	0.0596	0.0422	0.039	0.0153	0.0111	0.0596
	3	0.039	0.03616	0.0237	0.0186	0.0165	0.0706
4.0	0	0.1194	0.0823	0.053	0.0345	0.0224	0.0443
	1	0.0818	0.0699	0.05402	0.0460	0.0195	0.0798
	2	0.0612	0.0614	0.037	0.0267	0.0204	0.0655
	3	0.033	0.042	0.031	0.020	0.0061	0.0812

...../Cont.

TABLE C-5 MEASURED LONGITUDINAL VELOCITY DISTRIBUTION IN VERTICAL PLANES

RUN NUMBER 1 h_o = 0.1515 ft. b_o = 0.161 ft. U_o = 0.323 ft/sec. Ri = 0.152 R = 7588

Distance from Outlet x in ft.	Distance from Central Plane y in ft.	Longitudinal Velocity u in ft/sec in Vertical Planes (at z distance below the surface)					
		z = 0.0 ft	z = 0.025 ft	z = 0.05 ft	z = 0.075 ft	z = 0.10 ft	Half Velocity Depth h_u in Feet
5.0	0	0.113	0.051	0.0294	0.0236	-	0.0227
	1	0.0909	0.0662	0.0346	0.0224	0.0183	0.0414
	2	0.074	0.0591	0.0347	0.0204	0.0167	0.0475
	3	0.0623	0.05	0.022	0.0181	-	0.0418
6.0	0	0.08786	0.0577	0.0303	0.0111	0.006	0.0376
	1	0.0657	0.0578	0.0514	0.029	0.0122	0.0706
	2	0.0698	0.0554	0.0441	0.016	0.0126	0.0599
	3	0.0669	0.0578	0.0377	0.0147	0.0162	0.0546
7.0	0	0.0779	0.056	0.0185	0.0149	-	0.0363
	1	0.0801	0.0759	0.040	0.016	0	0.05
	2	0.0676	0.0572	0.0424	0.036	0.0214	0.0785
	3	0.0727	0.0499	0.033	0.023	0.0178	0.0450
8.0	0	0.0802	-	0.0412	0.0139	0.0098	0.0509
	1	0.0715	0.0602	0.0241	0.0183	0.0122	0.0419
	2	0.0622	0.0462	0.03	0.0119	0	0.0483
	3	0.0476	0.0388	0.0249	0.0114	0.0066	0.052

...../Cont.

TABLE C-5 MEASURED LONGITUDINAL VELOCITY DISTRIBUTION IN VERTICAL PLANES

RUN NUMBER 1 h_o = 0.1515 ft. b_o = 0.161 ft. U_o = 0.323 ft/sec. Ri = 0.152 R = 7588

Distance from Outlet x in ft.	Distance from Central Plane y in ft.	Longitudinal Velocity u in ft/sec in Vertical Planes (at z distance below the surface)					
		z = 0.0 ft	z = 0.025 ft	z = 0.05 ft	z = 0.075 ft	z = 0.10 ft	Half Velocity Depth h_u in Feet
9.0	0	0.0592	0.0361	0.0237	0.00824	0	0.038
	1.0	0.0575	0.047	0.0251	0.0689	0.0055	0.0458
	2.0	0.0394	0.0378	0.0272	0.0187	0	0.072

TABLE C-6 MEASURED LONGITUDINAL VELOCITY DISTRIBUTION IN VERTICAL PLANES

RUN NUMBER 3 h_o = 0.158 ft. b_o = 0.161 ft. U_o = 0.323 ft/sec. Ri = 0.56 R = 7727

Distance from Outlet x in ft.	Distance from Central Plane y in ft.	Longitudinal Velocity u in ft/sec in Vertical Planes (at z distance below the surface)					
		z = 0.0 ft	z = 0.025 ft	z = 0.05 ft	z = 0.075 ft	z = 0.1 ft	Half Velocity Depth h_u in Feet
1.0	0	0.174	0.150	0.121	0.0793	0.0205	0.0703
2.0	0	0.168	0.1299	0.0695	0.0507	0.0216	0.0448
3.0	0	0.165	0.0925	0.0335	0.0178	0.0155	0.0292
	1	0.123	0.0766	0.0458	0.0332	0.0284	0.0373
	2	0.083	0.0438	0.0286	0.0279	0.0314	0.0286
	3	0.0448	0.0373	0.0270	0.0194	0.0192	0.0354
4.0	0	0.130	0.0764	0.0419	0.0332	0.0344	0.0332
	1	0.109	0.0675	0.0498	0.0229	0.0331	0.0433
	2	0.101	0.058	0.0278	0.0216	0.01455	0.0312
	3	0.0661	0.0454	0.0207	0.0157	-	0.0375
5.0	0	0.124	0.0933	0.0202	-	0.0132	0.0357
	1	0.108	0.056	0.0498	0.075	0.0116	0.033
	2	0.0891	0.0786	0.0488	0.0182	-	0.0535
	3	0.065	0.029	0.01	-	-	0.0225
6.0	0	0.103	0.066	0.0398	0.0199	0.0107	0.0387
7.0	0	0.10	0.0833	0.0381	0.0205	-	0.0434
8.0	0	0.0915	0.0611	0.0246	0.0188	0	0.0355
9.0	0	0.0808	0.0621	0.0433	0.0345	0.0156	0.0576

TABLE C-7 MEASURED LONGITUDINAL VELOCITY DISTRIBUTION IN VERTICAL PLANES

RUN NUMBER 4 h_o = 0.0155 ft. b_o = 0.5 ft. U_o = 0.156 ft/sec. Ri = 0.79 R = 7049

Distance from Outlet x in ft.	Distance from Central Plane y in ft.	Longitudinal Velocity u in ft/sec in Vertical Planes (at z distance below the surface)					
		z = 0.0 ft	z = 0.025 ft	z = 0.05 ft	z = 0.075 ft	z = 0.1 ft	Half Velocity Depth h_u in Feet
1	0	0.175	0.131	0.115	0.066	0.0291	0.064
	1	0.091	0.081	0.064	0.046	0.043	0.075
	2	0.0485	-	0.0469	-	0.0205	0.0928
2	0	0.1683	0.0468	0.0447	0.0286	0.036	0.0173
	1	0.1136	0.094	0.0402	0.03	0.0259	0.0422
	2	0.0391	0.0425	0.037	0.03	0.004	0.085
	3	0.0334	0.026	0.0218	0.014	-	0.066
3	0	0.1455	0.0792	0.0434	0.0288	0.0193	0.0294
	1	0.123	0.0625	0.018	0.0174	0.0166	0.02507
	2	0.0769	0.0664	0.0244	0.0197	-	0.0416
	3	0.0225	0.0187	0.0125	0	-	0.0524
4	0	0.127	0.045	0.036	0.0177	0.0138	0.0193
	1	0.115	0.059	0.0322	0.027	0.025	0.0265
	2	0.102	0.033	0.0264	0.021	0	0.0184
	3	0.074	0.057	0.025	0.022	-	0.0406
5	0	0.117	0.0602	0.037	0.0255	0.0186	0.0268
	1	0.112	0.0723	0.030	0.0157	0.0089	0.0346
	2	0.087	0.053	0.0249	0.018	0.0182	0.033
	3	0.0425	0.037	0.0157	0.0155	0.0159	0.0434

...../Cont.

TABLE C-7 MEASURED LONGITUDINAL VELOCITY DISTRIBUTION IN VERTICAL PLANES

RUN NUMBER 4 h_o = 0.0155 ft. b_o = 0.5 ft. U_o = 0.156 ft/sec. Ri = 0.79 R = 7049

Distance from Outlet x in ft.	Distance from Central Plane y in ft.	Longitudinal Velocity u in ft/sec in Vertical Planes (at z distance below the surface)					
		z = 0.0 ft	z = 0.025 ft	z = 0.05 ft	z = 0.075 ft	z = 0.1 ft	Half Velocity Depth h_u in Feet
6	0	0.1044	0.0529	0.0318	0.0184	0.0159	0.0258
	1	0.0858	0.0618	0.0334	0.02	0.0178	0.0416
	2	0.0828	0.055	0.033	0.022	0.0093	0.0404
	3	0.0645	0.04687	0.0262	0.0244	0.0155	0.0427
7	0	0.096	0.0669	0.033	0.0229	0.0181	0.0389
	1	0.094	0.058	0.038	0.0257	0.0127	0.0387
	2	0.07	0.058	0.0327	0.0219	0.022	0.0477
	3	0.0495	0.0499	0.0275	0.0199	-	0.0589
8	0	0.0876	0.0837	0.0262	0.0248	0.0170	0.0423
	1	0.0856	0.0535	0.0399	0.0222	0.021	0.0446
	2	0.0740	0.0656	0.0327	0.0177	0.0159	0.0467
	3	0.0663	0.0428	0.0229	0.0161	0.0112	0.0371
9	0	0.0845	0.0495	0.0236	0.0225	0.0191	0.032
	1	0.0692	0.075	0.0524	0.0277	0.0274	0.0679
	2	0.0635	0.0634	0.0437	0.0223	0.0178	0.0639
	3	0.0552	0.0515	0.0314	0.0202	0.0153	0.0585

TABLE C-8 MEASURED LONGITUDINAL VELOCITY DISTRIBUTION IN VERTICAL PLANES

RUN NUMBER 5 h_o = 0.155 ft. b_o = 0.5 ft. U_o = 0.156 ft/sec. Ri = 1.14 R = 7784

Distance from Outlet x in ft.	Distance from Central Plane y in ft.	Longitudinal Velocity u in ft/sec in Vertical Planes (at z distance below the surface)					
		z = 0.0 ft	z = 0.025 ft	z = 0.05 ft	z = 0.075 ft	z = 0.1 ft	Half Velocity Depth h_u in Feet
2	0	0.186	0.0475	0.0385	0.0287	0	0.0168
	1	0.150	0.069	0.029	0.031	0.0156	0.0231
	2	0.0507	0.033	0.0314	0.0209	–	0.0566
	3	0.0317	0.0232	0.0153	0.0116	–	0.0482
3	0	0.161	0.0699	0.0318	0.0259	0.0179	0.0221
	1	0.132	0.058	0.021	0.016	0.017	0.0223
	2	0.0624	0.0325	0.0296	0.013	0.0054	0.0362
	3	0.05	0.0362	0.026	0.0178	–	0.053
	4	0.02925	0.0241	0.0291	0.0107	–	0.0603
4	0	0.138	0.0669	0.0382	0.0174	0.0175	0.0241
	1	0.1067	0.0692	0.02547	0.0182	0.0	0.03403
	2	0.097	0.0279	0.0393	0.0257	Small	0.021
	3	0.056	0.0391	0.0305	0.0293	0.0	0.0761
5	0	0.1147	0.0614	0.0265	0.0171	0.017	0.0278
	1	0.1002	0.0669	0.0333	0.0267	0.0182	0.0374
	2	0.0947	0.0428	0.0218	0.0214	0.0106	0.0228
	3	0.0411	0.035	0.025	0.0075	–	0.0563

...../Cont.

TABLE C-8 MEASURED LONGITUDINAL VELOCITY DISTRIBUTION IN VERTICAL PLANES

RUN NUMBER 5 h_o = 0.155 ft. b_o = 0.5 ft. U_o = 0.156 ft/sec. Ri = 1.14 R = 7784

Distance from Outlet x in ft.	Distance from Central Plane y in ft.	Longitudinal Velocity u in ft/sec in Vertical Planes (at z distance below the surface					
		z = 0.0 ft	z = 0.025 ft	z = 0.05 ft	z = 0.075 ft	z = 0.1 ft	Half Velocity Depth h_u in Feet
6	0	0.097	0.065	0.0262	0.0147	0.0143	0.0356
	1	0.0898	0.0744	0.0334	0.0297	0.0181	0.0429
	2	0.0929	0.0834	0.024	0.0161	0.0158	0.0405
	3	0.0645	0.0562	0.0217	0.0184	–	0.0423
7	0	0.0908	0.0738	0.0244	0.018	0.0099	0.0393
	1	0.0912	0.0518	0.0203	0.0186	0.0148	0.0299
	2	0.0673	0.0414	0.0240	0.0099	–	0.036
	3	0.0648	0.0484	0.03	0.025	0.013	0.0467
8	0	0.0819	0.0664	0.044	0.0266	0.0083	0.054
	1	0.07419	0.0581	0.029	0.010	0.0092	0.043
	2	0.0668	0.0478	0.0355	0.0159	0.0129	0.0509
	3	0.0304	0.0304	0.023	0.0159	–	–
9	0	0.078	0.0388	0.036	0.019	0.0067	0.025
	1	0.071	0.036	–	0.0266	–	0.025
	2	0.0615	0.055	0.0372	0.0183	0.0125	0.0585
	3	0.0341	0.0339	0.0319	0.0093	–	0.067

TABLE C-9 MEASURED "EXCESS TEMPERATURE" DISTRIBUTION IN HORIZONTAL PLANES

RUN NUMBER 1 h_o = 0.1515 ft. b_o = 0.161 ft. Ri = 0.15 R = 7588

Distance from Centerline y in ft.	Excess Temperature Distribution ΔT_s in °F at Surface (at x distance from outlet)							
	ΔT_o = 23.94°F				ΔT_o = 25.20°F			
	x = 1.0 ft	x = 2.0 ft	x = 3.0 ft	x = 4.0 ft	x = 5.0 ft	x = 6.0 ft	x = 7.0 ft	x = 8.0 ft
0	16.77	10.10	7.52	6.01	7.15	6.10	5.96	5.59
0.5	11.21	8.46	7.25	5.26	6.84	5.79	6.16	5.94
1.0	7.54	6.68	6.51	5.21	6.22	5.79	6.07	6.01
1.5	5,94	5.40	4.97	4.11	5.48	5.52	5.34	5.22
2.0	4.77	4.70	4.61	3.99	5.66	5.39	5.65	5.59
2.5	3.53	3.42	4.10	3.36	5.30	5.30	5.51	5.25
3.0	3.36	3.17	4.17	3.81	5.13	4.88	5.24	5.58
3.5	3.24	2.45	3.37	3.07	5.04	4.57	5.29	5.13
4.0	-	2.64	3.10	3.11	4.90	4.66	4.66	4.21
4.5	-	2.63	3.15	2.91	3.08	4.35	5.13	4.91
5.0	-	-	3.24	3.03	1.66	4.62	5.07	4.93
5.5	-	-	2.57	-	2.94	3.49	-	5.16
6.0		-	2.52	2.31	3.27	3.18	5.07	4.77
6.5		-	2.63	-	3.36	1.45	5.45	4.82
7.0	-	-	-	2.48	3.19	3.24	-	4.55

TABLE C-10 MEASURED "EXCESS TEMPERATURE" DISTRIBUTION IN HORIZONTAL PLANES

RUN NUMBER 2 h_o = 0.1515 ft. b_o = 0.161 ft. ΔT_o = 37.62°F Ri = 0.35 R = 6980

Distance from Centerline y in ft.	Excess Temperature Distribution ΔT_s in °F at Surface (at x distance from Outfall)									
	x = 0.5'	x = 1.0'	x = 2.0'	x = 3.0'	x = 4.0'	x = 5.0'	x = 6.0'	x = 7.0'	x = 8.0'	x = 9.0'
0	33.06	23.78	15.43	12.33	11.83	10.49	9.68	9.04	8.48	7.40
0.5	23.40	24.16	15.25	12.32	11.59	9.94	9.00	8.64	8.12	7.09
1.0	11.54	14.54	12.85	11.93	11.47	9.43	8.66	8.30	7.58	7.77
1.5	8.41	9.38	9.74	10.80	10.01	8.12	7.76	7.68	6.95	7.18
2.0	7.81	7.32	8.46	10.08	10.23	7.52	8.24	7.68	6.95	7.29
2.5	4.14	5.96	7.13	9.27	9.66	7.33	8.13	7.76	7.02	6.75
3.0	3.85	5.98	7.05	9.01	8.66	7.10	8.01	7.27	6.78	6.78
3.5	4.21	5.33	6.20	8.40	8.55	6.73	7.29	6.76	6.10	6.57
4.0	–	4.94	6.15	7.29	8.11	6.19	7.07	6.84	6.30	6.75
4.5	–	4.64	5.76	6.54	6.61	5.91	6.21	6.57	6.16	6.51
5.0	–	3.94	4.95	6.06	3.84	5.52	5.70	6.26	6.32	6.41
5.5	–	3.82	4.41	4.74	2.45	4.64	5.31	5.87	6.20	6.28
6.0	–	2.87	4.47	3.99	4.28	4.59	5.06	5.69	5.81	5.99
6.5	–	3.41	4.30	–	–	4.88	4.93	5.43	5.71	5.67
7.0	–	3.01	4.12	–	–	5.03	4.77	5.16	5.49	5.47

TABLE C-11 MEASURED "EXCESS TEMPERATURE" DISTRIBUTION IN HORIZONTAL PLANES ON THE SURFACE

RUN NUMBER 3 h_o = 0.158 ft. b_o = 0.5 ft. ΔT_o = 25.23°F Ri = 0.56 R = 7727

x = 1.0 ft		x = 2.0 ft		x = 3.0 ft		x = 4.0 ft		x = 5.0 ft		x = 6.0 ft		x = 7.0 ft		x = 8.0 ft		x = 9.0 ft	
y	ΔT_s	y	ΔT_s	y	ΔT_s	y	ΔT_s	y	ΔT_s	y	ΔT_s	y	ΔT_s	y	ΔT_s	y	ΔT_s
0	20.44	0	18.82	0	15.32	0	14.64	0	13.34	0	12.47	0	10.62	0	9.53	0	8.92
0.25	19.86	0.25	17.41	0.24	15.30	0.25	13.34	0.[illegible]	12.06	0.25	12.01	0.50	9.99	0.75	9.51	0.50	8.91
0.49	19.37	0.49	17.21	0.50	14.35	0.49	13.05	0.76	11.71	0.49	11.22	0.75	9.42	1.25	9.29	0.74	8.52
0.75	17.27	0.75	16.62	0.75	13.94	0.75	13.29	1.00	12.37	0.76	11.55	1.25	9.18	1.75	9.04	1.25	8.82
1.00	14.57	1.00	15.78	1.01	13.28	1.00	12.51	1.26	11.72	1.00	10.97	1.74	9.22	2.25	8.93	1.74	8.66
1.26	11.80	1.26	14.48	1.50	12.18	1.26	12.13	2.01	10.48	1.26	10.32	2.25	8.79	2.75	8.43	2.25	8.32
1.50	9.85	1.51	12.43	1.76	11.77	1.76	11.68	2.52	10.01	2.01	9.69	2.75	8.43	3.26	7.75	2.76	7.74
1.75	8.68	1.75	11.96	2.01	9.98	2.01	10.62	3.02	9.09	2.52	9.82	3.26	8.13	3.77	7.60	3.26	7.60
2.01	7.42	2.01	11.42	2.27	9.60	2.26	10.05	3.53	8.66	3.02	9.65	3.77	7.85	4.27	7.15	3.79	7.94
2.26	6.38	2.26	9.01	2.51	9.46	2.52	9.56	4.03	7.92	3.53	7.67	4.27	7.31	4.78	7.04	4.28	7.36
2.52	6.04	2.52	8.67	2.77	9.30	2.76	9.31	4.54	7.44	4.03	8.32	4.78	6.65	5.28	6.59	4.78	6.81
2.76	5.84	2.76	8.14	3.02	8.57	3.02	8.97	5.07	6.59	4.54	8.09	5.28	6.30	5.79	6.09	5.28	6.39
		3.02	7.64	3.28	8.02	3.27	8.39	5.54	5.93	5.07	6.90	5.79	5.57	6.30	5.66	5.79	6.56
				3.78	7.12	3.53	8.12	6.05	4.94	5.54	6.03	6.30	5.23	6.80	5.30	6.30	6.22
				4.03	6.76	4.03	6.95	6.55	4.58	6.05	5.64	6.70	5.13	7.05	5.12	6.80	5.84
				4.50	6.52	4.28	6.81	7.00	4.40	6.55	4.92	7.05	4.42	7.21	4.90	7.05	5.83
				5.30	6.22	4.75	5.06	7.21	4.20	7.06	4.20	7.21	4.79			7.21	5.74
						5.07	1.75			7.22	4.20						

TABLE C-12 MEASURED "EXCESS TEMPERATURE" DISTRIBUTION IN HORIZONTAL PLANES

RUN NUMBER 5 h_o = 0.155 ft. b_o = 0.5 ft. ΔT_o = 39.60°F Ri = 1.14 R = 7784

Distance from Centerline y in ft.	Excess Temperature Distribution ΔT_s in °F at Surface (at x distance from outfall)								
	x = 1.0'	x = 2.0'	x = 3.0'	x = 4.0'	x = 5.0'	x = 6.0'	x = [illegible]	[illegible]	x = 9.0'
0	32.35	25.76	22.61	[illegible]	15.				
0.5	27.00	27.07	23.02		16.40	13.52	13.32		
1.0	22.50	22.62	20.00		15.28	14.02	13.98	12.	
1.5	14.99	18.07	17.31	16.13	16.25	13.97	13.10	12.09	
2.0	11.03	14.85	15.69	14.83	14.04	13.55	12.89	11.95	11.95
2.5	7.27	11.97	13.35	12.76	13.37	13.39	12.17	11.70	11.86
3.0	6.91	10.29	11.95	12.35	12.27	11.88	12.01	11.70	11.37
3.5	5.76	7.81	10.28	11.55	11.36	11.79	11.21	10.75	10.82
4.0	6.44	8.91	8.91	9.13	9.76	10.78	10.19	10.42	10.53
4.5	6.64	8.06	8.84	7.36	8.86	9.48	9.54	9.38	10.08
5.0	–	7.52	8.10	5.85	7.22	8.78	9.18	8.71	9.05
5.5	–	7.38	8.08	8.46	6.84	8.42	8.46	8.61	8.48
6.0	5.44	7.29	7.99	8.06	6.95	7.38	7.56	7.92	7.81
6.5	–	6.78	7.16	8.01	7.00	6.71	6.84	6.75	7.16
7.0	4.79	6.51	7.02	7.95	–	6.30	6.66	6.71	6.55
7.25	–	6.44	7.34	7.56	6.84	–	6.66	6.78	6.66

TABLE C-13 MEASURED "EXCESS TEMPERATURE" DISTRIBUTION IN VERTICAL PLANES

RUN NUMBER 1 h_o = 0.1515 ft. b_o = 0.161 ft. ΔT_o = 23.94°F Ri = 0.15 R = 7588

Distance from Outlet x in ft.	Distance from Central Plane y in ft.	Excess Temperature in °F in Vertical Planes (at z distance below the surface)										Half Temperature Depth h_T in ft.
		z = 0.0 ft	z = 0.025 ft	z = 0.05 ft	z = 0.075 ft	z = 0.10 ft	z = 0.125 ft	z = 0.15 ft	z = 0.175 ft	z = 0.20 ft	z = 0.225 ft	
1.0	0	16.77	13.81	10.51	8.18	5.53	4.66	3.56	3.02	2.60	2.12	0.0726
	1.0	7.54	6.95	6.48	5.14	3.30	1.93	1.94	1.67	1.37		0.0935
	2.0	6.03	4.40	4.43	3.43	2.20	1.94	1.33				0.0834
	3.0	3.36	3.57	3.60	2.57	2.40	1.39	1.40				0.117
2.0	0	10.10	8.18	6.45	4.49	3.64	2.72	1.87	1.49			0.0678
	1.0	6.68	5.62	4.73	3.63	3.39	0.59	-				0.10
	2.0	4.70	4.11	4.26	2.91	1.34	1.10	0.68				0.0834
	3.0	3.17	2.69	2.34	1.04	0.62	0.92	0.60				0.0645
3.0	0	7.52	6.34	5.09	3.33	2.24	1.87	1.27				0.069
	1.0	6.51	5.60	4.23	2.55	1.30	0.20					0.0645
	2.0	4.61	4.51	2.66	1.66	0.53	-					0.059
	3.0	4.17	3.05	2.11	1.16	0.65	0.23					0.0506
4.0	0	6.01	4.87	3.35	2.37	1.68	0.85					0.0590
	1	5.21	4.77	2.71	1.12	0.34	0.10					0.0516
	2	3.99	2.81	1.78	0.72	0.07	-					0.0447
	3	3.81	3.47	2.09	1.87	0.27	0.51					0.071

...../Cont.

TABLE C-13 MEASURED "EXCESS TEMPERATURE" DISTRIBUTION IN VERTICAL PLANES

RUN NUMBER 1 h_o = 0.1515 ft. b_o 0.161 ft. ΔT_o = 25.20°F Ri = 0.15 R = 7588

Distance from Outlet x in ft.	Distance from Central Plane y in ft.	Excess Temperature in °F in Vertical Planes (at z distance below the surface)							Half Temperature Depth h_T in ft.
		z = 0.0 ft	z = 0.025 ft	z = 0.05 ft	z = 0.075 ft	z = 0.1 ft	z = 0.125 ft	z = 0.150 ft	
5.0	0	7.15	5.09	3.43	1.57	0.20			0.0477
	1	6.22	5.58	3.56	1.75	0.81	0.28		0.056
	2	5.66	4.53	3.09	1.52	0.77	0.38		0.054
	3	5.13	4.77	3.[illegible]	1.62	0.72	0.66		0.059
6.0	0	6.10	4.91	2.49	1.08	0.20			0.0442
	1	5.79	4.21	2.63	0.90	0.40			0.0458
	2	5.39	4.23	2.46	1.01	0.59	0.16		0.0466
	3	4.88	4.66	2.98	1.95	0.52			0.063
7.0	0	5.96	4.53	2.20	0.62	0.16			0.042
	1	6.02	3.60	2.44	0.87	0.43			0.0377
	2	5.57	4.15	2.46	1.21	0.54	0.32		0.0451
	3	5.12	4.17	2.71	1.36	0.80	0.58		0.0527
8.0	0	5.60	4.09	2.24	0.92	0.14	-		0.0425
	1	5.97	3.87	2.28	1.19	0.72	0.45		0.039
	2	5.51	3.70	2.37	1.25	0.74	0.65		0.0427
	3	5.46	3.60	3.39	1.91	1.32	0.92	0.29	0.0611

TABLE C-14 MEASURED "EXCESS TEMPERATURE" DISTRIBUTION IN VERTICAL PLANES

RUN NUMBER 2 h_o = 0.1515 ft. b_o = 0.161 ft, ΔT_o = 37.62°F Ri = 0.35 R = 6980

Distance from Outlet x in ft.	Distance from Central Plane y in ft.	Excess Temperature in °F in Vertical Planes (at z distance below the surface)								Temperature Half Depth h_T in ft.
		z = 0.0 ft	z = 0.025 ft	z = 0.05 ft	z = 0.075 ft	z = 0.1 ft	z = 0.125 ft	z = 0.150 ft	z = 0.175 ft	
0.5	0	33.06	28.15	22.91	17.64	10.48	3.62	1.31		0.0788
1.0	0	23.78	20.57	15.05	10.93	6.37	3.10	0.86		0.0691
	1	14.54	10.47	6.02	2.65	1.36	0.18	-		0.043
	2	7.32	6.81	5.67	3.81	2.30	0.93	0.04		0.0774
	3	5.98	4.60	2.09	1.35	0.72	0.33			0.041
2.0	0	15.43	14.17	10.29	6.71	4.03	1.57	0.67		0.068
	1	12.85	9.87	6.38	1.88	0.57	0.17	0.03		0.0496
	2	8.46	7.73	5.26	2.08	1.22	0.50	0.10	0.02	0.058
	3	7.05	7.11	5.77	4.23	2.09	0.99	0.22	0.01	0.083
3.0	0	12.33	10.62	7.59	4.35	2.25	0.81	-	-	0.0608
	1	11.93	8.30	2.83	1.54	0.42	0.20			0.036
	2	10.08	7.38	4.26	1.46	0.46	0.09			0.0437
	3	9.01	8.78	6.79	3.88	1.03	0.51	0.24		0.0696
4.0	0	11.83	10.46	6.98	4.63	1.93	0.63			0.061
	1	11.47	6.81	2.81	1.18	0.96	0.64	0.29		0.033
	2	10.23	6.82	2.90	1.13	0.047	0.06	0.23		0.036
	3	8.66	6.76	1.76	0.63	0.29	0.06			0.046

...../Cont.

TABLE C-14 MEASURED "EXCESS TEMPERATURE" DISTRIBUTION IN VERTICAL PLANES

RUN NUMBER 2 h_o = 0.1515 ft. b_o = 0.161 ft. ΔT_o = 37.62°F Ri = 0.35 R = 6980

Distance from Outlet x in ft.	Distance from Central Plane y in ft.	Excess Temperature in °F in Vertical Planes (at z distance below the surface)										Temperature Half Depth h_T in ft.
		z = 0.0 ft	z = 0.025 ft	z = 0.05 ft	z = 0.075 ft	z = 0.1 ft	z = 0.125 ft	z = 0.15 ft	z = 0.175 ft	z = 0.20 ft	z = 0.225 ft	
5	0	10.49	9.07	6.53	3.87	1.58	0.27					0.062
	1	9.43	5.81	3.21	1.32	0.99	0.81	0.76	0.57			0.036
	2	7.52	4.20	2.37	1.19	0.97	0.77	0.76	0.39			0.033
	3	7.10	5.06	2.79	1.60	1.47	1.20	1.34	0.84			0.042
6	0	9.68	8.33	6.33	3.42	1.47	0.25					0.0628
	1	8.66	5.67	2.34	1.58	1.24	0.99	0.81	0.72			0.035
	2	8.24	5.22	2.66	1.80	1.47	1.20	1.10	1.11	0.95		0.0357
	3	8.01	5.78	3.40	2.28	2.16	1.98	1.46	1.10	0.83		0.103
7	0	9.04	7.36	5.97	3.04	1.58	0.50					0.0623
	1	8.30	5.16	2.32	1.78	1.60	1.26	1.02	0.79	0.79		0.0338
	2	7.68	4.71	2.68	2.07	1.44	1.04	0.95	0.90	0.79		0.0357
	3	7.27	6.39	5.51	4.23	3.83	2.70	2.16				0.1043
8	0	8.48	6.78	4.79	2.88	0.90						0.0572
	1	7.58	7.67	6.08	3.85	3.15	2.70	1.87	1.33	0.90		0.077
	2	6.95	6.98	6.42	6.51	3.71	2.82	1.74	1.11	0.93		0.107
	3	6.78	6.89	6.21	5.31	4.14	2.70	1.62	1.26	0.90	0.54	0.113
9	0	7.40	7.07	4.68	2.16	0.99	0.14					0.0597
	1	7.77	7.65	6.12	5.36	3.96	3.24	2.16	1.53	0.72	0.54	0.0701
	2	7.29	7.18	6.50	4.68	3.42	2.34	1.92	1.26	1.08	0.81	0.0955
	3	6.78	7.06	6.57	5.24	4.75	2.56	1.98	1.71	1.17	0.72	0.115

TABLE C-15 MEASURED "EXCESS TEMPERATURE" DISTRIBUTION IN VERTICAL PLANES

RUN NUMBER 3 h_o = 0.158 ft. b_o = 0.5 ft. ΔT_o = 25.23°F Ri = 0.56 R = 7727

Distance from Outlet x in ft.	Distance from Central Plane y in ft.	Excess Temperature in °F in Vertical Planes (at z distance below the surface)								Temperature Half Depth h_T in ft.
		z = 0.0 ft	z = 0.025 ft	z = 0.05 ft	z = 0.075 ft	z = 0.10 ft	z = 0.125 ft	z = 0.150 ft	z = 0.2 ft	
1	0	20.22	13.58	9.37	3.15	1.65	0.93	0.79	–	0.045
	1	14.35	5.39	2.47	2.18	1.45	1.05	–	–	0.02
	1.75	0.35	6.19	4.44	3.43	2.63	2.24	2.14	2.19	0.056
	3	5.43	5.43	4.79	4.07	2.70	2.62	2.54	2.54	0.10
2	0	18.82	10.36	5.94	2.743	2.58	0.939	0.8856	0.70	0.031
	1	15.56	8.51	5.44	2.84	1.94	2.03	1.75	1.50	0.031
	2	11.20	5.96	2.75	1.57	1.41	1.09	0.83	0.68	0.028
	2.5	8.66	5.33	4.68	2.06	1.70	1.48	1.26	1.13	0.053
3	0	15.32	7.06	3.27	–	1.47	–	1.37	1.28	0.023
	1	13.28	6.30	2.68	–	1.144	–	0.81	0.72	0.023
	2	10.01	4.73	1.40	–	0.68	–	0.25	0.38	0.023
	2.5	9.46	4.70	2.10	–	0.977	–	0.505	0.575	0.025
4	0	14.64	5.215	1.063	0.373	–	0.373	–	–	0.019
	1	12.51	4.68	1.21	0.80	–	0.80	–	–	0.02
	2	10.62	3.69	0.60	0.49	–	0.49	–	–	0.019
6	0	12.47	4.31	1.58	1.38	–	1.30	–	–	0.019
	1	10.32	4.45	1.89	1.49	–	1.15	–	–	0.022
	2	9.69	4.23	1.80	1.69	–	0.93	–	–	0.022
	2.5	8.15	3.89	1.92	1.49	–	1.16	–	–	0.024

TABLE C-16 MEASURED "EXCESS TEMPERATURE" DISTRIBUTION IN VERTICAL PLANES

RUN NUMBER 5 h_o = 0.155 ft. b_o = 0.5 ft. ΔT_o = 39.60°F Ri = 1.14 R = 7784

Distance from Outlet x in ft.	Distance from Central Plane y in ft.	Excess Temperature in °F in Vertical Planes (at z distance below the surface)										Temperature Half Depth h_T in ft.
		z = 0.0 ft	z = 0.025 ft	z = 0.05 ft	z = 0.075 ft	z = 0.10 ft	z = 0.125 ft	z = 0.150 ft	z = 0.175 ft	z = 0.20 ft	z = 0.225 ft	
1	0	32.34	28.94	21.56	13.59	7.40	3.64	2.47	1.71	2.56	2.61	0.067
	1	22.50	15.17	9.52	4.91	3.06	1.60	0.97	0.23	0.02	–	0.042
	2	11.03	8.04	5.83	2.61	1.44	1.06	0.41	0.0	–	–	0.0524
	3	6.91	4.08	2.16	1.08	0.72	0.32	0.0				0.031
2	0	25.75	19.06	13.10	7.43	4.12	2.21	1.40	1.35	2.07	2.43	0.0516
	1	22.62	15.21	7.70	5.88	3.15	1.60	0.39	0.21	0.27	–	0.0373
	2	14.85	10.55	5.74	3.33	2.75	1.17	0.32	0.07	0.16	–	0.0412
	3	10.29	8.21	5.16	3.49	2.23	1.35	0.45	0.16	0	–	0.05
3	0	22.61	14.76	9.31	4.14	3.06	1.35	1.02	1.08	1.02	–	0.0408
	1	20.00	12.44	7.16	4.35	2.43	1.08	0.45	0.43	0.54	–	0.0365
	2	15.69	10.57	5.97	4.23	2.65	1.08	0.52	0.39	0.16	–	0.0398
	3	11.95	8.96	5.29	3.36	2.25	1.17	0.68	0.47	0.18	–	0.0453
4	0	18.50	11.52	6.64	3.85	1.83	1.08	0.65	0.54	0.63	–	0.0376
	1	17.84	11.47	6.87	3.36	1.53	0.81	0.30	0.32	0.27	–	0.038
	2	14.83	9.79	5.60	3.65	2.00	0.63	0.18	0.0	–	–	0.0392
	3	12.35	9.07	7.05	4.55	2.84	1.26	0.83	0.18	0.18	–	0.0587

...../Cont.

TABLE C-16 MEASURED "EXCESS TEMPERATURE" DISTRIBUTION IN VERTICAL PLANES

RUN NUMBER 5 h_o = 0.155 ft. b_o = 0.5 ft. ΔT_o = 39.60°F Ri = 1.14 R = 7784

Distance from Outlet x in ft.	Distance from Central Plane y in ft.	Excess Temperature in °F in Vertical Planes (at z distance below the surface)									Temperature Half Depth h_T in ft.
		z = 0.0 ft	z = 0.025 ft	z = 0.05 ft	z = 0.075 ft	z = 0.1 ft	z = 0.125 ft	z = 0.15 ft	z = 0.175 ft	z = 0.20 ft	
5	0	15.88	9.92	5.04	2.97	1.60	0.67	0.11	0.14	0.14	0.0326
	1	15.28	11.09	6.14	3.76	1.94	0.90	0.25	0.05	0.05	0.0424
	2	14.04	11.12	6.71	3.63	2.52	1.21	0.40	0.0	-0.09	0.0482
	3	12.28	10.35	6.35	4.00	2.32	0.99	0.38	0.0	-0.11	0.053
6	0	15.10	9.77	4.44	2.66	1.47	0.61	0.07	-0.11	-0.08	0.0354
	1	14.02	9.21	6.06	3.08	1.66	0.51	0.18	0.0	0.05	0.0424
	2	13.55	9.70	5.83	4.05	2.75	1.08	0.50	0.18	0.09	0.0439
	3	11.88	9.97	6.66	4.23	2.21	0.81	0.45	0.27	0.14	0.057
7	0	13.39	8.39	4.21	2.37	1.22	0.45	0.02	0.11	-	0.0351
	1	13.99	10.08	5.89	3.28	2.02	0.86	0.59	0.23	0.18	0.043
	2	12.99	9.31	5.71	3.33	1.87	1.53	1.08	0.36	0.27	0.0444
	3	12.01	9.99	7.43	3.94	4.05	2.34	1.08	0.54	0.45	0.065
8	0	11.90	8.19	4.91	2.61	1.39	0.72	0.43	0.18	0.09	0.042
	1	12.40	9.00	5.85	2.70	1.48	0.72	0.18	-0.07	-	0.0471
	2	11.95	9.61	6.86	3.74	2.88	2.29	1.35	1.21	1.35	0.0571
	3	11.70	10.39	8.42	7.40	4.91	2.50	1.47	0.54	-	0.088
9	0	11.70	8.10	5.26	3.08	1.84	1.13	0.97	0.61	0.54	0.0447
	1	11.57	9.45	6.86	3.20	2.05	0.90	0.63	0.47	0.83	0.0545
	2	11.95	8.46	4.99	3.65	1.57	1.51	0.81	0.47	0.47	0.0428
	3	11.37	10.46	10.32	7.85	4.57	3.19	1.49	1.35	0.70	0.085

APPENDIX - D

PLOT OF ISOTHERMS AND ITS AREAS

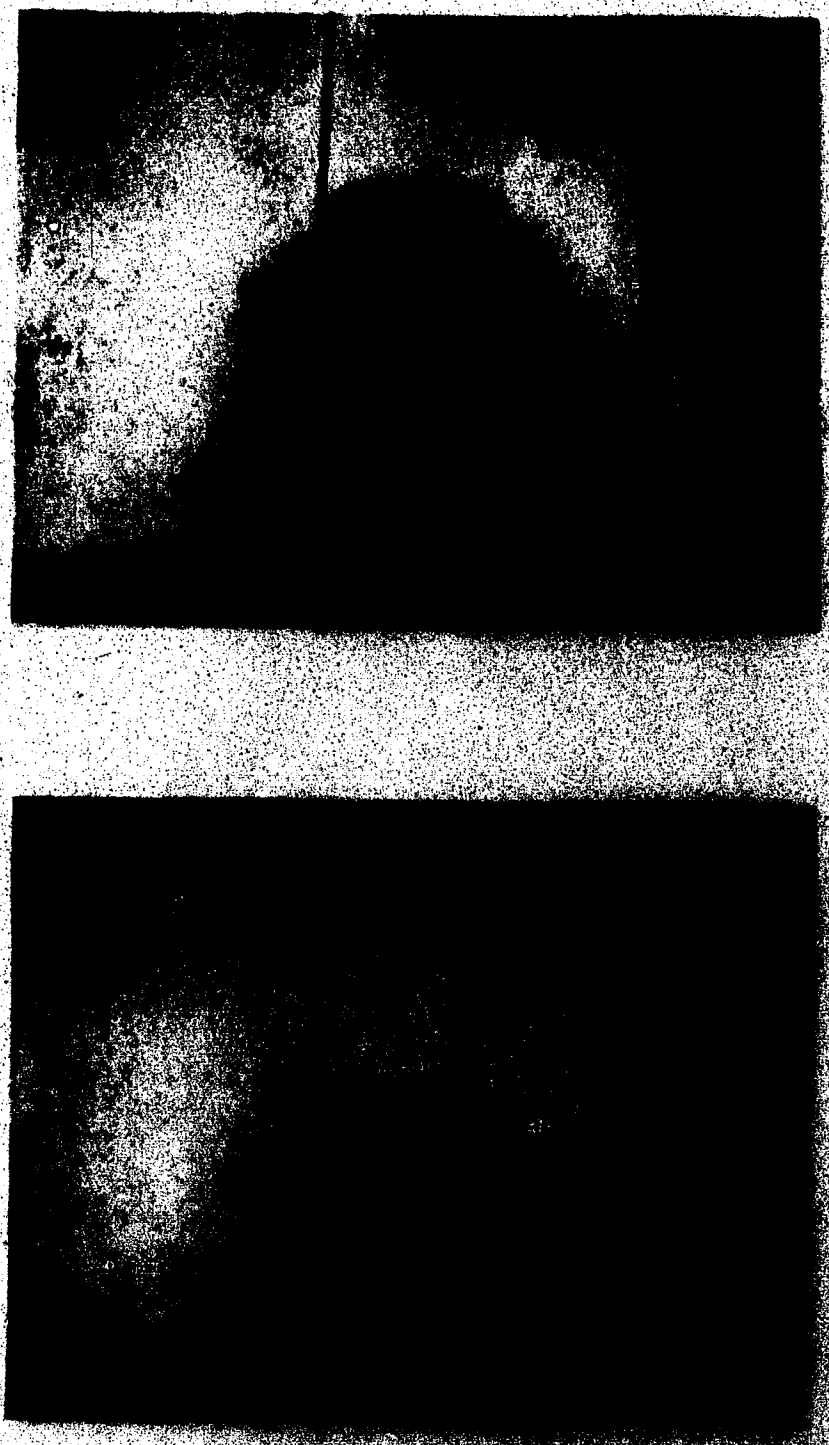

FIGURE D-1 PHOTOGRAPH OF JET [illegible] AT DIFFERENT TIME INTERVALS FOR [illegible]

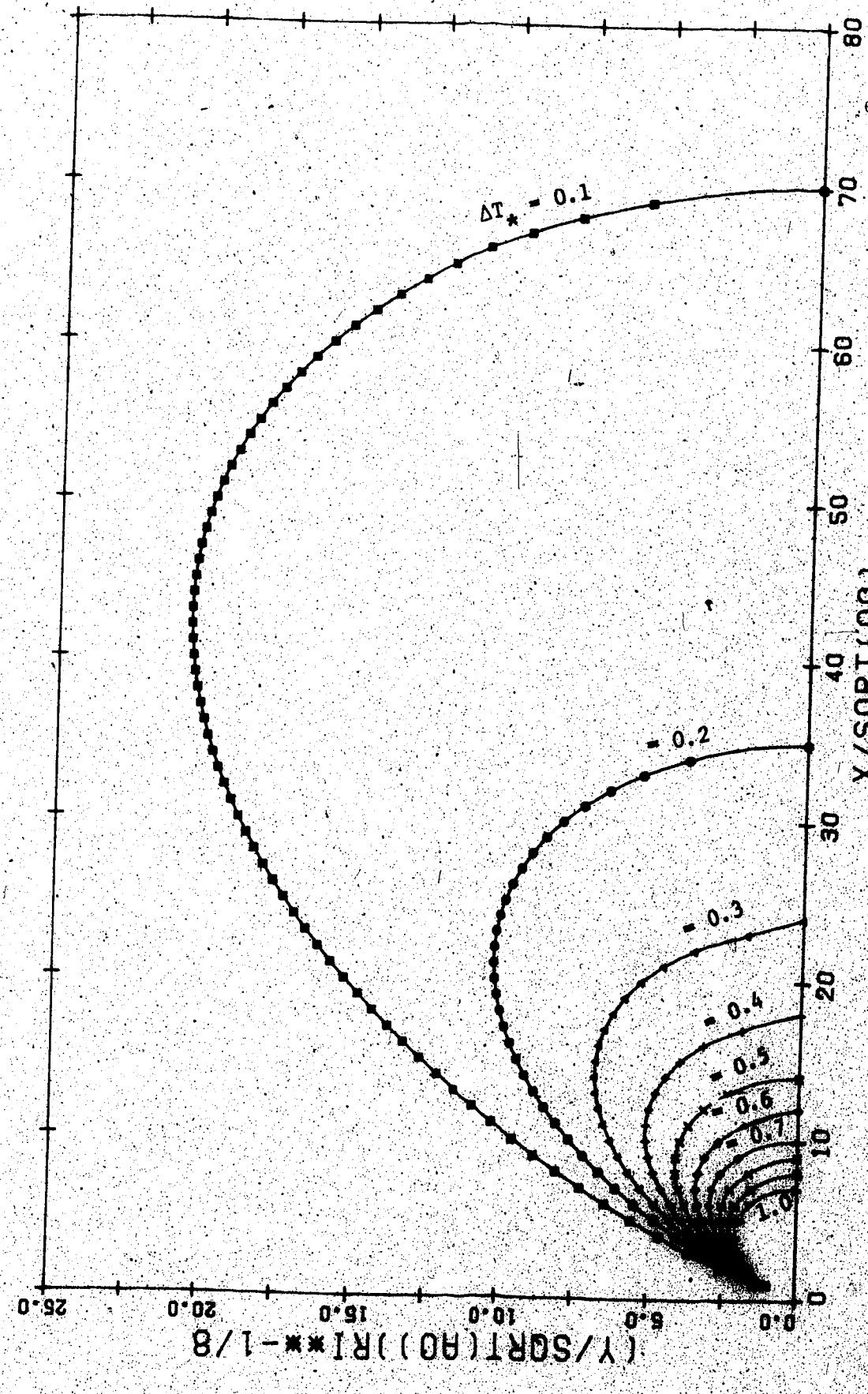

FIG.D-2 PLOT OF SURFACE ISOTHERM FOR SMALL RI.

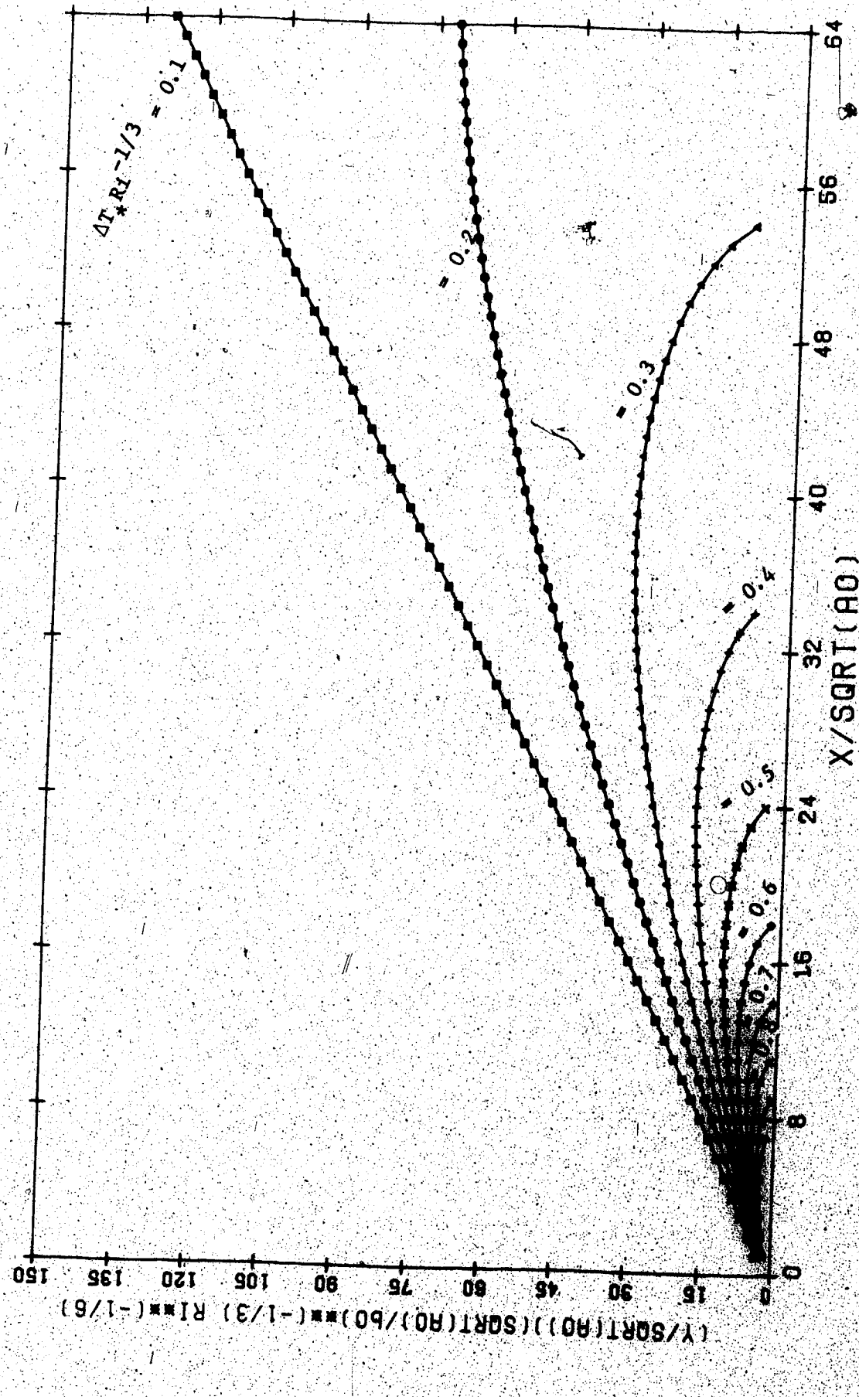

FIG.D-3 PLOT OF SURFACE ISOTHERM FOR MODERATE RI

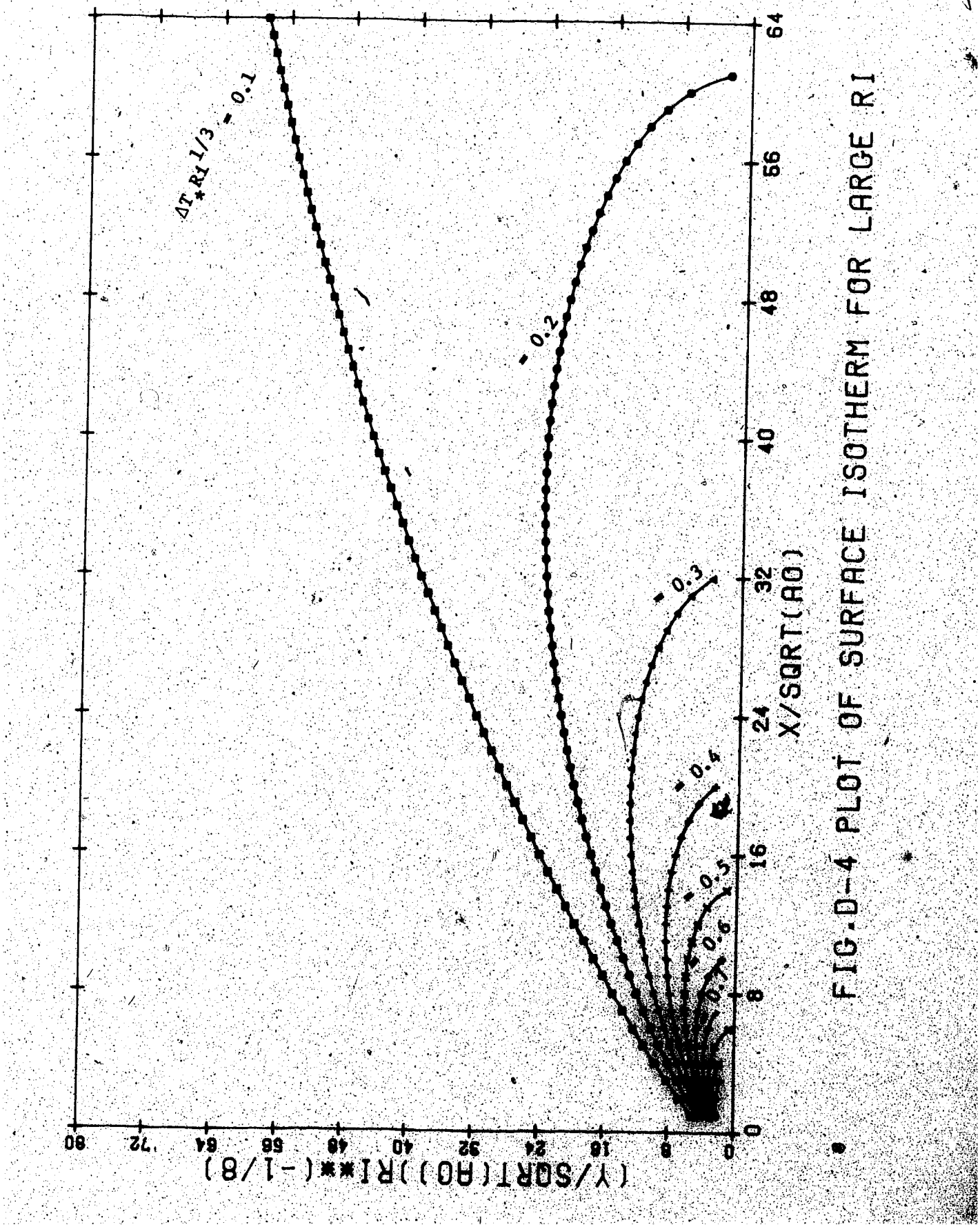

FIG.D-4 PLOT OF SURFACE ISOTHERM FOR LARGE RI

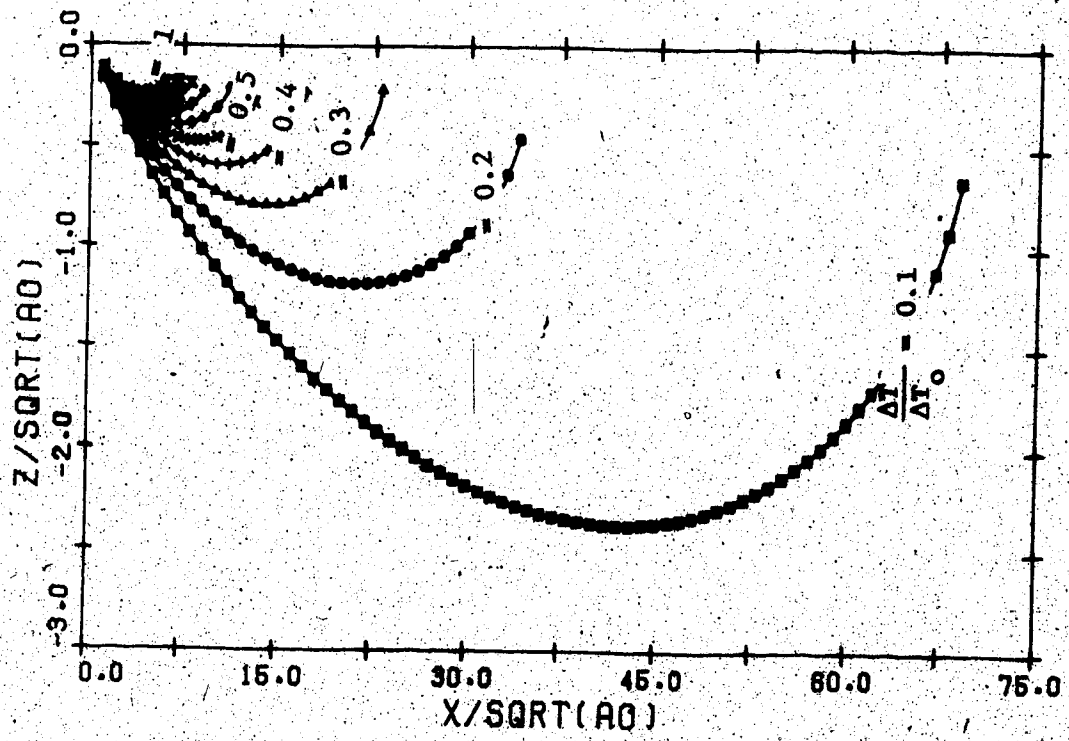

PLOT OF VERTICAL ISOTHERM FOR SMALL RI

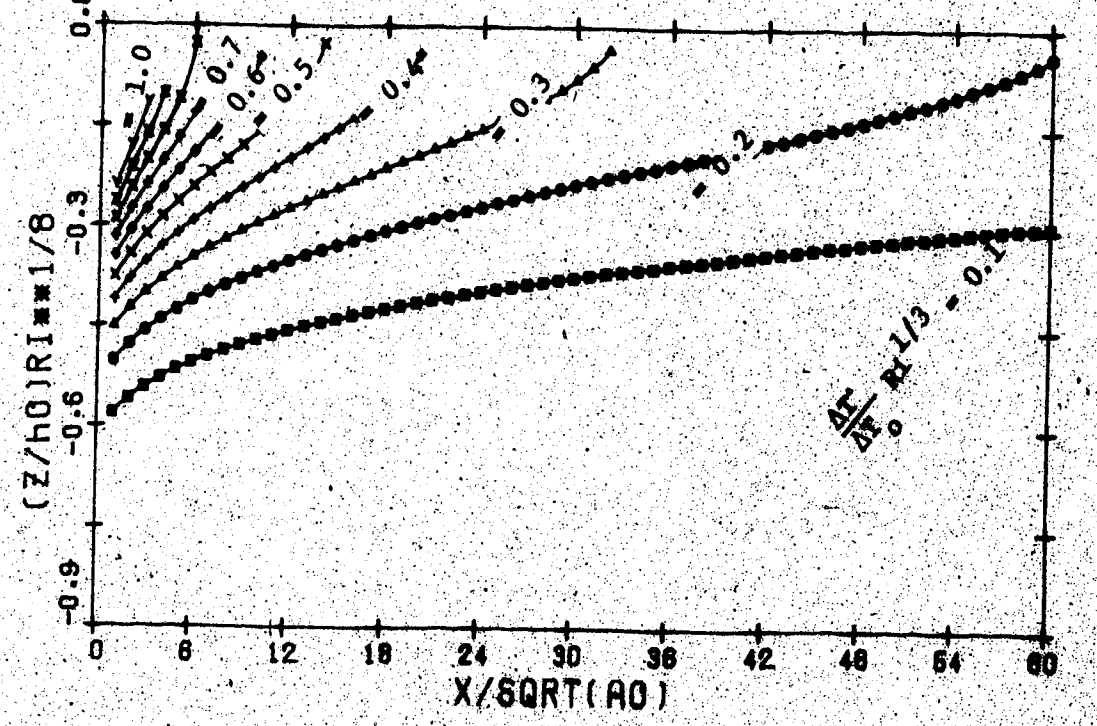

FIG.D-5 PLOT OF VERTICAL ISOTHERM FOR LARGE RI

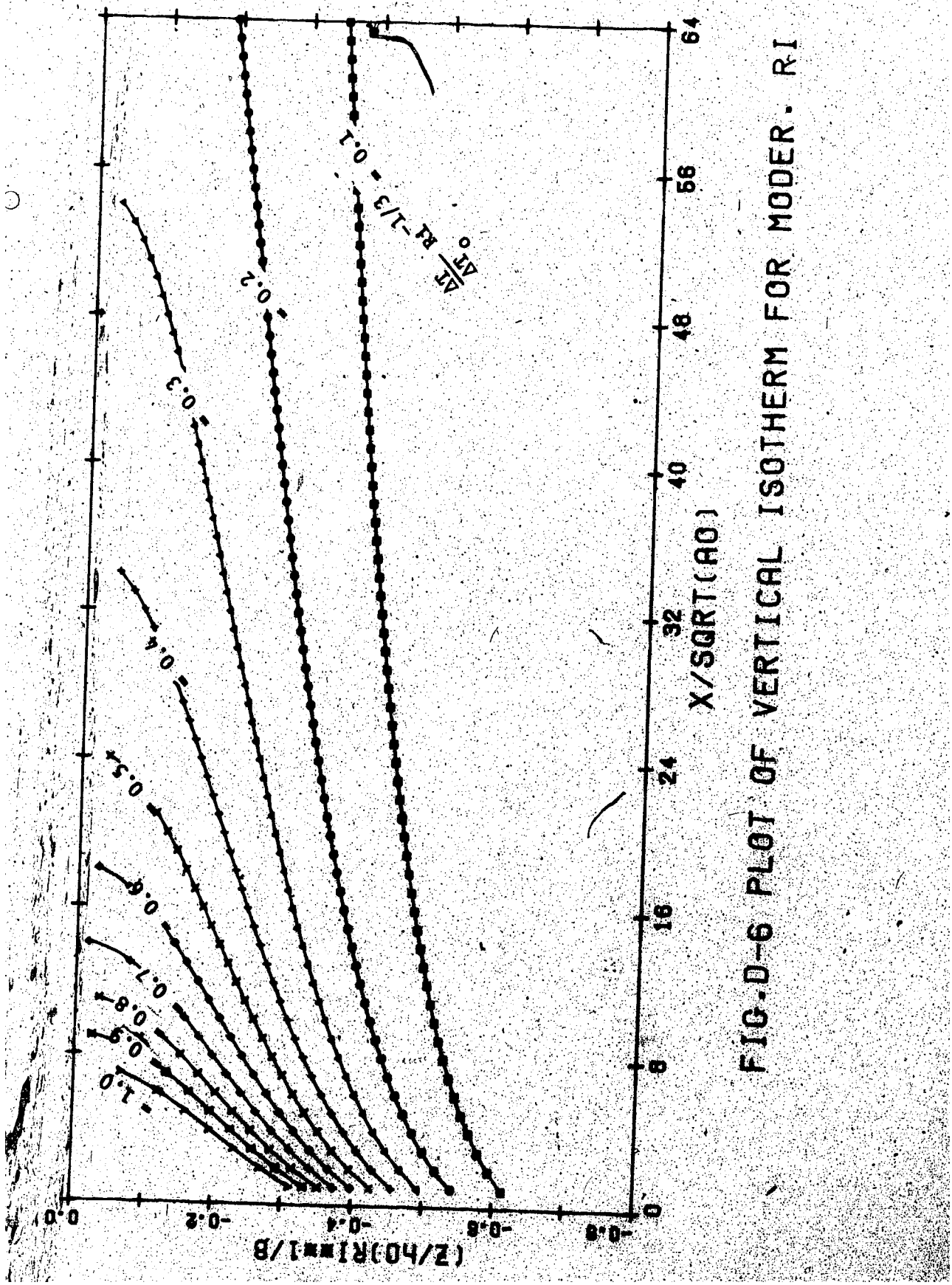

FIG-D-6 PLOT OF VERTICAL ISOTHERM FOR MODER. RI

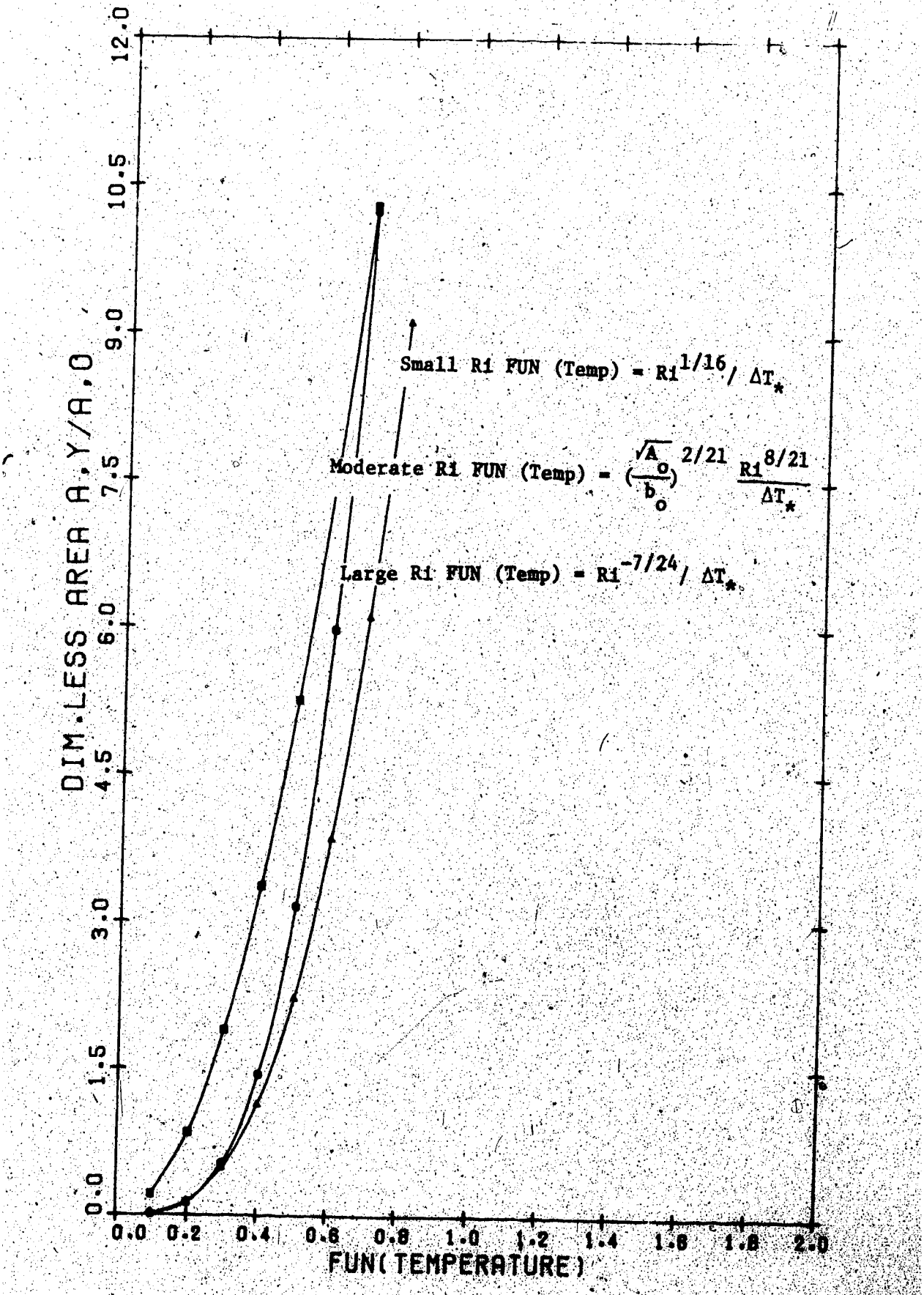

FIG.D-7 AREA OF SURFACE ISOTHERM

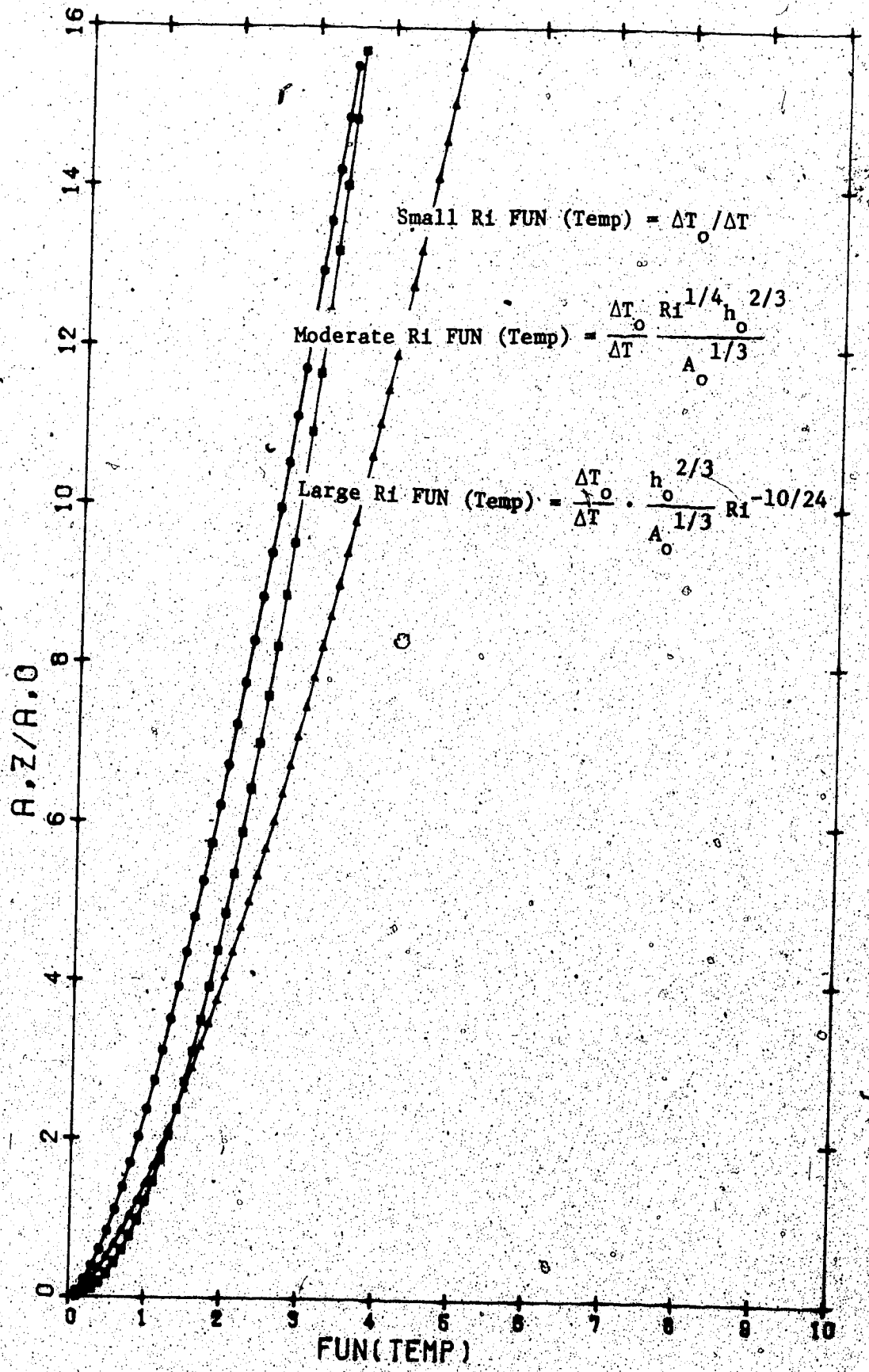

FIGD-8 AREA OF ISOTHERM IN C/L VERTICAL PL.